This is to certify that the

dissertation entitled

SPECTRAL ANALYSIS FOR OPTIMAL DESIGN OF A

VARIABLE ECCENTRICITY TRUNK SHAKER HARVESTER SYSTEM

presented by

Henry A. Affeldt Jr.

has been accepted towards fulfillment
of the requirements for

Doctor of Philosophy degree in Agricultural Engineering
(PhD)

John B. Gerrish
Major professor

Date 19 May 1987

SPECTRAL ANALYSIS FOR OPTIMAL DESIGN OF A VARIABLE ECCENTRICITY TRUNK SHAKER HARVESTER SYSTEM

By

Henry Albert Affeldt Jr.

A DISSERTATION

Submitted to
Michigan State University
in partial fulfillment of the requirements
for the degree of

DOCTOR OF PHILOSOPHY

in

Agricultural Engineering

Department of Agricultural Engineering

1987

SPECTRAL ANALYSIS FOR OPTIMAL DESIGN OF A VARIABLE ECCENTRICITY TRUNK SHAKER HARVESTER SYSTEM

By

Henry Albert Affeldt Jr.

Date: 19 May 1987

Approved: John B. Smith
Major Professor

Approved: Galen K Brown
Director of Research

Approved: Donald G. Edwards
Department Chairman

ABSTRACT

SPECTRAL ANALYSIS FOR OPTIMAL DESIGN OF A VARIABLE ECCENTRICITY TRUNK SHAKER HARVESTER SYSTEM

By

Henry A. Affeldt Jr.

Until the advent of mechanical harvesting in commercial cherry orchards of Michigan in the mid-1960's, the normal productive life of trees exceeded 40 years. Annual bark damage from trunk shaker harvesting had shortened orchard life to 15-20 years maximum by the mid-1980's. A dynamic analysis of a trunk shaker was needed to affect a shaker redesign and to establish physiologically safe operating procedures. A method to nondestructively monitor possible changes in tree growth resulting from mechanical harvesting was also needed.

A C-clamp, fixed-eccentricity trunk shaker was instrumented with transducers to measure instantaneous acceleration and position. A frequency-domain analysis technique was developed to obtain displacement from acceleration and compare with other events. Peak displacements during start-up and shut-down of the shaker vibration were found to be associated with destructive stress levels in the bark.

A fixed-eccentricity mass on a harvester was exchanged for a controllably variable eccentric mass. Starting and stopping transients that involved excessive displacement and

stresses were successfully eliminated with this design, even though the steady-state displacement remained equal to that of the fixed-eccentricity design. Several multi-mass, fixed-eccentricity designs are presented which could also reduce the trunk damage.

A spectral analysis package was developed to compare profile changes in trunk perimeters with time. Bandwidth, Fourier analysis, and invariant moments appear to indicate bark damage permeation (internal and external damage can be differentiated), and level of infection.

To my wife **Karen**
my mother **June**
my sister **Tara**
my father **Henry Sr.**

United in Time and Space,
Through Love, Sacrifice and Understanding,
We have sought Knowledge,
And learned the Questions.

ACKNOWLEDGMENTS

The author would like to express his deepest gratitude to the following persons and organizations for their contribution to this study:

To **Dr. John B. Gerrish**, my Major Professor, for his professional guidance, immortal support and incomparable, eccentric prescriptions for problem solving purveyed throughout the epoch of this graduate program.

To my Director of Research, **Dr. Galen K. Brown** (Research Leader, Fruit and Vegetable Harvesting, U.S. Department of Agriculture), for his unsurpassing, inimitable professionalism, logic, and dedication.

To my Guidance Committee, **Dr. Clark J. Radcliffe** (Associate Professor Mechanical Engineering), **Dr. Steven W. Shaw** (Assistant Professor Mechanical Engineering), and **Dr. Clyde L. Burton** (U.S. Department of Agriculture, Assistant Professor Botany and Plant Pathology) for their time, auspicious counsel, and professional collaboration.

To USDA Mechanical Engineering Technician **Richard Wolthius**, MSU Electronic Technicians **Joe Clemens** and **Sidney Ehlert**, MSU Horticultural Specialist **Nancy M. Schulte-Pason**, and Graduate Students **Thomas A. Esch** and **Ghassan Al-Soboh** who each contributed many hours of valuable assistance, experience, and seasoning to the project.

To cherry growers **David and Philip Friday** and the **Friday Tractor Company** (Hartford, MI) for their cooperative spirit and contributions of equipment which made this project feasible.

To the **Agricultural Research Service, U.S. Department of Agriculture** for subvention (Research Engineer Recruitment and Development Program) and continued aspirations for the agricultural foundations of these United States.

To my mother **June**, my sister **Tara**, and the orchestra of family and friends whose unabated love, confidence, and understanding have been an important and never ending source of strength and encouragement.

To my wife **Karen**, a highly unique and fluorescent spirit, who brought a wondrously enchanting love, exhilaration, and placid mystery into my once harmonic orbit.

TABLE OF CONTENTS

LIST OF TABLES

LIST OF FIGURES

CHAPTER 1

INTRODUCTION

Fruit and nut production around the world continues to be a costly, long term investment for growers (Brown, 1980). The onset of industrialization combined with problems in labor management and production economics has forced growers to mechanize crop production, harvesting and processing. Countries such as the U.S., Japan, Australia, New Zealand, Israel, South Africa, the Socialist Block Countries, Canada and many countries in South America currently have programs to mechanize labor-intensive fresh market crops. Improved means by which production can be made more efficient and reliable are necessary to meet the demands of the competitive world food markets and the 4,917 million people therein (United Nations, 1986).

Tree fruits have been mechanically harvested since the early 1920's (Abildgaard, 1923) but mechanization actually began with the development of the eccentric powered cable limb shaker for walnuts in 1946 by J. P. Fairbanks (O'Brien et al., 1983). Since that time, there have been extensive efforts to mechanize the harvest of the world's multitude of fruit and nut crops, thereby realizing increases in labor and economic efficiency. An unwanted side effect of

mechanization evolved, however; bark damage at the point of shaker attachment. The clamping and shaking forces from vibrating shake-and-catch harvest systems are transmitted to the tree limb or trunk through the bark and cambium causing subsequent fruit release onto a catching surface below. Worldwide, grower's have expressed concern as to the potential role dynamic shaker loading may play in internal tree damage and subsequent tree decline, particularly in younger orchards.

In Michigan, for instance, commercial cherry growers who mechanically harvest estimate 20-30% annual decline of cherry trees in some orchards (Brown, 1982). Until the advent of mechanical harvesting, manual cherry orchard productive life exceeded 40 years. Commercial orchard life degenerated to 30 years in the late 1960's and finally to 15-20 years with today's trunk shakers (Burton et al., 1986).

Trunk damage alone can result in the death of many trees, particularly young trees subjected to annual shaking. Mechanical harvesting, however, may simply initiate decline, presenting an opportunity for the infectious cankers or predisposing the tree to other stress factors such as cold injury, nematodes, borers, viruses, fungi, bacteria, etc.

USDA undertook an engineering analysis of a representative commercial inertial shaker in order to determine basic dynamic behavior which may be correlated to fruit harvesting success and bark strength failure. This

information is mandatory for design of a mechanical shaker which will cause minimum tree (bark) damage. It may also be of value in indicating the range of basic tree properties as limits for future harvester designs.

This research describes the hardware and methodology employed to characterize the dynamic behavior of an inertial trunk-shaking harvester clamped to different sizes of trees. The analysis of the data highlights a new criterion for shaker design. Subsequently, a new mechanical vibratory tree shaker is designed, built and tested. Finally, a method for studying the long term effect of shaking on tree trunk profiles is presented (spectral analysis).

1.1 Physics and Physiology

The first limb shakers transmitted forces in a linear reciprocating motion, practically devoid of any lateral forces on the tree when the clamps were correctly attached perpendicular to the limb. Due to the greater speed, lower harvest cost and lower labor requirement offered by trunk shakers, however, trunk shakers were adopted in the early 1960's. The trunk shakers applied large forces in epicyclic patterns such as cycloids, hypocyloids, cardioids, N-leaved roses and spirals. These patterns are quite efficient at fruit removal when transmitted at proper design frequency and amplitude for a given crop. Compared with limb shakers, the compressive, tangential and longitudinal forces associated with epicyclic trunk shakers are usually greater, the motion is non-linear and hence, some lateral forces

become apparent.

Research on cherry bark strength indicates that cherry tree bark is easier to damage than apple or peach tree bark in both longitudinal and tangential directions (Diener et al, 1968). The adoption of the epicyclic trunk shaker patterns also brought about obvious bark damage to the trees. Potential causes of bark damage include operator error, carrier slip, improper shaker and clamp adjustments, improper machine maintenance, inadequate orchard maintenance and poor choice of harvest date, harvest practice or production practice, and clamping and shaking forces too high or too low (Cargill et al., 1982).

By itself, bark damage from these and other causes would not be deleterious to tree production. Insect attack and fungus cankers often infect the damaged area, however, spreading and quickly causing premature tree decline (Devay et al., 1965). Fungal spores can be transported from tree to tree by shaker pads from diseased trees to healthy, undamaged plantings.

Damage can be greatly affected by the condition of the cambium at harvest. During periods of rapid growth and irrigation when the cambium is moist, the cell interiors and intercellular spaces become filled with liquid. Cell walls are thinner (Bukovac, 1984). When shear stress is applied, the bark slips easily over the wood. When the moisture content decreases or Fall dormancy sets, cell walls become thicker and less elastic and intercellular spaces lose their

liquid content (Priestley, 1930); the occurrence of slip is greatly reduced under these conditions (Fridley et al., 1970).

Rain and irrigation during periods of rapid growth increase the tendency for the bark to slip. Thus, cherry trees harvested in June and July are more susceptible to damage than peach, plum or apple trees which are harvested later. Bark damage that occurs as torn or split bark (visible) has been studied for the past 20 years. Research has been conducted to determine the limits on cherry bark strength and how to eliminate bark damage (Diener et al., 1968; Brown et al., 1982). Excessive clamping forces which were found to crush bark and internal tree tissues have been identified in the static, nonvibratory state (Frahm et al., 1983).

Responding to the recommendations of researchers, some manufacturers have redesigned clamp pads with increased contact area; larger pads transmit shaking forces at lower pressures (Brown et al., 1986). Forces transmitted by shakers have been studied; recommendations have resulted for stroke and frequency to remove fruit and minimize tree damage (Fridley and Adrian, 1960). Procedures on operations and maintenance of both machine and orchard have been suggested by other researchers (Brown et al., 1982; Cargill et al., 1982).

1.2 Importance - Tree Fruit Statistics

Mechanical trunk shaker harvesters are employed to some extent throughout the U.S. and abroad for apples, apricots, olives, peaches, pears, plums, prunes, cherries and citrus (Brown, 1980). Frequently, over 50% of the total labor required for these crops is dedicated to the harvesting process. Production quantity and a short harvest season often mandate the use of mechanical harvesting in some crops, especially in countries where hand labor is not available or affordable.

The soil condition, drainage, elevation, and climate combine to make the counties bordering Lake Michigan host to some of the most productive cherry orchards in the world. In 1985 Michigan ranked first in the nation in production value of tart cherries; Michigan ranked second in production value for sweet cherries (Table 1.1). Seventy-seven percent (100,000 tonnes) of the nation's tart cherries, worth 52.4 million dollars, are produced in Michigan along with 23% (28,000 tonnes) of sweet cherries worth 15.5 million dollars.

Cherries are high in nutritive value (Table 1.2) and are often used as a supplement to the diet. The primary market for Michigan tart cherries (95%) is in cherry pie filling and dessert toppings in frozen market packs. The remaining tart cherries go into juice, raisins, wine and jams. Sweet cherries are also mostly processed (90%), the light varieties being packed for juice, jelly, ice cream and

Table 1.1. Total 1985 U.S. cherry production.
(National Agricultural Statistics Service, 1986)

TART CHERRIES

	Total Production 1000 t	Value of Production 1000 Dollars (U.S.)
Michigan	100.0	52,395
New York	10.2	5,764
Utah	9.5	4,832
Wisconsin	3.9	1,549
Oregon	2.9	1,560
Pennsylvania	2.7	1,608
Colorado	0.8	390
U.S.	130.0	68,098

SWEET CHERRIES

	Total Production 1000 t	Value of Production 1000 Dollars (U.S.)
Washington	34.4	36,588
Michigan	28.2	15,500
Oregon	26.4	16,761
California	21.4	24,641
Montana	4.2	2,255
Idaho	2.0	2,065
Utah	2.0	1,624
New York	1.8	1,396
Pennsylvania	0.4	655
U.S.	120.8	101,485

frozen products, the remaining 10% going into maraschinos and fresh market.

Yield per tree depends on factors such as climate, cultural practice and variety but is generally categorized by age of the tree (Table 1.3). The yield for tarts in Michigan was up 5% from 1984 while sweet production was down 6% (Figure 1.1). The 1985 average productivities for Michigan were 1100 kg/ha (6000 lbs/acre) for tarts and 1285

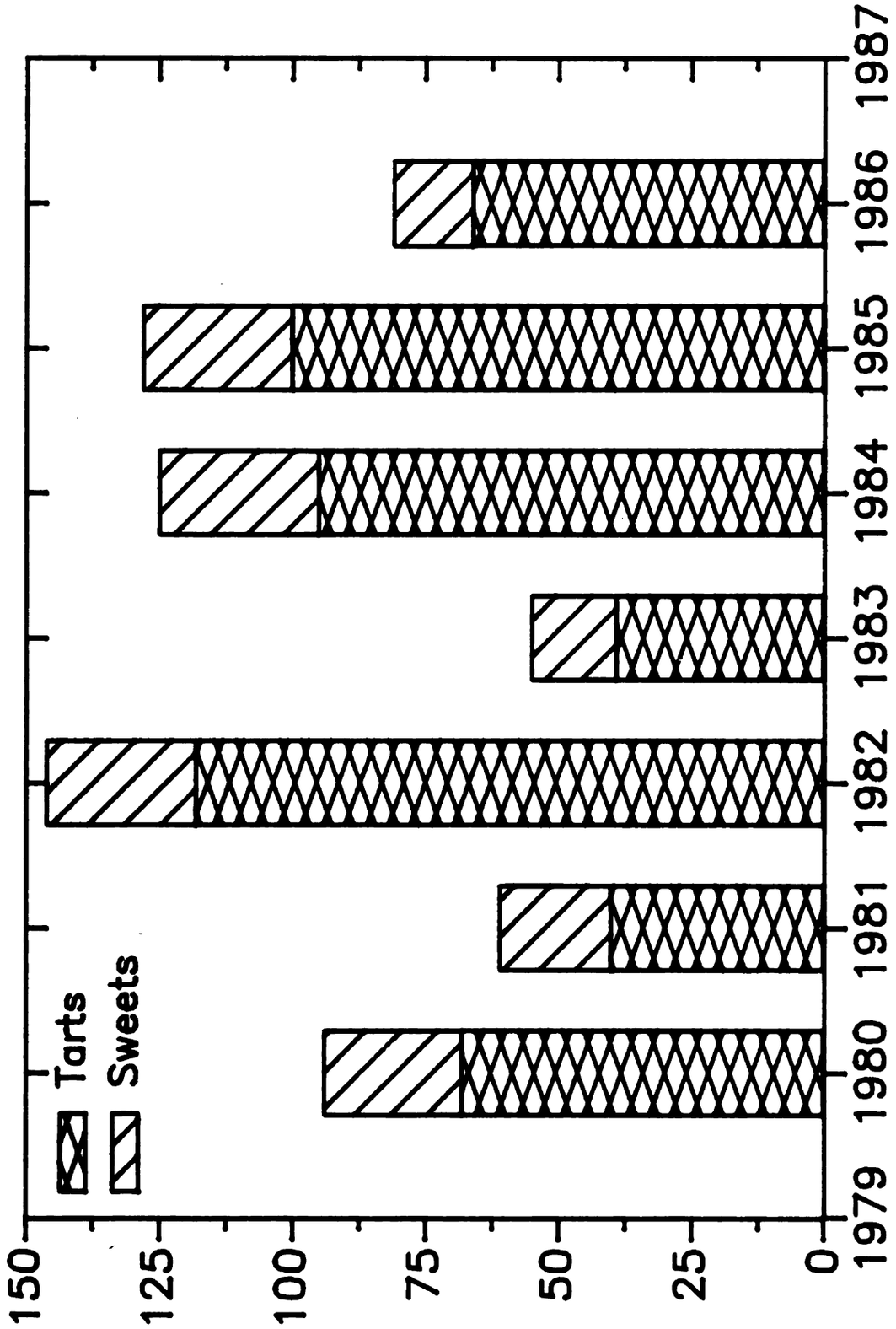

Figure 1.1 Michigan cherries: total production

Table 1.2. Nutritional composition of fresh raw cherries*. (Westwood, 1978).

	Sour Red Cherry	Sweet Cherry
Water (%)	83.7	80.4
Calories (kcal)	58	70
Carbohydrates (g)	14.3	17.4
Protein (g)	1.2	1.3
Ash (g)	0.5	0.6
Fat (g)	0.3	0.3
VITAMINS		
Vitamin A (I.U.)	1000	110
Ascorbic Acid Vitamin C (mg)	10	10
Niacin B-Vitamin (mg)	0.4	0.4
Riboflavin B_2 (mg)	0.06	0.06
Thiamine B_1 (mg)	0.05	0.05
MINERALS		
Potassium (mg)	191	191
Calcium (mg)	22	22
Phosphorus (mg)	19	19
Sodium (mg)	2	2
Iron (mg)	0.4	0.4

* Based on 100 g (3-1/2 oz, 110 cherries/lb).

kg/ha (7000 lbs/acre) for sweets with a reported 82,300 hectares (33,300 acres; 3.25 million tart trees) and 18,800 hectares (7,500 acres; 625,000 sweet cherry trees) of bearing age (Figure 1.2). There were 1383 tart cherry growers and 775 sweet cherry growers in Michigan in 1982; recently grower numbers have been decreasing and orchard acreage has been increasing.

Ninety-nine percent of the state's tart cherries are of the Montmorency variety. For sweet cherries, 31% are the Napoleon variety; Golds (17%), Schmidt's Biggareau (12%), Emperor Francis (11%) and other varieties (29%) make up the

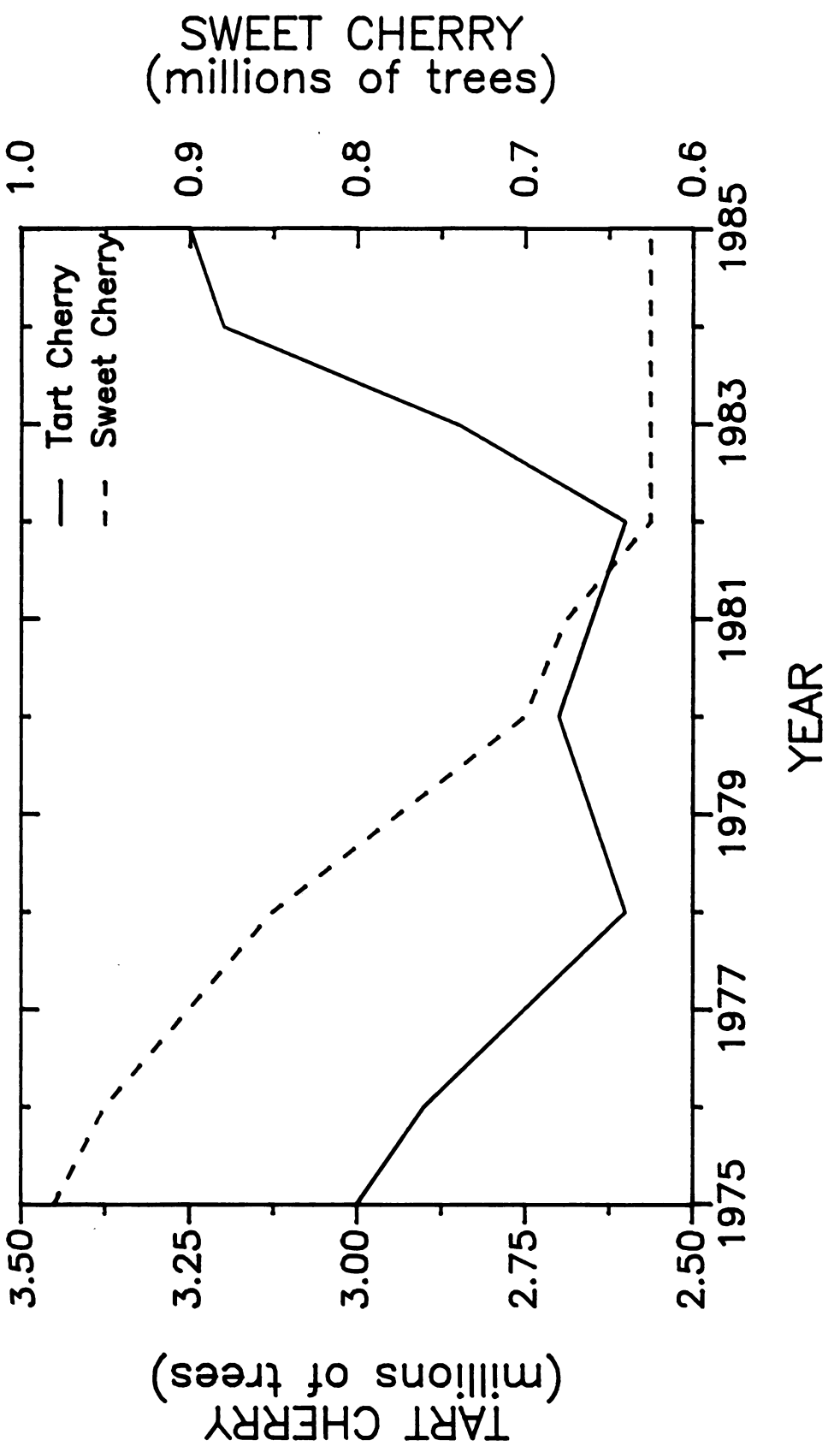

Figure 1.2 Michigan cherry trees of bearing age (Michigan Dept. of Agriculture; 1985, 1986).

Table 1.3. Cherry tree productivity categorized by tree age. (Fouch, 1986).

Tree Age (Years)	Average Annual Productivity (kg/tree)
4	22
5	33
6	44
7	88
8	132
9	176
10 - 18	176 - 220
19 - 20	176
21 - 22	132
23	110
24	66
25	55
26	44
27	33
28	22
29 +	0

General Classification of Bearing Age:

0 - 5	:	Non-bearing
6 - 9	:	Moderately Bearing
10 - 20	:	Prime Bearing
21 - 25	:	Rapid Decline

rest. Domination of the state's cherry trees by the tarts (84%), in particular by the Montmorency variety, facilitates design of mechanized harvesting systems because of the uniformity of tree size and structure.

Over the past eight years there has been an increase in the number of bearing trees. This increase will continue as nearly 50% of the state's tart trees and 30% of the sweets are currently of non-bearing age. New orchards signal even greater uniformity in terms of design for reduction of bark damage. New orchards also make urgent the need to eliminate

bark damage and tree decline factors before harvesting should begin on these younger, more susceptible plantings.

Bark damage leading to tree decline (loss of vigor and yield) is thought to be caused by excessive shear, compression stress or strain (Adrian et al., 1965). Limb shakers may damage one or more scaffolds but damage to the entire tree can occur when a trunk shaker causes damage. The flow of nutrients essential to tree vitality is interrupted when the xylem or phloem cells are damaged. The tree isolates damaged areas in a two step process to protect healthy wood and tissue (Santamour, 1986). The speed at which this process occurs depends on the area damaged and can determine the spread of decay and loss of tree vigor.

1.3 A Timely Goal

Visible bark damage has practically been eliminated for operators who accept current recommendations for shakers, pads, operations, pruning, and irrigation scheduling. Bark damage from excessive stress or strain may still occur in the form of cell-crushing which is not visible. The outer bark periderm on cherry trees is elastic and may hide the internal damaged areas for several weeks. This damage is later revealed in the form of open cracks, dead bark tissues, gummy areas, or abnormal bark growth (Brown et al., 1984).

Despite continued shaker and pad development and the adoption of enlightened operating procedures, growers continue to report some bark damage each year in commercial

orchards (Timm, 1986). Sweet cherry trees are more susceptible than tarts and young trees are more susceptible than older plantings. The productive life of mechanically harvested orchards appears to have decreased from 30 years to 10-15 years; bark damage may be a significant factor (Burton et al., 1986). When considering that mechanical shake-and-catch harvest systems are used to harvest over 95% of all sweet and tart cherries used for processing, this loss in productivity adds up to 3.0 million tart trees (30 million tree-years of productivity) and 536,000 sweet trees (5.36 million tree-years of productivity) in 1985 alone for existing orchards. Significant plantings of new orchards in the late 1970's and early 1980's (nearly 50% of the state's tart trees and 30% of the sweet trees in 1982) have made the elimination of bark damage an economic priority. These new orchards signify another 1.3 million tart trees and 312,500 sweet trees that will come to bearing age in Michigan orchards which may be harvested mechanically.

The U.S.D.A. Joint Council on Food and Agricultural Sciences (1986) lists as one of it's eight top research priorities for 1988: "to sustain the long term productivity and profitability of agriculture...Greater emphasis is needed on integrated farming systems which are based on the appropriate new and existing production technologies". The current problem of eradication of hidden bark damage requires the identification and control of safe limits on applied pressure and strain from mechanical shake-and-catch

harvest systems (Brown et al., 1984). Re-design of current shaker-pad-tree systems and modification of shaker operating procedures are just two of the many bio-physic interfaces that promise to benefit from engineering intervention.

1.4 Objective of this Research

The goal of this research was to analyze the dynamic displacement response of an inertial fruit tree shaker and attached cherry trees of varying size. Displacement data can aid in estimation of stress and strain applied to the bark. Critical maxima thought to be harmful to tree bark would be sought. Theoretical analysis and re-design of the inertial fruit tree shaker based on vibration results may then provide a key step in minimizing bark damage. A tree trunk profile analysis method, a possible hidden bark damage indicator, would be developed and presented for utilization in future studies. The specific objectives formulated for the needs of this research investigation were:

1. Collect and analyze dynamic displacement data from a typical commercial inertial fruit tree shaker and develop the methodology for required signal analysis processes.

2. Determine peak X and Y displacements of the tree and shaker for several vibration frequencies and tree sizes.

3. Design, construct, test and evaluate a modified shaking mechanism based on an analysis of the apparent vibration anomalies potentially harmful to the bark.

4. Develop and test a method for monitoring tree trunk profile changes over a several year period.

CHAPTER 2

LITERATURE REVIEW

The first manual harvesting of a tree fruit is attributed to Eve (Genesis 3:6). For millennia thereafter, fruits were harvested manually, requiring much time and labor. The amount of labor needed for harvesting was frequently over 50% of the total labor and cost requirements to raise a specific horticultural crop (Brown, 1980). Different tree fruits pose different difficulties for manual harvest. Date palms, for example, grow very tall (9-18 m, 30-60 ft.) and bear fruit at the top where skilled workers are needed to climb and cut the fruit bunches. Some citrus fruits like tangerines, lemons and limes, rapidly deteriorate if the stem is improperly removed from the fruit during picking. Apple, pear, peach and plum trees require ladder or platform work; the bulk of these fruits also necessitates frequent trips to empty the picking sacks.

Cherries, on the other hand, are not bulky, but are small and vastly abundant within a tree. It requires ten times as many man-h of labor to pick a tonne of cherries as are required to pick a tonne of apples, peaches or pears (Levin et al., 1960).

Most tree fruits also pose the problem of a short

harvest season and low yield per worker, particularly cherries (150 h season, 8 man-h per tree: Fridley and Adrian, 1968). When an orchard is ready to be harvested, a grower may have only a few days to harvest for prime quality. Until the late 1960's, the cherry growers in Michigan could rely on over 45,000 workers, 35,000 of whom were migrant workers, to meet the harvest need (Levin et al., 1960; ARS, 1964; Brown, 1980). Public Law (PL) 78, known as the "Bracero program", which permitted seasonal migratory workers to enter the United States, was terminated December 31, 1964. Investors in orchard crops were faced with the choice of selling out, switching crops, abandoning the orchards or mechanizing. As the problems of labor shortage, labor cost, labor unrest, transportation costs, rough handling and economics accumulated, growers learned that mechanization could be economical and eliminate many labor problems while maintaining steady product flow to the market (Drake, 1983).

2.1 Chronology of Tree Shaker Design

Mechanical vibratory tree fruit harvesting has seen an evolution from crude tools to current-day, highly complex mechanized shakers (Figure 2.1). The concept of these tree fruit harvesters remains quite simple: to transmit enough shaking force through the shaker and the clamp to overcome the inertia of the tree and provide limb acceleration sufficient to detach the fruit at the stem. This concept was first employed in hand tools used as knockers and

Mallets - Pre 1960

Boom Shakers - 1923, 1954

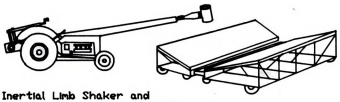

Inertial Limb Shaker and Mobile Catching Frame - 1960

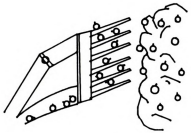

Combing Tines - 1962

Cable Shakers - 1946

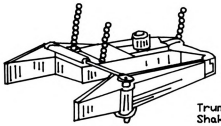

Trunk Shakers - 1960

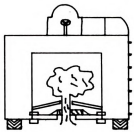

Over-the-Row Harvesters - 1973

Rotary Cone Harvester - 1984

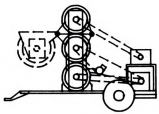

Air Blast Shaking - 1961

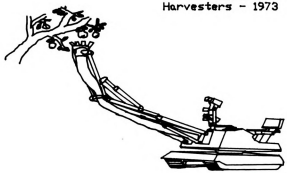

Optically Activated Robotic Pickers - 1985

Figure 2.1 A pictorial register of tree fruit harvester innovation.

shakers. Stiff trees where low amplitude, high frequency vibration could remove fruit were found to be good targets for mallet shakers, especially in the nut groves of California. A 1-m long wooden mallet with a hard rubber padded tip was used to beat limbs to remove fruit. Bark damage from this method, however, in conjunction with Ceratocystis fimbriata canker infestation, caused enough harm to nut trees in California that the canker earned the nickname "mallet wound canker" (Devay et al., 1960).

Long willowy poles have also been used to knock limbs, thereby jarring the fruit from the stem (Gaston et al., 1959; O'Brien et al., 1983). Fridley and Adrian (1966) describe manual limb shaking of prunes with a hook secured to a long pole. W. F. Rurup actually patented the first manual "tree shaking device" in 1927 consisting of a spring loaded metal hook on the end of a rod. Gustafson patented a similar concept in 1951 with an improved hook guide to shake nuts from tree limbs. Expectedly, the size of the limb was limited; weakened branches were easily broken, and workers quickly tired.

Hand-carried mechanically activated shaking devices were developed to replace poles in the shaking of small limbs (Gaston et al., 1959; Russel and Dowling, 1964; Plummer, 1969). Ferguson (1963) developed a hand held, spring loaded limb knocker which was activated by a hand crank. Several hand held motorized designs were based on the use of a chain saw type power unit with a pitman linkage

(Londo, 1965; Aulabaugh, 1965). A manually operated pulley system on a tractor frame was developed in 1959 to knock tree limbs for fruit removal (Roberts, 1959). Steingas and Gaul (1968) developed a portable hydraulic/air cylinder which had one end ratchet-clamped to a limb with the opposite end supporting a mass which was reciprocated; the unit was powered through a flexible hose coupled to a tractor unit. Watson (1970) had a similar idea with a PTO-powered pneumatic pump hose-connected to a hand held rotating motor unit which operated a pitman arm for limb reciprocation. Most of these hand-held shakers were not popular, however, due to the low rate of harvest, operator fatigue, shock transferred to the user, in effectiveness on large limbs and bark damage.

The next step in tree shaker evolution was changing the shaker carrier from man to machine. Abildgaard patented the first completely mechanized fruit and nut harvester in 1923. A spring loaded hook clamped to a trunk or main scaffold imparted linear reciprocating motion from a boom driven by a gasoline powered pitman-crank mechanism mounted on a carrier below. This was the first patented account of a "trunk shaker" of sorts. In 1927, Harold Bartlett patented a hydraulically activated boom shaker harvester (limbs or trunks) with a two-half tree encircling catching frame. Berger (1937) moved the standard reciprocating pitman-crank mechanism to the end of the boom on his design such that only the shaker head and the trunk or limb were oscillated

and not the boom itself. Berger was also the first of the tree shaker patentees to suggest using some padding at the tree contact surface to prevent bark damage.

Unfortunately, it took almost a quarter of a century after these first designs were patented before total mechanization found general acceptance. The first widely-noted "pioneering account" of mechanical tree shaking was published in 1946 by J. P. Fairbank, Extension Agricultural Engineer, at the University of California, Davis (O'Brien et al., 1983). Although many earlier designs employed rigid booms, Fairbank's design (for walnut trees) employed a cable with a hook at one end which was reciprocated by an eccentric crank on a farm tractor. The hook was placed over the limb, tension was applied to the cable. The eccentric was then started to apply reciprocating, large amplitude motion to the tree limb. The speed of the shaker was limited by the natural frequency of the limb, which accounted for the return stroke of the shake, as the cable was capable of applying only tension. In 1950, the first cable shaker was patented by Paul Balsbaugh; it consisted of a cylindrical housing in which a PTO driven crank attached to a pitman arm provided reciprocating motion to a cable attached to a tree. Other reciprocating mechanisms for cable shaker operation followed, often powered by a tractor PTO (Johnson, 1951; Avansino, 1953; Hess, 1962).

The boom shakers of the 1920's had been difficult to maneuver in many orchards due to tree shape and ground

conditions. Early models were expensive and were subject to frequent breakdowns. As a result, cable shakers outsold boom shakers for many years.

Eventually, however, the rigid boom design of the 1920's began to replace the Fairbanks cable shaker of 1946 in the design evolution (Gould and Gould, 1954). The boom eliminated the second operator who handled the cable hook. Two types of boom shakers simultaneously developed. One type of boom shaker was called a "knocker" and consisted of a padded member which simply maintained flush contact with the tree delivering a series of impulses to the tree and thus still relied on the natural frequency of the tree for return motion (Jones, 1961; Balsbaugh, 1961; Phelps, 1963). Knocker designs included eccentric boom bumpers, spring activated impulsers, and pressurized air cylinder impulsers. Fridley and Adrian (1966) developed an impulse shaker consisting of an air-accelerated piston in a tube which impacted a padded head next to the limb. A spring between the head and the piston prolonged the impact. Pellerin et al. (1978) designed a pendulum type of trunk impulse shaker with a variable mass and drop height.

Pacheco and Rehkugler (1980) developed a spring-activated impact shaker capable of delivering up to 1151 J (10,185 in.-lb) energy with an 86.6 kg (191 lb) mass moving at 516 cm/s (203 in./s). In 1982, Pellerin et al. designed a spring activated trunk impact shaker capable of both a double impact mode (second impact strikes tree in opposite

direction of first impact and at a time when the tree reaches maximum displacement from the first impact) and a recoil impact mode (tree is pulled toward shaker by a spring recoil force, then impacted to move away).

The second type of boom shaker simply replaced the cable with a boom and the hook with a mechanically activated clamp which could be remotely fastened around a limb by the tractor operator (Lowe, 1955). The tension-compression member with clamp had the advantage of allowing the frequency of vibration to be set by the operator, independent of the natural frequency of the limb or tree.

The majority of the boom and cable shakers which provided a linear motion utilized a cam, piston-crankshaft or pitman-crank drive mechanism. Some innovative deviations from these designs had arisen, however. Goodwin (1954) used a linear hydraulic actuator (cylinder) to reciprocate the boom as fluid was switched in and out of opposing cylinder sides. Balsbaugh (1963) developed a journaled swash plate to reciprocate the shaker boom. In a rigid boom limb shaker, Anderson (1963) used a rotating eccentric to pull a cable attached to a sliding shaker head for retracting motion and used a built-in compression spring to provide the extending motion. Sumner et al. (1975) used a four bar crank-rocker mechanism including a flywheel to provide linear motion at the tree. Khalilian et al. (1978) added a spring between the mass and the limb shaker boom to reduce the maximum force and peak power necessary at frequencies

above the second natural frequency (mode) without affecting limb displacement.

Cherry tree shaker mechanization made its debut in 1958 in Michigan. Levin et al. (1960) recorded 95% fruit removal on sour cherry trees with a Gould tractor-mounted, hydraulically-activated boom shaker designed for West Coast nut crops. Operation was at 12 - 17 Hz with a 3.8 cm (1.5 in.) stroke for 3-5 s. A bear-hug style clamp with rubber padding was used. Tart cherry tree bark damage ranged from no damage to very serious damage depending on clamp slip, clamp pressure, or deviation from a 90^{o} clamp angle. Sweet cherry harvest with this same machine caused severe bark damage due to the violent, long shaking periods required to remove immature fruit for brining (the maraschino process).

Boom shakers, where the boom was fixed to the carrier, required the mass of the carrier to be greater than the mass of the tree, otherwise the carrier would shake more than the tree due to the reactions. The development of the floating inertial limb shaker (Adrian and Fridley, 1965) relaxed this requirement, however, since the suspension of the shaker from its center of gravity allowed free body motion relative to the tractor and thus absorbed some of the reactions.

Fridley and Adrian (1960) experimented with a double eccentric mass boom shaker where masses weighing 2.3 kg (5 lb) were mounted on a common shaft, had 6.4 cm (2.5 in.) eccentricity, and rotated at 7-18 Hz (400-1100 c/min). Herbst (1964) patented a boom shaker activated by two

eccentric masses on the same shaft capable of running in apposition or opposition. Read's (1965) boom shaker patent was similar to Fridley and Adrian's model of 1960 actuated by two eccentric masses on separate shafts rotating synchronously in opposition to produce linear motion. Whitfield (1971) designed a pivoted boom shaker activated by a single rotating eccentric mass.

Fridley (1968) used a crankshaft arrangement to oscillate a mass thus providing a "linear inertially-excited" shake. Brandt (1965) developed a general two eccentric mass vibration generator capable of real-time phase/velocity indexing between the two masses thus producing a multidirectional shake. Brandt's was the first multidirectional vibration generator for inertial shakers. Two rotating eccentric masses were mounted atop one another on a common shaft and driven by a common hydraulic motor and V-belt. Twisting of the V-belt provided reverse rotation for one mass and different eccentric mass pulley diameters permitted slight speed differences. Shipley (1970) patented a plural eccentric mass harvester, each driven by its own hydraulic motor on a C-clamp frame to provide a multidirectional shake.

In 1967, Shipley patented a complete multidirectional trunk shaker design which used two masses in line with the tree, one on either side of the tree, operated hydraulically by individual motors on a free hanging suspended body. Direction of rotation was by hydraulic design, velocity was

by hydraulic flow control and eccentricity was adjustable by manual adjustment of the masses on their eccentric arms. Fridley and Adrian (1966) produced a multidirectional shake by placing two masses on opposite sides of a tree, rotating the masses in the same direction and at the same speed for a circular translation of the trunk, or rotating the masses in opposite directions at equal or different speeds to produce various translational patterns.

Gould and Richter (1969) developed a two mass hydraulically driven multidirectional trunk shaker with two masses in line with the tree but adjacent on the same side of the tree. The masses rotated in opposition and were chain linked for pattern fixation. This design is claimed to achieve minimal bark damage with increased shake yield due to the extra "twisting" of the tree. Savage (1981) developed a C-clamp shaker that uses two chained eccentric masses rotating in the same vertical plane but on spaced axes and synchronized such that a linear horizontal forcing vector is generated to vibrate the tree.

Gentry (1980) developed a citrus shaker for lemons in 1978 utilizing two rotating masses totaling 114 kg (250 lb) in a housing weighing 565 kg (1245 lb). The shaker was attached to trunks up to 40 cm (16 in.) in diameter at heights of 36 cm to 1 m (14 - 40 in.) above the ground. The frequency of shaking was less than 5 Hz (300 c/min). Debarking of the lemon trunks forced Gentry to switch to grapefruit; trees which had smoother trunks and tougher

bark.

Trunk shakers usually deliver an output of relatively high frequency (12 - 40 Hz), short stroke (5 - 20 mm, 0.2-0.8 in.) and varying pattern (O'Brien et al., 1983). These parameters can be varied by modifying the relative masses, the eccentricities, the relative direction of rotation and the relative speeds of rotation. Overstreet (1969) developed a three-mass triangular (isoceles) arrangement of eccentric masses around the tree, which were chain-linked to provide a circular motion of the trunk shaker and tree. This design was used in conjunction with a tri-clamp to effectively transmit forces with minimal bark damage. Fruit removal is a function of stroke and frequency and is also influenced by pattern. Inertial shaker stroke can be approximated by (Adrian and Fridley, 1965):

$$S = 2*m*r/(M_{shaker} + M_{limb})$$

S = Peak to peak stroke
m = Eccentric mass of shaker
r = Eccentricity of shaker
M_{shaker} = Total mass of shaker
M_{limb} = Total mass of limb = 0.2 kg/mm diameter for limbs
= 2.0 kg/mm diameter for trunks

The development of the trunk shakers throughout the 1960's saw larger power units transmitting larger forces. Unrecognized at the time, the general design of some shakers inherently induced tree damage. Torques generated by counter-rotating masses induced twisting effects at the pad which must be absorbed as friction at the tree bark.

Redesigned clamps and pads were necessary to fit the trunk diameters and allow the bark to survive the increased

stresses (radial, tangential, longitudinal) imposed on the trunk. Clamp design (Burke, 1951; Gould, 1962; Gould, 1964; Gerrans, 1968; Gerrans, 1971), pad design (Gerrans, 1966), pad lubrication (McEwen, 1965), increased pad contact area and reduced clamping forces (Edgemond, 1967) have all been means by which researchers have attempted to reduce shear and torque transmitted to the tree.

The first tri-clamp pad design was patented in 1969 by L. B. Overstreet. Three pads comprised the clamp, grasping the tree approximately 120^{o} apart, via one fixed arm and two hinged arms; the tri-clamp made for better grip and less slip within the clamp system. A tri-clamp design by Friday (1981) incorporates a single hydraulically-driven rotating mass in each of two arms. These arms pivot about the trunk so two pads make contact at approximately 120^{o} and 240^{o} from the approach angle, and combine with a third stationary pad at 0^{o}. The forcing vectors developed by the masses are thus nearly in-line with the tree, although torque may still be a problem.

To study relative levels of bark damage, two shakers were utilized by Hedden et al. (1984) to harvest Valencia and Hamlin oranges. One shaker provided linear motion, the other multidirectional motion. Minimal bark damage was observed in all tests, even for growing Valencia orange trees when clamping 16.2 cm (6.4 in.) average diameter trunks at 640 kPa (93 psi) average contact pressure for the linear shaker and 1215 kPa (176 psi) for the

multidirectional shaker.

No obvious trunk damage was apparent when Millier et al. (1983) tried a recoil impact shaker for apple harvest. The linear impact shaker performed better on Y-shaped trees than did a multidirectional shaker on limbs parallel to the applied force. Violent action was needed to remove fruit on limbs perpendicular to the applied force.

With the advent of mechanical harvesting, tree crops frequently needed pruning or retraining to make the operations efficient. Tree modification could increase the speed of harvesting, promote uniform maturity, improve recovery, decrease product and plant damage and improve overall economics (Brown, 1980). Often new harvester designs were based on a particular tree-orchard pruning configuration, particularly when continuous harvester designs were being investigated.

Conventional low density orchards (75 - 200 trees/ha) are presently harvested at acceptable rates with stop-and-go shaker harvester systems (Tennes and Brown, 1981). Trunk shakers with self propelled catching frames harvest 60 - 120 cherry trees per h. High density orchards (200 - 400 trees/ha), however, may have lower yield per tree and therefore necessitate higher speeds for equivalent volumetric harvest rates. As a result, various continuous harvesters for tree crops have been designed.

Tennes and Burton (1977) developed a sway-bar shaker for continuous harvest of tree crops consisting of a pair of

equi-spaced horizontal bars pivoted at the front end and powered by two synchronized rotating eccentric masses at the back end. A roller assembly mounted along each bar formed a free wheeling contact surface for tree trunks. Tennes and Brown (1980) expanded upon this design such that the oscillating sway-bars were combined with a pendulum system for absorbing vibrations otherwise transmitted to the power frame. Bark damage was still a problem, however, as the harvester moved 3 - 6 cm (1 - 2 in.) during each cycle of the sway bar, causing probable shearing impact on the bark as discussed by Fridley et al. (1970).

Peterson and Monroe (1973,1974) developed an automatic sequencing continuous over-the-row trunk shaker harvester. Harvest rates were increased 100% on a time basis, reaching 200 trees/h. In 1985, Peterson et al. combined a recoil impact shaker with an over-the-row sequencing harvester frame to provide continuous detachment of apple fruits without some of the apple damage and bark damage problems associated with compact high-power inertial trunk shakers.

Continuous over-the-row tree harvesters with two eccentric masses on separate shafts using a scissors type grasping unit have also been developed by Peters (1980). Orlando and Fitzmaurice (1981) built an over-the-row harvester with a vertical scissors-type clamp suspended from the top of the frame and shaken by a non-positive oscillatory eccentric pair of masses at the upper end of the frame. The entire assembly was pivoted by a single axis to

alternately impact opposite sides of the trunk.

Gebendinger (1973) created a three mass shaking unit with all three masses concentric on the same shaft to prevent twisting of the shaker axis. This effectively was a two-mass shaker however, as the top and bottom masses rotated synchronously and were each half the weight of the middle mass. Westergaard et al. (1983) discuss a true three-mass concentric shaft design where the three eccentric masses would be driven by various combinations of motors and sheaves to impart a plurality of distinct shaking patterns to a tree trunk or limb. Tempkins (1973) developed a scissors type shaker head pivotally coupled to the distal end of a transportable boom and having two counter-rotating masses on a common axis, driven at different angular velocities by a twisted V-belt; this could develop a 360^{o} progression of the shaking force vector.

Variable amplitude shakers have been developed to change the shaking characteristics of the tree, sometimes even while running. These often consist of adjustable eccentrics with pitman arms (Harrett, 1963). Fridley (1970) developed a mechanism to create any desired shaking pattern by having a variable offset mass on a common shaft with a fixed offset mass, chain-linked for a fixed phase relationship. Gould and Richter (1971) used hollow cylindrical shells to vary eccentricity by varying the amount of flowable heavy matter (such as BB's, lead shot, etc.) in the cylinder. Because the amount of unbalance depended on movement of the material

in the shell, the moment of inertia was a function of the shell's rotational velocity during operation. Hood et al. (1979) created a unique scissors-type trunk shaker by using eccentric masses mounted on sun gears which "walked" around the inside of planet gears. As the eccentricity of the mass was capable of being offset by the offset of the "walking" sungear shaft, various shake patterns were realizable.

Brown and Perkins (1967) used a light weight, hand-carried hydraulically powered eccentric mass C-clamp vibrator for successful and complete fruit removal from date palm bunches with a 3 s shake.

Tree fruit harvester mechanization improvements over the past 25 years have reduced 65 man-h of hand picking per hectare down to 4 and 8 man-h per hectare for mechanized harvest of tart and sweet cherries, respectively. Improvements in tree shaking and other fruit removal methods will undoubtedly continue as technology advances in sensors, controls and actuators.

2.2 Root Damage

Bukovac (1983) suggested that shaking with "unnecessary force" may result in "breaking of roots, interfering with conduction systems and doing other harm which is not so apparent". The use of plant growth regulators which would loosen fruit and increase removal rate may prevent an operator from shaking extra hard and long, thereby stressing the tree and causing premature orchard death.

Early experiments by Levin et al. (1960), however, found no adverse affects on cherry root systems when limb shaking to harvest fruit. Halderson (1966) also found that root movement during trunk shaker harvesting ceased approximately 15.2 cm (6 in.) below the soil surface and did not appear to cause root or tree decline.

Beljakov et al. (1979) found no adverse effect on tree growth either with only an insignificant number of roots severed (less that 0.05% of the roots by weight of diameter 0.1 cm (0.04 in.) or smaller) when sweet and sour cherries, peaches and plums were trunk shaken. An eccentric mass trunk shaker clamped 20 cm (7.9 in.) above the ground operating at 15 - 18 Hz with 2.4 - 3.0 cm (1.0 - 1.2 in.) strokes was used.

Lyons and Yoder (1981) found that 7.6 - 12.7 cm (3 - 5 in.) diameter peach trunks which were poorly anchored had deeper crown roots and were susceptible to breakage by wind and shaking.

More recently, however, Brown et al. (1984), in attempts to find a nondestructive, convenient method of detecting hidden bark damage, suggest that increased ethylene production found in samples taken beneath trunk shaken cherry trees may result from injury to the root system, though this has not yet been verified. The question of root damage from mechanical harvesting and its effect on tree decline is still under inquiry.

2.3 Tree Injury - Prelude

Tree damage generally occurs in three different forms: 1) damage to the bark at the point of shaker attachment, 2) breakage of large stiff limbs, and 3) breakage of small branches or detachment of leaves and other new, young growth (Cargill et al., 1982). The authors list 19 possible factors that can result in bark damage, much of which can be serious.

Breakage of large limbs generally results from excessive stroke length, shaking at a natural frequency or shaking for a long period of time. Weak, grafted or low-crotched trees are most susceptible. Breakage of small limbs results from high frequency vibration. Long periods of shake are likely to magnify the damage.

Bark damage normally occurs as a total stripping of the bark from limbs or trunk or as a separation of the bark from the cambium (Brown et al., 1982). The latter can seldom be detected except by trained personnel. Tapping of the bark for presence of a hollow sound is one method used to detect internal damage; other more sophisticated methods of detecting hidden bark damage have also been investigated (Brown et al., 1984). Neglected bark damage combined with adverse winter weather, insect and disease attack, poor nutrient supply from the soil, improper use of growth regulators or poor irrigation practices can cause rapid orchard decline. Diener et al. (1968) found that the amount of bark damage accumulated by a limb or trunk is determined

by the bark properties, the radius of the limb or trunk, and the resistive forces of the shaken object.

Preventing bark damage is of prime importance with today's harvester which clamps to a tree trunk. Ironically, Sturos and Erickson (1977) of the USDA Forest Service use a compression debarking device consisting of two stiff rollers which squeeze wood samples in order to intentionally separate the bark. The adverse effect of poor tree clamping mechanisms on bark damage has reinforced concern over what is happening in Michigan orchards.

2.4 Tree Vibration

Fruit detachment is the prime objective in shake-harvesting. Much work has been done to study fruit detachment. When shaking is used for fruit detachment, efficiency depends on the pull force required to remove the fruit (the lower the better), the fruit mass (the higher the better), the location of the fruit on the tree structure, and the stem length (the shorter the better). For example, pull force for Windsor sweet cherries never gets as low as that for Schmidt's sweet cherries while Windsor cherries seldom get as large as Schmidt's; thus Windsors are more difficult to shake harvest.

Since mechanical shakers are attached to the tree trunk or limb, factors like the limb's natural frequency, efficiency in transmitting vibration, damping effect of the leaves, damping effect of the fruit, mass of the limb and direction of vibration are important. With inertia shakers,

the mass of the shaker and its parts must also be considered. Adrian and Fridley (1958) concluded that the four variables affecting fruit removal were: 1) the frequency of shake, 2) the length of the stroke, 3) the force/weight ratio required to remove the fruit, and 4) the number of limber fruit bearing hangers in the tree.

Cooke and Rand (1969) describe the three important modes of vibration for a fruit (Figure 2.2). Instability and fruit-stem resonance have been important in creating high stress for fruit detachment. However, limb characteristics are very important in successful vibration transmissibility (Fridley and Yung, 1975).

Coffee, cherries and macadamia nuts are easily removed because the stiff tree structure allows excitation of resonant frequencies at the fruit-stem interface. Olives, however, are more difficult to remove because the flexible stem and branch act as vibration absorbers, isolating the fruit from the excitation.

At low frequencies, fruit tends to detach by failure of the stem or branch near the fruit, leaving a variable length stem or branch attached to the removed fruit. The stem may also be pulled or broken from the fruit causing a stem-tear or similar damage at the area of stem attachment. At high frequencies, the inertia of the fruit causes it to remain stationary and stem failure normally occurs at an abscission layer between the stem and fruit or the stem and branch. In the cherry industry, excitation of the pendulum mode (low

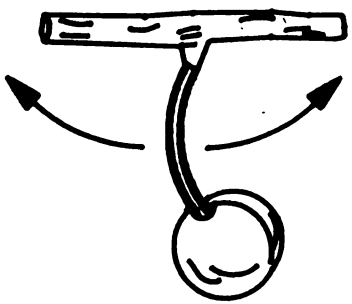

Pendulum mode

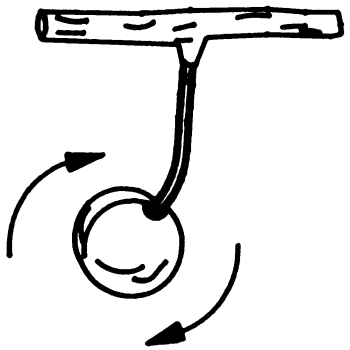

Tilting mode

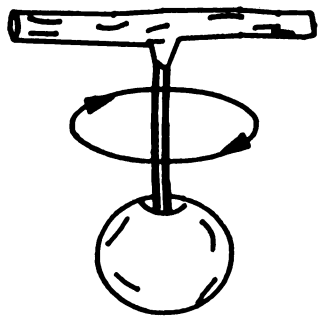

Twisting mode

Figure 2.2 The three modes of oscillation of a fruit (Cooke and Rand, 1969).

frequency) provides sweet cherries with stems for maraschinos and fresh market, excitation of the tilting mode (higher frequencies) provides stemless cherries for processing.

High frequencies (25 - 40 Hz) and short strokes (20 - 25 mm, 0.8-1.0 in.) have been proven most effective at fruit removal when the tree structure and fruit attachment are relatively rigid (O'Brien et al., 1983). Low frequencies (1.5 - 6.0 Hz) and long strokes (100 - 125 mm, 4.0-5.0 in.) have been found superior for long branched and willowy trees that hang down under the load of the fruit (Table 2.1).

Kronenberg (1964) found the detachment force of fruit to decrease as the fruit ripened. The difference between the force 10 days before harvest and that on the traditional picking day varied according to the equation:

$$Y = -48 \cdot X + 428$$

Where: X = 9 - Number of days before harvest
Y = Detachment force, g

Ripe cherries detached without stems whereas unripe cherries detached with stem.

Discovery of satisfactory frequency and stroke for fruit removal has provided researchers with the following empirical means by which to estimate fruit removal for cherries, prunes, olives and macadamia nuts (Markwardt et al., 1964; Halderson, 1966; Fridley and Adrian, 1960, 1966; Fridley et al., 1971; Peterson et al., 1972):

$$\text{Percent Removal} = 100 \cdot (1 - \exp(-k s^{a} \omega^{b}))$$

Table 2.1 Tree characterization and tree shaker inputs for several tree fruits (O'Brien et. al., 1983).

Crop	Tree Character	Shaker Utilized	Typical Input to Tree: Frequency (Hz)	Typical Input to Tree: Stroke (mm)
Apricots	1	Trunk	15-30	12-8
		Limb	10-20	40-25
Almonds	1	Limb	15-20	40-25
		Trunk[2]	15-25	12-8
Apples	2	Limb	10-20	40-35
		Trunk	15-25	12-8
Prunes	2	Trunk	15-25	14-10
		Limb	10-20	40-25
Walnuts	3	Limb	7-16	50-30
		Trunk[2]	15-20	14-10
Pecans	3	Limb	10-16	50-35
		Trunk[2]	15-20	14-10
Peaches	3	Trunk	15-25	16-12
Red Tart Cherries	3	Limb	10-15	40-30
		Trunk[3]	10-24	40-20
Sweet Cherries	4	Limb	10-20	60-35
		Trunk[2]	12-24	16-12
Olives	5	Limb	20-35	75-50
Oranges	5	Limb	1.6-6	125-100
		Trunk	10-15	16-12

[1] A rating of 1 indicates a stiff tree structure and fruit stem; 5 indicates willowy structure and long flexible stem.
[2] In large trees, multidirectional trunk-type shakers are mounted on booms and used to shake major scaffold branches.
[3] Source: Bruhn, 1969.

Where: Constants a, b, and k have been tabulated
s = Stroke delivered to the limb, mm
ω = Shaking frequency, Hz

Unfortunately, however, increasing either stroke or frequency does not necessarily increase fruit removal since

increasing the frequency may decrease the stroke or the effective vibration transmission through the limbs to the fruit stem (Fridley and Adrian, 1966; Fridley et al., 1971). In fact, Diener et al. (1969) found limb transmission efficiencies (ratio of end of limb stroke to shaker stroke) ranging from 25-130%.

Direction of shake influences removal of fruits and has had a significant role in shaker design. McLaughlin et al. (1976) found that vertical shaking on apple limbs removed 16% more fruit than horizontal shaking for a 1 s period. Lenker and Hedden (1968) used a variable stroke, variable frequency FMC hydraulic cylinder (square wave) inertia shaker and a crank-type inertia shaker to harvest Pineapple and Valencia oranges. They found that more fruit in Pineapple oranges were removed with smooth limb shaking action than with the square wave.

Shaking patterns can be present on some machines; on others there is an undefined continuous change of motion either by design or from the operator's controls. Shaking frequency and shaking force are related by the square of the frequency. Increasing the frequency on any shaking pattern requires more power. This frequency increase requires both higher hydraulic system flow rate and pressure, resulting in excessive clamping pressure between the pad and bark on machines where the shaking and clamping circuits are interconnected. Force transmission of most shaking patterns can also cause excessive radial stress, tangential stress or

longitudinal stress on the bark due to reactive forces at the clamp.

Direction of shake has more influence on fruit damage than on fruit removal. Pellerin et al. (1979) state that minimum damage occurs when fruit is removed by several short bursts rather than longer, more intense shaking. Fruit tend to move very little before detaching and falling straight down when shaking by impact shakers (Upadhyaya et al., 1981a).

Fruit detachment is complicated by the existence of combined tension, bending and shear stresses at the stem (Alper and Foux, 1976). As the angle at which tension is applied increases, bending and shear stresses on the stem increase while tension stress decreases. Desired shaking characteristics (frequency, stroke, direction) to get the proper stress combination for removal of a particular fruit are difficult to optimize due to the vibration transmissibility. Fruit remaining attached to trees after shaking are commonly hanging on limber fruiting branches near the tree surface.

Fridley and Adrian (1960) conducted studies to determine the power and optimal frequency of vibration of prune trees such that fruit removal was high but fruit and tree damage was avoided. Vibrations at the natural frequency of the fruit, which would be the most efficient in terms of power, were difficult to transmit through the branched tree structure because of the damping by leaves and

the collision of limbs. Vibrations at the natural frequency of a limb caused both limb and fruit damage. Attempts to vibrate prune tree limbs at the natural frequency indicated that selection of the proper natural frequency was dependent on the stroke required to remove the fruit at that frequency, the power required and the resulting tree and fruit damage (Fridley and Adrian, 1960). As expected, minimum force and power were needed to vibrate a tree when clamping was at an anti-node and shaking speed was at a natural frequency. Less power was needed with longer strokes and lower frequencies. Tree and fruit damage tended to increase as stroke or frequency increased, although the stroke effect was more predominant.

Alper et al. (1976) studied the effect of frequency and the point-of-force application on resultant amplitudes at the points of fruit suspension and at the zone of force application on orange trees. Vibration amplitudes in a shaken branch at points of fruit suspension were found to increase as the force application point was moved further from the main branching point. Vibration amplitudes at points of fruit suspension remained the same with and without attached fruit. With multidirectional trunk shakers, Berlage and Willmorth (1974) found that the nodes and antinodes of a vibrating limb move along the limb as frequencies change, thus preventing dead spots with zero displacement.

Halderson (1966) found the first resonant frequency of

a vibrating tart cherry tree to be very low (e.g. 50 c/min). Bruhn (1969) found that, except at very low values, changing applied frequency and amplitude had little effect on cherry fruit removal unless the combination resulted in a change in acceleration. Accelerations in the outer fruiting zone of the tree exceeded those applied to a trunk or limb base in all cases. These conclusions were confirmed by Tennes and Brown (1981) in over-the-row apple harvesting tests with a sway bar shaker.

The response of each individual tree to vibration and damage is different, and can vary from orchard to orchard as well. The force and power required to shake trees varies with stroke and frequency of shake, type of shaker, position of tree attachment, limb or trunk size and tree species (Fridley and Adrian, 1966). As expected, force was found to be proportional to the stroke and to the square of the frequency. Power was proportional to the square of the stroke and the cube of the frequency. Power for increasing trunk displacement was proportional to the square of the ratio of the increased displacement to the original displacement (Cargill et al., 1982). Limb shakers operating with hydraulic motors typically average 8 kW (11 Hp) while trunk shakers require 30 to 40 kW (40 - 54 Hp) (O'Brien et al., 1983).

Hoag et al. (1971) studied the damping properties of almond tree limbs. They found a log decrement of 0.0667 to 0.1015 when limb moisture content was near the saturation

point of fiber (30%). External damping due to limbs moving through the air was nonlinear and proportional to the velocity squared. Air drag on vibrating olive tree limbs could be described by a constant drag coefficient of 1.5; the leaf area turned out to be important. With leaves removed, external damping was negligible unless limb velocities were very high.

2.5 Shaker Clamps

The most likely point of tree injury is at the point of shaker attachment. Here, longitudinal, tangential and radial forces from epicyclic pattern trunk shakers are transmitted through a pad which must act as a cushion, damper and spring. The pad must be firm enough to conduct vibrational energy so that excessive stresses are not imposed on the bark yet conform to the trunk such that the pad does not slip. If pad contact area is too small or clamping pressure too low, observable scarring of the bark or excessive shear stress may result, observable as a slipping action (tangential or longitudinal) or beating action (radial). On the other hand, excessive clamping pressure can crush or split the bark. Excessive clamping pressure also stiffens pads (smaller pad deflection per force increment), reduces internal pad flex, and reduces belt-system slip but a very stiff pad system can generate large peak contact pressures and large torques during shaking.

Brown et al. (1982) found peak pressures between the C-clamp pad and the bark of 2345 kPa (340 psi), 3450 kPa (500 psi) and 4140 kPa (600 psi) on an 11 cm (4.5 in.) diameter trunk when clamping at manufacturer's recommended pressures. Results indicated that all current commercially utilized pads developed pressures that exceeded the suggested limit when clamped at the manufacturers recommended circuit pressure. Reducing circuit pressure to limit peak pad contact pressure was not possible on some pad designs because tree contact area became insufficient. Contact area on limbs of 50-165 mm (2.0-6.5 in.) diameter ranged from 5000-25000 mm^2 (8-39 $in.^2$) per pad for pads that were acceptable relative to peak pressure and shake transmission. Frahm et al. (1983) suggested 2070 kPa (300 psi) as an ultimate bark pressure under a pad since the average ultimate compressive strength of tree bark was found to be 2415 kPa (350 psi) on sour cherry trees and 1035 kPa (150 psi) on sweet cherry trees. Zero compressive failure is preferred under shaker pads but a practical limit of 15% of the pad area is stated as reasonable without necessitating pad redesign (Brown et al., 1986).

Bark injury is usually caused by excessive tangential or radial stresses at the cambium under the clamp (Fridley and Adrian, 1966). The stresses at which the cambium is damaged increase with age, decrease with cell turgidity and increase from spring to fall (Fridley et al., 1970). Cambial failure from compressive stress (radial) was

initiated at lower pressure on sweet cherries (1000 kPa, 145 psi) than on tart cherries (2310 kPa, 335 psi). Shear strength ranged from 350-700 kPa (50-100 psi) and should be assumed to be the lower value of 300 (43 psi) to eliminate shear damage. Bark strain at failure ranged between 4.5° and 11.6° and should be limited to 5° for design purposes (Brown et al., 1982). Bark damage is also more likely to occur during morning operation since the trees experience diurnal moisture fluctuations, having greater moisture in the cambium during the morning (Burton et al., 1986).

Early padding in shaker experiments consisted of cloth, belting or rubber wrapped around a tree attachment point when clamping circuit pressure was 8280 kPa (1200 psi) (Levin et al., 1960). Pads have been formed as hollow tubes, bags filled with sand or ground nutshells (Martin, 1968; Brandt, 1967), solid rubber pads with small holes drilled parallel to the tree trunk axis (Kilby, 1972), preformed clamp jaws and rubber pads, belting mounted on spring and universal joint assemblies (Brandt, 1964) and other conforming materials (Brandt, 1985). Adrian and Fridley (1963) suggested pads in the form of sacks filled with magnetic particles and oil or viscous fluid. Flat belts on parallel rollers and bolts placed in trees were also investigated. Pool and Steingas (1969) employed "bouncing putty", a non-Newtonian silicone fluid, on their shaker head to conform to tree shape and prevent bark damage during force transmission. Pool (1971) filled airtight

pouches with a combination of silicone putty, tire carcass discs and air to clamp to the tree. Savage (1971) took another approach and used a hydraulically manipulated chain to clamp firmly around the tree to prevent slip during shake. Most manufacturers now place a flap over the clamp pad with lubrication between to provide a slip surface, thereby limiting shear stresses during cherry harvesting.

Affeldt et al. (1984) observed a shaker pad relaxation effect, a change in contact pressure distribution of the pad around the tree after a settling time. Settling time may complicate the ability to maintain adequate contact force for vibration transmission.

The Friday Tractor Company (1982) utilized a commercial "tri-clamp" composed of three pads 120^{o} apart which completely surrounded the tree. An eccentric mass on each side of the shaker was centered in-line with the tree. This design is claimed to prevent slip between the bark and pads and to direct all forces to the center of the trunk to minimize torque on the bark.

Research by Burton et al. (1986) indicated, however, that after four years of mechanical harvesting, 58% of the trunks in a 9 year-old tart cherry orchard had moderate-to-severe trunk damage regardless of whether the Friday tri-clamp system or experimental reduced pressure pad systems were used to clamp to the trees. A low-pressure scissors-clamp kit was developed in 1985 for further testing for trunk damage control. In 1986, this kit resulted in almost

zero damage on 6.5 cm (2.6 in.) diameter trunks, whereas the tri-clamp severely damaged 20% to 90% of the trunks. The low-pressure kit appears to eliminate the damage experienced with previous clamp systems (Brown, 1986).

Timm (1986) compared three beltings and five lubricants to study the static and dynamic friction properties and their relation to bark damage. Static and dynamic friction forces were greater for neoprene-lubricant combinations than for either polyurethane or nitrile-lubrication combinations. Polyurethane belting had a lower nominal intermittent operating temperature compared with nitrile, and delaminated under high clamping pressure and long shaking periods. Silicone spray was a better lubricant than Modoc oil, light bearing grease, food grade grease or Crisco shortening due to its tenacity, easy application, easy cleanup, low friction, and minimal heat and dirt buildup. Furthermore, the nitrile belting combined with the silicone spray lubricant was found by researchers and growers to produce minimal visible bark damage.

The optimal clamp pad system should have adequate contact area to limit peak radial pressures, exert only radial forces upon the tree (to eliminate tangential and longitudinal bark stresses) and efficiently transmit shaking motion from the shaker to the tree. A properly designed pad can minimize bark damage due to peak pressures. Even the best pad, however, will not eliminate tree damage caused by improper operation, thus highlighting the need for both good

design and good operator training.

Some designs have come about as alternatives to clamping the tree with pads. Adrian et al. (1965) attempted to reduce shaker clamp injury to fruit and nut trees by using permanent style installed fasteners in trees for shaker attachment; the idea was to transmit shake force directly to the structural wood. Fasteners included lag screws, eye hooks and nut and bolt arrangements. Shaking force transmission was adequate to remove fruit but problems with initial installation, screws pulling out, screws bending, tree gumming, structural failure and decay offset any advantages. Coblentz (1973) developed several types of permanent tree frames and fasteners to which the shaker could be attached each season for fruit removal by shaking. These included frames bolted to a group of limbs, eyehooks bolted to individual tree limbs, spring loaded C-clamps and multiconnector C-clamp hardware.

2.6 Modeling

Experimental study has provided a basic understanding of the forced vibration of fruit trees but details required by engineers to design shakers or by growers to make optimum use of shakers are difficult to obtain experimentally. Therefore, many researchers have attempted to model the shaker and a typical tree utilizing various mathematical analysis methods. Alper et al. (1976) found good correlation when modeling dynamic forces and displacements of a shaken fruit suspension twig. Optimal removal of fruit

occurred at 10 Hz (600 c/min) with a 30 mm (1.2 in.) stroke using minimum power.

Phillips et al. (1970) used finite element analysis to study a branched system consisting of a straight primary limb with straight lateral branches all having viscous, proportional damping. Hoag et al. (1970) also used finite element analysis for a branched system where the elements could be arranged to create curved branches. A Rayleigh-Ritz procedure was used to find the undamped mode shapes and natural frequencies. Hutchinson et al. (1970) found that nonlinear damping gave better predictions than linear or viscous damping. Most of these methods used lumped mass systems.

Cooke and Rand (1969) developed a linearized three degree-of-freedom model of a fruit-stem system excited by sinusoidal periodic horizontal and vertical planar displacements. Dynamic instability and modal shapes were inferred from the coupled nonhomogeneous Hill's equations allowing prediction of frequency conditions for fruit separation or detachment with, or without, the stem attached. Results indicated that the greatest dynamic instability of the fruit occurred at a drive frequency twice the natural frequency when the upper stem underwent small, planar elliptical displacements.

Ghate and Rohrbach (1980) used a transfer matrix technique with lumped parameters to account for the generalized structural geometry and interdependence of

bending, longitudinal and torsional vibrations when solving for vibrational characteristics of a continuous structure having a rigidly fixed base, a fork with two branches, and an arbitrary geometric configuration. The model accurately predicted response of an aluminum forked structure and was subsequently applied to blueberry cane vibrations.

Yung and Fridley (1975) used finite element analysis and a consistent mass matrix (mass not lumped) to model coffee and olive trees bearing fruit. Their model used truncated conical segments which formed a trunk and two branches supporting fruits. Natural frequencies, mode shapes, dynamic internal stress, and vibration response of the complete tree structure correlated well with the steady-state forced vibration of a similar steel model.

Moini et al. (1980) also used a consistent mass finite element model to simulate cone harvesting in the forest industry, modeling the limbs and branches as truncated conical beams and the fruit as short circular beams with concentrated masses at the end. Leaves and twigs were treated as distributed loads along corresponding elements.

Analytical studies of tree vibration have supported the concept of shaking at several frequencies to develop a multitude of vibrations throughout the tree, as the structural variation from tree-to-tree has not permitted the designation of any one optimum frequency or range of frequencies for shaking (Liang et al., 1971; Hussain et al., 1975). Analysis shows the waveshape is important: high

frequency components account for more fruit detachment and potentially more damage to the bark.

Transient analysis using finite elements has been conducted for impact shakers with good correlation between experimental and analytical results (Upadhyaya et al., 1981a; Upadhyaya and Cooke, 1981b).

Upadhyaya and Cooke (1981) used a finite element model to study the transient response of a limb impacted on its underside at 90° to its vertical inclination. They found that impacting the limb transversely was superior to impacting the limb in any other direction. The optimal direction for branch inclination in Y-shaped open center trees was 45°-60° from horizontal for a transverse impact from below. The percent of harvested apples having a stem pull (rather than an intact stem or stem and spur) was dependent on stem-spur angle of attachment, spur-limb angle of attachment, impact direction, and stem physical properties.

Upadhyaya et al. (1981c) were able to show that a simple one-degree-of-freedom model adequately represented the impact response of a tree and concluded that physical properties relevant to design of impact harvest equipment (dynamic mass, damping coefficient, spring stiffness and Young's modulus) could be obtained from a pendulum test. The mechanical energy loss may be as high as 40-50% and must be accounted for when attempting to impact harvest tree fruits.

2.7 Tree Injury - Bark

Cherry bark consists of a thin, nonliving outer periderm, a large, spongy, nonfunctioning phloem in the center and a thin, functioning phloem next to the cambium. Phloem cells have their long axis in a longitudinal (vertical on the trunk) direction, whereas periderm cells have their long axis in the tangential (horizontal on the trunk) direction. This gives cherry bark its characteristic greater strength in the longitudinal direction. The periderm consists of dead cells encrusted with waxes; the waxes lubricate the tissue allowing slippage between cells (Esau, 1965). The periderm on cherry trees is elastic and can hide compression damage to the phloem, xylem and cambium for several weeks.

When cells are crushed, cell liquids are freed and small cracks usually occur in phloem (bark) tissue. Damaged bark often separates from the wood (xylem) interrupting the flow of vital nutrients. Hairline cracks in the bark tissue form, then air enters and oxidizes cambial tissues turning them brown quite rapidly (Adrian and Fridley, 1963; Adrian et al., 1965). Insects and disease, can then enter and infect the damaged tissue, slowly spreading to healthy tissue and causing tree death. Devay et al. (1960) describe the canker attack as a depression in the infected tissues, accompanied by the production on an orange frothy gum. Pseudomonas syringae, a serious bacterial canker disease of stone fruits in Michigan, is almost identical to C.

fimbriata, except that it is active only when the tree is dormant and early in the spring months; at other times it is inactive (Devay et al., 1960). P. syringae is normally more infectious to young trees (4 to 8 years old), and is rarely found in the older orchards.

Live canker fungi spread rapidly as soil moisture and insect activity increase. The first few weeks after irrigation in an orchard is the time when fungus development is most pronounced. Continued trunk shaker damage to the tree base can spread spores and mycelial fragments of diseased tissue to healthy trees, causing tree death within a few years.

The strength of fruit tree bark has been studied by researchers trying to develop design parameters for mechanical harvest systems (Table 2.2). Fridley et al. (1970) found the bark strength of prune, peach, apricot, almond and olive trees to be directly related to seasonal factors such as moisture content and cambial activity. When the moisture and cambial activity are high, the bark strength is low and the bark "slips" easily. "Slip" is the separation of the bark from the wood at the cambial zone (Cargill et al., 1982).

Diener et al. (1968) found the periderm strength of cherry bark to be highest in the tangential direction perpendicular to the vertical axis of the tree. Phloem strength was greatest in the longitudinal direction, parallel to the long axis of its cells and weakest in the

Table 2.2 Comparison of radial stress causing browning at cambium and tangential stress causing bark failure for various species and varieties (Cargill et. al., 1982).

Crop and Variety	Radial Stress (kPa)	Tangential Stress (kPa)
Apricots, Tilton[1]	5500-6200	1720-1830
Apricots, Blenheim[1]	5500-6200	1480-1690
Peaches, Dixon	4830-5500	1380-1590
Almonds, Non Pariel	3800-4140	
Almonds, Peerless	3800-4140	
Prunes, French[1]	4140-5170	1000-1210
Prunes, French	4830-6210	1310-1720
Olives	3450-4140	960-1100
Cherries, Tart[2]	2410	550-690
Cherries, Sweet[2]	1030	410-480

[1] Trees approximately 6 years old; other trees tested were mature.
[2] Source: Brown et. al, 1982; trees approximately 4 years old.

tangential direction. The periderm could elongate five-to-six times that of the phloem in the tangential elongation before rupture. These facts indicate that tangential shear stress or strain from shaker torsion or clamp pressure can cause the phloem underneath to rupture without periderm rupture, thus concealing the hidden damage.

Brown et al. (1982) studied bark failure on sweet cherry and sour cherry. Sweet cherry bark was damaged about twice as easily as tart cherry bark on equal diameter trees. The bark of young cherry trees (up to 8 cm (3 in.) trunk diameter) damaged more easily than the bark of older trees and was more likely on 4-8 year-old trees than on 10-20

year-old trees. Contact pressure limits, subject to moisture content and cambial activity, were accepted as 1035 kPa (150 psi) and 2415 kPa (350 psi) for sweet and sour cherry trees, respectively.

Adrian et al. (1965) found that tangential shear failure in fruit and nut trees always resulted in complete bark failure. Cambial browning was initiated by average dynamic stresses which were only 75% of average static stresses which caused browning. This indicates that acceptable average static clamping pressures may be much too high to prevent tree damage in a dynamic state.

Cherries are harvested earlier in the growing season than most other fruit crops; cambial activity and moisture content are very high and the bark is very susceptible to slip. In addition, variations in use of trickle irrigation, use of growth regulators, location, climate, soil, and production methods may adversely affect bark strength.

2.8 Suggestions for Eradicating Bark Damage

The success of a shake harvesting system depends on factors such as age and structure of the tree, cultural practices, equipment, operator care and supervision. Adjusting the shaker properly, proper pruning of the trees to accommodate the shaker, employing attentive operators, and avoiding canker infected areas on trees were all significant factors in maintaining orchard vitality.

Proper design of shaker pads (Adrian and Fridley,

1963), proper clamping pressure and maintaining perpendicularity at the point of shaker attachment have all been valuable suggestions (Brown et al., 1982).

Prevention and control of Ceratocystis fimbriata canker by avoiding bark injury, shaving away bruised bark tissue, dressing wounds with an appropriate fungicide (Cerano, for example), surgically removing and dressing internal wounds and severing infected limbs or scaffolds have been promoted by Devay et al. (1965). Diseased tissue should be immediately collected and burned.

One of the current odious tasks facing researchers is the nondestructive detection of bark damage. At present, detection of hidden bark damage is possible only through destructive tests that are subjective. Either sections of bark are removed for visual inspection or the tree is cut down and the trunk sectioned for inspection (Brown et al., 1984; Santamour, 1986).

Nondestructive methods of detecting hidden damage have been investigated by Brown et al. (1984); the methods include electrical resistance measurements, infrared thermography, ultrasound spectrum analysis, scanning electron microscopy (SEM), and energy dispersive X-ray spectrophotometry (EDS). None of these methods were both nondestructive and effective in the field. EDS analysis of core samples revealed an accumulation of K and Ca and a decrease in P in damaged tree tissue; the test was somewhat destructive and time consuming.

2.9 Trunk Shape Analysis

Proper training of operators, better designs for clamp pads, safe recommended pressures for clamping, stopping irrigation prior to harvest and checking fruit for maturity level prior to harvest are all means by which recognizable bark damage has been reduced (Brown et al., 1982; Frahm et al., 1983). Bark damage that is not visible may still occur during trunk shaker harvesting. Damage is currently evaluated by assessing the delayed decline symptoms of the tree: loss of yield, bark splitting, insect and disease infestation, dead branching structures, and decay spots.

Many trees never show signs of decline when damage is minor or occurs only once. A young tree can segregate a wounded area from undamaged tissue (Santamour, 1986). First, a chemical barrier is set up to limit the spread of decay, then the cambium develops a decay resistant wall to protect new growth in the wood. Some tree species are more successful than others at this process and individual trees among a species may also vary. Stressful events requiring a healing process draw heavily upon the energy reserves of the tree. If wounded annually for several years, a mature tree can become weak, develop poor growth patterns, and decline in fruit productivity.

Santamour's work indicated that growth rates in the tree may vary within a zone depending upon the degree of recovery undertaken to prevent decay. Therefore, even though the conventional signs of decline may never surface,

the shape of a tree limb or trunk may change within the clamp attachment region during the seasonal growth period.

Because trunk shakers are designed to shake mature trees, most growers have delayed starting mechanical harvesting operations in their new orchards until the tree trunks were at least 13 cm (5 in.) in diameter: about 9 years old. In recent years, however, because of economic incentives and lack of labor, growers have begun to mechanically harvest trees of trunk diameters as small as 5 cm (2 in.) (tree about 4 years old). These young trees are particularly susceptible to trunk damage (Burton et al., 1986). Young trees (3-6 years old) suffering major wounds or a series of lesser wounds may never realize their full production capacity.

Nondestructive continuous measurements of circumferential growth on stems of woody plants utilizing a strain gage dendograph have been conducted by Burger et al. (1982). Light and temperature controlled growth chambers provided the environment for experimental young trees. Data correlated well with young tree growth and could provide a means to estimate the effects of environmental changes in these and other growth factors as a means for following orchard progress.

The shape of a tree trunk, particularly when young, is rather smooth and circular. As age increases, the bark becomes rougher. Tree limbs which are undamaged are still nearly circular to elliptical in older trees and are usually

expressed by an average diameter. Kenworthy (1974) reports that tart cherry trees may exhibit terminal shoot growth from less than 25 cm (10 in.) to more than 46 cm (18 in.) with corresponding changes in shoot girth, depending on tree vigor. The peripheral shape of a trunk would only be a planar number so other means are needed to classify the tree trunk shape and express shape changes over time.

Means to classify trunk shapes that vary between circular and elliptical may be similar to investigations in the literature on microscopic particle size analyses. Classical methods to classify particle shapes are revealed in Table 2.3.

Stockham (1977) demonstrates some of the means by which nonspherical particles can be expressed (Figure 2.3). The most common is the area-projected-diameter: the diameter of a perfect circle with equal area. Martin's diameter is the mean length of a line, parallel to the fixed direction of scan, that divides the particle profile into two equal areas. Ferets' diameter is the mean length between two tangents on opposite sides of the particle profile, perpendicular to the fixed direction of scan. The maximum horizontal intercept is the longest diameter from particle edge to edge in the direction of scan. The perimeter-projected-diameter is the diameter of a perfect circle with the same perimeter.

Hausner (1966) has displayed a set of common general shapes described by an elongation factor X, a bulkiness

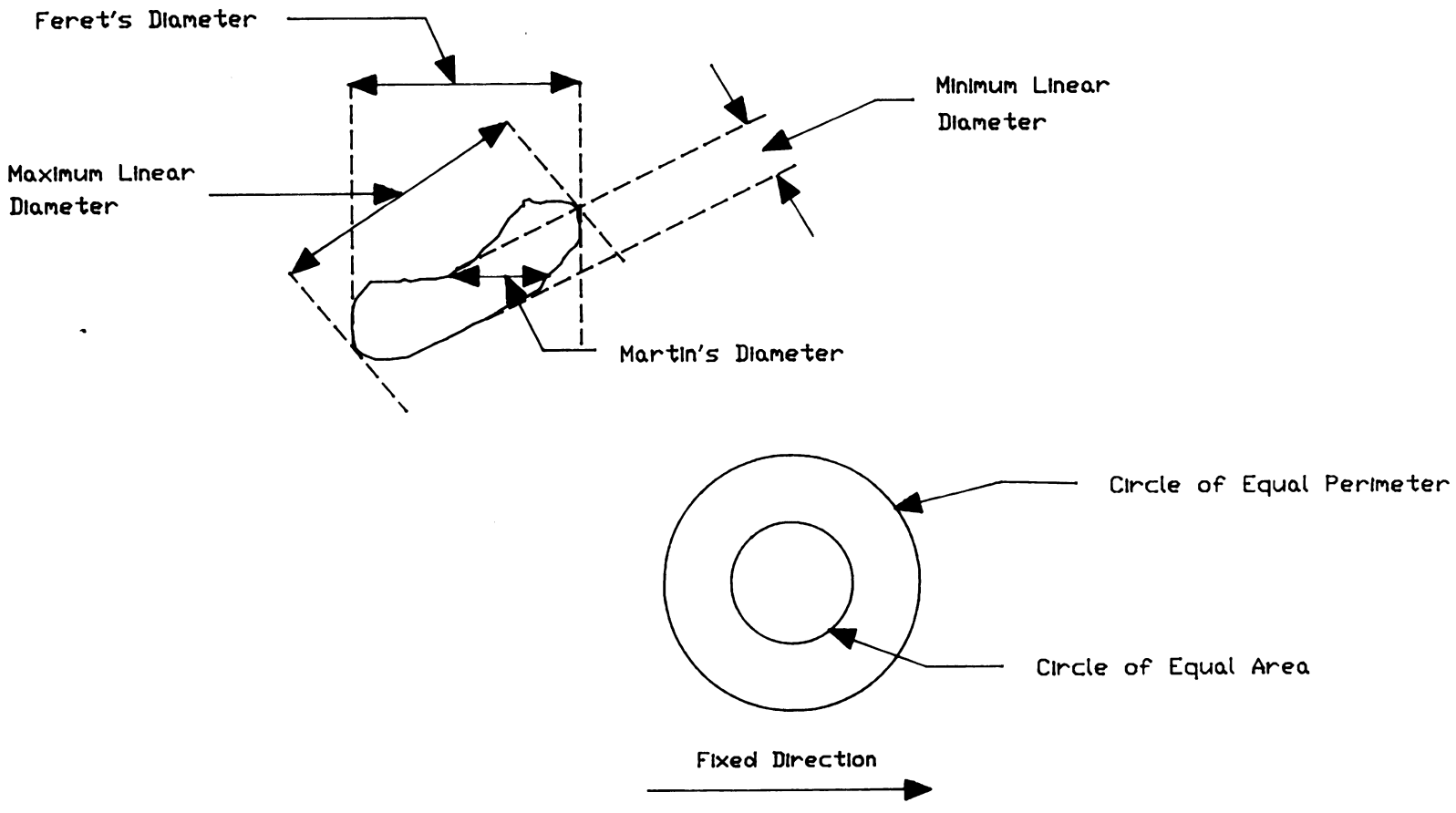

Figure 2.3 Methods of measuring the diameter of non-spherical particles (Stockham, 1977).

Table 2.3 Classical methods of describing particle shape.

Author (Year)	Parameter	Formula
Curray (1951)	Roundness	RD=Object Area/Circle Area
Hausner (1966)	Elongation X	X=Length/Width
	Bulkiness Y	Y=Area/(Length•Width)
	Surface Z	$Z=Perimeter^2/(12•6•Area)$
Graf (1966)	Form Factor	$FF=Area/Perimeter^2$
Duda and Hart (1973)	Thinness Factor	TF=4•π•FF
Segerlind and Weinburg (1973)	Shape by Harmonics	Fourier Transforms
Stockham (1977)	Area Projected Diameter	$D=2•(Object\ Area/\pi)^{0.5}$
	Perimeter Projected Diameter	D=Object Area/π
	Martin's Diameter	D: $A_1 = A_2$ || Scan
	Feret's Diameter	D: Dist. Between Tangents || Scan
	Maximum Horizontal Intercept	D: Maximum D || Scan
Sites and Delwiche (1985)	Invariant Moments	See Reference

factor Y, and a surface factor Z. When X = 1, the particle is equiaxed; when Y = 1 the particle fills the rectangle and when Z = 1, the particle is spherical and smooth. Clarenburg (1966) suggested that the side lengths of a rectangle, a and b, in Hausner's description could be symmetrically reduced

to equal the area 'A' of the particle thus eliminating the need for 'A'. 'Y' would then become unity and thus superfluous.

Curray (1951) described the roundness of an object using the measured projected area and the smallest circumscribing circle. Graf (1966) separated objects based on the 'form factor' which creates a distribution for selected objects such as circles even when triangles and rectangles exist in the same field.

Similarly, Duda and Hart (1973) defined the roundness of near-circular objects by a property known as the thinness ratio 'T', a dimensionless property independent of the object's size, which was used by Parrish and Goksel (1977) in attempts to design an automated robotic harvesting machine for apples. The maximum 'T' value is 1 which occurs for a perfect circle. As the object's shape changes, 'T' decreases.

Segerlind and Weinberg (1973) classified various types of grain kernels using a Fourier series expansion of the radial distance from the two dimensional center of gravity to the grain kernel periphery. The first ten harmonics of each grain kernel shape were calculated and statistically compared. Interspecies discrimination among relatively different kernels resulted in only 1% error but intraspecies discrimination resulted in an error range of 11-25% when utilizing only ten harmonics.

Sites and Delwiche (1985) utilized various vertical,

horizontal and central moments of inertia combined with area and perimeter for feature extraction as the means for locating tree fruit for robotic harvesting. As machine vision becomes more popular, many algorithms will become available for shape analysis of real world objects (Sarkar, 1984).

CHAPTER 3

TRUNK SHAPE ANALYSIS - FOURIER AND CORRELATION

3.1 Tree Trunk Profile Measurement

In 1985, peripheral shape of nine Montmorency cherry trees, located at the Michigan State University Horticultural Research Orchards, were measured for profile analysis. These trees were first trunk shaken in 1983. Circumferal traces of tree trunks were first made in September 1985 before experimental trunk shaker harvesting tests. Successive corresponding measurements were made on the same trees in September 1986.

A perimeter measuring device designed and constructed by the USDA Plant Pathology and Agricultural Engineering teams at Michigan State University was utilized to perform the measurements. The contour tracer (Figure 3.1) consisted of a toroidal aluminum table (a), hinged on one side (b), with a spring loaded clasp opposite (c). The device encircled the tree (d). Three adjustable legs (e) allowed positioning and leveling. A leveling bubble (k) ensured consistent alignment. A sliding pointer (f) mounted on the table's rail border (g) consisted of a teflon pen carrier (h) precisely fitted with an aluminum cam-follower (i) at its head.

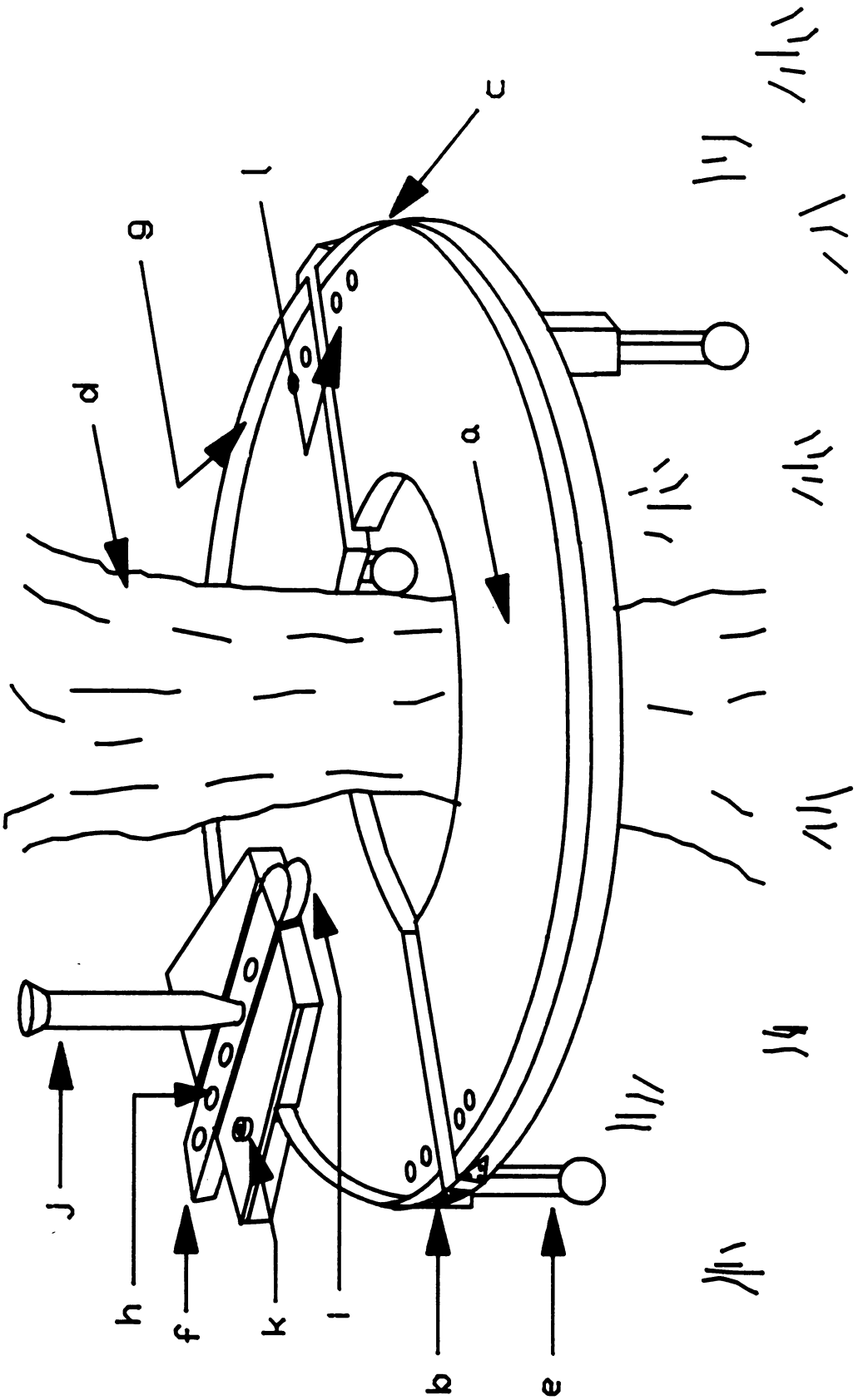

Figure 3.1 Tree trunk profile contour tracer.

The height of shaker clamp attachment at harvest time on each of the nine trees was marked with indelible white tree paint. Each tree was also marked for magnetic north as a reference and alignment point for the following year's measurements.

The contour tracer was centered, leveled, and clamped around each tree at shaker clamp height. A pre-cut, toroidal-shaped piece of paper was aligned on pins (l) on the table and taped onto the contour tracer table. A pen (j) was inserted into the teflon pen carrier (h) until the point made contact with the paper. Light downward pressure was applied to the pen as the follower (f) was moved around 360^{o} of the tree's perimeter to trace the profile of the tree trunk at this height. The largest of the nine sample trees outgrew the contour tracer size and was therefore not measured in 1986.

Each trace was identified by orchard, row and tree number. Magnetic north, as marked on the tree, was also labeled correspondingly on the paper trace. The two halves of the paper trace were then removed from the table, taped together, and stored for later analysis.

Accuracy in following the tree profile was estimated to be ± 1 mm (± 0.04 in.) on smooth trees and ± 2 mm (± 0.08 in.) on rough bark trees due to the width of the pointer tip "filtering" the valleys in rough bark. The cam radius of curvature ($\rho(t)$ = 5 mm, 0.20 in.) was slightly larger than the average radius of curvature of valleys on rough tree

bark ($\rho(t)$ = 2-3 mm, 0.08-0.12 in.). This radius was selected to provide a continuously smooth motion in tracing tree bark. Narrower tipped cams (small radius of curvature) had a tendency to lodge in tree bark abnormalities, thus shifting the burden of accuracy to the operator's dexterity. Repeatability in measurements was approximately ± 1 mm (± 0.04 in.).

Accuracy in realigning the measuring table in 1986 to the magnetic north mark made on the tree in 1985 was estimated to be ± 3^{o}. This was also the repeatability in realignment. Repeatability in vertical alignment was estimated at ± 5 mm (± 0.20 in.).

It should be noted that the accuracy of measurements on some smooth trees decreased in 1986 due to severe damage resulting from intense shaking tests in 1985 which caused the bark to deform. This introduced measurement error of valleys in the bark not previously a factor with smooth bark. Expected overall profile measurement tolerance was found to be ± 2 mm (± 0.08 in.) on rough bark trees, a figure I chose to accept.

In the laboratory, a transparent acetate overlay containing 360 radial lines emanating from the center (1^{o} resolution) provided equally spaced polar coordinates for digitization and analysis of the near-circular tree profiles. Each profile trace was visually centered under the transparent acetate grid and taped onto a Tektronix 4954 Graphics Tablet (1080 mm x 880 mm, 42.5 in. x 35 in.). The

graphics tablet was connected to a Prime 750 Mainframe located in the MSU Engineering Computing Facility via a Tektronix 4014 Graphics Terminal. The points at which each radial line intersected the periphery were digitized starting at north as 0^{o} and proceeding 360^{o} ccw back to north. The first point was redigitized along with one point directly north of the periphery for a total of 362 points. These last two points provided computer identification of magnetic north in the data. Digitized values were put into an IBM AT Personal Computer for disk storage and analysis.

The block diagram for the data preparation phase of the shape analysis project is shown in Figure 3.2. In the calibration phase, digitized data were converted from digitizing tablet coordinates to paper trace measurements via multiplication by a simple ratio. Calibration was then necessary to convert from paper trace measurements into actual tree profile values by adjusting the radial lengths from the profile center to each digitized coordinate to compensate for the constant radial offset of the measuring table's cam follower (Figure 3.3) determined from the equation:

$$\text{Cam Radius (mm)} = (\text{HOLE} - 1) * 25 + 58.5$$

The trace radius for each digitized point was:

$$\text{Radius}_{trace}\ (\text{mm}) = \sqrt{(X_i - X_C)^2 + (Y_i - Y_C)^2}$$

$$\text{for } i = 1,2,\ldots 360$$

Where:

$$X_C = X_{center}$$
$$Y_C = Y_{center}$$

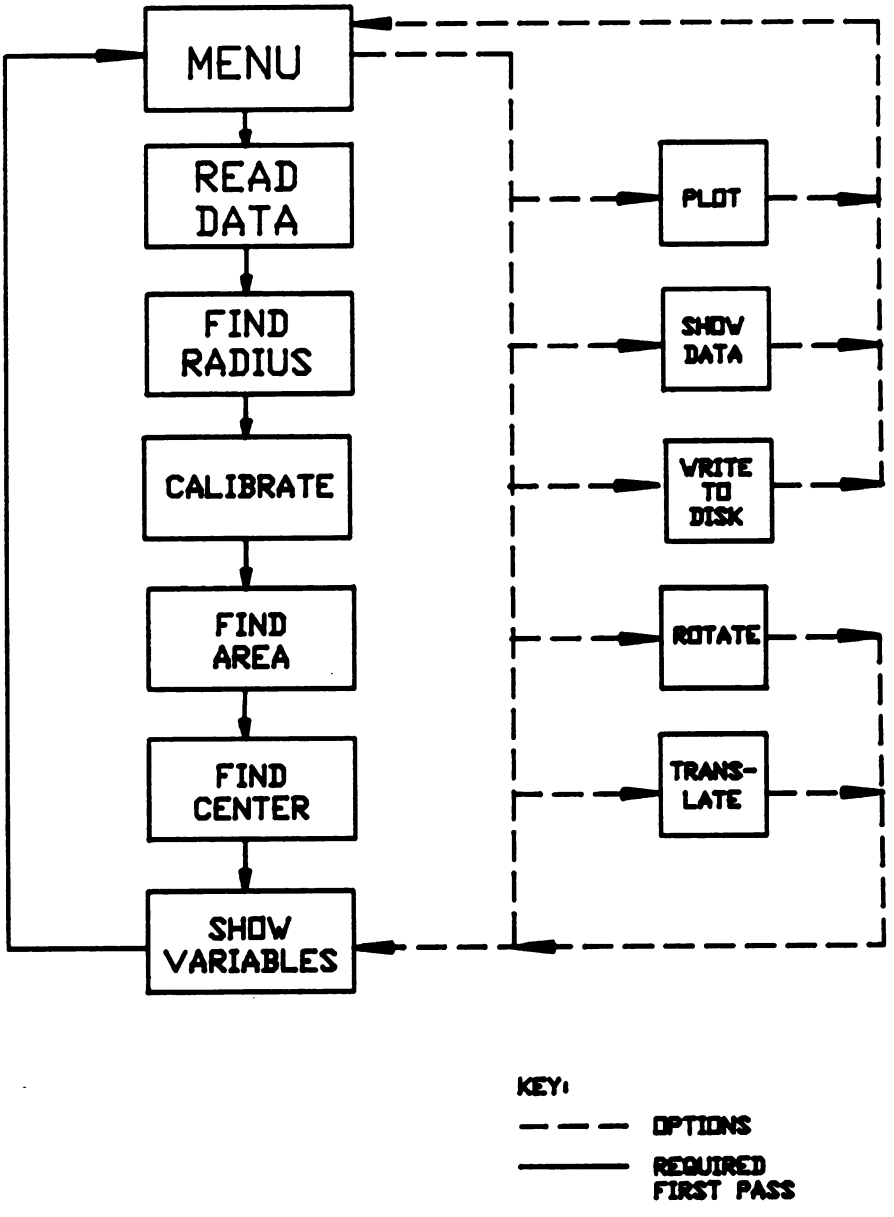

Figure 3.2 Block diagram of profile data calibration.

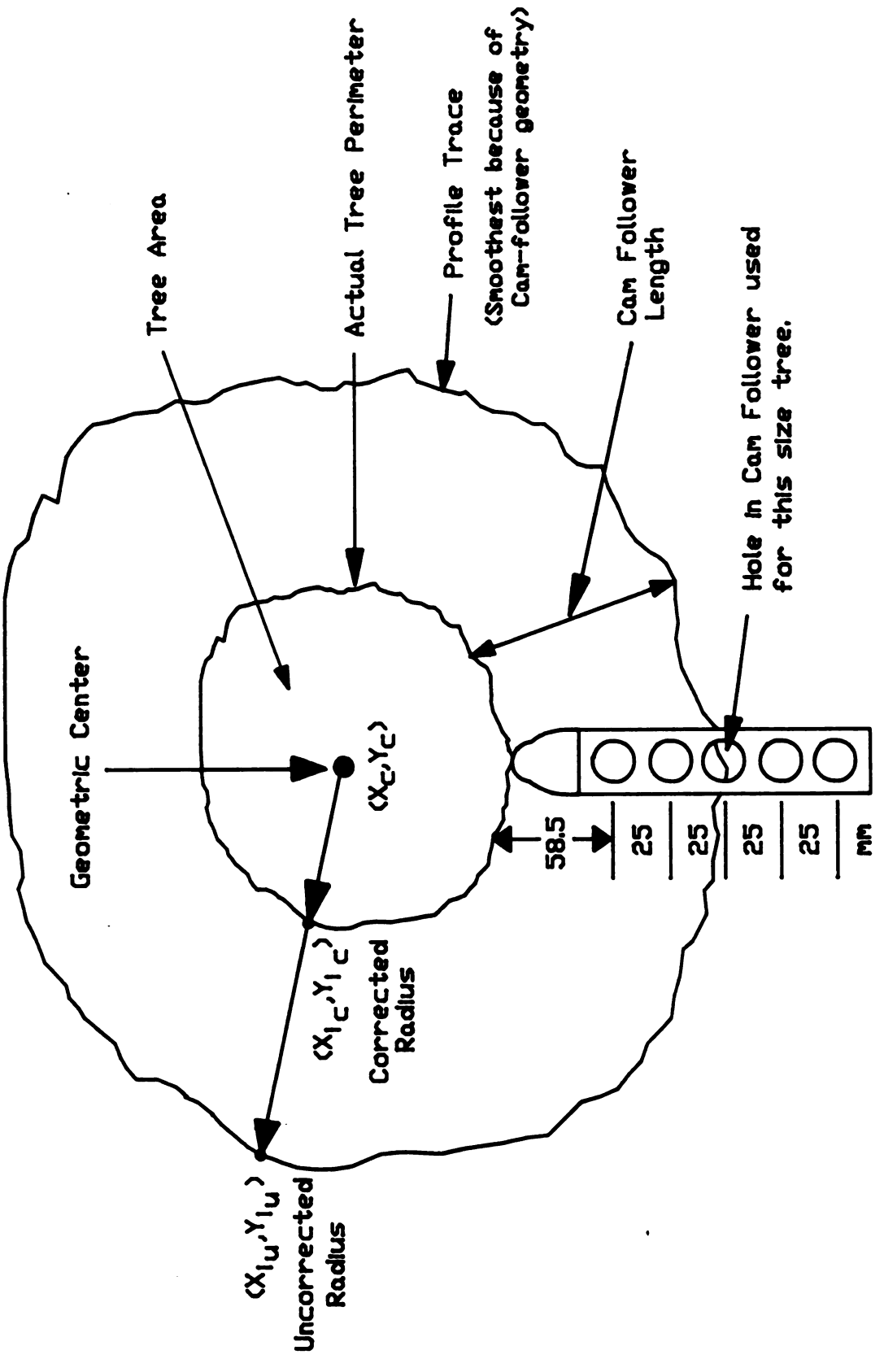

Figure 3.3 Profile calibration from periphery trace.

X_i, Y_i = (X,Y) coordinates of the i_{th} digitized data point of the trace

The uncorrected area was calculated using the survey area coordinate method (Brinker and Wolf, 1984) as follows:

X_1 Y_1

X_2 Y_2

. .

. .

X_n Y_n

$SUM_{pos} = X_i * Y_{i+1}$

$SUM_{neg} = X_{i+1} * Y_i$

$AREA = (SUM_{pos} - SUM_{neg})/2$

Area-projected-radius (APR) is often used to define near-circular particles and is defined as the radius of a circle with area equal to the object area under consideration. The area-projected-radius of the trace is then:

$$APR_t = \sqrt{\text{Trace Area} / \pi}$$

Where:

APR_t = Area-projected-radius of trace

The corrected profile radius for each point is then:

$$Radius_{correct} = Radius_{trace} - Length_{cam}$$

And the corrected (x,y) profile coordinates which give the corrected profile radius are then:

$$X_{i\text{-correct}} = X_i * \frac{APR_t - Length_{cam}}{APR_t}$$

$$Y_{i\text{-correct}} = Y_i * \frac{APR_t - Length_{cam}}{APR_t}$$

The valid profile area was then recalculated using the survey area coordinate method. Profile area (A_p) and profile radii (APR_p) were compared with hand measured estimates.

The profile center was defined utilizing a least squares fitting procedure, i.e., the point which minimized

the sum of squares distance from all the circumferal points (Kasa, 1975).

Letting (x_i, y_i) represent the x,y coordinates of the i_{th} measured data point, N the number of data points $(1 \leq i \leq N)$, (X_c, Y_c) the coordinates of the center, and R the radius of the circle, the least squares error criterion for locating the center is:

$$\sum_{i=1}^{N} (R_i - R)^2 = \min$$

Where:

$$R_i = \sqrt{(X_i - X_c)^2 + (Y_i - Y_c)^2}$$

for $N \geq 3$

This expression is not easy to solve analytically. Consequently, Kasa (1975) uses a modified least squares error criterion defined as:

$$\sum_{i=1}^{N} (R_i^2 - R^2)^2 = \min$$

This form presents no analytic difficulties and can be written in the form:

$$\mu = \sum_{i=1}^{N} [(X_i - X_c)^2 + (Y_i - Y_c)^2 - R^2]^2 = \min$$

A best fit circle is then found by searching for the unknowns X_c, Y_c and R.

Since the sum μ is a second-order function of X_c and Y_c without constraints, the extrema can be simply evaluated by setting derivatives of μ equal to zero. Taking derivatives with respect to X_c, Y_c, and R, setting them equal to zero, and simplifying, the new variable C can be introduced to

linearize resulting equations:

$$C = R^2 - X_C^2 - Y_C^2$$

Resulting equations appear as (all summations are over i=1 to N):

$$X_C 2\Sigma X_i + Y_C 2\Sigma Y_i + CN = \Sigma(X_i^2 + Y_i^2)$$

$$X_C 2\Sigma X_i^2 + Y_C 2\Sigma X_i Y_i + C\Sigma X_i = \Sigma(X_i^3 + X_i Y_i^2)$$

$$X_C 2\Sigma X_i Y_i + Y_C 2\Sigma Y_i^2 + C\Sigma Y_i = \Sigma(X_i^2 Y_i + Y_i^3)$$

Introducing the matrix DM and the vectors EM and QM respectively:

$$DM = \begin{pmatrix} 2\Sigma X_i & 2\Sigma Y_i & N \\ 2\Sigma X_i^2 & 2\Sigma X_i Y_i & \Sigma X_i \\ 2\Sigma X_i Y_i & 2\Sigma Y_i^2 & \Sigma Y_i \end{pmatrix}$$

$$EM = \begin{pmatrix} \Sigma(X_i^2 + Y_i^2) \\ \Sigma(X_i^3 + X_i Y_i^2) \\ \Sigma(X_i^2 Y_i + Y_i R) \end{pmatrix}$$

We can write:

$$EM = DM * QM$$

and solve:

$$QM = DM^{-1} * EM$$

by the classical Gauss or other appropriate method.

If R from Kasa's solution was within 2% of APR_t, then the geometric center found from Kasa's equations was accepted. If not, this meant that the tree trace was not bilaterally symmetric and hence, the center of the tree trace would not correspond to the center of a best fit circle through its coordinates (Figure 3.4). Therefore, a least squares error criterion was used to iterate through the profile to find the best center:

$$E = ((X_i - X_C)^2 + (Y_i - Y_C)^2)^2 = \min$$

irrespective of R

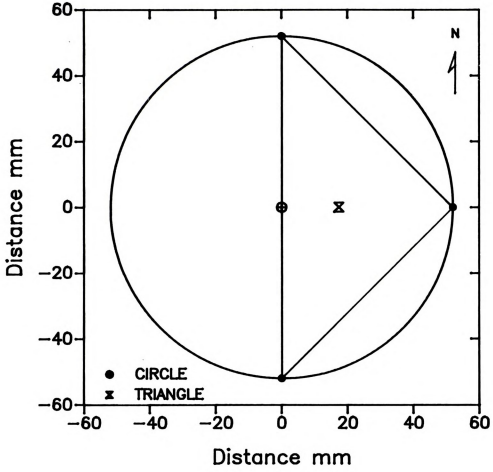

Figure 3.4 Inequality of centroids with a least squares best fit circle procedure.

The geometric profile center calculated by either method does not necessarily correspond to the tree's center of mass, however, due to density variations in material content.

Once calculated, the center of a tree profile plot could be translated to any desired X,Y location for further analysis via:

$$X_{new} = X_{old} - X_{translate}$$

$$Y_{new} = Y_{old} - Y_{translate}$$

Where $(X_{translate}, Y_{translate})$ usually equal (X_C, Y_C) in order to center profiles at (0,0). For uniformity, all centers were subsequently translated to (0,0) for plotting and analysis.

Rotation was also performed to align the profile on the plot as desired. The angle of rotation θ could be specified by the user or it could be calculated so as to set magnetic north at the top of the plot according to the routine:

$$\Delta X = X_{361} - X_C$$
$$\Delta Y = Y_{361} - Y_C$$

$$\theta = \text{ARCTAN}(\Delta Y / \Delta X)$$

Rotation was accomplished by matrix multiplication:

$$QM = DM * RM$$

Where:

QM is the N*3 output matrix of rotated X,Y values
DM is the N*3 input matrix of nonrotated X,Y values
RM is the 3*3 rotation matrix:

$$RM = \begin{pmatrix} \cos(\theta) & \sin(\theta) & 0 \\ -\sin(\theta) & \cos(\theta) & 0 \\ -X_C(\cos(\theta)-1)+Y_C\sin(\theta) & -X_C(\sin(\theta)-1)-Y_C(\cos(\theta)-1) & 1 \end{pmatrix}$$

Rotation was necessary in the 1986 profile data in

order to increase the accuracy (and repeatability) of alignment of plots with magnetic north. A time domain cross-correlation procedure was used on the 1985 - 1986 profile plan to determine a rotation angle for best alignment as follows:

$$\psi_{12}(\zeta) = \frac{1}{\phi_1} \cdot \int_{\phi=0}^{\phi_1} f_1(\phi) f_2(\phi+\zeta)\, d\phi$$

or in discrete formulation:

$$\psi_{12}(\zeta) = \frac{1}{\phi_1} \cdot \sum_{\phi=0}^{\phi_1} f_1(\phi) f_2(\phi+(\zeta-1))$$

$$\zeta = 1 \ldots \zeta_1$$

This provided the required angle of rotation of the 1986 plot which would provide best alignment with the 1985 plot. Assuming accurate directional traces on each years profile plot, this would improve alignment repeatability to $\pm$ 0.5^{o} from magnetic north.

Now that successive profiles are calibrated and aligned, multiple shape discriminators can be calculated. The perimeter (needed for several shape discriminators) was calculated as:

$$P\ (mm) = \sum_{i=1}^{359} \sqrt{((X_{i+1}-X_i)^2 + (Y_{i+1}-Y_i)^2)} + \sqrt{(X_1-X_N)^2 + (Y_1-Y_N)^2}$$

3.2 Geometric and Linear Profile Plots

Much work has been devoted to image analysis and shape discrimination. Unfortunately, most of this work has been targeted towards keeping similar shapes in the same category

(rectangles, ellipsoids, circles: Figure 3.5). This presents a problem in trunk profile analysis because, while it is clear that successive annual profiles will have similarity, my goal is to identify those small differences which may provide indicators of tree deformation and damage.

Tree shapes have received little attention as indicators of damage. In a first attempt to make small discriminations in shape, the simplest methods of discrimination were approached - observation of the geometric profile plots produced by the digitization and calibration procedures of Section 3.1. Three of the nine tree profiles analyzed were selected as examples for what follows. Tree 11 (Figure 3.6) has a small trunk (dia<100 mm, 4.0 in.), Tree A (Figure 3.7) has a medium trunk (100 mm<dia<150 mm, 4.0-6.0 in.) and Tree 2S (Figure 3.8) has a large trunk (150 mm<dia, 6.0 in.). Plots are not to-scale. Dashed lines indicate a circle of area equal to that of the corresponding trunk profile (Area-projected-radius circle).

Tree 11 in 1985 had a nearly circular cross section. In 1986, after having been shaken once in 1985, the shape has become less circular, having a radius smaller than APR in the SW and NE octants and a radius larger than average in the NNW and SE octants. Visual inspection of this tree indicates no external damage except for a slightly scuffed bark patch in the WSW sector.

Tree A appeared to have some slight malformation in 1985; visual inspection in 1985, however, failed to reveal

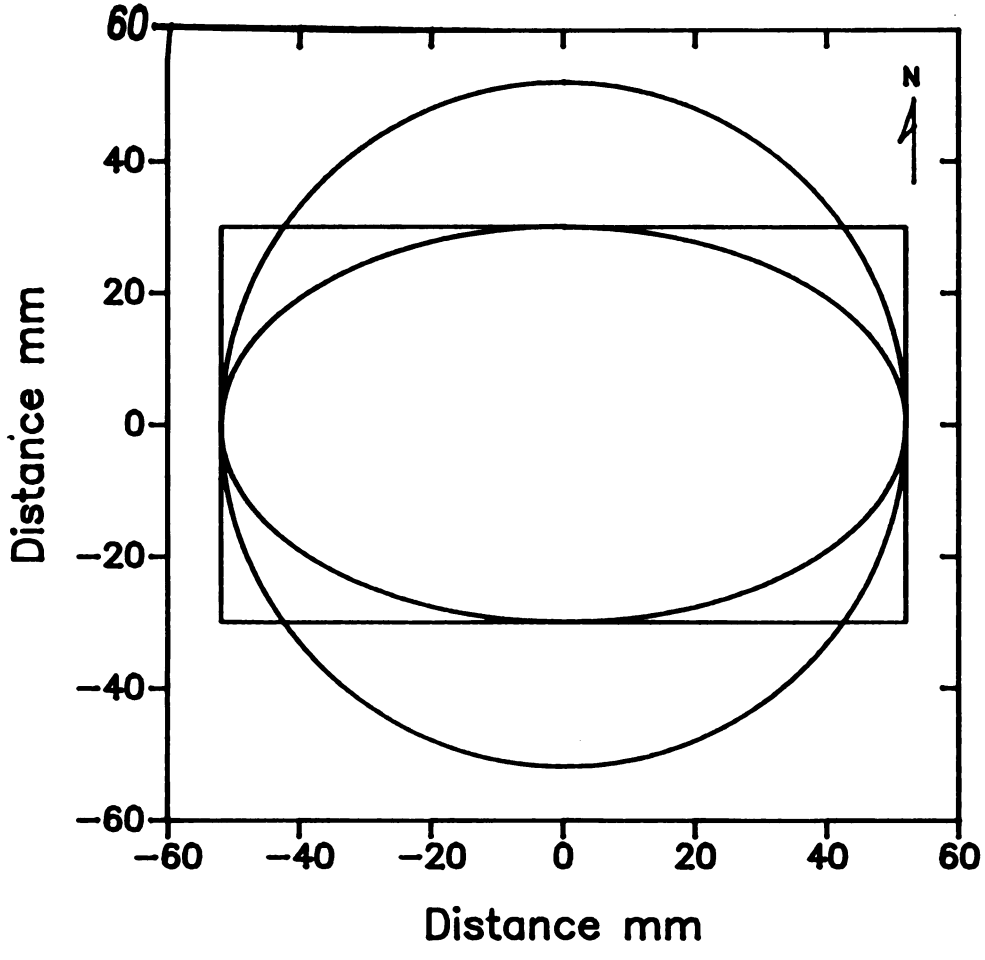

PROFILE ID.

RECTANGLE
ELLIPSE
CIRCLE

PROFILE AREA

7200.0 mm^2
4897.0 mm^2
8481.9 mm^2

PROJECTED RADIUS

44.6 mm
39.5 mm
52.0 mm

Figure 3.5 Standard geometric shapes referenced in profile analysis.

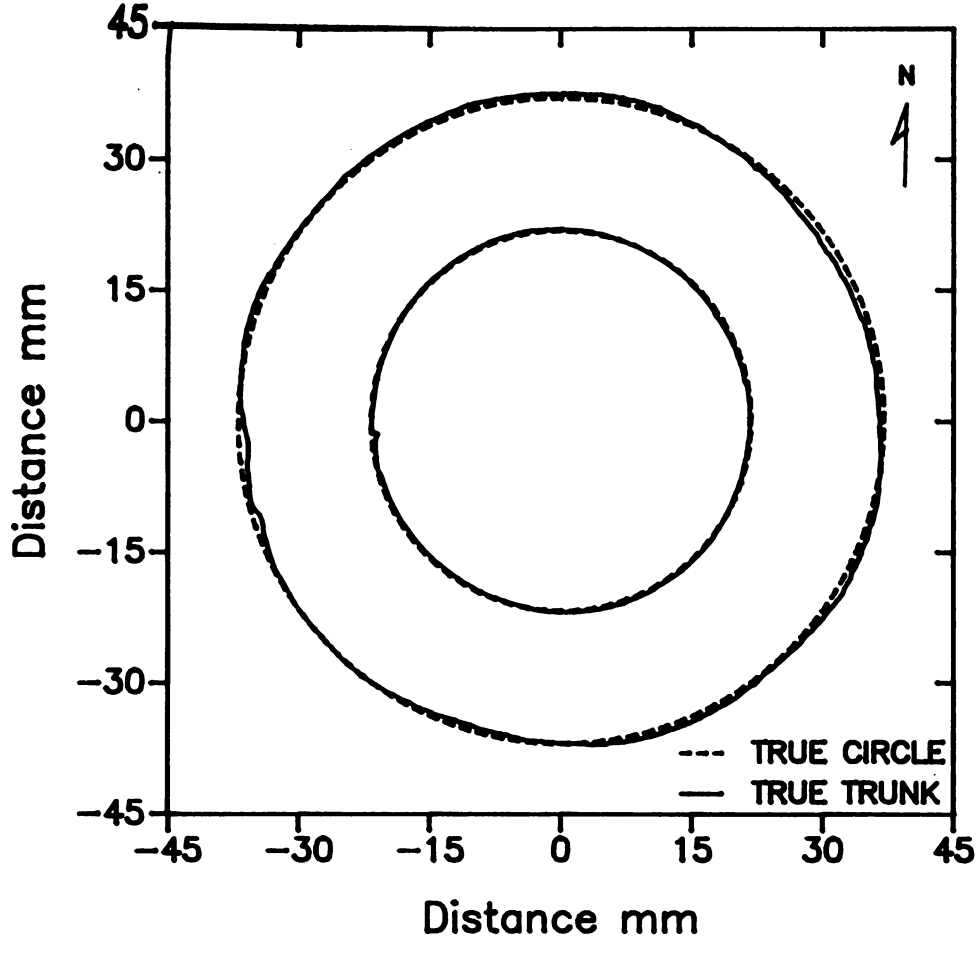

PROFILE ID.

Tree 11: 1985
Tree 11: 1986

PROFILE AREA

1487.1 mm²
4306.8 mm²

PROJECTED RADIUS

21.8 mm
37.0 mm

Figure 3.6 Tree trunk shape/area analysis — trunk profile 11.

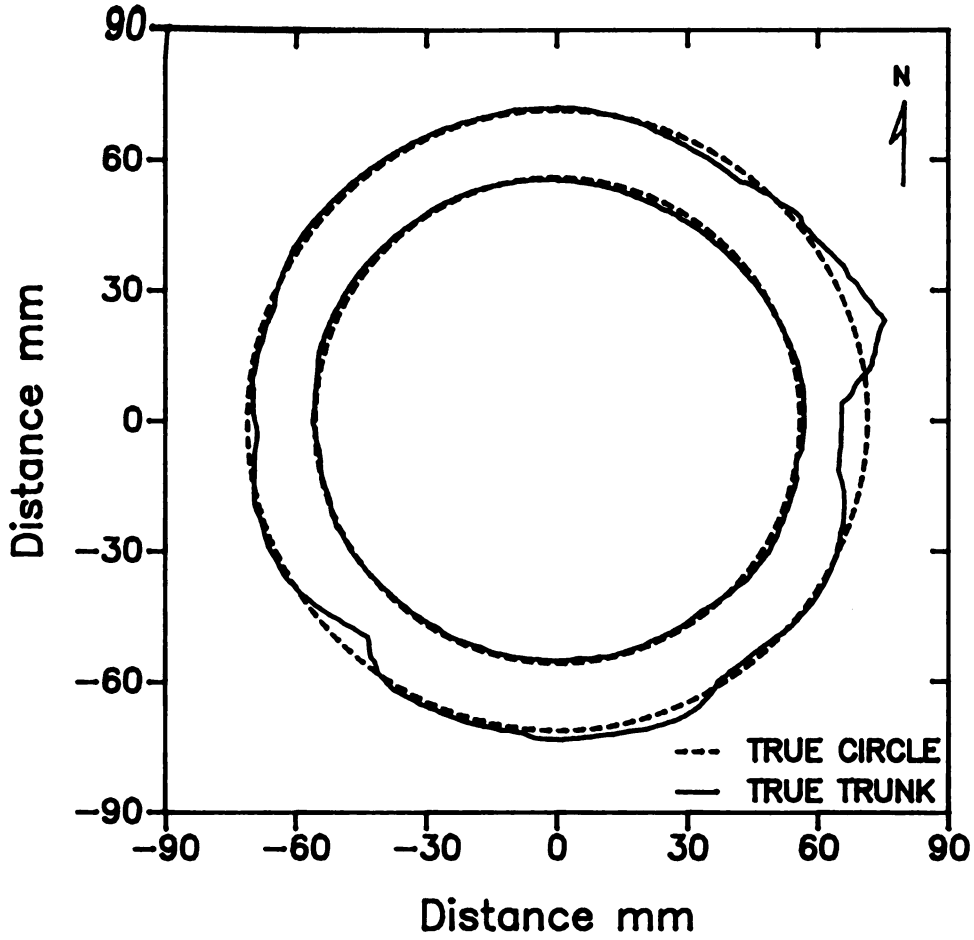

PROFILE ID.

Tree A: 1985
Tree A: 1986

PROFILE AREA

9771.7 mm^2
15985.0 mm^2

PROJECTED RADIUS

55.8 mm
71.3 mm

Figure 3.7 Tree trunk shape/area analysis — trunk profile A.

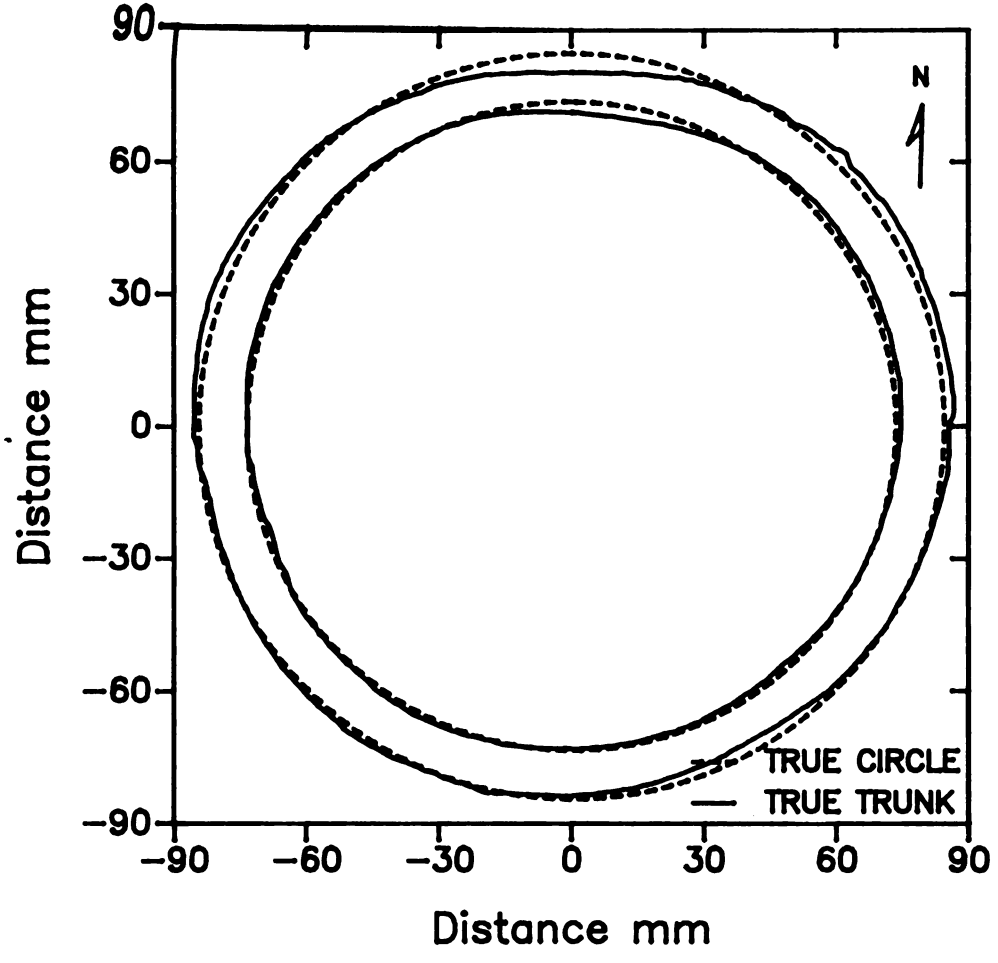

PROFILE ID.

Tree 2S: 1985
Tree 2S: 1986

PROFILE AREA

16981.1 mm^2
22443.3 mm^2

PROJECTED RADIUS

73.5 mm
84.5 mm

Figure 3.8 Tree trunk shape/area analysis – trunk profile 2S.

any external damage. The 1986 profile shows drastic changes in shape; in addition severe bark splitting, bark folding, and decay can be seen.

Tree 2S also showed some malformation in 1985. Visual observation revealed slight external bark scuffing in the NNE sector. The 1986 profile appears to amplify the profile distortion observed in 1985. In general, the periphery is similar to 1985 except for slight bark protrusion in the NE quadrant, possibly the result of splitting. This tends to agree with 1986 observations; minor external change has taken place except for uniform radial growth.

Profile plots were subsequently linearized by transforming from Cartesian coordinates to polar coordinates and plotting the radius from the calculated geometric center versus the angular displacement from magnetic north (positive CCW). This plot transformation appears as:

$$X_i = \theta_i$$
$$Y_i = \text{Radius}(\theta_i)$$
$$\theta_i = 0 \ldots 360^{o} \text{ CCW}$$

This provides a means to observe and compare the profile perimeter in 1985 with that in 1986. Difference between successive annual plots indicates a radial change in shape for the growth period. It also provides a means for evaluating the circularity of the profile each year. For example, a linearized perfect circle would map to a perfect straight line, y=R, assuming the geometric center of the circle was accurately calculated (Figure 3.9).

More importantly, however, this method also provides a

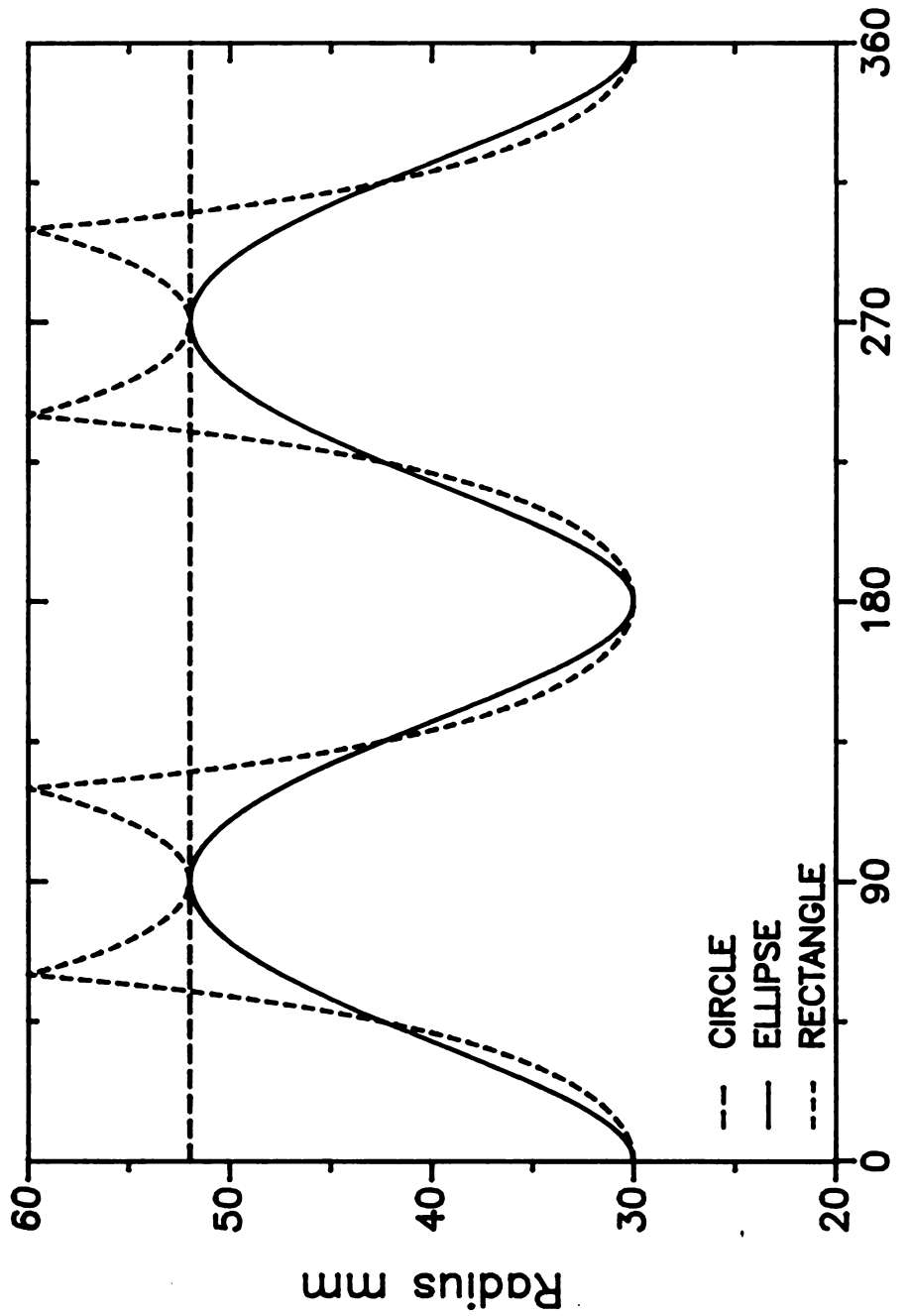

Figure 3.9 Polar map of standard geometric shapes.

check on the accuracy of the previously calculated geometric center of the profile. For example, if the profile was a perfect circle but the calculated geometric center was not the true geometric center, then the polar transformation would reveal a cycloid. This is not to be confused with actual perimeter malformations in non-circular profile plots, however.

Figure 3.10 is a linearization of the Tree 11 profile for 1985 and 1986. As shown, the calculated geometric centers are accurate. In 1985, Tree 11 was nearly a perfect circle. By 1986, however, some change in shape had occurred. Low magnitude changes with no sharp peaks may indicate internal cell damage causing redirected radial growth without visible external damage.

Tree A (Figure 3.11) shows minor non-circularity (via nonlinearity) in 1985 with drastic shape changes in 1986. The sharp changes correlate with visual observation of external bark damage. Valleys in the plot indicate decay or exposed wood. Peaks correlate with bark protruding due to splitting and peeling.

Tree 2S (Figure 3.12) exhibits a tri-lobed shape in 1985; by 1986 little more than radial growth has taken place. The jagged look of the 1986 data seems to indicate some bark scuffing and an increase in "rough bark". The fact that the two valleys do not show growth proportionate with the peaks may indicate slight internal damage.

The differences between 1985 and 1986 linearized

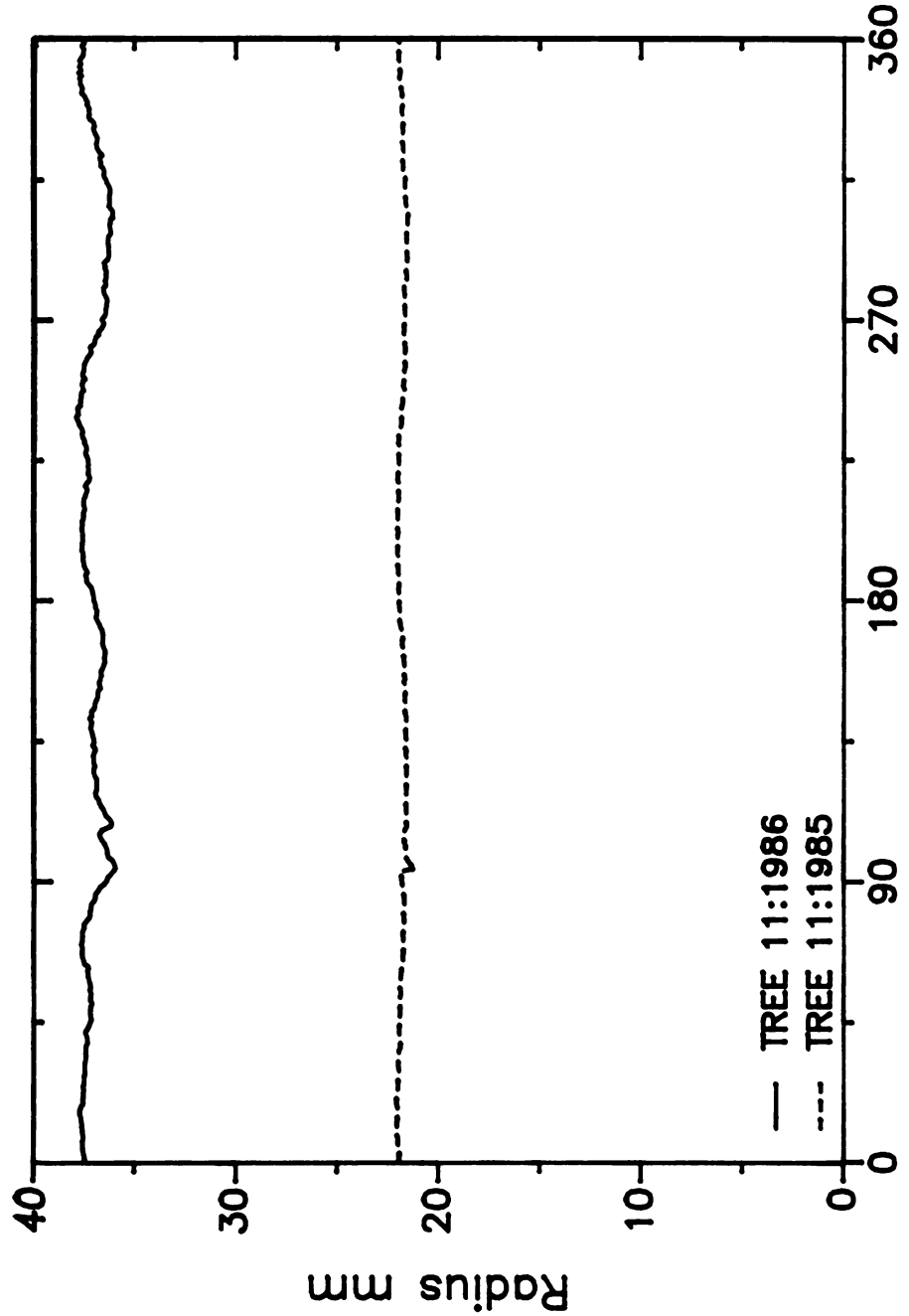

Figure 3.10 Polar map of tree trunk profile 11.

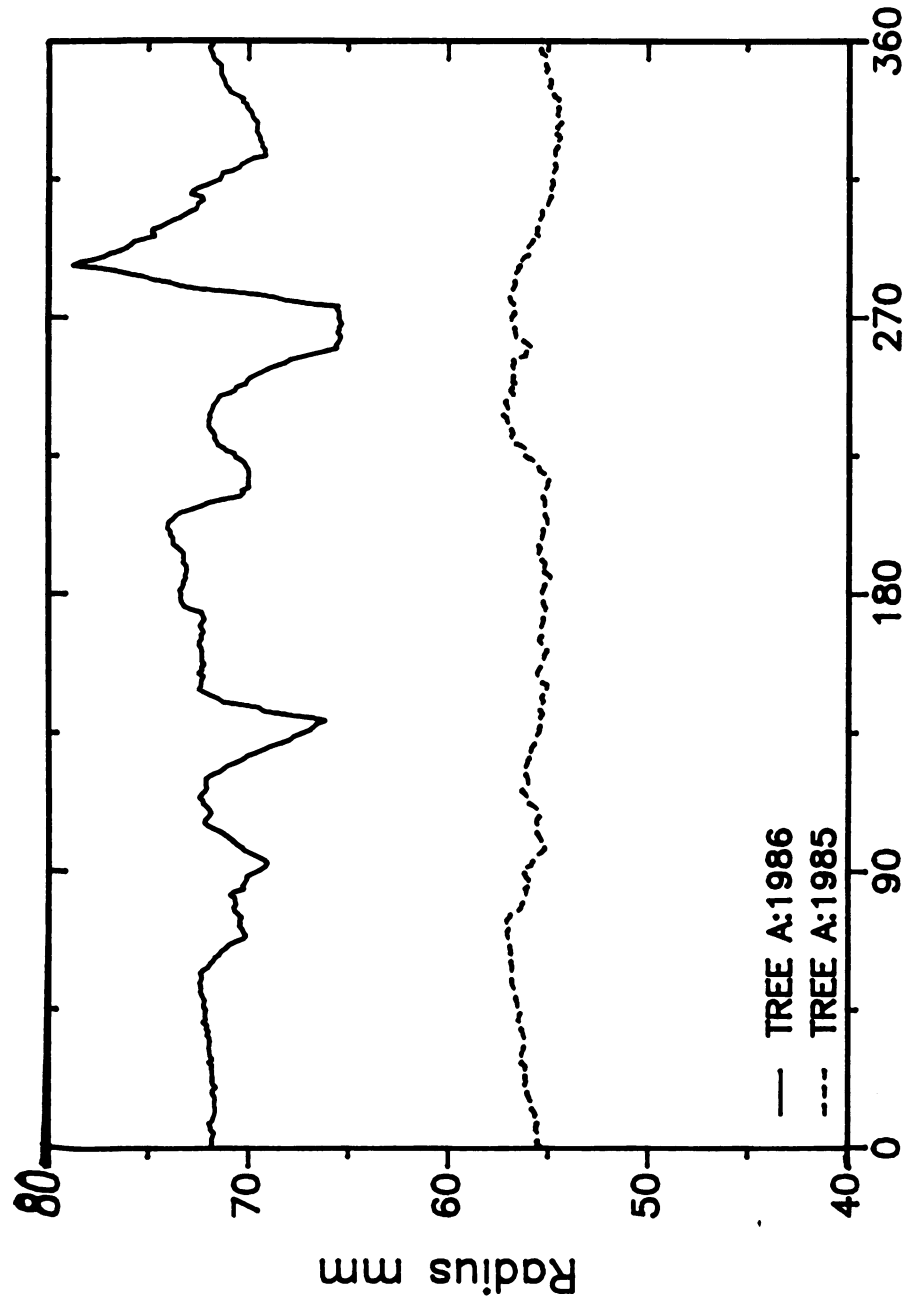

Figure 3.11 Polar map of tree trunk profile A.

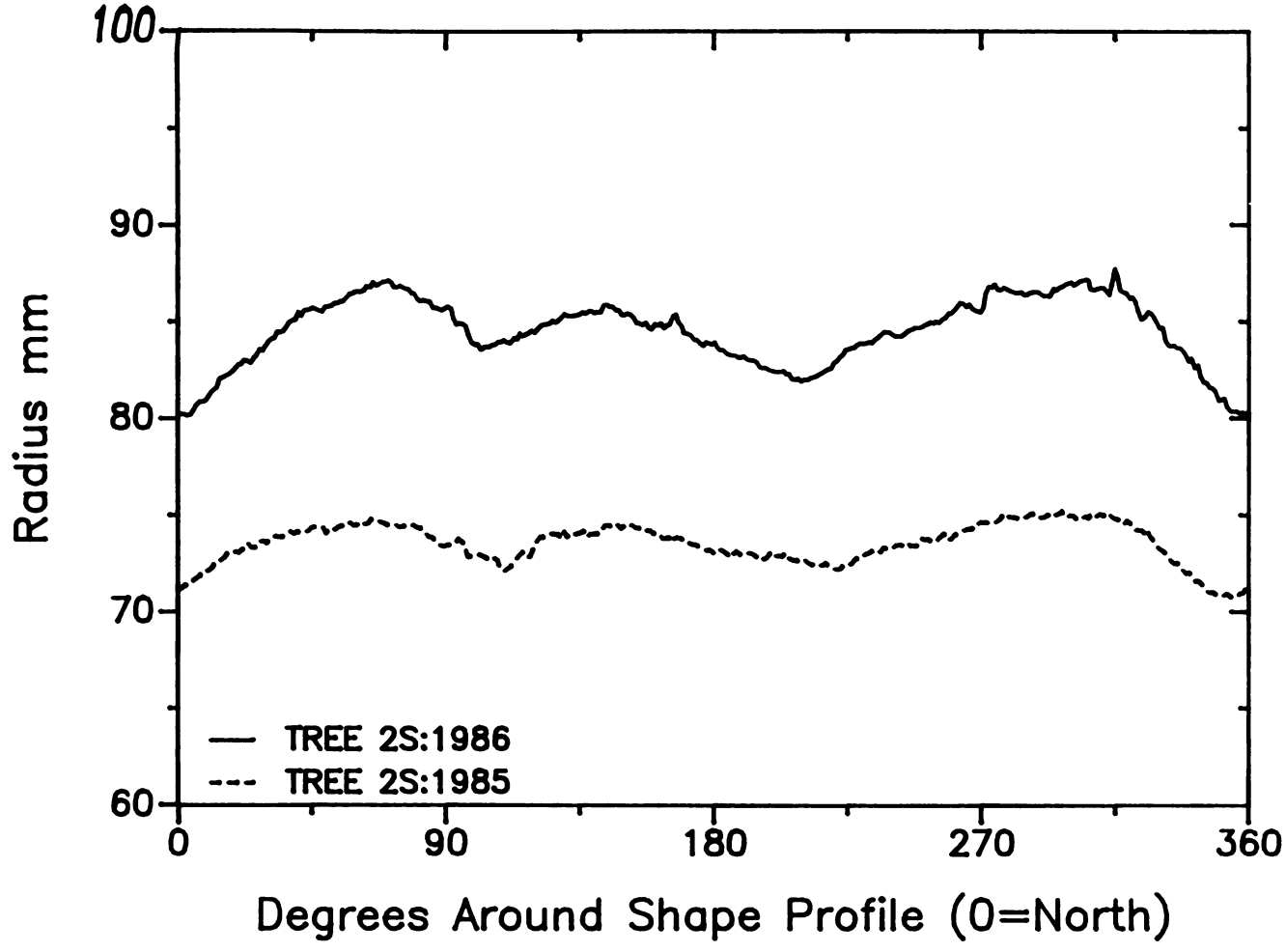

Figure 3.12 Polar map of tree trunk profile 2S.

profiles are shown in Figures 3.13 - 3.15. These plots provide an assay of radial growth among trunks of the same size class. If a perfectly circular tree has grown uniformly from 1985 to 1986, then a straight line would be expected at a Y-axis value equivalent to the measured radial growth. Deviation from a straight line indicates less growth (valleys) or more growth (peaks) than the average. Note the vertical axes are broken so that minor fluctuations will be emphasized.

Of the three small trees, Tree 11 appears to have developed most uniformly. Slight lack of growth is visible on the SW (90^{o}+) and NE (270^{o}+) sides of the tree. This happens to reflect the clamp location for the 1985 and 1986 harvests.

Tree A (Figure 3.14) shows drastic changes at the SW (90^{o}+) and NE (270^{o}+) quadrants agreeing both with location of clamping for the 1985 and 86 seasons as well as the visibility of external bark damage.

Tree 2S (Figure 3.15) clearly shows two areas of uniform growth and two areas of superior growth, differing radially by approximately 5 mm (0.20 in.). The fact that these two valleys are very close to 180^{o} apart agrees well with the hypothesis that slight internal damage at clamping points may have caused slight redirection in growth with no external markings.

The preceeding data indicate that degeneracy of circular shape occurs to varying extents as these trees

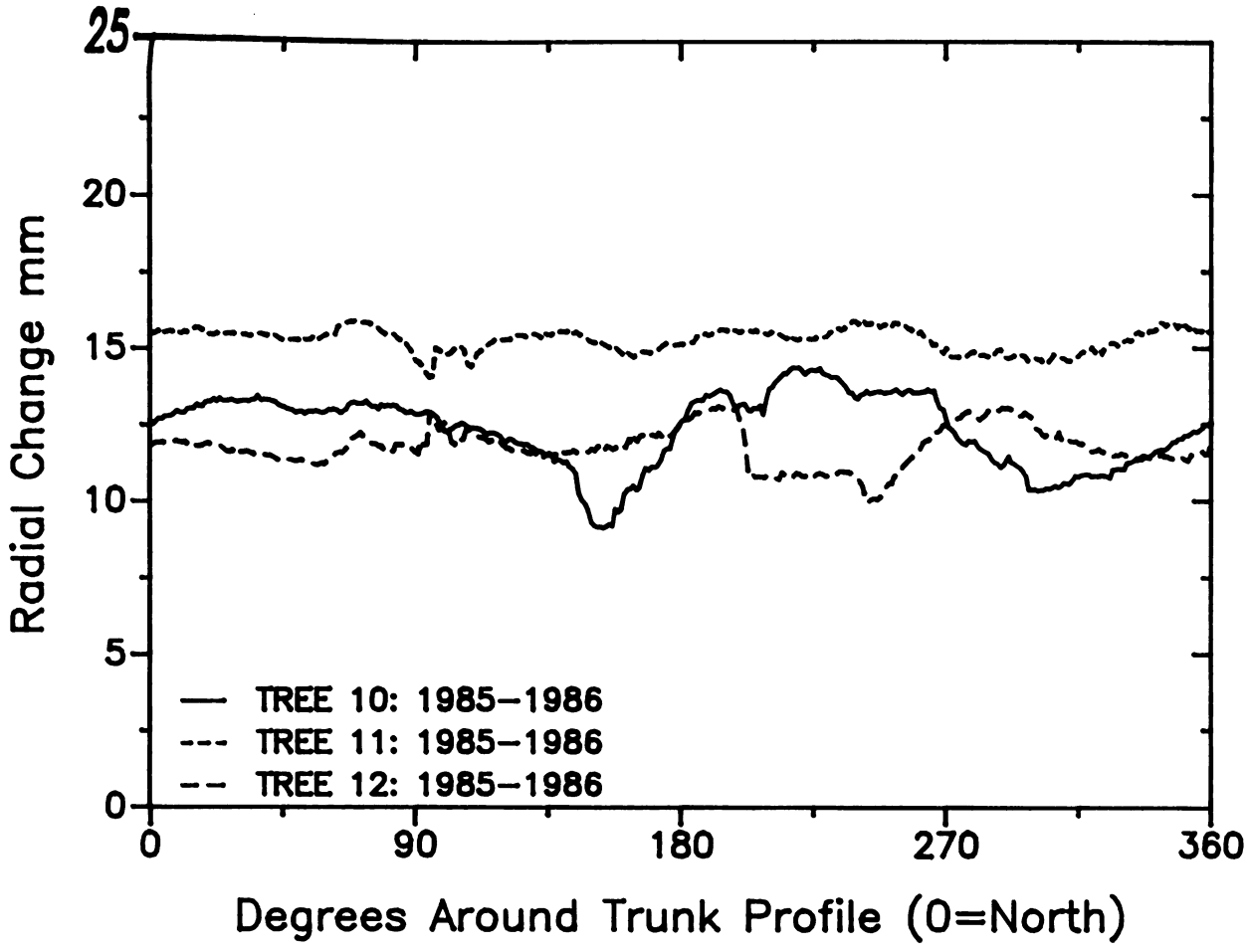

Figure 3.13 One year's radial change in trunk profile – trees 10, 11 and 12.

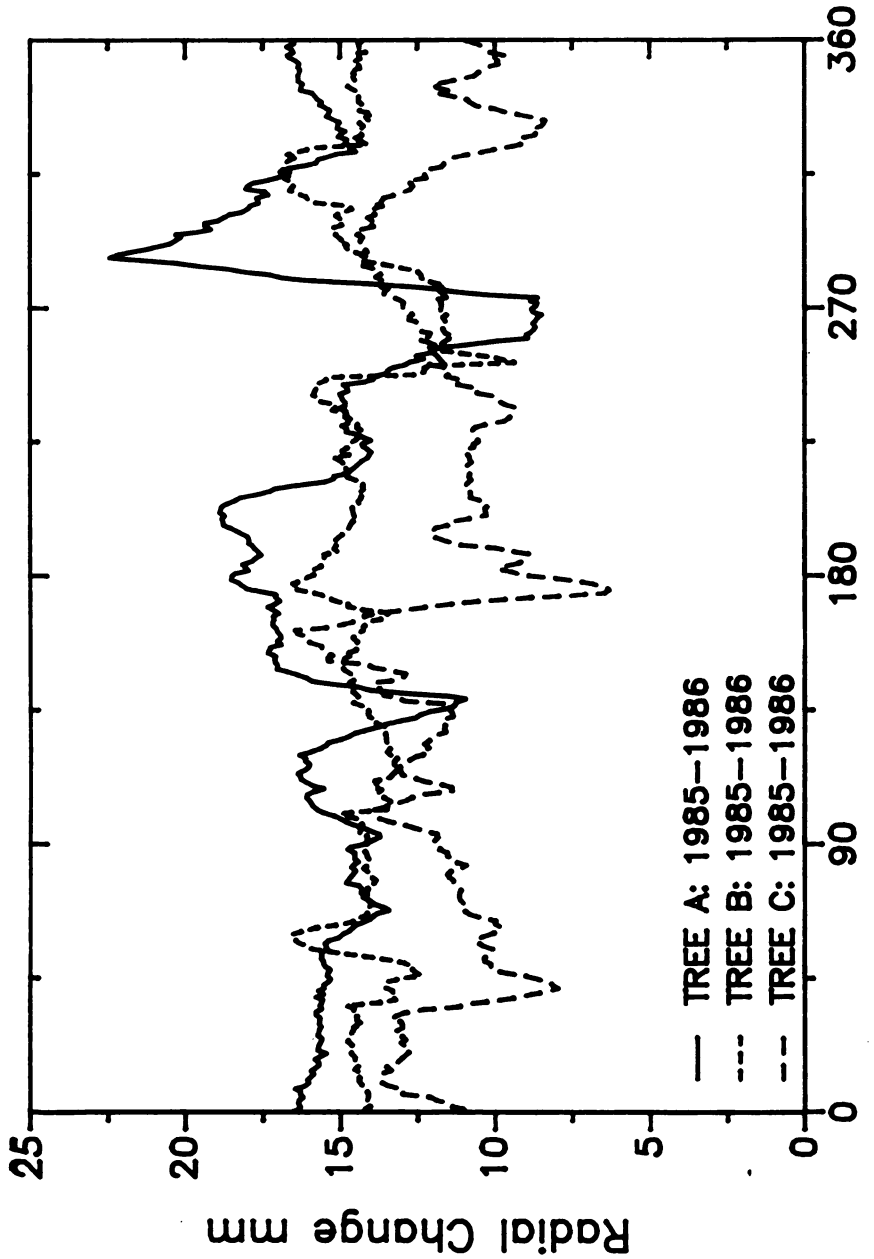

Figure 3.14 One year's radial change in trunk profile – trees A, B and C.

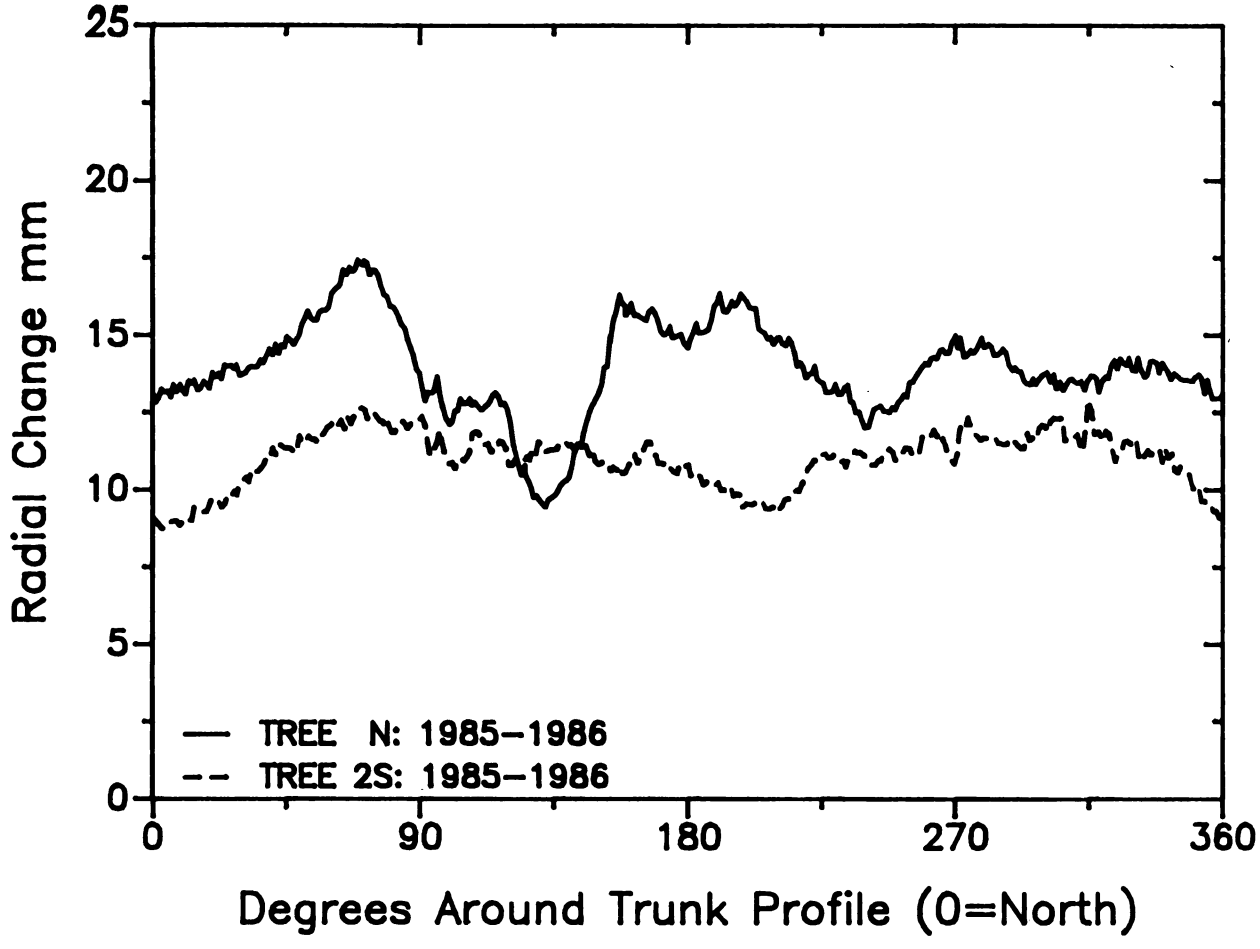

Figure 3.15 One year's radial change in trunk profile – trees N and 2S.

grow; the common causal agent appears to be trunk-shaking. Profile peaks above the mean difference may indicate bark protrusion and callus development while valleys below the mean difference may indicate compressed bark, decay areas, or dead wood. The trees in this test were shaken more severely than may be typical in commercial operations.

Live control trees were not available for profile analysis but several control cross sections of disected Montmorency cherry trees are shown in Figures 3.16-3.17. These cross sections indicate that trees generally take on a near-circular shape when young and continue to maintain the shape of the previous year's growth ring as they mature (Figures 3.16a, 3.16b). Shape can be influenced, however, by factors other than shaker damage such as wind, light intensity and direction, pruning, and staking. These factors change the fiber stress level and/or distribution of plant growth regulators which, in turn, change the growth distribution (pattern) of new cells.

Damage to trunks can often change the shape of the trunk when associated with splitting, pealing, and cracking. The tree healing process will then tend to reshape trunks to the predamage growth ring profile as shown in Figure 3.17a. Slight shaker damage may often become exhibited by a thin, dark-stained arc or by stain pockets (Figure 3.16a, 3.17b). Stains may show up as patches, patches which extend towards the heartwood but stop short, or patches that extend all the way to the heartwood (Figure 3.17b). Stains are often

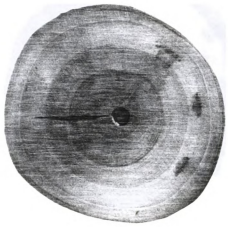

(a)

(b)

Figure 3.16 Cherry tree trunk cross sections:
a) shaker damage b) bark compression.

(a)

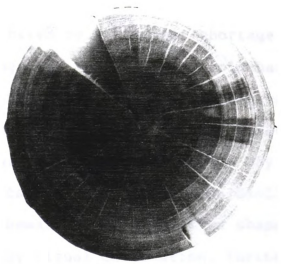

(b)

Figure 3.17 Cherry tree trunk cross sections:
a) contour rejuvenation b) staining.

evidenced with shaker damage and usually accompany decay. Decay, however, does not necessarily accompany staining. The physiological initiation, makeup, and activity of stains are not yet understood (Burton, 1987).

Slight changes in trunk shape may be caused by compression of the large phloem cells between the vascular and cork cambium layers (Figure 3.16b). These cells are larger and less rigid than most other bark cells and hence, are more likely to fail under stress. If damaged, these cells cannot provide passage of sugars from the leaves to the roots for over-winter storage. During a food shortage, available energy is allocated in a hierarchical manner with fruit yield and new shoot growth having lesser priority than maintenance of existing structure. Postwinter rejuvenation may also be inhibited by a nutrient shortage such as this.

Food shortage may reduce winter cold hardiness. Thin, dark growth rings often signify temperature or moisture extremes beyond a tree's physiological tolerances. Over a period of several years, periodic damage may accumulate and become a significant factor in the tree decline episode.

Having mathematically identified shape changes that were confirmed by visual observation, further more complex indicators for shape discrimination were investigated to find a convenient accurate index for bark damage.

3.3 Bandwidth and Historic Shape Indicators

Several geometric indices were calculated for the tree profile plots in an attempt to identify bark damage and

discriminate between external and internal damage. Some of these methods are used in digital image processing and have been converted for this application. Area and perimeter have already been calculated for the profiles. These two properties are invariant to rotation and translation and are considered good indicators of "multiple" versus "non-multiple" objects.

The area-projected-radius, as previously mentioned, is calculated for a shape as the radius of a perfect circle having the same area as the shape under investigation:

$$APR\ (mm) = \sqrt{Profile\ Area\ (mm^2) / \pi}$$

A similar parameter, the perimeter-projected-radius is the radius of a perfect circle having the same perimeter as the shape under investigation:

$$PPR\ (mm) = Perimeter\ (mm) / 2\pi$$

A 'bandwidth' factor was defined for this application as:

$$BW\ (mm) = Max\ Radius - Min\ Radius$$

Where:

$$Max.\ Rad.\ (mm) = Max\ \left(\sqrt{(X_i - X_c)^2 + (Y_i - Y_c)^2} \right)$$

$$Min.\ Rad.\ (mm) = Min\ \left(\sqrt{(X_i - X_c)^2 + (Y_i - Y_c)^2} \right)$$

$$i = 1...N$$

'Percent bandwidth' can then be defined as:

$$\%\ BW = BW\ (mm) / APR * 100$$

Compactness, CPR, (Agin, 1976) is a dimensionless feature that is invariant to translation, rotation, and size and has been used to distinguish "single fruit" objects from

"noise objects". It is defined as:

$$CPR = Area / Perimeter^2$$

The thinness ratio, TR, was defined by Duda and Hart (1973) as:

$$TR = 4\pi * CPR$$

Finally, Curray (1951) identified an object's roundness (RDNESS) as:

$$RDNESS = Object\ Area / Circle\ Area$$

Where:

Object Area = Calculated Area in the shape
Circle Area = Area of a circumscribing circle about the shape

$$= \pi * RLONG^2$$

Where:

$$RLONG = LONG\ DIA. / 2$$

And:

$$LONG\ DIA. = MAX \left[\sqrt{(X(\theta_i)-X_c)^2 + (Y(\theta_i)-Y_c)^2} + \sqrt{(X(\theta_i+180)-X_c)^2 + (Y(\theta_i+180)-Y_c)^2} \right]$$

$$\theta_i = 0...180$$

Shape indicators for standard geometric figures are given in Table 3.1. Application of these methods to the tree trunk profiles results in the data of Table 3.2.

Elongation, a measure of length to width ratio, is invariant to translation but only semi-invariant to rotation when defined as the minimum moment of inertia divided by the maximum moment of inertia (Gonzales and Wintz, 1977). Since rotation is important when defining damage areas on tree profile plots, the rotation-sensitive elongation factor was not calculated. However, a more in-depth moment approach has been used to calculate shape descriptors invariant in

Table 3.1 Geometric shape indicators of standard geometric shapes (All measurements in mm unless noted otherwise).

Profile	AREA (mm^2)	APR	MIN. RAD.	MAX. RAD.	PERIM	LONG DIA.
RECTANGLE	7200.0	44.6	30.0	60.0	360.0	120.0
ELLIPSE	4897.0	39.5	30.0	52.0	262.1	104.0
CIRCLE	8481.9	52.0	52.0	52.0	326.5	104.0

	BW	%BW	PPR	CPR	TR	RDNESS
RECTANGLE	30.1	67.7	52.2	0.0580	0.7290	0.5568
ELLIPSE	22.0	55.6	41.7	0.0713	0.8956	0.5773
CIRCLE	0.0	0.0	52.0	0.0796	1.0000	1.0000

translation, rotation and size. Gonzales and Wintz (1977) define seven invariant moments which combine to reveal features for object classification where the features are composed of second and third order moments divided by an area factor defined as [(moment's order/2)+1].

A moment of order (p + q) is defined for a two dimensional continuous function f(x,y) of an image as:

$$m_{pq} = \int_{-\infty}^{\infty} \int_{-\infty}^{\infty} x^p y^q \cdot f(x,y)\, dx\, dy$$

$$p,q = 0,1,2,\ldots$$

The center of gravity of an object can then be determined from:

$$\bar{x} = m_{10} / m_{00} \qquad \bar{y} = m_{01} / m_{00}$$

The central moments are expressed as:

$$\mu_{pq} = \int_{-\infty}^{\infty} \int_{-\infty}^{\infty} (x - \bar{x})^p (y - \bar{y})^q \cdot f(x,y)\, dx\, dy$$

Table 3.2 Geometric shape indicators of cherry tree trunk profiles (All measurements in mm unless noted otherwise, listed in size categories in order of damage).

Profile	ED*	AREA (mm^2)	APR	MIN. RAD.	MAX. RAD.	PERIM	LONG DIA.
11-1985	1	1487.1	21.8	21.0	22.0	137.9	44.1
11-1986	2	4306.8	37.0	35.9	37.8	234.5	75.2
12-1985	1	1749.3	23.6	22.7	24.0	150.1	48.0
12-1986	3	3927.6	35.4	33.4	36.9	225.2	72.4
10-1985	2	1739.5	23.5	23.1	23.8	148.5	47.5
10-1986	5	4048.7	35.9	32.7	38.0	229.6	75.0
C-1985	1	10348.5	57.4	54.3	60.2	367.9	119.1
C-1986	3	15006.8	69.1	65.8	74.2	445.5	143.3
B-1985	2	10734.7	58.5	56.8	60.0	369.4	118.7
B-1986	4	16622.2	72.7	68.6	75.1	467.8	149.3
A-1985	2	9771.7	55.8	54.3	57.2	353.9	114.1
A-1986	5	15985.0	71.3	65.3	78.8	461.9	151.0
N-1985	1	20399.0	80.6	78.3	82.6	510.0	164.6
N-1986	2	28074.8	94.5	90.6	97.8	599.1	193.9
2S-1985	1	16981.1	73.5	70.7	75.2	464.4	149.1
2S-1986	3	22443.3	84.5	80.1	87.7	535.5	173.2

	BW	%BW	PPR	CPR	TR	RDNESS
11-1985	1.0	4.7	21.9	0.0783	0.9833	0.9754
11-1986	2.0	5.3	37.3	0.0783	0.9840	0.9692
12-1985	1.3	5.5	23.9	0.0777	0.9763	0.9678
12-1986	3.5	10.0	35.8	0.0775	0.9736	0.9534
10-1985	0.7	3.0	23.6	0.0789	0.9913	0.9823
10-1986	5.3	14.8	36.5	0.0768	0.9655	0.9156
C-1985	5.9	10.3	58.5	0.0765	0.9610	0.9284
C-1986	8.4	12.2	70.9	0.0756	0.9501	0.9299
B-1985	3.1	5.4	58.8	0.0787	0.9888	0.9708
B-1986	6.5	9.0	74.5	0.0759	0.9544	0.9493
A-1985	3.0	5.4	56.3	0.0780	0.9802	0.9560
A-1986	13.5	18.9	73.5	0.0749	0.9414	0.8931
N-1985	4.3	5.3	81.2	0.0784	0.9854	0.9581
N-1986	7.2	7.7	95.4	0.0782	0.9828	0.9507
2S-1985	4.5	6.1	73.9	0.0787	0.9893	0.9720
2S-1986	7.6	9.0	85.2	0.0783	0.9835	0.9524

* Estimated Damage: 1-(No Visible Damage), 3-(Moderate visible damage, no cracking or peeling), 5-(Severe visible damage, cracking, peeling, or sapping).

which, in format for digital processing becomes:

$$\mu_{pq} = \sum_x \sum_y (x - \bar{x})^p (y - \bar{y})^q \cdot f(x,y)$$

After expansion and simplification, the central moments to order 3 can be summarized as:

$$\mu_{00} = m_{00} \qquad \mu_{11} = m_{11} - \bar{y}m_{10}$$

$$\mu_{10} = 0 \qquad \mu_{30} = m_{30} - 3\bar{x}m_{20} + 2m_{10}\bar{x}^2$$

$$\mu_{01} = 0 \qquad \mu_{12} = m_{12} - 2\bar{y}m_{11} - \bar{x}m_{02} + 2\bar{y}^2 m_{10}$$

$$\mu_{20} = m_{20} - \bar{x}m_{10} \qquad \mu_{21} = m_{21} - 2\bar{x}m_{11} - \bar{y}m_{20} + 2\bar{x}^2 m_{01}$$

$$\mu_{02} = m_{02} - \bar{y}m_{01} \qquad \mu_{03} = m_{03} - 3\bar{y}m_{02} + 2\bar{y}^2 m_{01}$$

The normalized central moments are defined as:

$$\eta_{pq} = \mu_{pq} / \mu^{\gamma}_{00}$$

Where:

$$\gamma = ((p + q)/2) + 1 \qquad p+q = 2,3...$$

From the above second and third order moments, a set of seven moments (ψ_i), invariant to translation, rotation and size, are defined as descriptors for the continuous region:

$$\psi_1 = \eta_{20} + \eta_{02}$$

$$\psi_2 = (\eta_{20} - \eta_{02})^2 + 4\eta^2_{11}$$

$$\psi_3 = (\eta_{30} - 3\eta_{12})^2 + (3\eta_{21} + \eta_{03})^2$$

$$\psi_4 = (\eta_{30} + \eta_{12})^2 + (\eta_{21} + \eta_{03})^2$$

$$\psi_5 = (\eta_{30} - 3\eta_{12})(\eta_{30} + \eta_{12})[(\eta_{30} + \eta_{12})^2 - 3(\eta_{21} + \eta_{03})^2] + (3\eta_{21} - \eta_{03})(\eta_{21} + \eta_{03})[3(\eta_{30} + \eta_{12})^2 - (\eta_{21} + \eta_{03})^2]$$

$$\psi_6 = (\eta_{20} - \eta_{02})[(\eta_{30} + \eta_{12})^2 - (\eta_{21} + \eta_{03})^2] + 4\eta_{11}(\eta_{30} + \eta_{12})(\eta_{21} + \eta_{03})$$

$$\psi_7 = (3\eta_{12} - \eta_{30})(\eta_{30} + \eta_{12})[(\eta_{30} + \eta_{12})^2 - 3(\eta_{21} + \eta_{03})^2] + (3\eta_{21} - \eta_{03})(\eta_{21} + \eta_{03})[3(\eta_{30} + \eta_{12})^2 - (\eta_{21} + \eta_{03})^2]$$

The function f(x,y) is defined as a continuous image function over the region of scan. In the case of profile plots, this function must be defined since only the profile

boundary is stored in the data. Two methods are available to do this. The first consists of plotting the boundary on a screen and then filling the boundary regions by varying levels of contrast (grey tones). F(x,y) is then defined as the screen area in pixels. The value of f(x,y) for each iteration is dictated by the grey level of the pixel at (x,y).

In the case where the image is not too complex, it may be easier to analytically define image boundaries and then check to see if each (x,y) lies within. This second method was used with the profile plots by converting the Cartesian coordinates (x,y) of the boundary to polar coordinates (R,θ) and scanning an area which is known to include the largest profile. A value $f(x_s,y_s) = 1$ is returned if the scan coordinate $(x_s,y_s) = (R_s,\theta_s)$ lies inside the minimum profile radius R_{min} or $f(x_s,y_s) = 0$ if $(x_s,y_s) = (R_s,\theta_s)$ lies outside the maximum profile radius R_{max}.

If the scan coordinate lies "in the bandwidth" between R_{min} and R_{max}, the angle θ_s is used to find the two boundary points (x_{s-1},y_{s-1}) and (x_{s+1},y_{s+1}) which border (x_s,y_s). A linear interpolation is then performed between (x_{s-1},y_{s-1}) and (x_{s+1},y_{s+1}) to determine a "virtual boundary radius" $(R_{virtual})$ at θ_s. The scan radius R_s is then compared to $R_{virtual}$ to determine relative internal or external location. The number of calculations using this method is thereby dependent on the bandwidth.

The standard geometric shapes have moments as shown in

Table 3.3 Moment invariants for standard geometric shapes.

	Moment (Log)						
Profile ID	Ψ_1	Ψ_2	Ψ_3	Ψ_4	Ψ_5	Ψ_6	Ψ_7
RECTANGLE	0.120	0.885	6.174	7.021	14.251	7.923	13.800
ELLIPSE	0.132	0.859	5.520	6.525	12.621	7.205	12.720
CIRCLE	0.196	7.276	6.666	9.769	17.890	13.407	0.000

Table 3.4 Moment invariants for tree trunk profiles.

	Moment (Log)						
Profile ID	Ψ_1	Ψ_2	Ψ_3	Ψ_4	Ψ_5	Ψ_6	Ψ_7
11-1985	0.196	4.085	4.589	9.140	15.983	11.272	15.779
11-1986	0.196	3.553	4.330	8.122	14.117	10.463	14.126
12-1985	0.196	4.274	4.998	8.805	15.706	10.942	15.706
12-1986	0.196	3.803	3.611	6.521	11.376	8.424	11.573
10-1985	0.196	3.984	3.806	6.875	12.086	8.942	12.666
10-1986	0.194	2.621	3.568	6.042	10.622	7.360	10.746
C-1985	0.195	2.869	3.338	6.722	11.732	8.235	11.826
C-1986	0.195	3.319	2.900	6.355	11.529	8.671	11.364
B-1985	0.196	3.870	3.579	7.232	12.557	9.411	13.065
B-1986	0.196	3.405	5.416	7.516	14.182	9.219	13.935
A-1985	0.196	3.477	3.924	7.669	13.634	9.752	13.473
A-1986	0.195	3.726	3.820	5.601	10.736	7.465	10.426
N-1985	0.196	3.091	4.743	7.855	13.939	9.432	14.194
N-1986	0.195	3.072	4.164	6.683	12.995	8.911	12.120
2S-1985	0.196	3.704	3.656	7.173	12.589	9.510	12.749
2S-1986	0.195	3.162	3.703	6.582	11.562	8.363	11.981

Table 3.3. Application of these seven invariant moment equations to the tree profiles reveals the data of Table 3.4.

These results show that the first moment ψ_1 is practically invariant for a set of profiles of near circularity. From 1985 to 1986, ψ_2 tends to decrease for

all profiles except for A and C which are the two profiles with the largest perimeter "bumps" from bark distortion. From inspection of the profile plots, ψ_4 - ψ_7 tend to decrease for all three example trunks (11, A and 2S) proportional to the amount of shape change. With further data, ψ_2 and ψ_4 may provide adequate indication of direction and magnitude of shape change. ψ_1 alone seems to be inadequate for separation of similar shapes. ψ_2 and ψ_6, in combination with perimeter measurements, have been used to separate single objects from multiple objects of the same shape and may provide an indicator of "bumps" on trunk perimeters. Therefore, a combination of ψ_1, ψ_2, and ψ_7 may provide a bark damage envelope upon which judgement can be based.

3.4 Fourier Continuum and Cross-Correlation

Pattern recognition techniques have often been based on the Fourier series expansion of the linearized functions such as Figures 3.10, 3.11 and 3.12 (Ehrlich and Weinberg, 1970). The Fourier series coefficients contain information about an object's shape and thus can be used for identification. I wrote a discrete Fourier transform program to calculate the Fourier coefficients of the periphery radius of the tree profiles about their center of gravity in the form (Segerlind and Weinberg, 1973):

$$R(\theta) = R_o + \sum_{n=1}^{\infty} A_n \cdot \cos(n\theta) + \sum_{n=1}^{\infty} B_n \cdot \sin(n\theta)$$

Where:

$$R_o = \frac{1}{2\pi} \cdot \int_0^{2\pi} R(\theta)\, d\theta$$

$$A_n = \frac{1}{\pi} \cdot \int_0^{2\pi} R(\theta) \cdot \cos(n\theta)\, d\theta$$

$$B_n = \frac{1}{\pi} \cdot \int_0^{2\pi} R(\theta) \cdot \sin(n\theta)\, d\theta$$

The polar form is employed since the profile radius is a function of the angle about the center of gravity from a select reference line. Peripheral points are mapped to polar coordinates and the values of A_n and B_n for each value are calculated from the discrete form:

$$R(k) = \frac{1}{N} \cdot \sum_{\theta=1}^{N} R(\theta) \cdot e^{-2\pi i k\theta/N}$$

Then the expansion becomes:

$$R(\theta) = R_o + \sum_{n=1}^{\infty} R_n \cdot \cos(n\theta + \phi_n)$$

Where: $R_n = A_n^2 + B_n^2$

and: $\phi_n = \text{Arctan}\ (B_n/A_N)$

The R_o term in the series identifies the average radius while the R_n terms identify added "bumps" superimposed on the average radius properly placed by their corresponding phase.

The number of points needed to evaluate the Fourier series coefficients must be at least twice the number of the highest desired harmonic. Utilizing the acetate grid with 1^o spaced radials, 360 points were collected, providing data for the zeroth through the 179th harmonics. The zeroth

harmonic gives a centered circle with an area equal to the total area, the first harmonic is a offset circle, the second is a figure eight, the third a trefoil and so on. Frequency spectra for the standard geometric shapes are shown in Figures 3.18-3.20. Note from Figure 3.20 that some digital numerical error is evident around 0.001 to 0.005 magnitude. Values above 0.01 are considered accurate.

Figures 3.21 - 3.23 show the spectral content of Trunks 11, A, and 2S, respectively. The data are not normalized; therefore, differences in the projected area between profiles for the same trunk are apparent as the zeroth harmonic. Frequencies at the low end of the spectrum represent slower changing shapes and are more reliable than frequencies at the higher end where vision, dexterity, and digital numerical error begin to play an important role in frequency decomposition.

Figure 3.23 reveals that Trunk 2S did not significantly change shape from 1985-1986. Referring back to Figure 3.8, this agrees with visual observation. Significant magnitude changes in the low frequency spectral content of Trunk 11 and Trunk A would, however, indicate significant shape changes.

The profile of Trunk 11 shows significant changes up to approximately the 40th harmonic whereas Trunk A has an obvious extension up to about the 100th harmonic. Referring to the profile plots, Trunk A has significant shape changes with sharp valleys and peaks. High frequencies are

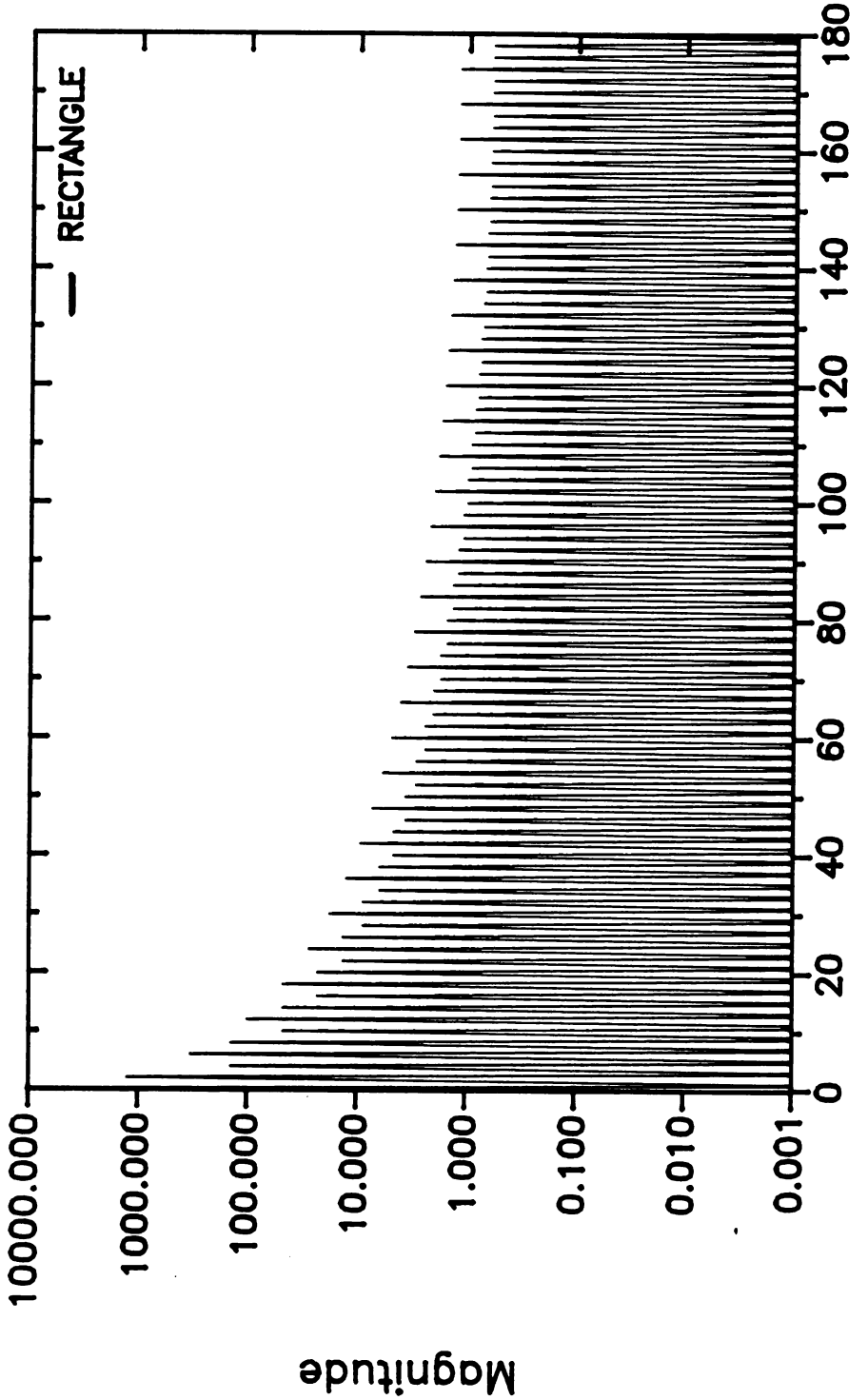

Figure 3.18 Spectral content of a standard rectangular profile.

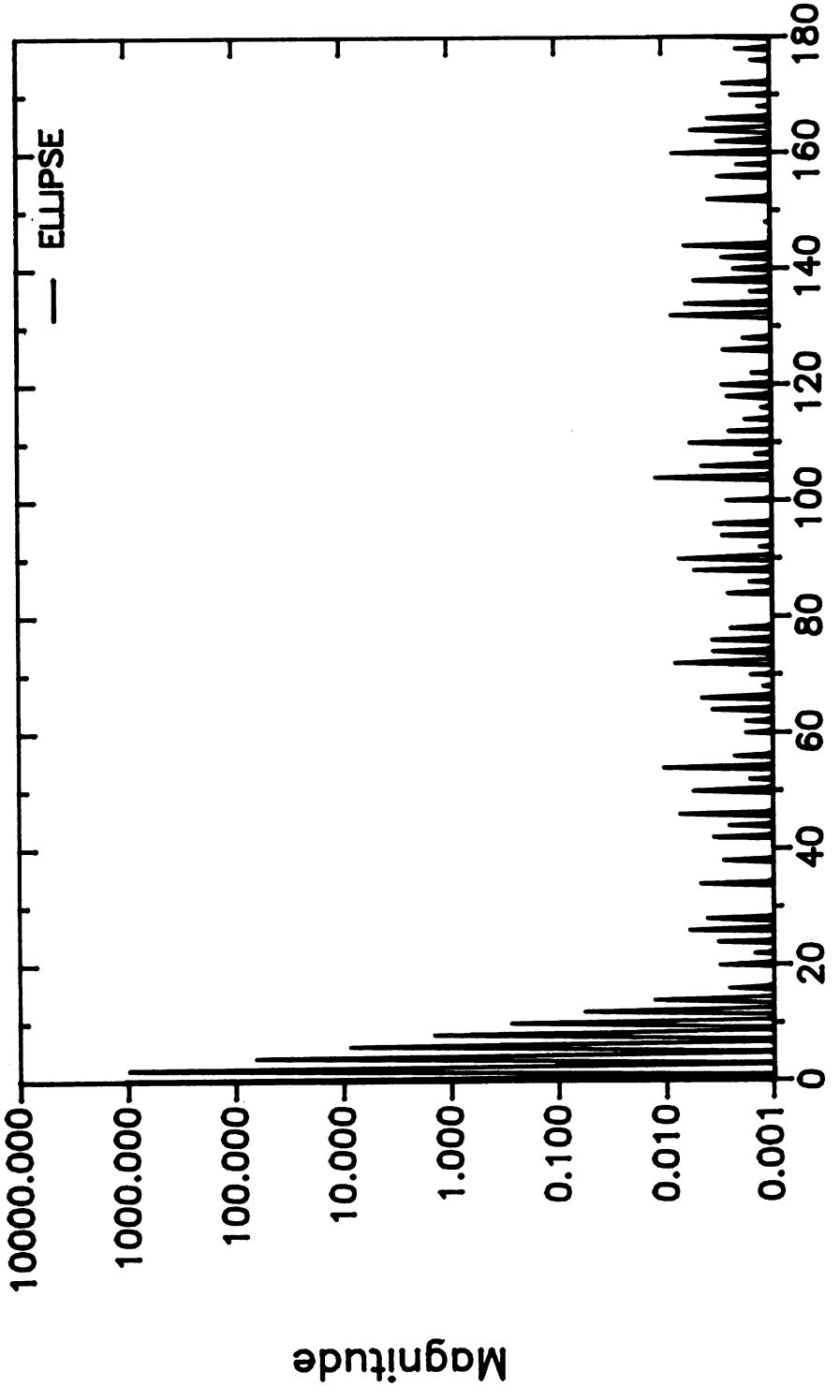

Figure 3.19 Spectral content of a standard elliptical profile.

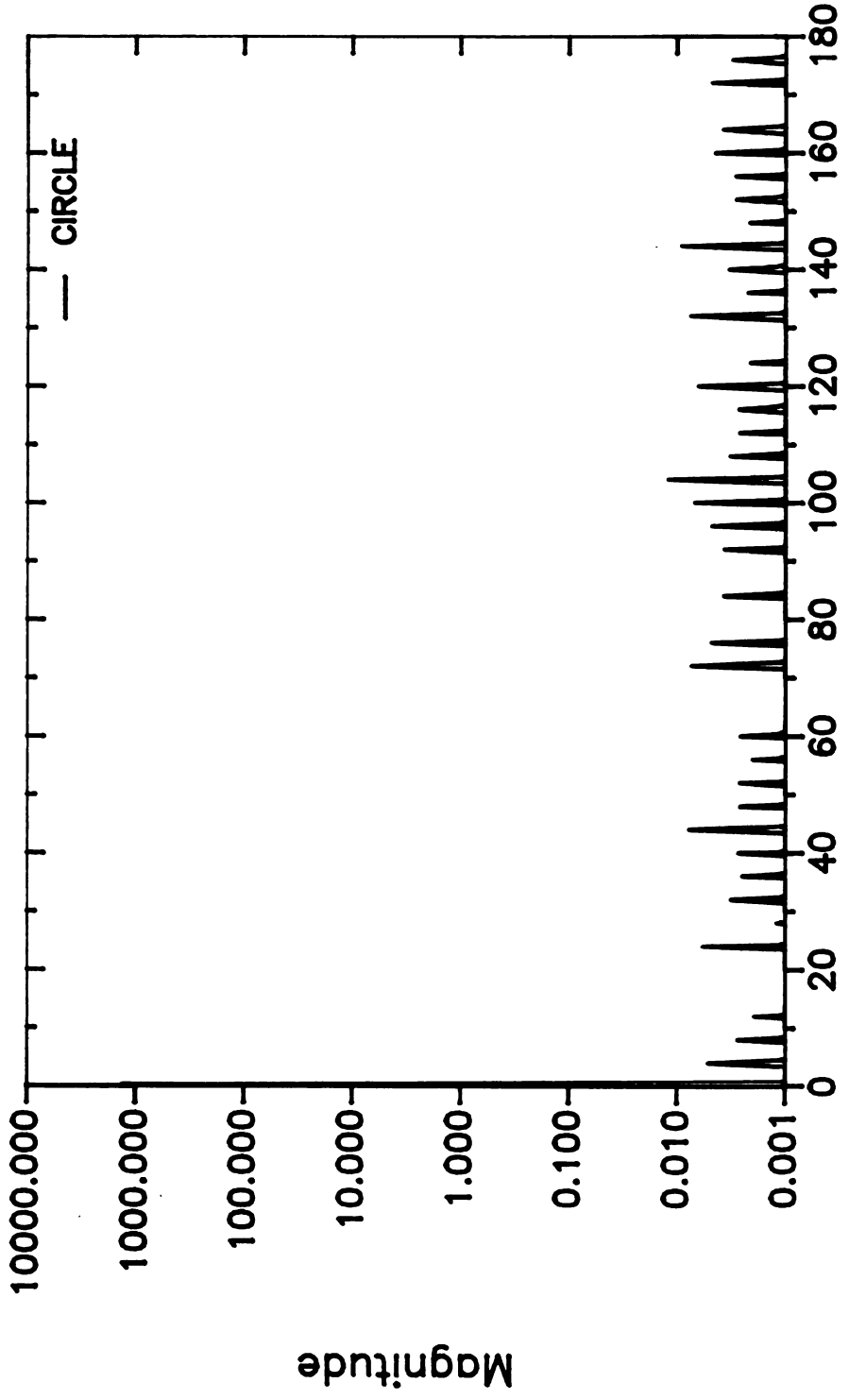

Figure 3.20 Spectral content of a standard circular profile.

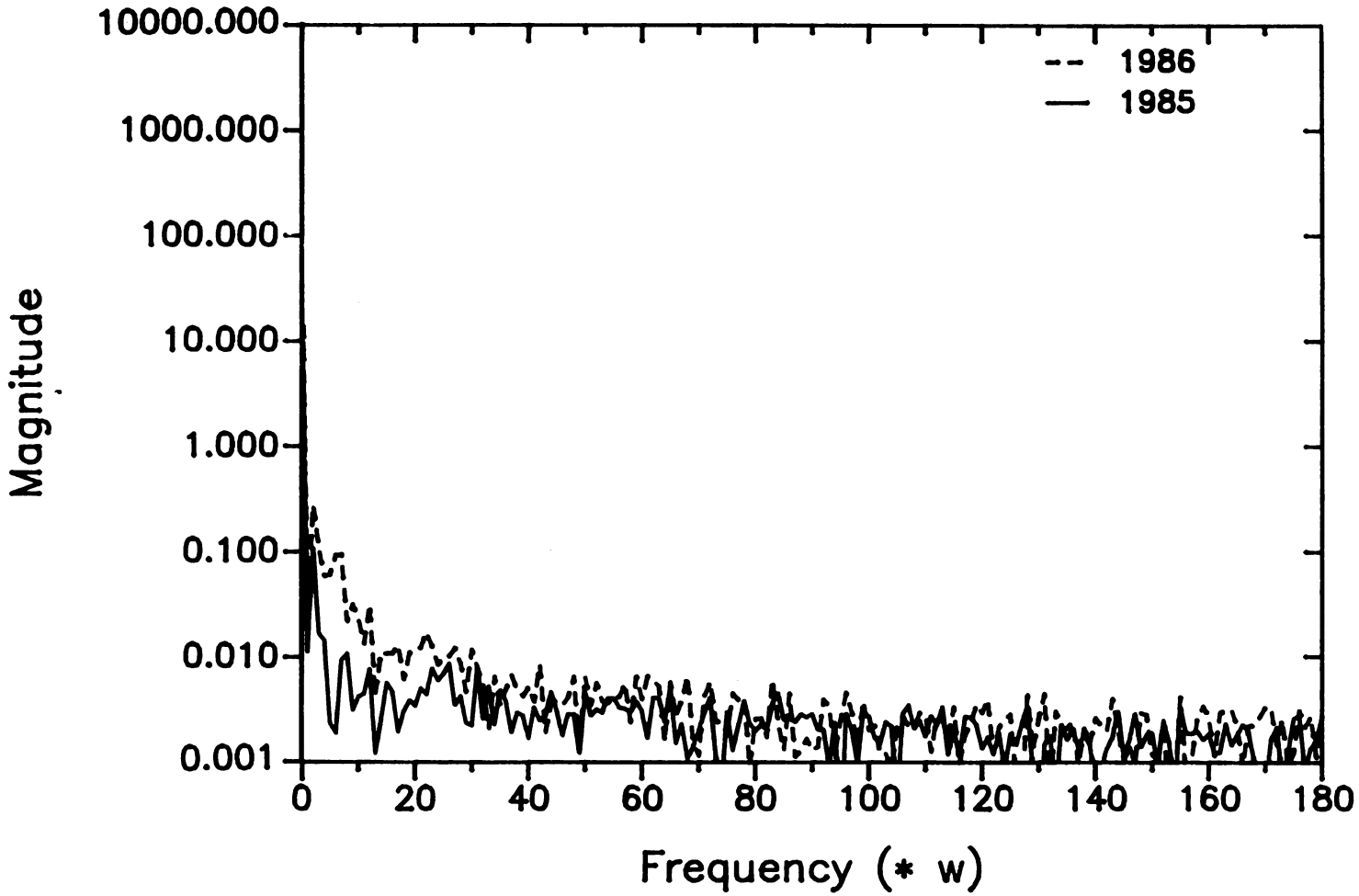

Figure 3.21 Spectral content of trunk profile 11.

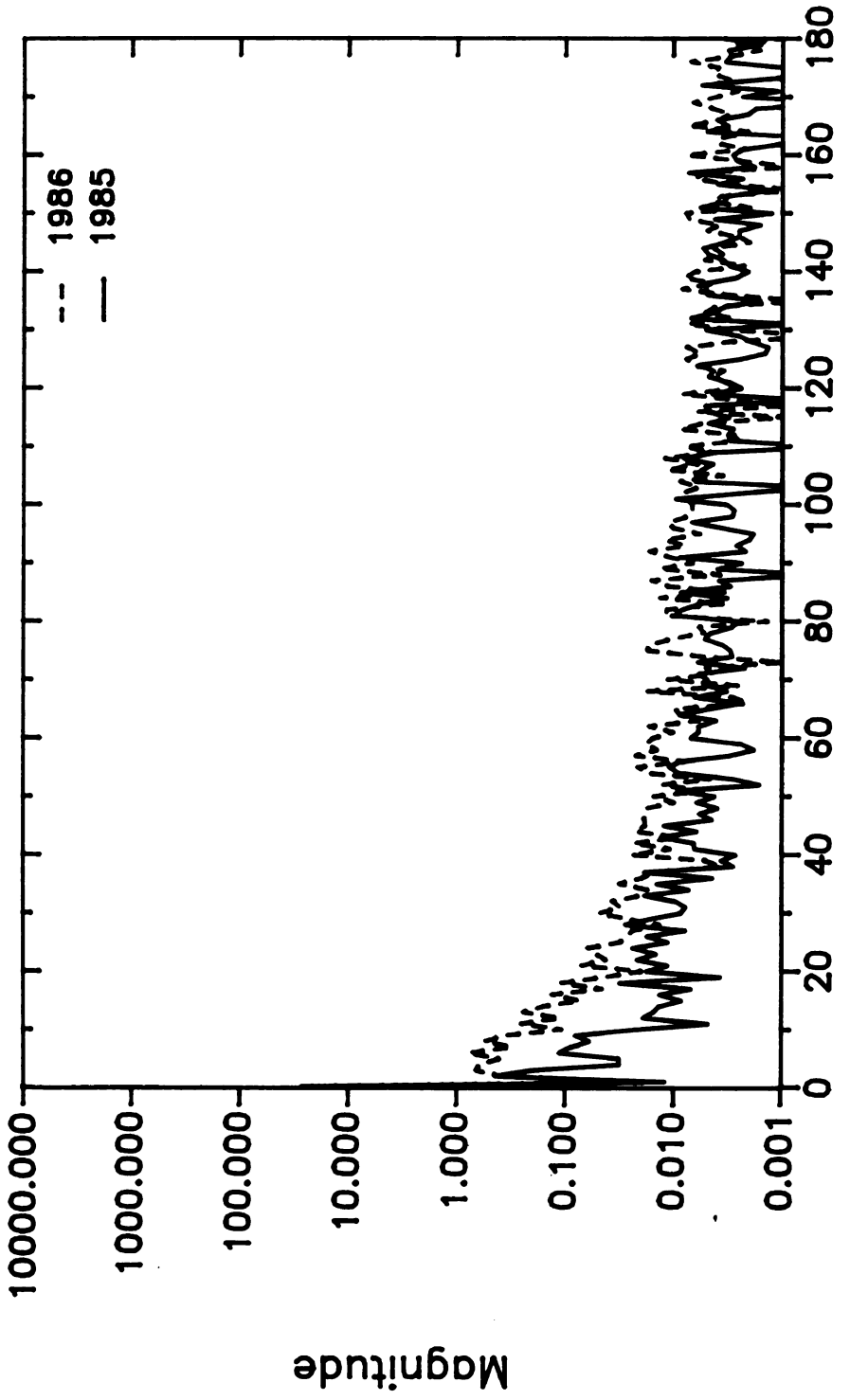

Figure 3.22 Spectral content of trunk profile A.

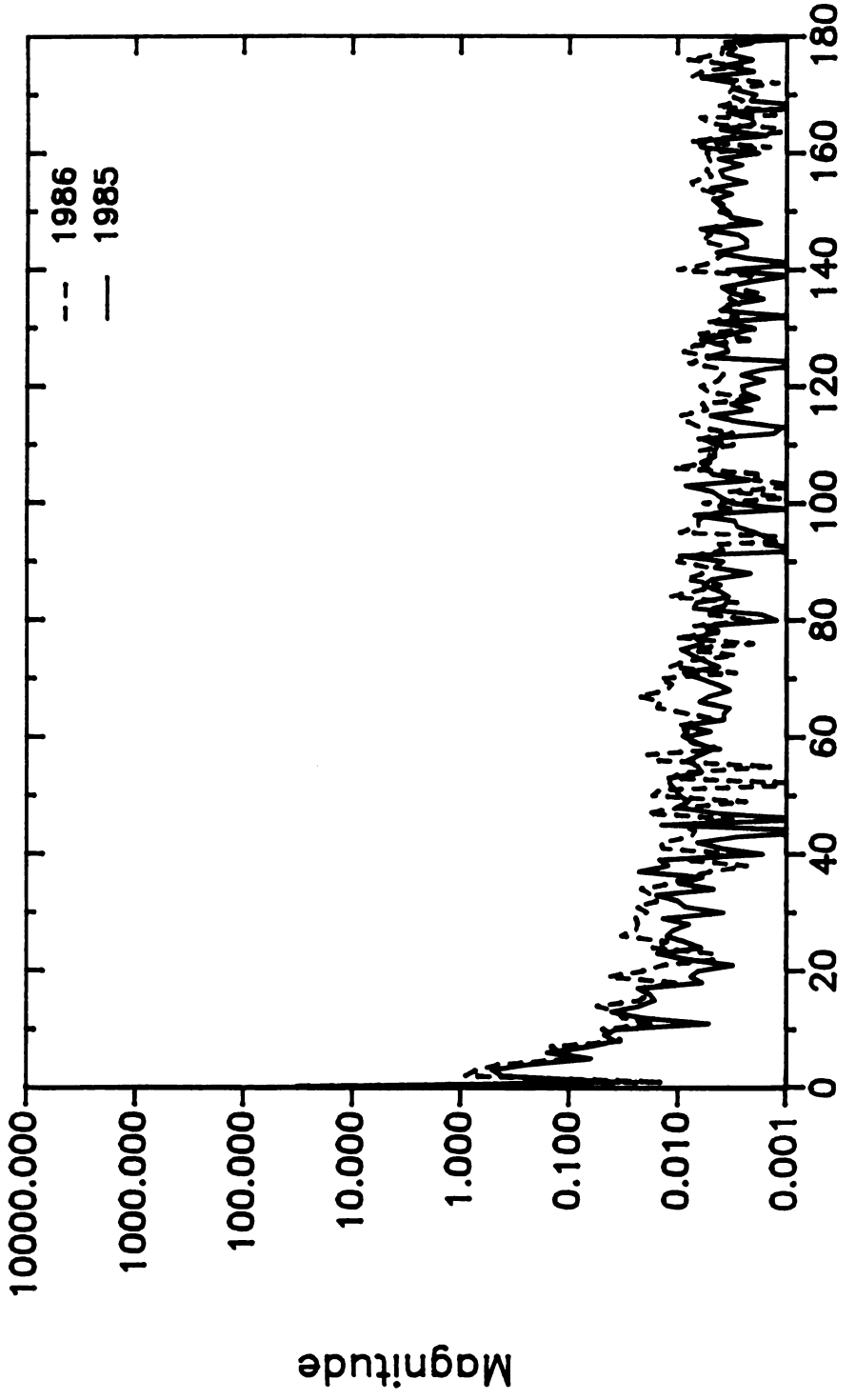

Figure 3.23 Spectral content of trunk profile 2S.

developed from rapidly changing signals. Since Trunk A was observed to have external damage and Trunk 11 had none, it may be possible to distinguish frequencies which identify external from internal damage.

Figures 3.24 to 3.26 reveal the ratio of frequency spectra for the sample profiles. Values for frequencies having original spectral contents above 0.01 are considered accurate. Trunk 2S, which had very little change is shape, shows a low spectrum ratio for the two years. Trunk 11, which had a gentle change in shape, shows a significant peak at about the 7^{th} harmonic with significant area of change from the 2^{nd} to the 15^{th} harmonics. Trunk A, on the other hand, presents its gradual peak at about the 12^{th} harmonic with important side peaks at the 4^{th}, 14^{th} and 19^{th} harmonics. Area change extends from the 2^{nd} to the 80^{th} over the other two samples.

With evidence of frequency decoding in these plots, the first 20 harmonic frequency coefficients (R_1-R_{20}) of each profile plot were normalized by dividing by R_o to eliminate the projected area differences. Frequency coefficients are tabulated in Table 3.5 for the standard geometric shapes and in Tables 3.6-3.8 for tree trunks.

A low value for the first harmonic in all profiles indicates that the origin was located at the centroid of the profile. As symmetry decreases, the odd harmonics increase in amplitude. The second harmonic is generally associated with elliptical shaping, therefore as circularity decreases

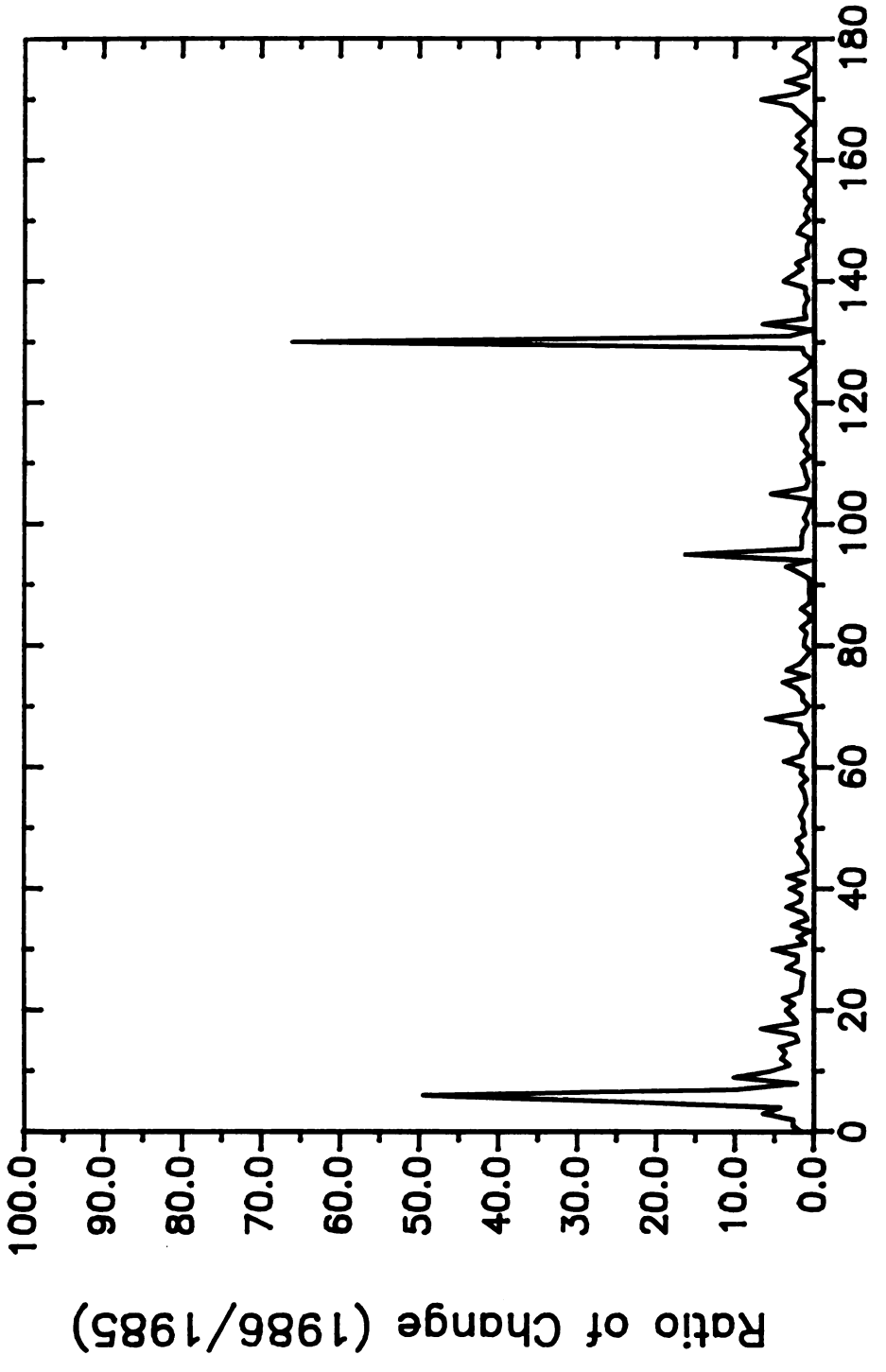

Figure 3.24 Change in spectral content – trunk 11.

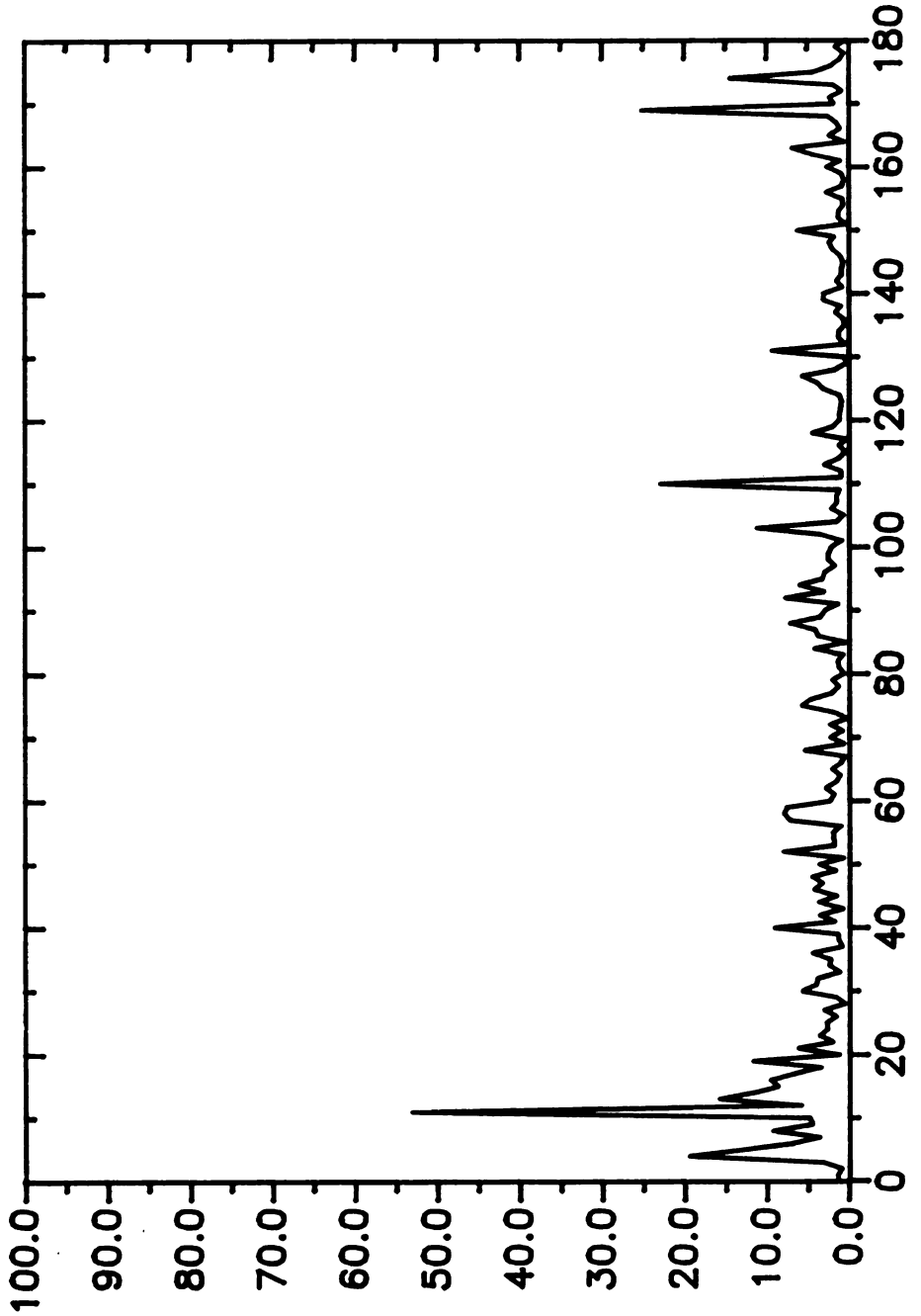

Figure 3.25 Change in spectral content – trunk A.

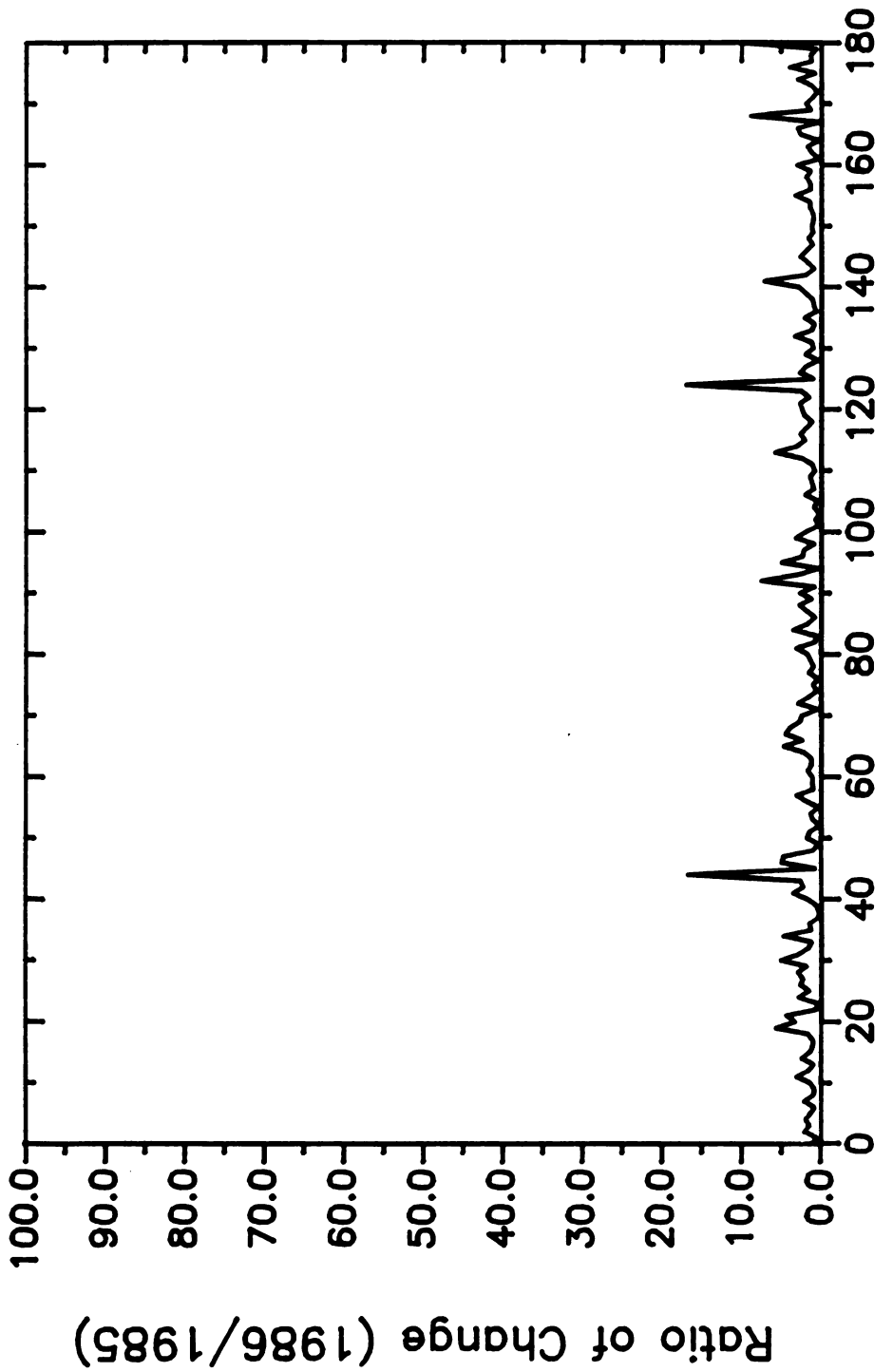

Figure 3.26 Change in spectral content – trunk 2S.

Table 3.5 Normalized Fourier coefficients for standard geometric shapes (coefficient * 10^{-3}).

Harmonic	Shape Identification		
	RECTANGLE	ELLIPSE	CIRCLE
1	0.00	0.00	0.00
2	161.16	130.41	0.00
3	0.00	0.00	0.00
4	18.10	8.65	0.00
5	0.00	0.00	0.00
6	42.52	1.15	0.00
7	0.00	0.00	0.00
8	18.11	0.00	0.00
9	0.00	0.00	0.00
10	6.03	0.04	0.00
11	0.00	0.00	0.00
12	12.82	0.00	0.00
13	0.00	0.00	0.00
14	6.03	0.00	0.00
15	0.00	0.00	0.00
16	2.92	0.00	0.00
17	0.00	0.00	0.00
18	6.02	0.00	0.00
19	0.00	0.00	0.00
20	2.92	0.00	0.00

due to tree damage, the second harmonic increases. A change in shape from circular to elliptical tends to increase even harmonics.

Cracks, which often show up in shear damage, usually occur one per tree. This appears to relieve enough strain in the bark to prevent a second crack. A crack has the effect of adding frequency content to the 1st harmonic and the higher harmonics, particularly the 3^{rd}-7^{th}.

Young trees which are of particular interest to commercial growers in terms of investment, longevity, and productivity are more adversely affected by severe shake harvesting than older, tougher trees. From the normalized frequency spectra of the young trees, it appears that in all

Table 3.6 Normalized Fourier coefficients for small trunk profiles (coefficient * 10^{-3}).

	Trunk Identification					
Harmonic	10-1985	10-1986	11-1985	11-1986	12-1985	12-1986
1	0.98	1.06	0.50	0.80	0.37	0.38
2	1.55	19.86	4.98	7.44	4.41	5.09
3	2.57	9.02	0.75	2.88	1.84	7.50
4	2.12	4.00	0.64	1.56	2.09	7.66
5	0.22	4.02	0.11	1.64	0.44	0.77
6	0.87	2.52	0.09	2.50	0.65	0.64
7	0.82	2.63	0.43	2.47	0.43	1.83
8	0.82	3.21	0.49	0.58	0.41	1.74
9	0.31	1.93	0.14	0.85	0.26	2.63
10	0.50	1.65	0.19	0.61	0.18	2.06
11	0.31	0.68	0.21	0.36	0.51	1.83
12	0.42	1.31	0.35	0.85	0.88	1.23
13	0.18	0.58	0.05	0.11	0.35	0.16
14	0.42	1.17	0.12	0.30	0.33	0.33
15	0.36	1.33	0.26	0.29	0.37	0.91
16	0.26	0.40	0.21	0.29	0.23	0.69
17	0.33	0.63	0.09	0.35	0.41	0.63
18	0.22	0.39	0.14	0.16	0.13	1.11
19	0.14	0.38	0.18	0.29	0.40	0.55
20	0.11	0.38	0.15	0.32	0.07	0.51

Table 3.7 Normalized Fourier coefficients for medium trunk profiles (coefficient * 10^{-3}).

	Trunk Identification					
Harmonic	A-1985	A-1986	B-1985	B-1986	C-1985	C-1986
1	0.21	0.23	0.44	0.28	0.31	0.30
2	7.85	5.25	4.23	7.65	13.92	6.42
3	3.63	9.15	5.90	0.79	7.63	13.26
4	0.55	8.40	3.74	6.53	5.05	2.47
5	0.55	5.59	1.82	3.33	4.50	4.77
6	2.03	10.84	0.42	2.94	2.01	3.24
7	1.54	4.23	0.29	0.97	1.04	4.05
8	1.05	7.64	0.26	2.00	0.46	4.46
9	1.43	4.88	0.30	1.16	2.32	3.44
10	0.39	1.49	0.55	2.50	2.04	2.37
11	0.08	3.49	0.35	1.61	1.89	2.63
12	0.34	1.51	0.53	2.01	0.12	2.44
13	0.27	3.35	0.60	0.42	2.32	2.63
14	0.24	2.16	0.34	1.98	0.33	2.24
15	0.15	1.00	0.37	1.95	1.90	0.66
16	0.24	1.82	0.47	0.99	1.21	2.18
17	0.12	0.63	0.33	1.25	2.65	1.04
18	0.57	1.48	0.32	0.89	1.28	0.94
19	0.06	0.59	0.28	0.72	0.08	0.20
20	0.32	0.27	0.08	0.06	0.94	0.12

Table 3.8 Normalized Fourier coefficients for large trunk profiles (coefficient * 10^{-3}).

Harmonic	Trunk Identification			
	NAN-1985	NAN-1986	2S-1985	2S-1986
1	0.26	0.36	0.45	0.16
2	10.77	11.40	5.63	10.61
3	2.35	6.17	7.04	8.30
4	1.65	3.68	3.11	5.17
5	1.81	2.20	0.84	0.92
6	0.80	1.49	2.18	1.42
7	1.17	2.77	0.93	1.73
8	0.78	1.99	0.50	0.39
9	0.63	1.53	0.65	0.43
10	0.70	1.02	0.49	0.59
11	0.23	0.31	0.07	0.19
12	0.12	0.35	0.29	0.38
13	0.18	0.08	0.56	0.42
14	0.24	0.08	0.30	0.65
15	0.26	0.14	0.22	0.26
16	0.20	0.09	0.24	0.21
17	0.11	0.35	0.32	0.26
18	0.18	0.26	0.08	0.12
19	0.19	0.14	0.10	0.52
20	0.13	0.16	0.09	0.24

cases, both circularity and symmetry have decreased after the second year of shaking. This indicates that shake harvesting may be causing tree damage and hence, a redirection of growth.

Small trees tend to exhibit most of their shape (frequency) change in the low harmonics (2^{nd}-4^{th}) indicating gradual, smooth shape changes. This may result from the fact that although the tree is smaller than a mature tree in relation to the magnitude of shaking force, the young tree puts up less mechanical resistance to vibration and hence, is more susceptible to internal damage. Furthermore, in young trees, the bark system is more sensitive to compression and shear failure. Older trees, on the other

hand, exhibit a greater resistance to shaking and thus, with an equivalent clamping pressure induce more energy dissipation at the clamp pad-tree interface and thereby invite greater external damage via splitting and stripping. Older trees therefore display their shape (frequency) change more conspicuously at the higher harmonics.

Frequency shifting was investigated in order to determine the similarity between the two profiles from year to year. Cross-correlation of the frequency spectra of the two profile plots for each tree was calculated as follows:

$$\psi_{12}(\theta) = \frac{1}{\theta_1} \cdot \int_{\omega=0}^{\omega_1} f_1(\omega) f_2(\omega+\theta)\, d\omega$$

In digital form, this appears as:

$$\psi_{12}(\theta) = \frac{1}{\theta_1} \cdot \sum_{\omega=0}^{\omega_1} f_1(\omega) f_2(\omega+\theta)$$

Cross-correlation plots are shown in Figures 3.27 - 3.29. The high values are at $\omega=0$ for all plots indicating that for the most part, frequency distribution within a profile remains the same. However, a comparison of the figures reveals that as change in shape decreases, the peak around $\omega=0$ becomes narrower. Trunk 2S for example, changes very little in shape, which evidences a sharp narrow peak in the cross-correlation plot. Trunk A on the other hand, changes shape significantly and reveals a wide peak near $\omega=0$. Therefore, changes in profile may also be revealed in cross-correlation plots.

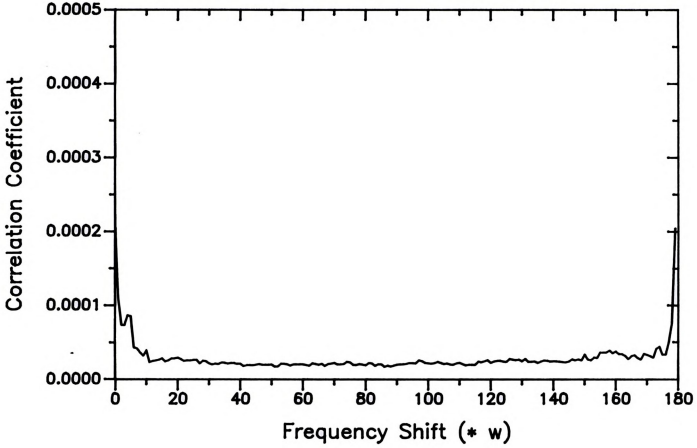

Figure 3.27 Cross–correlation of the time–spaced frequency spectra of trunk 11.

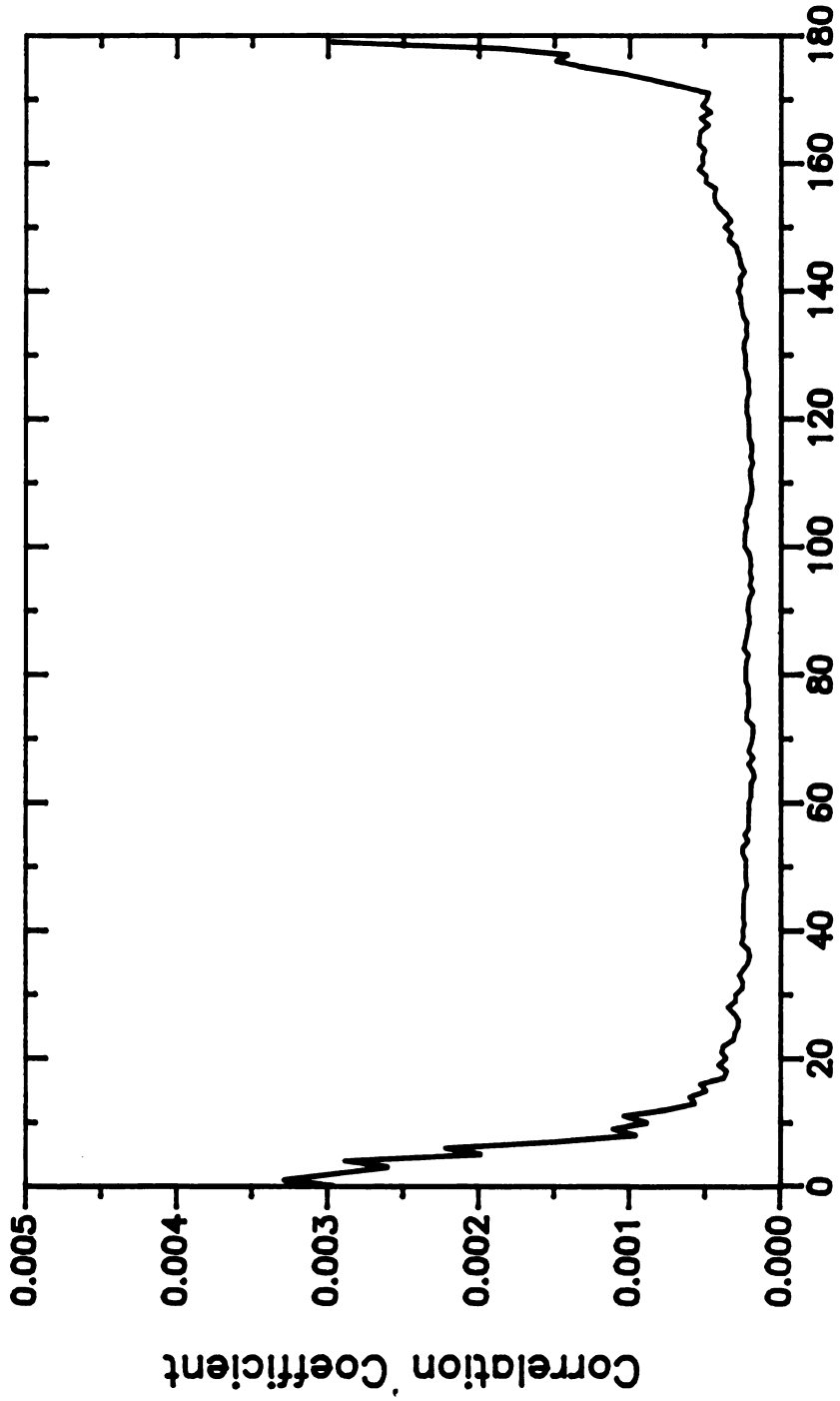

Figure 3.28 Cross-correlation of the time-spaced frequency spectra of trunk A.

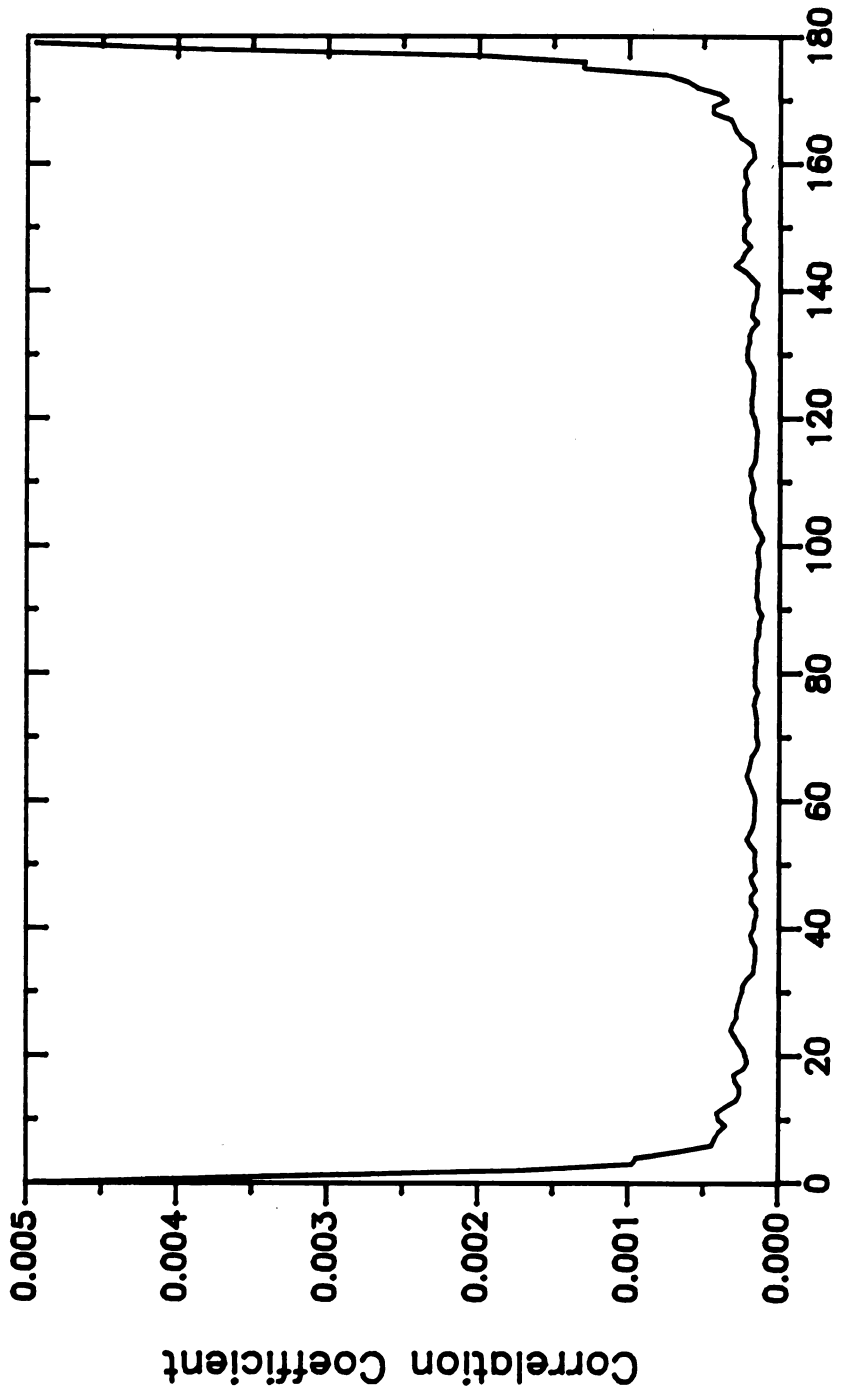

Figure 3.29 Cross-correlation of the time-spaced frequency spectra of trunk 2S.

3.5 Comment

Although this was a preliminary investigation, the methods presented in this chapter for analysis of tree trunk profiles have suggested some indicators of tree damage. Bandwidth, invariant moments, and frequency decomposition seem particularly suited to analyze the problem. Further experiments should be conducted with many tree sizes and a set of experiment controls to compare statistically the effects of wind, light, pruning, and staking, as well as shaker damage, on tree trunk shape.

The implementation of all of these techniques is quite tedious due to the effort required for digitization and processing. Advances in current technology, however, such as minicomputer imaging systems and dedicated coprocessors would make this type of analysis fast and simple. Laser optic systems capable of performing Fourier transformations optically are another possible mechanism by which this could be simplified. Advances in image processing equipment will surely aid in an endeavor of this nature.

CHAPTER 4

SPECTRAL CHARACTERIZATION OF SHAKER PATTERNS

Direct clamping of a mechanical shaker to a tree trunk has proven to be a very effective method of harvesting cherries (at least in the short run). High-powered machines currently harvest 60-100 trees/h. In recent years, orchard life expectancy has decreased from 30 years in the late 1960's to 15 to 20 years currently (Burton et al., 1986). The shaking of young trees (4 to 8 years of age), with trunk diameters as small as 5 cm (2 in.), is believed to contribute to this degeneration. Bark stripping, bark splitting, and cell damage in the phloem and cambium layers resulting from excessive shear, radial or tangential stresses induced by undesirable dynamic shaking patterns are all suspected causes of tree decline. Excessive relative displacements between the trunk and shaker may provide an indication of excessive transient dynamic stresses.

Real-time vibrations of a commercial trunk shaker and a cherry tree were analyzed and characterized according to shake pattern. Sensors and signal conditioning devices provided representation of X and Y accelerations of the tree and shaker, and the positions of the rotating masses. Waveforms were digitized, calibrated and

characterized in both time and frequency domains. Accelerations were integrated twice to give absolute displacements at the trunk shaker and the tree. Integrations were performed in the frequency domain rather than in the time domain because the time domain integrations were unstable and dominated by low frequencies.

Resulting patterns revealed extreme displacement transients during shaker start-up and shut-down resulting from passage through a low natural frequency in the system. Low frequency shaker tests confirmed this resonance phenomenon. Elimination of potentially high transient stress necessitates shaker redesign.

4.1 Commercial Trunk Shaker Design

A C-clamp fixed-eccentric mass inertial trunk shaker was obtained from the Friday Tractor Co. (Hartford, MI) for characterization of the real-time dynamic behavior of shaker-tree vibrations (Figure 4.1). The total mass of the shaker was 635 kg (1400 lb) including two 40 kg (88 lb) semi-circular unbalanced rotating masses. The radius of each mass was 17.1 cm (6.75 in.). Each mass was attached to a shaft, chain-driven by its own 2.8 L/s (44 gpm) 10,345 kPa (1500 psi) counter-rotating Vickers hydraulic vane motor.

The shaker was mounted on a 2250 Mount-O-Matic loader frame of a 42 PTO kW (56 PTO Hp) Hydro-84 International Tractor (Figure 4.2). A frame was constructed to suspend the shaker at the three points recommended by the manufacturer. Rubber bushings on both ends of the three

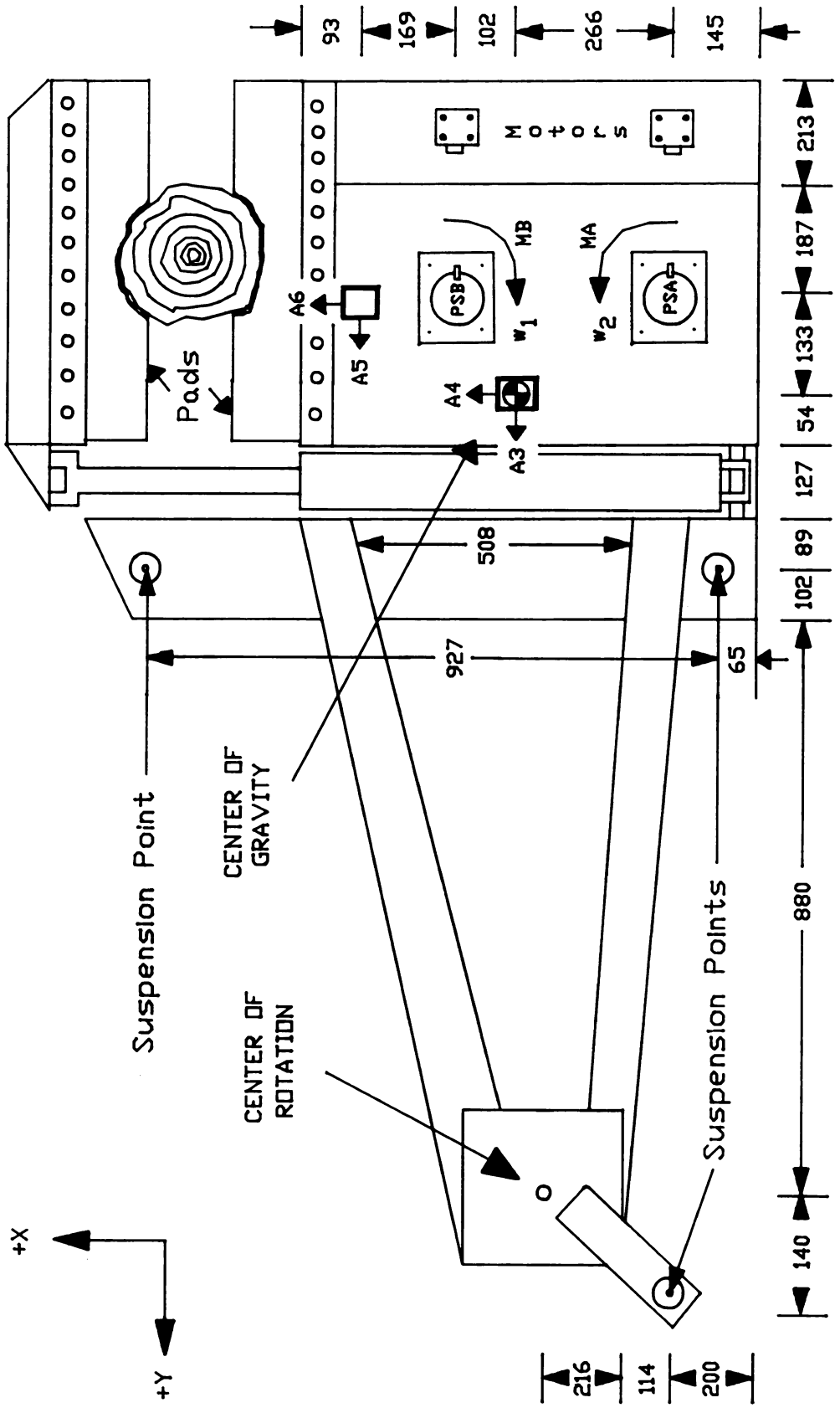

Figure 4.1 Dimensioned C-clamp trunk shaker showing accelerometer and proximity sensor locations. (All measurements in mm).

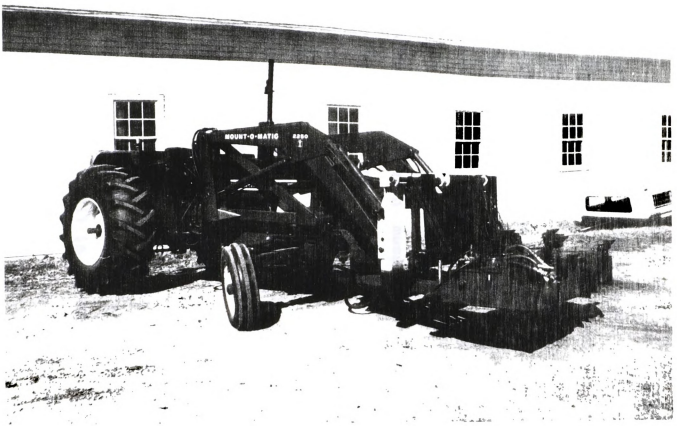

Figure 4.2 C–clamp trunk shaker harvester for cherries mounted on a Hydro–84 International Tractor.

suspension bars isolated shaker vibrations from the tractor.

A separate PTO-driven hydraulic system mounted on the rear of the tractor powered the shaker drive motors. A 35 tooth sprocket on the PTO stepped up the pump driven speed 2.7:1 to a 13 tooth sprocket on a Hydreco hydraulic gear pump. A 150 L (40 gal) reservoir, equipped with a return line oil filter and master shut off valve, was mounted above the PTO and pump. Hoses of 1.9 cm (0.75 in.) ID distributed fluid from the pump to a flow divider for equal allocation to continuously variable, pressure-compensated flow control valves controlling each shaker drive motor. Separate valves regulated oil flow to each shaker drive motor such that the angular velocity of each mass could be independently selected. A 45 tooth motor sprocket then stepped up mass velocity by chain driving an 18 tooth sprocket on the mass shaft.

A double acting 8 cm ID x 61 cm stroke (3 in. x 24 in.) hydraulic cylinder activated the C-clamp for trunk gripping. Cylinder pressure was derived from the tractor's hydraulic system. At 12,415 kPa (1800 psi), the hydraulic system could provide 0.4 L/s (6.3 gpm) at 1500 engine r/min and 0.7 L/s (11.0 gpm) at 2200 engine r/min. Clamping pressure was set at 4,830 kPa (700 psi) in a separate circuit; the clamping pressure was unaffected by operation of the shaker motor drives.

Two cylindrical rubber pads (19 cm OD, 8 cm ID, and 55 cm long, 7.5 in. x 3.0 in. x 21.5 in.) were fastened in

support slings in the clamping jaw. A lubricant was applied to each sling per manufacturer's recommendations; the sling was then covered with an attached rubber flap prior to shaking to reduce shear force on the tree bark by providing a slip surface between the sling and flap.

During operation, the loader frame tilt mechanism was used to set the shaker perpendicular the the trunk at the point of tree attachment (thereby minimizing shear forces). Clamping pressure for shaking 6.5 cm (2.5 in.) to 16.5 cm (6.5 in.) diameter trunks was set at 4,830 kPa (700 psi) as recommended by Frahm et al. (1983) and monitored on the hydraulic system with a 10,345 kPa (1500 psi) pressure gage. Clamping circuit check valves prevented clamp movement during shaking (Affeldt, 1984).

During shaking, engine speeds of 1500 and 2200 r/min, corresponding to pump outputs of 1.9 L/s (30 gpm) and 2.5 L/s (40 gpm), respectively, at 10,345 kPa (1500 psi) provided shake frequencies of 9-10 Hz (560-600 c/min) and 14-15 Hz (840-900 c/min) according to the design equation:

$$\text{Frequency (Hz)} = \frac{[\text{Engine R/MIN} - 100] * 0.4}{60}$$

Engine and PTO r/min were monitored on the tractor tachometer.

I needed the engineering parameters for the trunk shaker in order to analyze the tree-shaker system. The shaker center of gravity (shown in Figure 4.1) was found by balancing the machine on the tip of a 5 cm x 5 cm (2 in. x 2

in.) piece of angle iron on two orthogonal axes (Affeldt, 1984).

Spring and damping coefficients for the three-point shaker suspension design were found by testing (Esch, 1986). A rectangular, rigid steel test frame was constructed around the trunk shaker body and attached to the tractor loader frame which supported the shaker. One side of the test frame was then attached to a vertical steel girder in the engineering machine shop to provide absolute rigidity. The shaker (suspended from the loader frame in its operating position) could then move with no vibration feedback from the loader frame.

Spring coefficients for the shaker were found by applying a force to the shaker body in one of the three directions X, Y, or θ, and measuring the corresponding displacement (Table 4.1). The point of force application on the shaker for each directional test was selected as the point which, when force was applied, caused motion only in the desired direction. A Linear Variable Differential Transformer (LVDT), mounted between the rigid test frame and the shaker, provided an electric signal proportional to shaker displacement. A 2.2 cm ID x 7.6 cm stroke (0.875 in. x 3 in.) 48,275 kPa (7000 psi) hydraulic cylinder, also mounted between the rigid frame and the shaker body, equipped with a pressure transducer provided a signal proportional to cylinder pressure.

Transducer signals were collected in an Analogic Data

Table 4.1 Linearized spring and damping coefficients for a C-clamp eccentric mass inertial trunk shaker for cherries.

Direction	Masses Installed		Masses Not Installed
	Damping (ζ) (%)	Spring (K) (N/mm)	Spring (K) (N/mm)
X	0.18	86.0	70.4
Y	0.16	153.2	137.2

6000 Waveform Analyzer (Analogic Data Precision, Danvers, MA) for calibration. Pressure signals were converted to forces via multiplication by the appropriate cylinder inside area. Data were plotted as force versus displacement with the slope equal to the suspended shaker spring constant. Calculations revealed linear spring constants of 86.0 N/mm (490 lb/in.) in the X direction and 153.2 N/mm (875 lb/in.) in the Y direction with small displacements of 7.6 cm (3.0 in.) about the shaker's equilibrium point. For larger displacements, spring coefficients became nonlinear.

The same system was used for determination of the damping ratio (ζ). The hydraulic cylinder was equipped with a quick release mechanism. The shaker was displaced to a maximum position in the desired test direction (X, Y, θ), then released instantaneously to allow free swing. Displacement traces from the LVDT provided data for determination of damping ratios via the Logarithmic Decrement Method.

Table 4.2 Linearized spring (K) and damping (ζ) coefficients and natural frequencies (ω_n) for Montmorency cherry trees.

Property	Tree Diameter (cm)		
	6.5	11.0	16.5
K (N/mm)	12.7	144.5	657.9
ζ (%)	0.12	na	na
ω_n (r/s)	2.8	na	na

na: not available

A similar procedure was used to obtain the spring and damping coefficients for several cherry trees of different sizes (Table 4.2). The higher spring coefficients of larger trees made determination of damping coefficients unreliable with the equipment utilized.

Damping ratios for the shaker appeared constant over the displacement range tested. Cherry tree shakers normally operate at less than 3.8 cm (1.5 in.) peak-to-peak displacement. Since spring and damping coefficients were linear over this range in laboratory testing, a linear, second-order, lumped mass vibration model was used to compare spring and damping coefficients found in the laboratory with values calculated from free (unloaded) shaker displacement traces:

$$X = x + e \cdot \sin\omega t$$

$$(M-m)\ddot{x} + m \frac{d^2}{dt^2}(x + e \cdot \sin\omega t) = - Kx - C\dot{x}$$

$$M\ddot{x} + C\dot{x} + Kx = (me\omega^2)\sin\omega t$$

Where:

M = Mass of shaker
m = Mass of rotating unbalance
C = Shaker damping property
K = Shaker spring property
e = Eccentricity of rotating unbalance

The general solution is:

$$X(t) = X_1 e^{-\zeta\omega_n t} \cdot \sin(\sqrt{1-\zeta^2}\ \omega_n t + \phi_1) + \frac{me\omega^2 \cdot \sin(\omega t - \phi)}{\sqrt{(K - M\omega^2)^2 + (C\omega)^2}}$$

Where:

ω = Natural system frequency (rad/s)

$\zeta = C/C_n = C/2m\omega_n$ = Damping Ratio

$$\text{Tan}\ \phi = \frac{C\omega}{K - M\omega^2} = \frac{2\zeta(\omega/\omega_n)}{1 - (\omega/\omega_n)^2}$$

The resonant amplitude is then:

$$\frac{MX}{me} = \frac{(\omega/\omega_n)^2}{\sqrt{(1 - (\omega/\omega_n)^2)^2 + (2\zeta(\omega/\omega_n))^2}}$$

Therefore:

$$X = \frac{(me/M)}{2\zeta} = X_{res}$$

And:

$$X = \frac{me}{M} = X_{ss}$$

Finally:

$$\zeta_i = \frac{X_{ss}}{2X_{res}}$$

Data for theoretical calculations are shown in Table 4.3.

Table 4.3 shows close agreement with the actual coefficients for free shake. Very little change from free shake to tree shake was observed; this indicates that in a

Table 4.3 Theoretical damping ratios for a C-clamp eccentric mass trunk shaker.

Shake Condition	Damping Ratio			
	ζ_1	ζ_2	ζ_3	ζ_{ave}
Free Shake	0.19	0.22	0.18	0.20
6.5 cm Trunk	0.25	0.25	0.27	0.26
11.0 cm Trunk	0.22	0.25	0.19	0.22
16.5 cm Trunk	0.25	0.30	0.33	0.30

dynamic state, the shaker appears to dominate. Tree properties tend to have little effect on the shaker vibration possibly because of the large mass of the shaker body and rotating masses in comparison with the effective mass and stiffness of the tree.

Finally, the center of rotation of the shaker (shown in Figure 4.1) was found by locating the coordinates of the node where no X or Y displacement occurred during torsional vibration. This center of rotation is greatly displaced from the shaker center of gravity due to the force distribution in the suspension bars created by the suspension system. The center of rotation with the tree attached may likely differ from this free suspension rotation point.

4.2 Instrumentation for Vibration Sensing

Three accelerometers, two at one location and one at a third, were strategically placed on both the trunk shaker

and a tree in order to characterize planar motion (X, Y, θ) in real time. On the shaker, two accelerometers were placed at the base of the pad on the shaker frame (Figure 4.1) to detect X and Y motion (A5, A6) while a third was placed at the shaker center of gravity to detect X motion (A4). A fourth sensor (A3) was placed in the Y direction at the shaker center of gravity to verify corresponding signals.

Two 0.8 cm (0.3 in.) diameter holes were drilled radially in each tree trunk 90^{o} apart and 46 cm (18 in.) above the ground plane. A single X axis accelerometer was placed in one hole while a 16 cm^3 (1 $in.^3$) aluminum block was mounted in the second hole with an X and Y accelerometer attached (A0-A2, Figure 4.3).

Sunstrand (Sunstrand Data Control, Inc., Redmond, MA) accelerometers were used in all tests. The accelerometers had natural resonant frequencies of 40 kHz, well above the shaker vibration range, and time constants of 20 μs, providing frequency response of 0.02 to 5000 Hz with 5% underestimates at the low frequency end and 5% overestimates at the high frequency end. With an expected shaker-tree response spectrum of 0.1 to 30 Hz (complex vibration of two 15 Hz rotating masses), the transfer function of these sensors for this application was almost exactly 1.0. The acceleration range was ± 250 g (1 g = 9.8 m/s^2) with ± 1 % amplitude linearity.

Calibration of accelerometers was accomplished by constructing a vibration table consisting of a 40 oz (1135

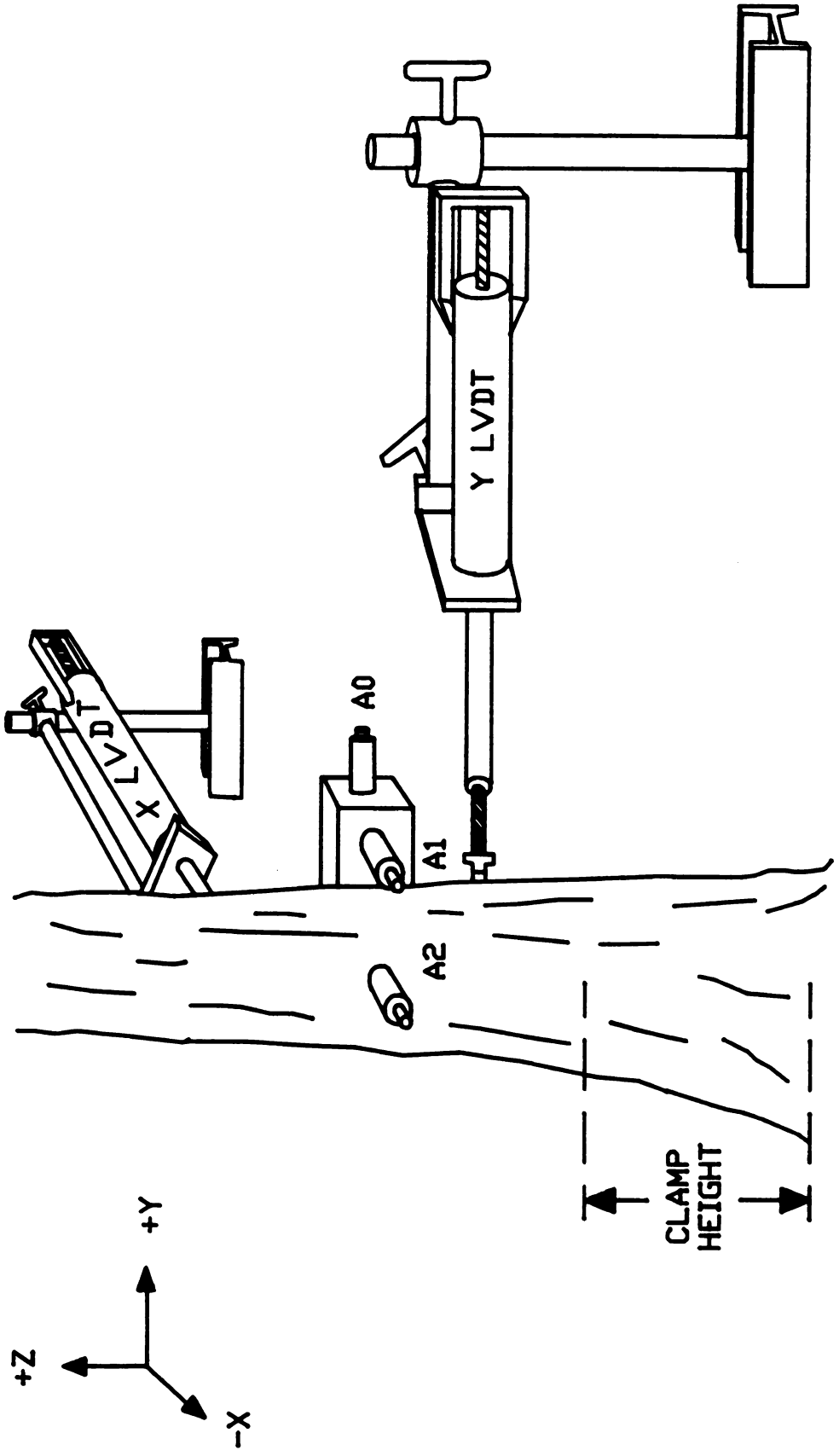

Figure 4.3 Sensor locations on a cherry trunk.

g) magnet loud speaker firmly mounted onto a laboratory frame. A test accelerometer was mounted onto the speaker along with with a calibrated (National Bureau of Standards (NBS) traceable) accelerometer of the same frequency specifications. The speaker was driven by a frequency generator capable of generating white noise. The driving signal was band-limited from 0 to 100 Hz.

Output signals from the two accelerometers were fed into a Hewlett Packard 5423A Structural Dynamics Analyzer through an HP 54410A A/D Converter. Spectra for each signal were calculated and then the transfer function, in magnitude and phase, was derived between the two. This provided a calibration reference to the NBS-traceable standard for all test accelerometers.

Since the vibration amplitude of the speaker was very small in comparison with vibration amplitude of the mechanical shaker, the accelerometers were also calibrated in a separate test for output voltage per unit displacement by mounting them on a swash-plate driven, reciprocating plunger (Affeldt, 1984). Plunger displacement was 1.09 cm (0.43 in.) at an operating frequency of 11.3 Hz (676 c/min). The signal output was amplified with a Piezotron Coupler or a Kistler Model 503 charge amplifier, then integrated twice by hardware integrators. Displacement signals were recorded on the Data 6000 and analog tape recorders for reference and calibration.

Proximity sensors (PSA & PSB, Figure 4.1), operating on

electromagnetic induction principles, were mounted to monitor frequency and angular position of each eccentric mass. A steel gear was mounted on each shaft to cause the flux changes in the magnetic field necessary for sensing by the nearby coil. Each gear had one tooth removed. This gap was aligned with the radial position corresponding to the center of mass of the rotating mass, thereby providing a reference mark to determine mass position in the output data.

Proximity sensor pulse shape was uniform except at the gap where an extra half pulse was produced. Pulse voltage was proportional to angular shaft velocity and was adjusted by changing the gap between the sensor head and the gear teeth. Mass position at any time was determined by counting the pulses since the last reference pulse and referring this to the number of teeth on the particular gear in use. The more teeth on the gear, the higher the angular resolution. Because of waveform analyzer speed and memory limitations, the pulse frequency was limited to 25% of the digitizer frequency (Nyquist demands at least 50%), thereby limiting the number of teeth.

Two LVDT's were available for vibration sensing along with the accelerometers. LVDT's are more accurate at low frequencies and would therefore complement the accelerometer response as verification. These sensors were connected to measure displacement in both the X and Y Cartesian directions on the tree (Figure 4.3). The LVDT's were just

below and vertically aligned with the X and Y accelerometer sensors to directly record trunk displacement. In free shake tests, a small 5 cm x 10 cm (2 in. x 4 in.) board was placed in the clamp, to which all tree sensors were attached. A Daytronic Model 300C amplifier with a type 61 module provided a 3 V excitation for the LVDT. Output voltage was linearly proportional to rod displacement on the ± 0.025 cm (± 0.010 in.) scale and ranged from ± 40 mV DC.

Planar motion of the tree (X,Y) made it necessary to modify the attachment mechanism of the LVDTs such that "crosstalk" caused by motion perpendicular to the LVDT's sensing direction would be minimized. This was accomplished by constructing a frame around each LVDT to which the back end of the LVDT slide rod could be attached via a light spring (Figure 4.3). This spring provided tension on the rod to pull it away from the trunk and eliminate binding. The front end of the rod was then fitted with a 3.0 cm (1.2 in.) long 0.2 cm (0.08 in.) diameter spring which provided no flexure in the longitudinal direction but maximal deflection in the lateral direction. By preforming the spring with a small vertical bend, "crosstalk" from motion perpendicular to the desired sensing direction was minimized.

Finally, displacement was recorded simultaneously through a high-speed photography system (Marshall, 1986). A matrix of high intensity light emitting diodes (LED's) strategically located at points on the tree and harvester

was filmed at high speed from a stationary camera during shaking. Developed film was then projected frame-by-frame onto a screen with a movie camera, imaged onto a color monitor, and digitized to record the position of each LED as a function of time in order to trace the motion of the shaker with time. In analyzing the data, this provided an excellent check on lower frequency vibrations not limited in accuracy by film speed, optic distortion, LED point source dimension, or imaging resolution.

Three Piezotron couplers provided a current source and amplified the accelerometer signals on the tree. Six Kistler Model 503 charge amplifiers coupled the accelerometer signals from the shaker. All direct and amplified transducer signal carrier lines were connected to recording devices. A four and a fourteen channel Racal Instrumentation Tape Recorder (Racal Recorders Inc., Covina, CA) were used to record accelerometer and mass position sensor signals. These instruments provided a bandwidth of DC to 5000 Hz on a tape speed setting of 190.5 mm/s (7.5 in./s) with a signal-to-noise ratio of 48 dB at 0.35% P-P Flutter and ± 0.2% tape speed inaccuracy. An Analogic Data 6000 Waveform Analyzer was capable of recording another four channels of data at 100 kHz and storing data on a floppy disk. During most field tests, recording equipment was stationed in an air-conditioned van which provided protection from dust and temperature effects.

A Vanner Model 80-500 (12 VDC to 120 VAC, 60 Hz, 500 W)

voltage inverter was connected to the van battery to provide 120 VAC instrument power (Vanner Corp., Columbus, OH). Ground potential was obtained through a #12 stranded copper wire clamped to a galvanized steel rod driven 76 cm (30 in.) into damp soil at a distance of 1.5-2.5 m (5-8 ft.) from the van.

4.3 Displacement Tests

Displacement tests were conducted on Montmorency tart cherry trees in the Michigan State University Horticultural Orchards. All trees were in the same general location and were presumed to have the same soil base. Nine trees were shaken, each at 1500 shaker r/min and then at 2200 shaker r/min. These speeds provided individual mass frequencies of 9 and 16 Hz. The actual vibration transmitted to the tree was a complex combination of frequencies.

Three trees of 6.5 cm (2.5 in.), three of 11.0 cm (4.5 in.), and three of 16.5 cm (6.5 in.) trunk diameter at clamp height were selected for testing. The shaker clamp was positioned orthogonal to the tree trunk at 25 to 30 cm (10 to 12 in.) clamp height according to common practice and was closed with the tree centered in the pads. Clamping pressure was 4,830 kPa (700 psi). The pad slings and flaps were greased prior to each test series. A test at each engine speed was also conducted for free shake (no tree in the clamp).

The following were recorded: date, engine r/min, tree identification data, clamp height above soil surface and

accelerometer location with respect to the trunk center and the soil surface.

All amplifiers were zeroed before each test. The LVDT slide rods were centered for zero readout. The desired engine speed was obtained and the data recorders were initialized. After 1 to 2 s, the operator was signaled to begin the shake. A shake lasted 3 to 6 s. The operator was then signaled to end the shake; there were 2 to 3 s of shut down data at the end of the acquisition period.

Data were recorded on magnetic tape and floppy disk. While data were being stored on the floppy disk, the LVDT's were rezeroed and the shaker body was propped with blocks to prevent vertical clamp slippage on the tree due to hydraulic system relaxation. The process was repeated for each tree such that all instrument settings and clamping pressures were the same at the start of every run.

Data digitized into the Data 6000 Waveform Analyzer were collected at a speed of 500 Hz over a 16.4 s trial period for a total of 8192 (2^8) points per waveform. This point count was significant for the Fourier Transforms used in the data analysis.

4.4 Frequency Domain Analysis

In the laboratory, acceleration and LVDT data were transferred from magnetic tape to the Analogic Data 6000 Waveform Analyzer for digitization and storage on a floppy disk. The LVDT data were calibrated directly in the memory

of the Data 6000 using the appropriate linear calibration equation, then plotted using a Hewlett Packard 7475A plotter.

Mass position data on magnetic tape were also digitized in the Data 6000 as well as transferred to the input port of a 16 channel 12 bit analog-to-digital converter (Interactive Structures, Inc.) for digitization into an Apple III minicomputer. Although the Data 6000 is capable of digitization rates up to 10 MHz, memory limitations (14 kbytes per channel) prevented capture of long, high frequency waveforms. The Apple III can digitize up to 20 kHz with memory allocations up to 256 kbyte. Digitized proximity data were then transcribed to floppy disk for later retrieval and analysis.

Proximity sensor data existed in the form of sinusoidal pulses over the period of the test with interspersed half pulses resulting from the missing tooth indicator of the mass' center of gravity. For analysis, a UCSD (University of California, San Diego) Pascal program was written to convert pulse data to frequency by converting the time between pulses into frequency, averaging frequency over one half mass revolution if the frequency was within 10% of the desired operating frequency, and storing/presenting output as frequency versus time with markers identifying the points at which the mass center of gravity passed the proximity sensor. If frequency was not within 10% of the desired operating value, no averaging was performed. Instead,

frequency was plotted directly with the assumption that a rapidly changing start-up, shut-down, or disturbed zone of operation of prime interest was occurring.

Time domain integration of accelerometer data on the Data 6000 Waveform Analyzer produced unrealistic results for displacements because integrated low frequencies masked the higher frequency shaker vibration of interest. To circumvent this problem, frequency domain analysis of the accelerometer data was performed on an IBM PC AT. Data 6000 floppy disks were IBM format compatible although file headers and data were stored in a non-standard binary-coded integer format. I wrote a Microsoft Pascal program (Microsoft Corp., Bellevue, WA) on an IBM PC AT to read a Data 6000 data diskette, decode the header and data values, and restore the information in ASCII format. Data were then suitable for normal programming access.

I also wrote a Spectral Analysis Program in IBM Professional Fortran (Ryan-McFarland Corp., IBM Corp., Boca Raton, FL) to read decoded acceleration files, calibrate data, and convert time domain information into the frequency domain with a Decimation-In-Time (DIT) Cooley-Tukey Fast Fourier Transform (FFT) algorithm which uses the discrete Fourier Transform in a bit-reversed butterfly routine:

$$A(k) = \sum_{n=0}^{N-1} A(n) \cdot \exp^{-i2\pi nk/N}$$

$$k = 0 \ldots N-1$$

Double integration of time domain data was performed on the

frequency domain acceleration data by dividing complex frequency components by ω^2:

$$f(t) = F(\omega) \cdot e^{j\omega t} \cdot \frac{d\omega}{2\pi}$$

$$\frac{df(t)}{dt} = F(\omega) \cdot e^{j\omega t} \cdot j\omega \cdot \frac{d\omega}{2\pi}$$

$$g(t) = \frac{df(t)}{dt} \quad \text{where} \quad g(t) = G(\omega) \cdot e^{j\omega t} \cdot \frac{d\omega}{2\pi}$$

$$G(\omega) = j\omega \cdot F(\omega)$$

Therefore:

$$F(\omega) = \frac{G(\omega)}{j\omega}$$

Then, with the data:

$$A(k) = Ae^{i\omega t} = A\cos\omega t + i\sin\omega t = c + di$$

$$k = 0 \ldots N-1$$

$$\omega_0 = (2\pi * f_{sampling})/N$$

$$\omega = \omega_0 * k$$

$$X(k) = A(k)/\omega^2$$

$$k = 1 \ldots N-1$$

Integration of the zero frequency is simply integration of a constant (DC):

$$A(k) = Ae^{i\theta t} = A\cos\theta t + iA\sin\theta t = c + 0i$$

$$X(k) = c * t^2$$

and was not performed since any DC in the data was a result of amplifier bias. The DC was thus zeroed out in the frequency domain since integration would allow it to obliterate the higher displacement frequencies of interest.

The boundary conditions for double integration were as

follows:

$$x(0) = 0 \qquad \dot{x}(0) = 0$$
$$x(\infty) = 0 \qquad \dot{x}(\infty) = 0$$

Low frequencies resulting from amplifier drift (often exponential with a very long period) obscured true data and were filtered by modifying the frequency sequence with a Hanning (cosine squared) Window:

$$w(t) = \cos^2 \frac{\pi t}{\tau} = \frac{1}{2} \cdot (1 + \cos \frac{2\pi t}{\tau}) \text{ for } |t| \leq \frac{\tau}{2}$$

$$= 0 \text{ elsewhere}$$

The Fourier Transform of the Hanning Window is then:

$$W(f) = \frac{\tau}{2} \cdot \frac{\sin \pi f\tau}{\pi f\tau} \cdot [1/(1-(f\tau)^2)]$$

Cutoff frequencies used in the filtering process were determined by comparing the frequency content of the contaminated acceleration signal with an uncontaminated acceleration signal from another sensor and with the LVDT displacement traces. LVDT's were very accurate at low frequency response and were reliable as a standard for comparison.

Convolution of a time domain sequence for filtering purposes transforms into a frequency domain multiplication. Therefore, by multiplying the frequency domain acceleration data with the Fourier Transform of the window function, time domain filtering results:

$$A(n) = A(k) * W(f)$$

$$= \sum_{k=0}^{N-1} a(k) \cdot w(n-k)$$

Initial filtering in some displacement traces indicated an insufficient frequency filter weighting. Therefore, the acceleration data (originally 8192 points) were doubled in number by linearly interpolating a midpoint between every two successive data points. All other factors remaining the same, the resolution doubled, the filter weighting thereby changed, and the filtering process for these waveforms was significantly more effective.

Although this process appears to contradict the Nyquist theory, the error introduced is small when the waveform is periodic and repeatable. The sacrifice made is in accuracy of peaks and areas of rapidly changing signal, which may be drastically over or under-estimated. Here, where the waveform is known and verifiable, the application of this method provides the weighting necessary for data filtering.

An Inverse Fourier Transform was performed to transform the data back into the time domain by reprocessing data through the same FFT routine with the sign of the exponent reversed and dividing final coefficients by N:

$$X(n) = \frac{1}{N} \sum_{n=0}^{N-1} X(k) \cdot \exp^{i2\pi nk/N}$$

$$k = 0 \ldots N-1$$

Final displacement data were plotted as X versus time, Y versus time, and X versus Y; the latter of which provided a planar view of the tree or shaker vibration pattern.

Piezoelectric accelerometers are more accurate at higher frequencies and the LVDT is more accurate at lower

frequencies. Therefore, linear X and Y displacement traces of the tree derived from acceleration data were compared with LVDT traces for verification.

4.5 Displacement Results

Excessive displacements occurring during the transient start-up and shut-down phases of shaker operation have been referred to as shaker "gallop". Gallop is an unintended magnification of shaker displacement beyond the design, operating, safe, or steady-state limits. This motion is normally but not necessarily transmitted to the tree in an observable fashion. By analysis of the dynamics of shaker and tree, gallop and its causes may be identified and controlled or eliminated.

The rotating masses of the shaker tended to come up to speed in about 0.35 s in these tests, and to overshoot or "gallop" as shown in Figures 4.4-4.12. This is typical of an underdamped second order linear system and can be modeled by a system where $\zeta < 0.707$. Overshoot may result from loading of the hydraulic pump with the full inertia of the masses. This loading is transmitted to the power source (the tractor) which relies on the governor to bring the engine speed back to steady-state. Shut-down of mass rotation required 2 to 3 s and often exhibited a gallop at about 1.5-2.0 Hz rotating frequency, possibly due to low natural modes of the shaker and tree resulting in a "beating" or "frequency pulling" phenomena.

Figure 4.4 and 4.5 show the inner and outer rotation

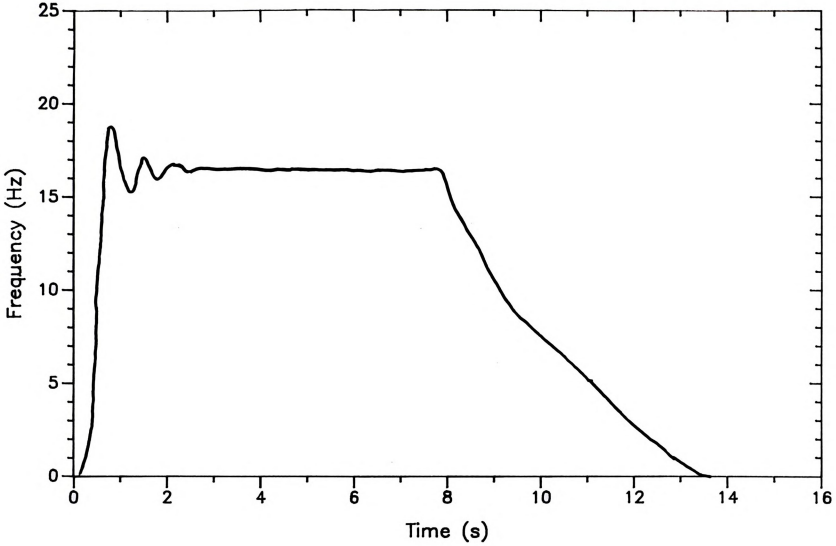

Figure 4.4 Angular velocity of inner mass during a 15–16 Hz free shake when both masses are operating.

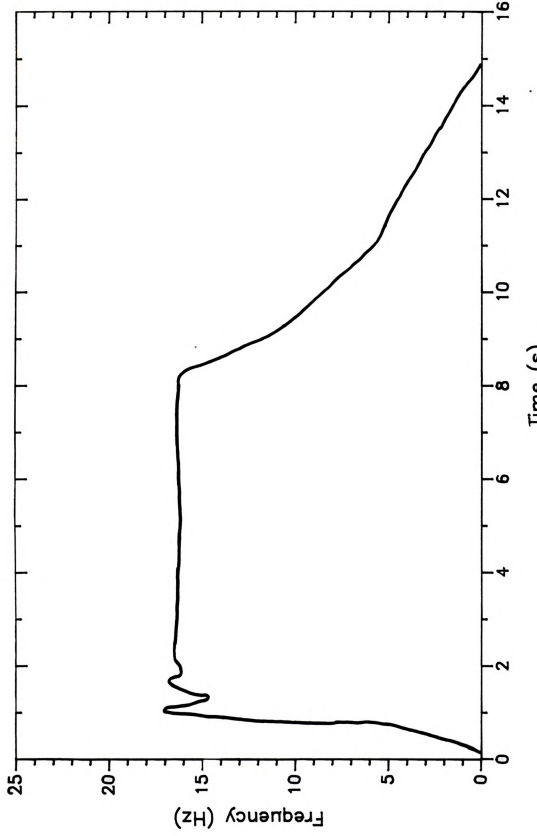

Figure 4.5 Angular velocity of outer mass during a 15–16 Hz free shake when both masses are operating.

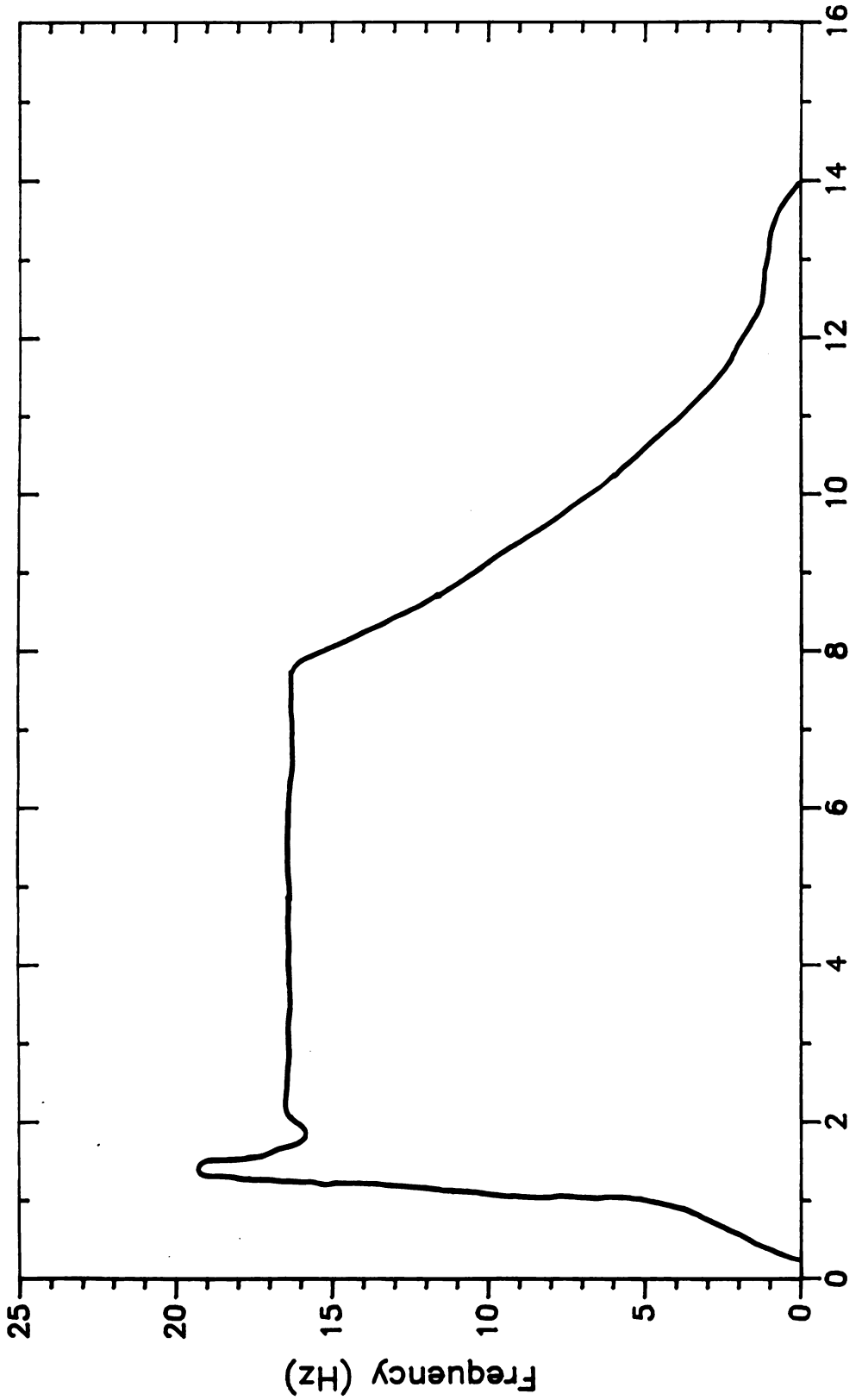

Figure 4.6 Angular velocity of outer mass during a 15–16 Hz free shake with only the outer mass operating.

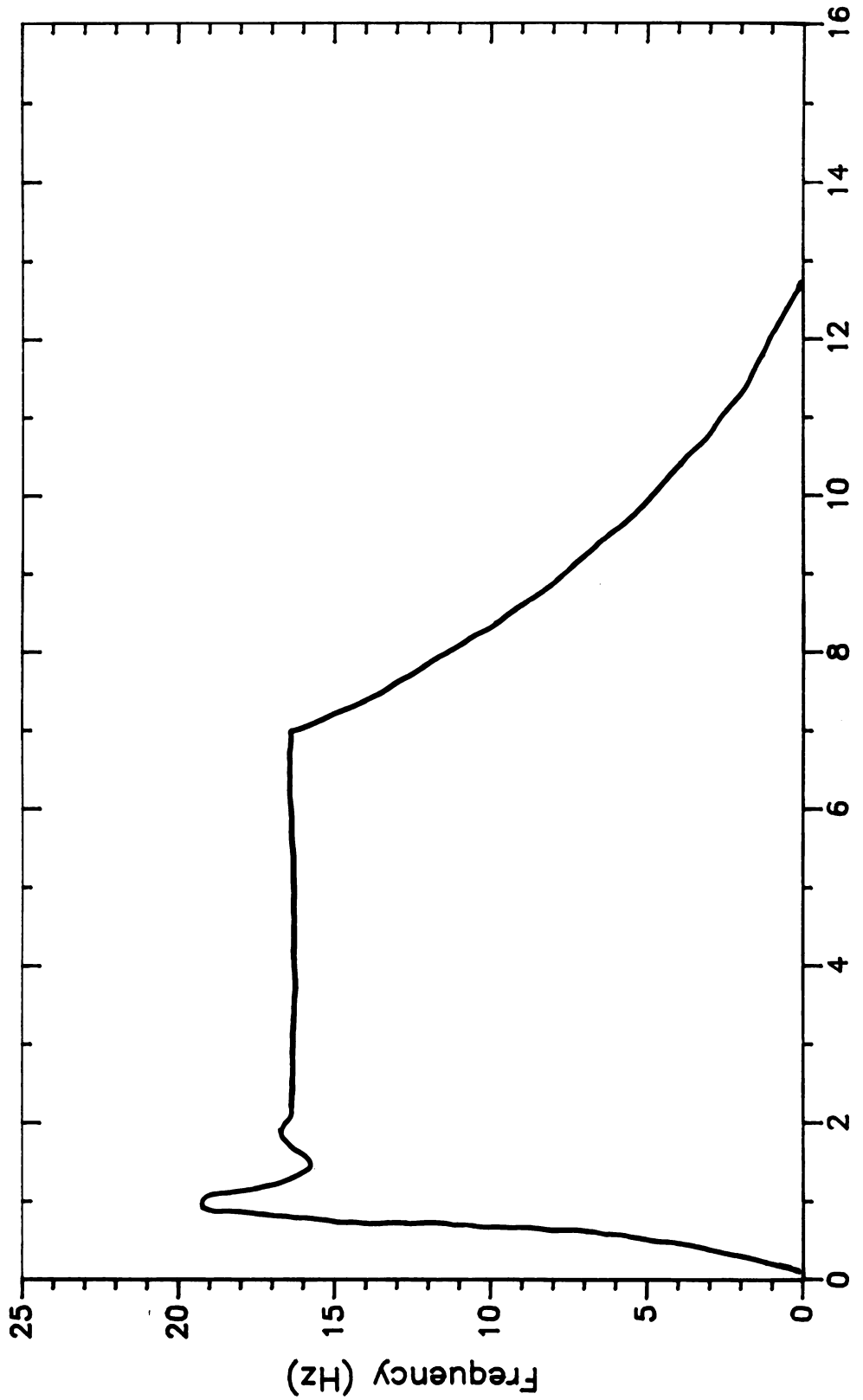

Figure 4.7 Angular velocity of inner mass during a 15–16 Hz free shake with only the inner mass operating.

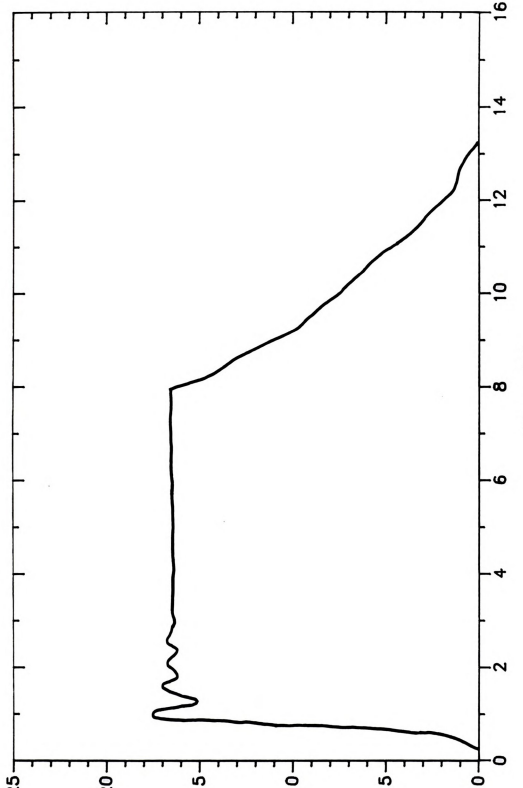

Figure 4.8 Angular velocity of inner mass during a 15–16 Hz 6.5 cm tree shake when both masses are operating.

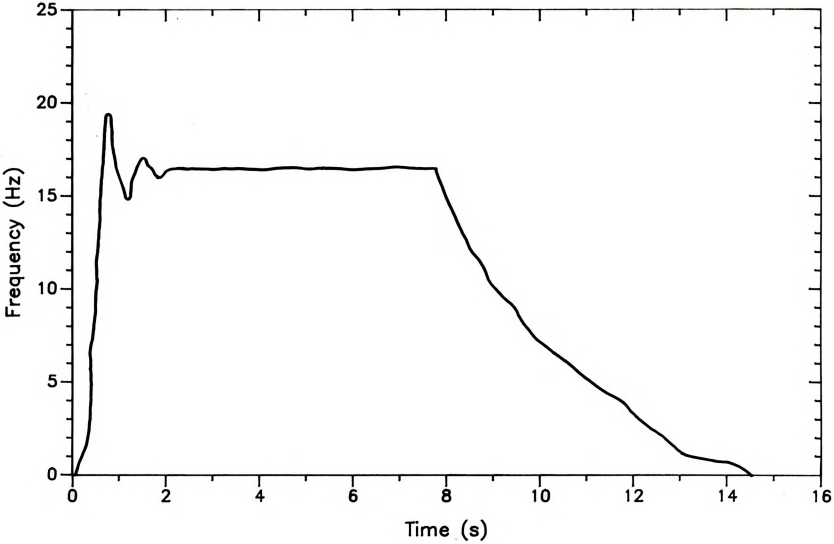

Figure 4.9 Angular velocity of outer mass during a 15–16 Hz 6.5 cm tree shake when both masses are operating.

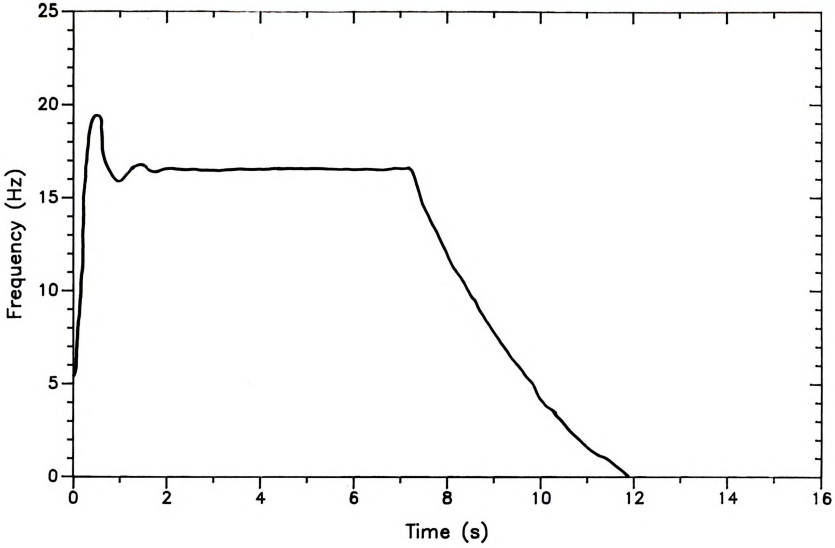

Figure 4.10 Angular velocity of outer mass during a 15–16 Hz 6.5 cm tree shake with only the outer mass operating.

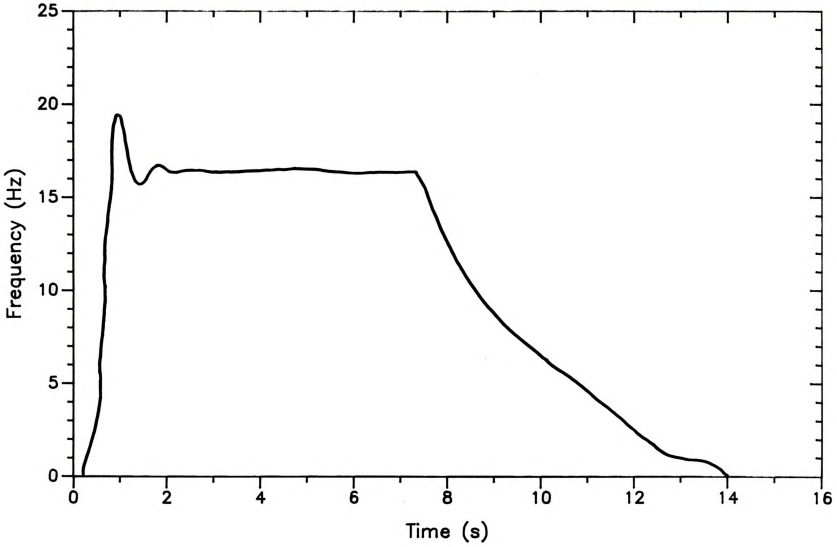

Figure 4.11 Angular velocity of inner mass during a 15–16 Hz 6.5 cm tree shake with only the inner mass operating.

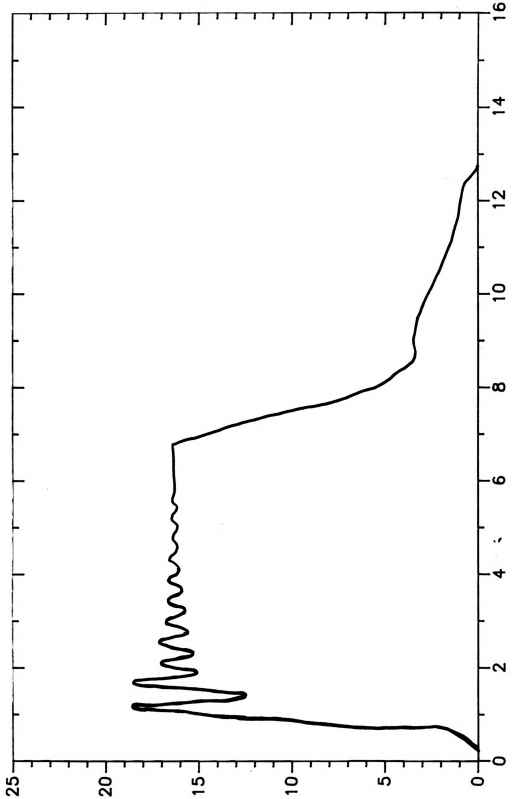

Figure 4.12 Angular velocity of inner mass during a 15–16 Hz 11.0 cm tree shake when both masses are operating.

when both masses are operating in a conventional fixed-mass shaker. These plots exhibit the overshoot and oscillation (1-2 Hz) to steady-state as might be expected when full power is suddenly applied to both masses, again loading the power source. Note that although the inner mass shuts down quickly, the outer mass continues to run for 1.5-2.0 s longer. Figures 4.6 and 4.7 display fixed-mass rotation when only one mass operates during a shake. Overshoot is as large or larger than with both masses operating, and settling to steady-state is more rapid. This most likely results from the elimination of the second mass which acts as an absorber (filter) of energy peaks. Again, at low frequency, the outer mass tends to hit a low resistance state and extend the period of rotation.

Figure 4.8 and 4.9 show the inner and outer mass rotation when both masses are operating in a conventional fixed-mass shake of a small 6.5 cm (2.5 in.) tree. These plots correspond well with the free shake data of Figures 4.4 and 4.5, though absolute overshoot and oscillation to steady-state differ slightly, possibly due to the response of the hydraulic pump loading and circuit flow divider. Slight unsmoothness on the downslope end of rotation tends to indicate that the masses were periodically absorbing extra energy and speeding up slightly. This could be the result of an inertial phasing action resulting from energy input from the tree-shaker system displacements on shut-down. As will be shown, shut-down displacements are quite

nonuniform.

Single mass operation in Figures 4.10 and 4.11 do not exhibit this 'energy pickup' by the masses in the shut-down period, although the outer mass still exhibits a free-wheeling period at the tail. Figure 4.12 is evidence of an extreme case of mass oscillation when an 11.0 cm (4.5 in.) tree is shaken. Displacement response from this tree may be interfering with the inertia of the rotating masses as they tend to settle to steady-state.

When attached to the tree, it was observed that displacement maxima normally occurred during start-up and shut-down of the shaking mechanism, probably because the forcing of vibration coincided with the lowest natural frequency of the tree and/or that of the shaker. The lowest natural mode of the shaker was found to be 1-2 Hz in both X and Y directions. Harmonic magnification of system displacement can result in potentially destructive reactive forces. When passing through these low frequencies, fluctuating shaker displacements may require unusual reactive forces by the tree. These vibrations were evident in shut-down, possibly due to the forces synchronizing at system resonance.

Figure 4.13 shows X and Y linear displacement plots for a conventional fixed-mass shaker in free shake when both masses are operating. Transients on start-up, resulting from sudden power application, overshoot steady-state values by 50% or more. Oscillation in both the X and Y directions

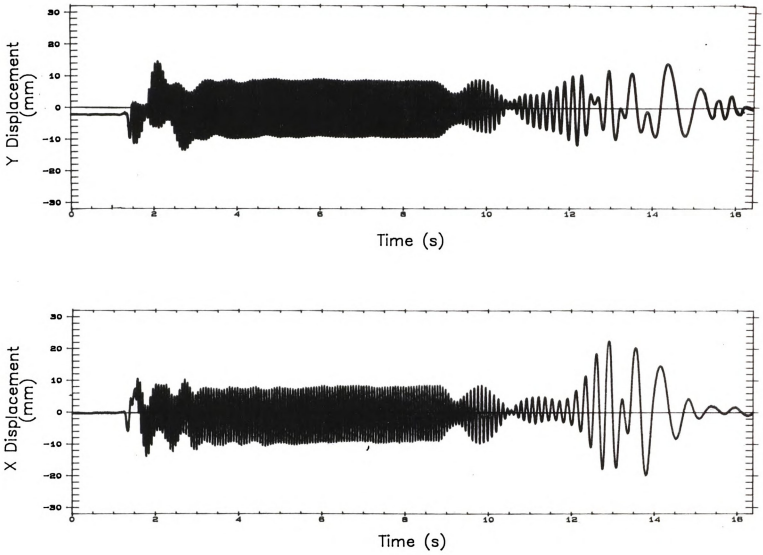

Figure 4.13 X and Y motion at shaker clamp with both masses operating 15–16 Hz in free shake.

require several cycles to settle. Frequency of this oscillation envelope is about 1-2 Hz; the same as the first natural mode of the shaker. Transients often reach 30 mm (1.2 in.) amplitude while steady-state is usually about 10-15 mm (0.4-0.6 in.). Though start-up transients may result from a sudden power transfer from the masses to the shaker inertia, the shut-down transients appear to occur as a result of low first natural modes of vibration of the shaker and tree, combined with some phasing of the masses. Displacement on shut-down tend to decay, then increase to potential maximums of 50 mm (2.0 in.). These shut-down or resonant phenomena normally occur at frequencies around 1.0-2.0 Hz often starting to build up while at 3.0-4.0 Hz. Double-peaked maxima and zero displacement values indicate rapid changes in shake direction and can be seen in the planar X-Y plot of Figure 4.14. Shut-down, with both masses operating, may impose significant stress and strain in tree bark as a result of these amplitude and direction changes.

Figures 4.15 and 4.16 exhibit the same phenomena when shaking a 6.5 cm (2.5 in.) tree, as in commercial operation, with both masses. With the current shaker suspension system, X direction displacements occur slightly larger than Y displacements. The vector sum causes a shake at angles between +X and +Y. Y motion normally ends prior to X motion, possibly from the damping in the different directions of shake.

By observation, the majority of fruit is removed at

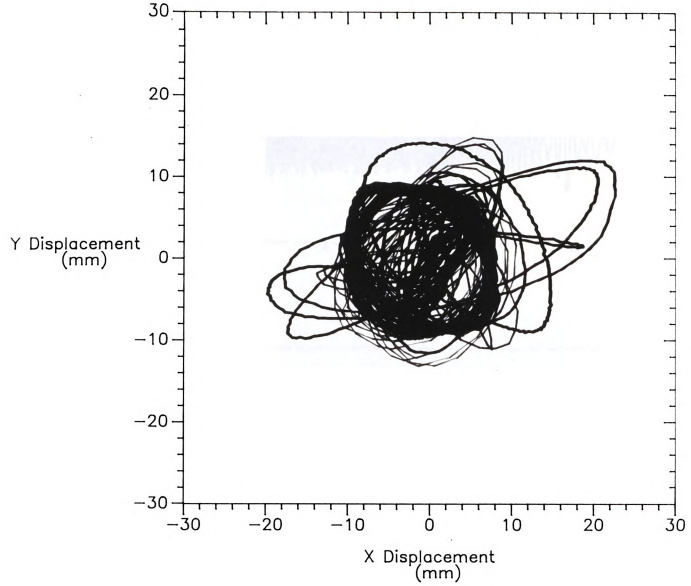

Figure 4.14 X–Y planar motion at shaker clamp with both masses operating 15–16 Hz in free shake.

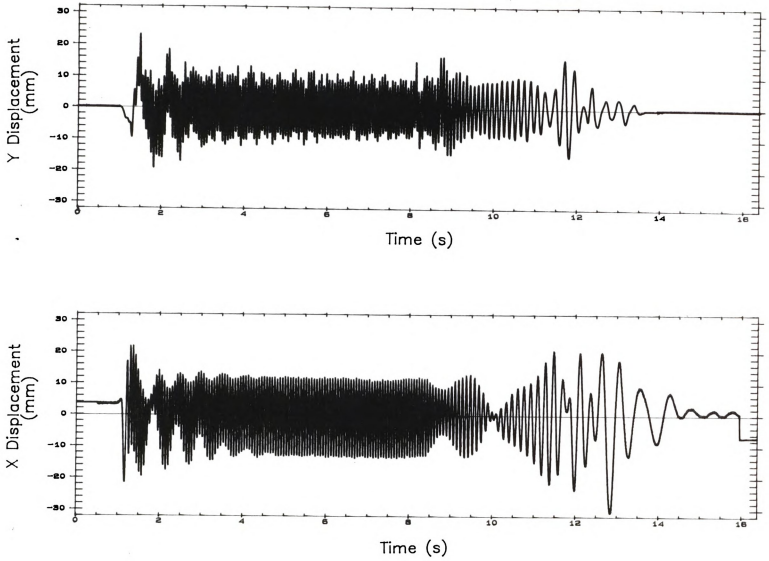

Figure 4.15 X and Y motion at the tree with both masses operating 15–16 Hz on a 6.5 cm tree.

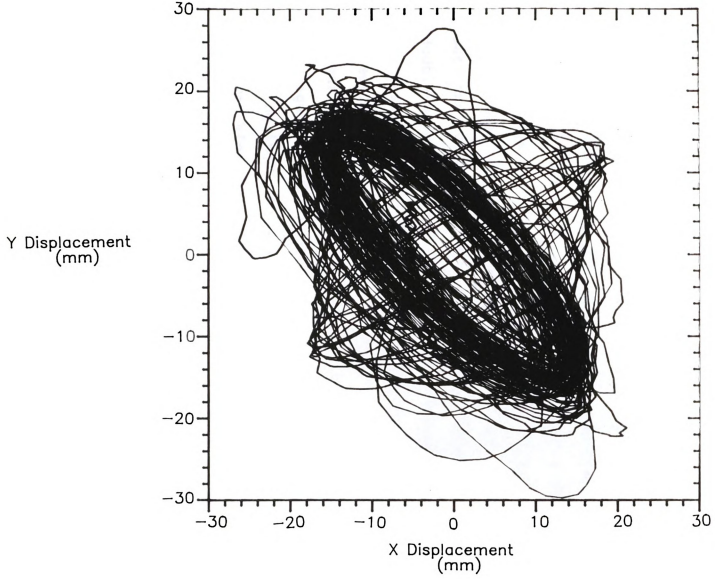

Figure 4.16 X–Y planar motion at the tree with both masses operating 15–16 Hz on a 6.5 cm tree.

start-up and during the high frequency steady-state operation. Insignificant amounts of fruit are detached during shut-down, even though displacements reach maximum values there. This is a key effect which will aid in elimination of high-stress displacements while maintaining shaker efficiency. Growers who indicate that stopping and starting the shaker during harvest results in an increase in fruit removal are likely observing the effect of a change in shake pattern resulting from a change in mass phasing.

Displacements of a single inner fixed-mass operating in free shake are shown in Figures 4.17 and 4.18. Start-up oscillations ($\simeq$ 1.0 Hz) are more pronounced and take longer to settle. Shut-down resonance ($\simeq$ 1.0 Hz) is also present but the sudden change in shake direction, evidenced by double-peaked maxima and zero displacements in the progression of shake, are not present, even though the direction of shake does similarly change as shown in the planar plot. Frequency content of this free shake is shown in Figure 4.19 as compared to that with both masses operating in Figure 4.20.

The single fixed-mass shake of a small tree is shown in Figures 4.21 and 4.22 with frequency content in Figure 4.23, as compared to the frequency content with both masses in Figure 4.24. Contrary to free shake performance, a transient peak occurs immediately upon start-up. Oscillatory decay to steady-state is faster. Finally, shake of a very large tree (16.5 cm, 6.5 in.) is shown in Figures

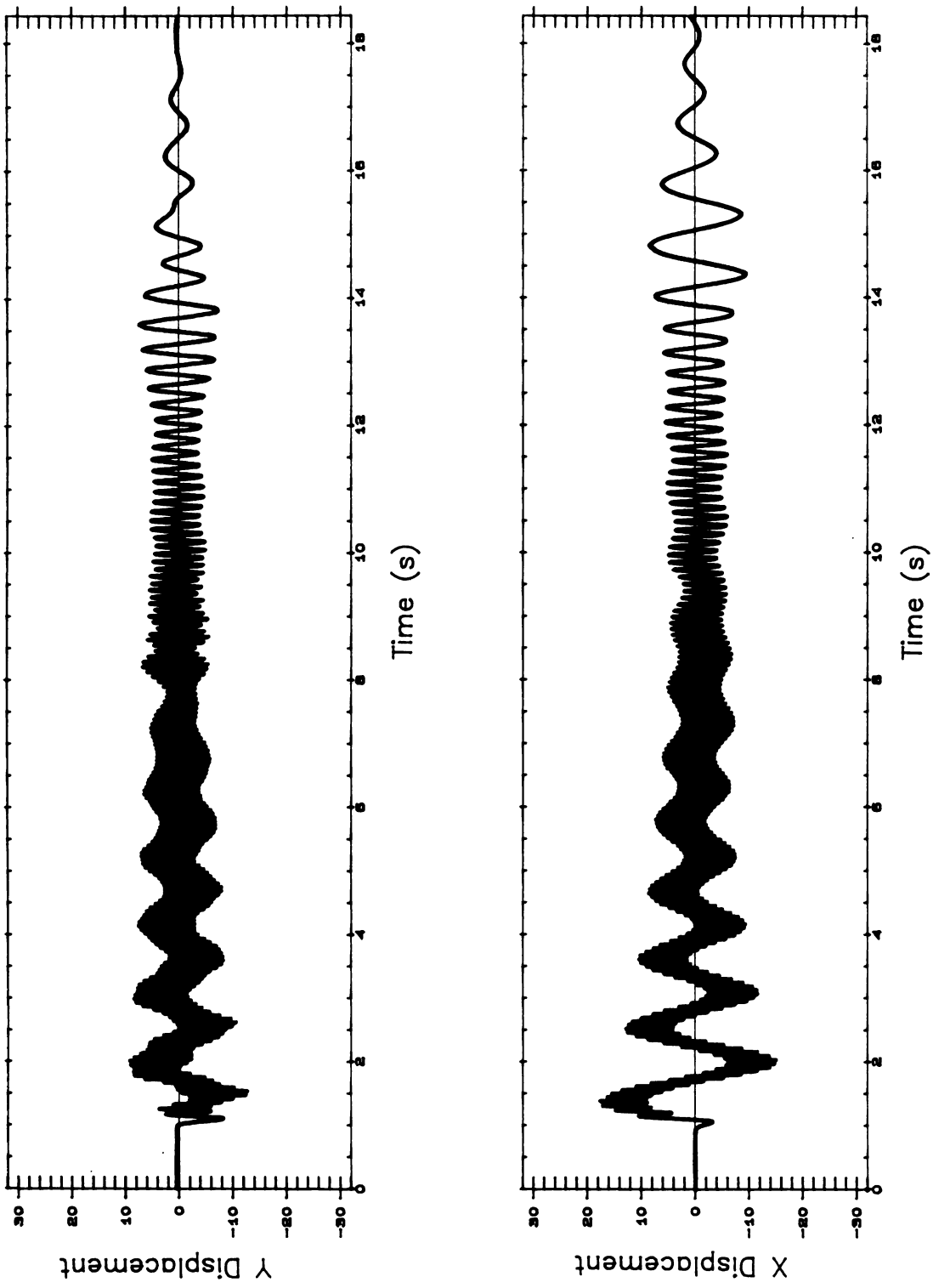

Figure 4.17 X and Y motion at shaker clamp with a single inner fixed—mass at 15—16 Hz in free shake

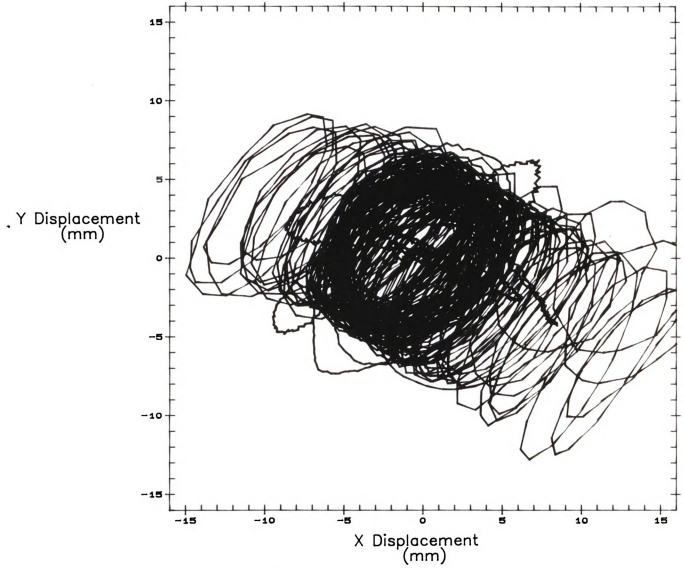

Figure 4.18 X–Y planar motion at shaker clamp with a single inner fixed–mass at 15–16 Hz in free shake.

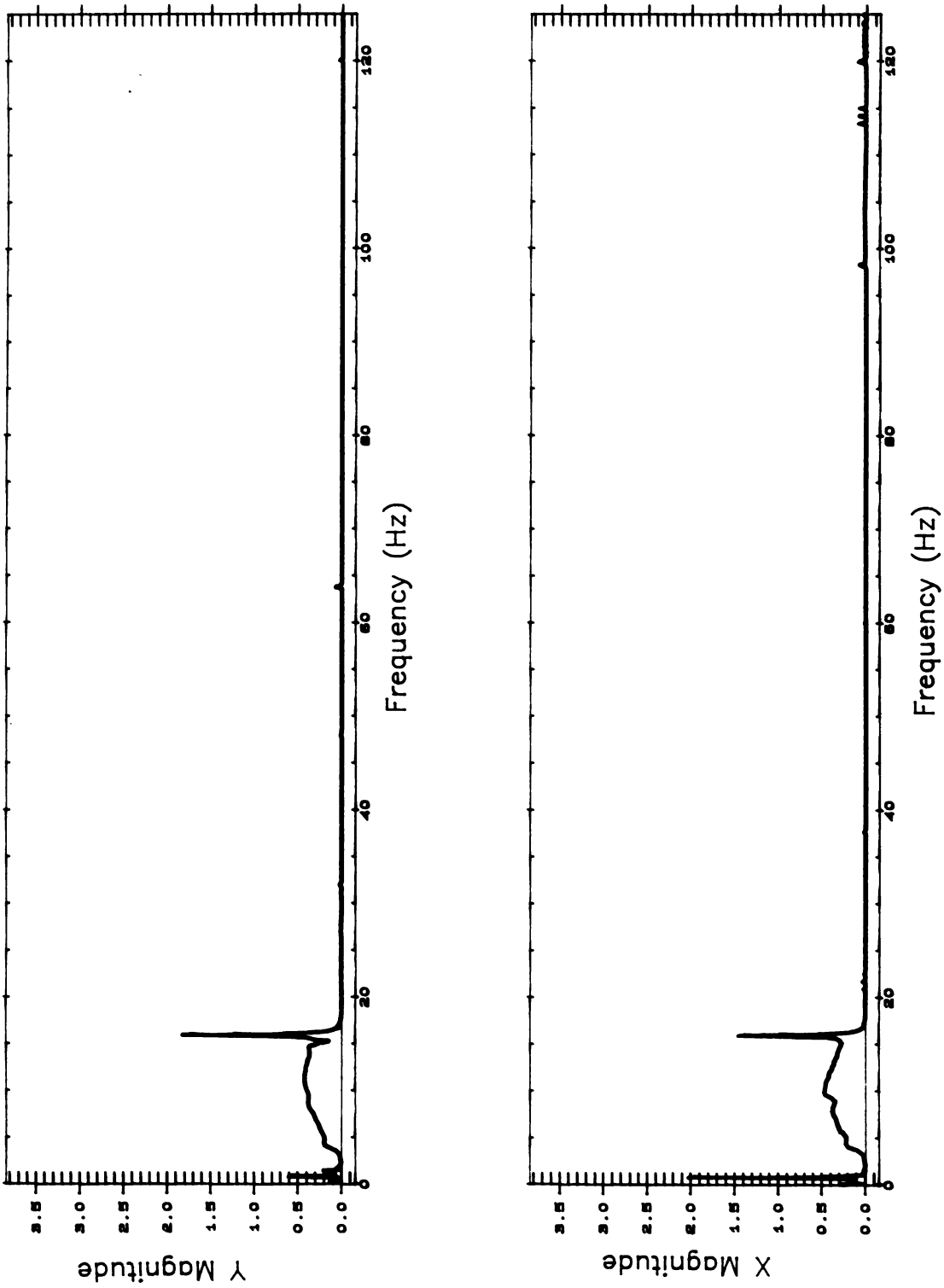

Figure 4.19 Spectral content of vibration with a single inner fixed-mass at 15-16 Hz in free shake.

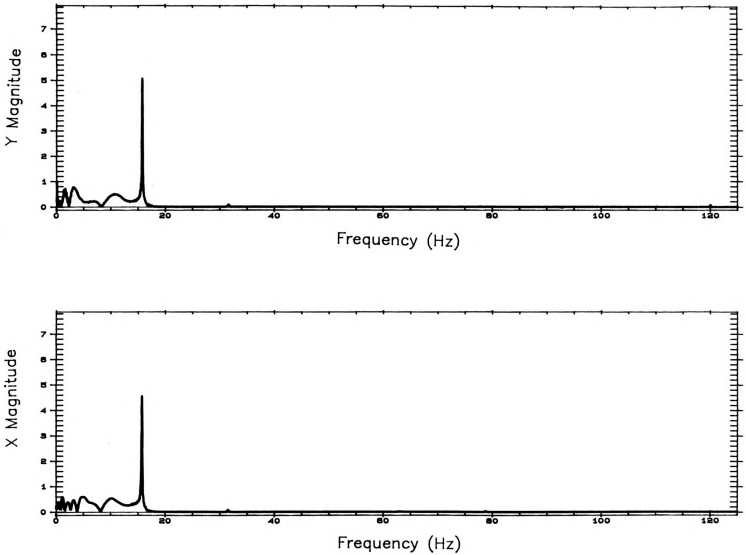

Figure 4.20 Spectral content of vibration when free shaking at 15–16 Hz with both fixed–masses operating.

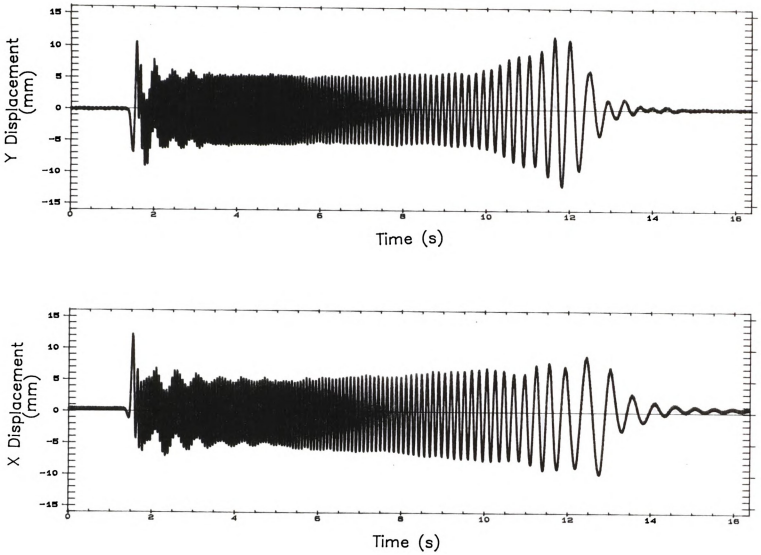

Figure 4.21 X and Y motion at the tree with a single inner fixed–mass at 15–16 Hz on a 6.5 cm tree.

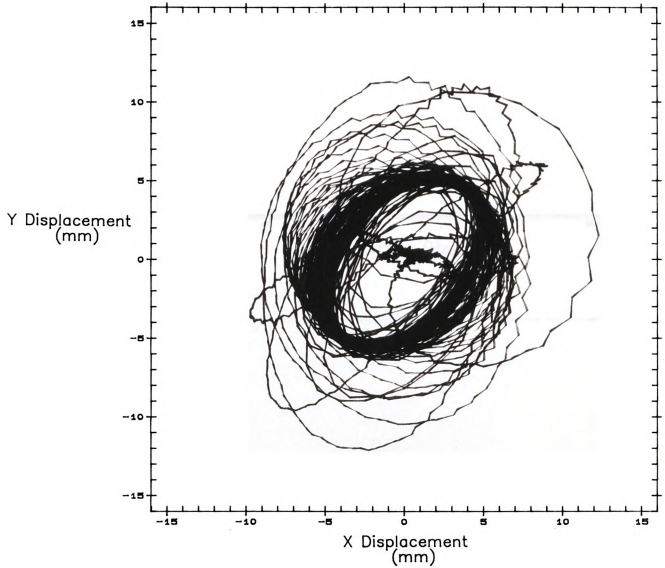

Figure 4.22 X–Y planar motion at the tree with a single inner fixed–mass at 15–16 Hz on a 6.5 cm tree.

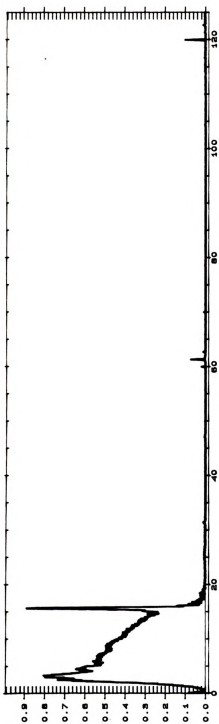

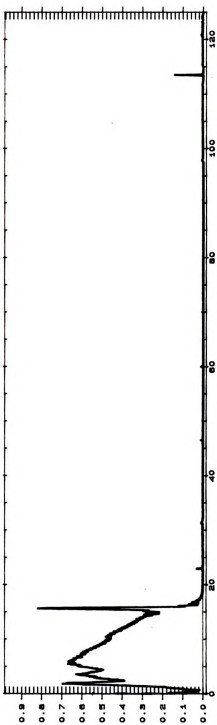

Figure 4.23 Spectral content of vibration when shaking a 6.5 cm tree at 15–16 Hz with a single inner fixed–mass.

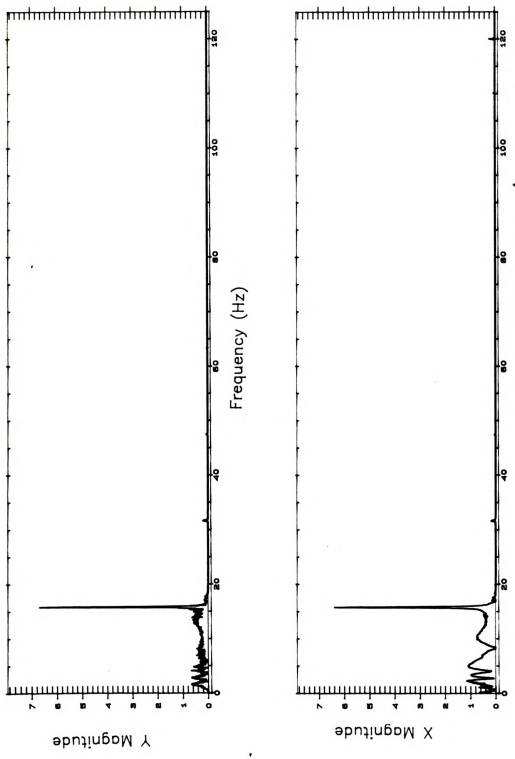

Figure 4.24 Spectral content of vibration when shaking a 6.5 cm tree at 15–16 Hz with both fixed–masses operating.

4.25 and 4.26 with frequency spectra in Figure 4.27. Start-up transients are smaller as well as shut-down resonance, though it appears that resonance may be occurring at a higher frequency; about 5 Hz. The first natural mode of the larger tree, with more heartwood, may be slightly higher. An extreme transient case is shown in Figure 4.28 where a medium (11.0 cm, 4.5 in.) tree is shaken with both fixed-masses at 15 Hz. In agreement with the rotating mass plots, there appears to be a tree size which is capable of inducing very large shaker transients.

In summary, displacements resulting from fixed-mass conventional shakers usually involve transient start-up and shut-down peaks with sudden direction changes. Single mass operation is similar and appears to be appropriate as a basis for analysis and design. Removal of fruit occurs mainly at high frequency steady-state operation and therefore, should not be significantly affected by presence or absence of transients; the maxima which may induce excessive stress and strain in tree bark.

4.6 Trunk Shaker Analysis

The Friday C-Clamp trunk shaker, during steady-state operation, does create an omni-directional displacement pattern. The individual masses which rotate asynchronously (they are connected only by the hydraulic system) may start with any phase difference, but eventually seek a minimum energy level at which to operate, though they must "beat" in order to develop the omni-directional shake. When both

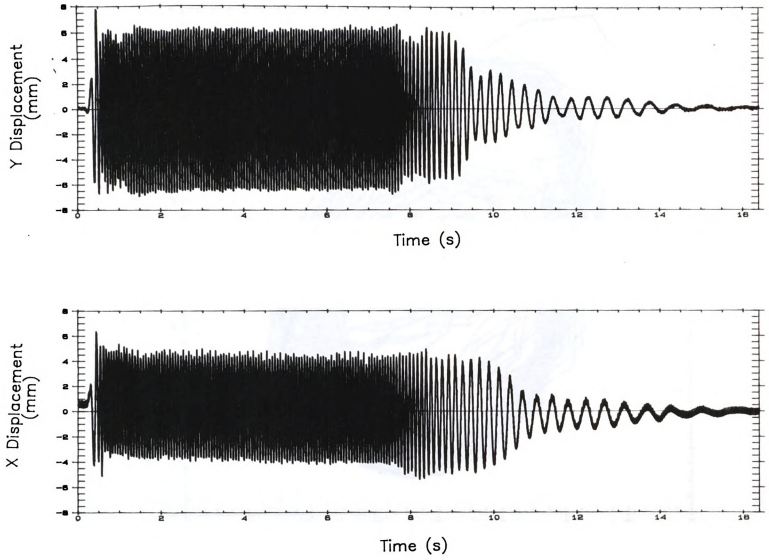

Figure 4.25 X and Y motion at the tree with a single inner fixed–mass at 15–16 Hz on a 16.5 cm tree.

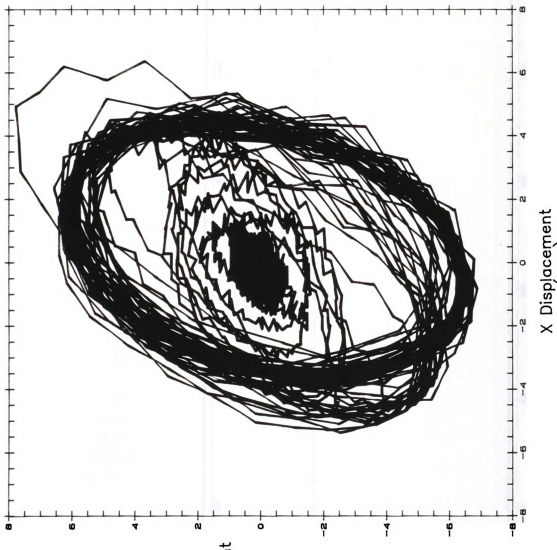

Figure 4.26 X–Y planar motion at the tree with a single inner fixed–mass at 15–16 Hz on a 16.5 cm tree.

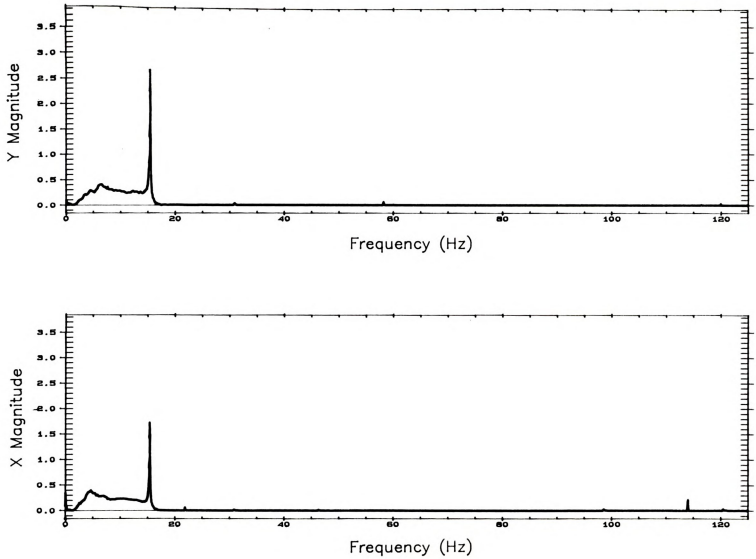

Figure 4.27 Spectral content of vibration when shaking a 16.5 cm tree at 15–16 Hz with a single inner fixed–mass.

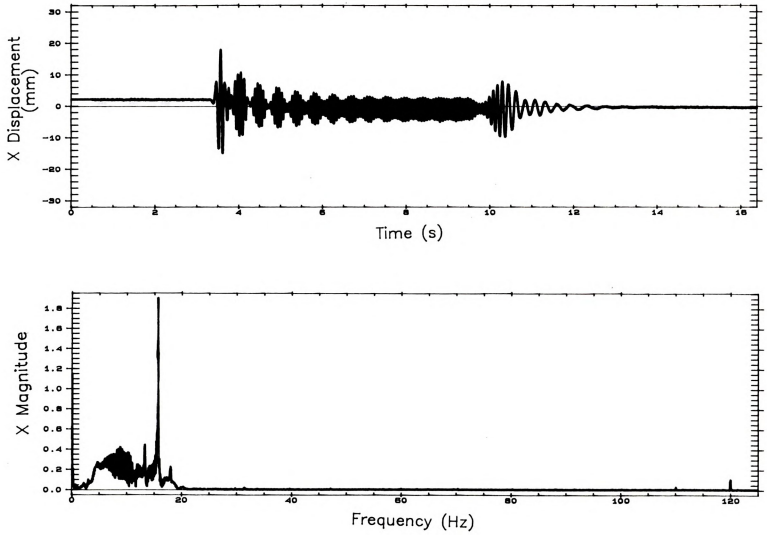

Figure 4.28 X displacement and frequency spectra at the tree with both fixed–masses operating 15–16 Hz on an 11.0 cm tree.

masses are operated in free shake (no tree), the resulting shaker motion is only omni-directional on start-up and shut-down, otherwise it is linear and appears to be a function of the suspension system parameters (Figure 4.29 and 4.30). Note that in Figure 4.29, the patterns are very nearly that which is expected, even though the shaker properties have been found to be nonlinear and difficult to analyze. For example, the one mass operation would appear as in Figure 4.31a with forces:

$$F_n = m_1 * r_1 * \omega^2$$
$$F_t = m_1 * a_t$$

Neglecting the suspension system (spring force F_k, damping force F_c), we see that:

$$\Sigma F = Ma = F_n + F_t$$

A single driving function would appear as in Figure 4.31b with resultant planar motion as in Figure 4.31c. This occurs simply due to the centrifugal force F_n. If a slight radial acceleration occurs due to the hydraulic system (which is very likely), this small force will shift the circular planar pattern. The restoring force caused by gravity (a pendulum support system) then acts against the tangential force F_t and a pendulum oscillation is superimposed on the planar circular pattern as in Figure 4.29a. Start-up transients likely excite pendulum motion.

Figure 4.29b shows a different phenomenon and relies on the assumption that without resistive motion of a tree, the two masses synchronize into a minimum energy state in which forces begin to cancel as shown in Figure 4.32a with near

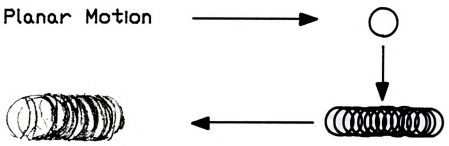

(a)

(b)

Figure 4.29 Free shake test: a) one mass operational b) two masses operational.

(a)

(b)

Figure 4.30 Free shake pattern with two masses operational: a) test one b) test two.

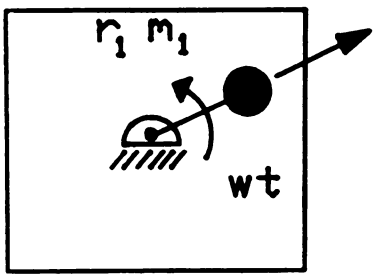

$$F_n = m_1 r_1 w^2$$

$$F_t = m_1 a_t$$

(a)

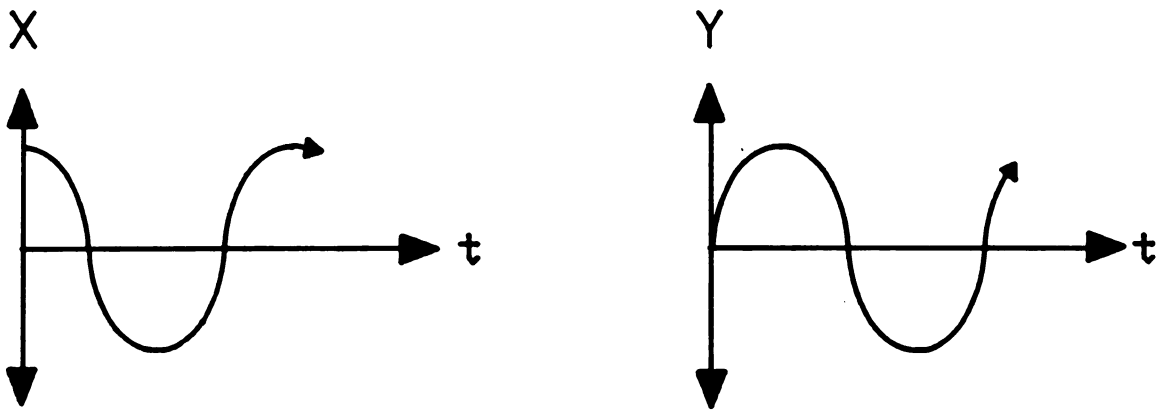

(b)

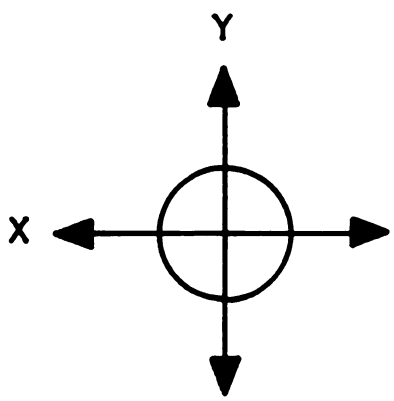

(c)

Figure 4.31 Single mass oscillator: a) free body diagram b) resulting X and Y motion c) resulting planar motion.

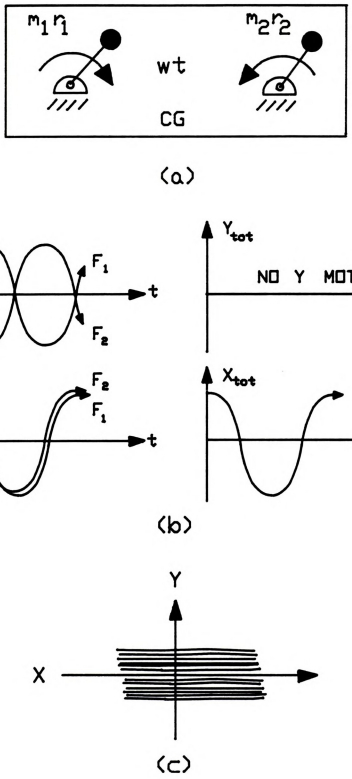

Figure 4.32 Two mass oscillator: a) free body diagram b) resulting X and Y motion c) resulting planar motion.

pure centrifugal normal forces:

$$F_1 = m_1 * r_1 * \omega_1^2$$
$$F_2 = m_2 * r_2 * \omega_2^2$$

Since $m_1 = m_2$ and $r_1 = r_2$, we can assume that $\omega_1 = \omega_2$ at steady-state in free shake. Thus, with the masses in phase, but rotating opposite, we have a flip-flop effect of the forcing function as shown in Figure 4.32b with resulting motion shown in Figure 4.32c.

This shake will therefore be linear with about twice the amplitude of a one-mass shake. Any tangential acceleration of the masses will induce some shifting motion. This again could be induced from the start-up transient (which reveals itself as an omni-directional shake at the beginning of Figure 4.29b). This theory agrees with the data shown in Figure 4.29b. The addition of springs and dampers from the suspension system will tend to rotate this line off-phase.

The assumption was made that the masses were in phase. This does not have to hold. If the masses are 180° out of phase, the same result occurs except that the motion will be shifted 90° to the Y direction (with spring and damping effects neglected). A force couple or torque will also be present, however.

Figure 4.30 shows the desired omni-directional response when shaking a tree. Notice that the motion is actually cycloid-shaped, thus pushing and whipping the tree to the side (assuming trunk motion resembles shaker motion). The current Friday shaker, however, has transient gallop

problems presumably due to the low natural frequency of the system (tree and shaker) which we are required to pass through to get to ω_{drive} as shown in Figure 4.33.

From previous displacement data, it has been stated that gallop will reach twice the steady-state displacement i.e. XM/me = 2.0. From Figure 4.33, we see that this occurs at about $\omega/\omega_n = 1$ (resonance) where $\zeta = 0.25$. In fact, damping ratios found earlier in Table 4.1 agree very closely with this theoretical value.

The current design then has the problem that the system natural frequency is too low. As a first look, we see that the mass of the shaker is much greater than the mass of the tree for small trees. Therefore, by decreasing the mass of the shaker or increasing the spring constant of the shaker, the natural frequency of the shaker could be increased beyond the drive frequency and thus gallop, which occurs partially due to resonance, would not occur. With $\omega_n = K/M_{effective} > \omega_d$, amplitude could be limited.

Unfortunately, however, as trees get larger than 16.5 cm (6.5 in.) diameter, their mass becomes significant and the system requires an actual multi-degree of freedom analysis which becomes quite complex and has been attempted by many researchers with a multitude of approaches.

The normal solutions for resonance problems are to: 1) move the drive frequency; 2) move the natural frequency; 3) increase damping; or, 4) power-up through and brake-down through the resonance point. Other more elaborate schemes

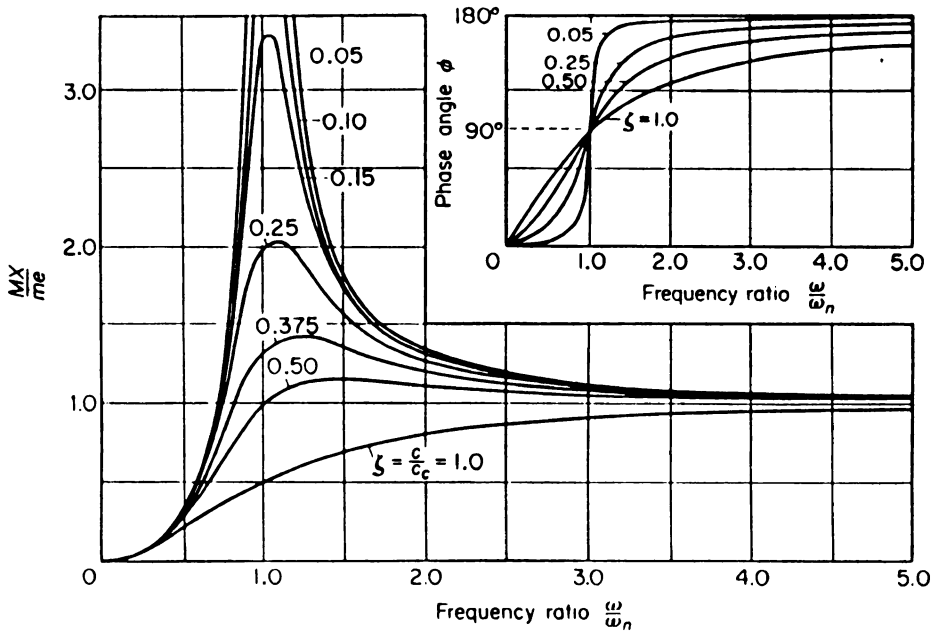

Figure 4.33 Amplitude and phase of a linear, second order system.

exist but are rare and not economical for this application.

The drive frequency cannot be shifted. Previous researchers in the past 30 years have determined the optimal stroke and frequency for cherry removal by mechanical shaking, and it is well above the problematic natural mode.

Shifting the natural frequency has just been discussed but poses realistic problems in material properties (mass, strength) as well as problems with different tree sizes. Not much can be done about the natural frequency of the tree (about 1 to 3 Hz).

Increasing the damping may help to reduce gallop but will probably reduce the steady-state value too, simply dissipating needed energy. A time-varying damper may potentially permit a high shaker damping ratio on start-up and shut-down to avoid resonance with a subsequent low damping ratio during steady-state shake. Undesirably, however, the shaker carrier would be required to absorb more vibration during transients.

Power-up and brake-down are simple concepts but difficult to implement directly with this system. I tried to power-up through resonance before the system could respond. However, with all the available tractor power, there was little evidence that start-up gallop had dissipated. Brake-down has not been tested directly but would require strong materials to ensure "braking" of the masses and not "breaking" of the unit. Braking also requires a secondary power unit, or energy sink, to rapidly

decelerate the rotating masses. Brake-down through resonance, however, would theoretically reduce bark damage.

4.7 Need for Shaker Redesign

Vibratory displacement patterns resulting from mechanical shaking of cherry trees with a fixed-eccentricity inertial trunk shaker reveals displacement maxima at transient start-up and shut-down periods. These transient extremes exceed steady-state amplitudes by as much as 100% and may impress dynamic stresses and strains not previously recognized in static analyses. Biological limits of cell strength in bark and cambium may well be exceeded since stress and strain from this phenomenon is superimposed on static clamping pressures.

From an engineering standpoint, the tree acts as a complex beam, with a stiffness and a damping property. In the static or motionless sense, a push on the tree causing displacement creates a force 'F_k' from the spring property of the tree. If the shaker and tree move, a damping force is created 'F_c', which in a simple sense is proportional to the velocity of the motion. An inertial force 'F_m' is also present from acceleration of the shaker and tree masses. Hence, the sum of these three forces may exceed previous static compressive force recommendations.

Both the tree and the shaker individually have very low natural frequencies. During start-up and shut-down then, with fixed-eccentric masses, both tree and shaker natural frequencies are encountered. Vibrations in machinery are

often eliminated by changing physical properties of the system or by conventional vibration absorbers. Tree properties, however, are fixed and vibration absorption is counter to the harvesting process. Therefore, we need a method of reaching the desired shake frequency while transferring minimal energy at the critical resonance frequencies when passing-through. Typical engineering methods to avoid resonance, as discussed in section 4.6, are difficult if not unreasonable to implement in this application. Hence, a new method of getting masses up to rotational velocity with minimal energy transfer at resonance, is needed.

CHAPTER 5

SHAKER REDESIGN AND EVALUATION

5.1 On the Prospect of Mode Evasion

Shaking force is the resultant of all forces acting on the frame of a shaking mechanism. Shaking motion is usually produced by inertial forces. If the resultant of all forces due to inertial effects acting on the frame is zero, then no shaking (linear displacement) is produced. Although linear shaking forces may sum to zero, there may nevertheless be a shaking couple (rotational displacement) present. Balancing the mechanism thus consists of eliminating both the shaking force and the shaking couple. In most mechanisms, it is usually not practical to provide a means for completely eliminating both. In fruit harvesting however, it is important to eliminate shaking couples at all frequencies (to prevent torsion on tree bark) and all linear shaking forces near the low natural frequencies (to prevent "gallop").

The low natural frequency modes of the tree, the shaker, and the tree-shaker system cause unstable, unproductive, and damaging vibrations when the driving force is oscillating near these same frequencies. A means to circumvent these vibration "gallops" with minimal economic

investment and minimal change in design was sought.

The customary methods of altering vibration characteristics of a mechanism, as mentioned in Section 4.6, are not practical in this application. Total vibration isolation is contrary to the shake-harvesting objective and a power-through resonance method requires an impractical power source which could potentially damage both the tree and shaker outside the resonant region.

A more promising approach, therefore, is to isolate vibration near the low resonance frequencies and deliver shaking energy near higher shake frequencies. In this investigation, two methods are discussed to accomplish this task. The first method involves the concept of vibration balancing by the phasing of oscillators. The second method involves changing the eccentricity of a single mass or a pair of masses.

a. Phasing

Oscillators, or vibration exciters, usually consist of a fixed-eccentric mass rotating in a plane. The displacement of a shaker body can be considered as a linear displacement of some point on the body plus an angular displacement of the body about this point. For example, if the acceleration of a point B (Figure 5.1a) is known as A_B, then the acceleration of any other point C is:

$$A_C = A_B + A_{C/B_{normal}} + A_{C/B_{tangential}}$$

given the angular velocity ω and the angular acceleration α

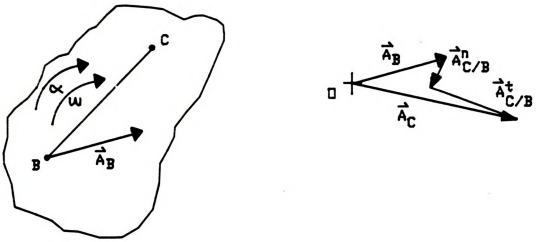

(a)

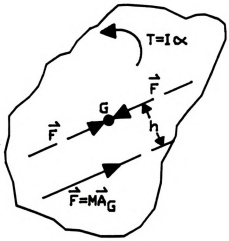

(b)

Figure 5.1 Geometry of rigid body motion a) relative motion b) force and torque.

of the body. Given the body of Figure 5.1b, with G as the center of gravity and A_G the acceleration of G with α known in magnitude, then a force and torque can be found that must correspond to produce A_G and α as:

$$F = MA_G$$
$$T = I\alpha$$

where I is the mass moment of inertia of the body about an axis which passes through G and is perpendicular to the plane of rotation. A single force F can act at a location h units from G and replace both the force F and the torque T where:

$$T = Fh = I\alpha$$

$$h = I\alpha/F$$

The inertial force is then defined as the reversed resultant force and the inertial torque is the reversed resultant torque. By D'Alembert's Principle, an inertial force and an inertial torque can be added to a body which is acted upon by a resultant force and a resultant torque to bring the body to equilibrium. This is a key concept that will be applied to a system of rotating masses in a shaker body to avoid low frequency resonance.

A single oscillator can be attached to the center of gravity G of the shaker body M_S, as shown in Figure 5.2a, with the shaft rotating at a constant speed ω_d and a single concentrated mass m_1 at radius r_1. This planar analysis provides the three degrees of freedom (X, Y, θ) which must be force-constrained and moment-constrained for prevention of shaking motion. The forces on this rotating mass are

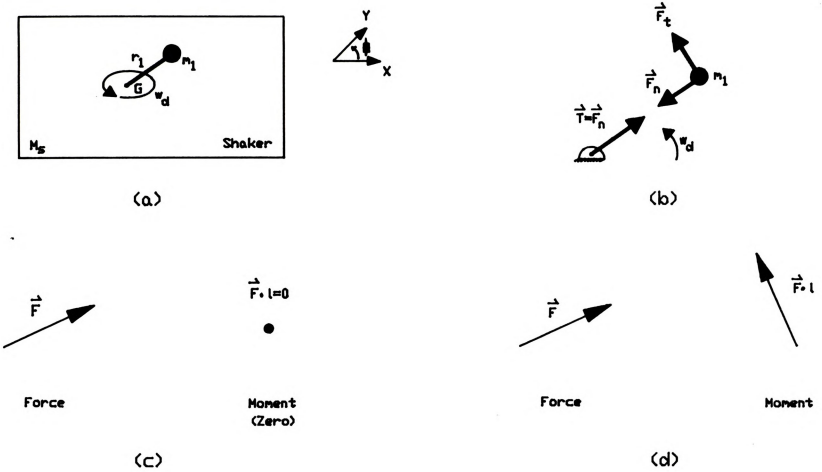

Figure 5.2 Single oscillator shaker excitation (a) in free space (b) acting forces (c) force and moment polygons at CG (d) force and moment polygons off the CG.

shown in Figure 5.2b where:

$$F_t = ma_t \qquad a_t = 0 \text{ when } \omega_d \simeq \text{constant}$$

$$a_n = V^2/\rho = (\omega\rho)^2/\rho = \omega^2\rho$$

$$F_n = ma_n = m\omega^2\rho$$

The conditions to balance the shaker body M_s are:

$$\Sigma M = I\alpha = 0$$
$$\Sigma F_i = ma_i = 0$$

Neglecting tangential forces, the force vector of a single oscillator m_1 is always directed through G thereby causing no rotational moment:

$$F_n \times \rho = 0 = \Sigma M = I\alpha \text{ with } F \parallel \rho$$

With only one oscillator, however, there is no cancellation of the forcing vector F and thus, motion is imparted to M_s through G:

$$\Sigma F = ma_i = ma_n = F \neq 0$$

Rigid body motion, in free space, will then occur unless m = 0 and r = 0. Force and moment polygons for the single oscillator case at the center of gravity and off the center of gravity are shown in Figures 5.2 c,d.

Seeking a solution to the vibration "gallop" phenomena using D'Alembert's Principle, the concept of vibration analysis for dynamic rigid bodies is extended to multiple masses $m_1 \ldots m_n$ with multiple radii $r_1 \ldots r_n$ with the following assumptions:

1) The shaker body lies in planar free space and is capable of X, Y, and θ motion.

2) Oscillator masses $m_1 \ldots m_n$ and radii $r_1 \ldots r_n$ are not necessarily equivalent.

3) Oscillator location in the rigid body is not constrained.

4) The center of gravity of the system can be located and referenced; the center of rotation is unconstrained, however.

An arrangement of oscillators is sought which will provide a configuration in which no motion is imparted to the body and which can provide a desirable shaking pattern for fruit removal with proper phasing control above the resonant frequencies. If all masses are constrained to rotate at the same r/min, then any phase relationship set up by the operator will repeat every 2π radians. If masses rotate in the same direction, a phase difference ϕ between them will not be a function of time $\phi(t)$ but will remain constant $\phi = \gamma \; \forall t$, even if $m_i = m_j$ and $r_i = r_j$. If $m \cdot r$ differences exist, they will be evident in the forcing functions.

The two oscillator system, quite common in shaker design, yields to two analytic approaches: the first being the simplest and most obvious Figure 5.3a. Here, both masses are fastened to the same shaft. By analysis:

$$\Sigma F = m_i a_i = 0$$

$$F_1 i - F_2 \cos(180-\theta) i + F_2 \sin(180-\theta) j = 0$$

$$F_1 i + F_2 \cos\theta i + F_2 \sin\theta j = 0$$

For equilibrium:

i: $F_1 + F_2 \cos\theta = 0$ $\quad \cos\theta = -1$ or $\theta = \pi$

j: $F_2 \sin\theta = 0$ $\quad \sin\theta = 0$ or $\theta = \pi$

For forces to cancel, the phase difference must remain at π radians $\forall t$ and:

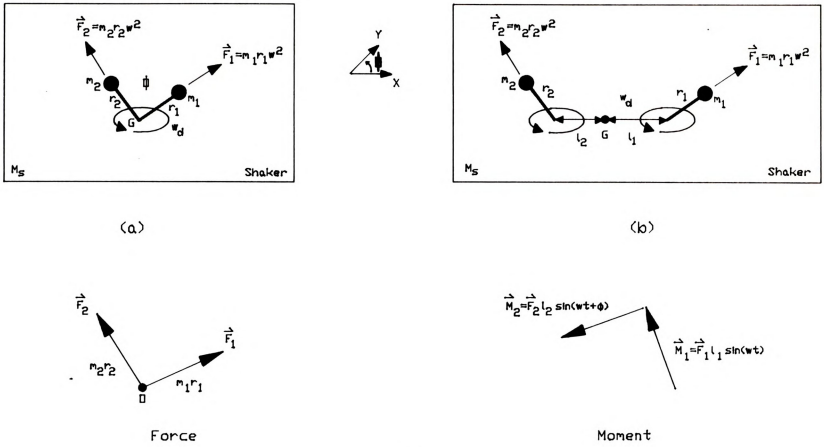

Figure 5.3 Two oscillator shaker excitation (a) both at CG (b) other than CG (c) general force and moment polygons.

$$F_1 = F_2$$
$$m_1 r_1 = m_2 r_2$$

For moments:

$$\Sigma M_{CG} = I\alpha = 0$$
$$F_1 * r_1 + F_2 * r_2 = 0$$

But $F_1 \parallel r_1$ and $F_2 \parallel r_2$ so $\Sigma M = 0$

Therefore, on the same shaft, two oscillators with this frequency and phase relationship will impart no force or moment to the platform. For all practical purposes, however, the tree can be considered to be the center of rotation. Therefore, moments will occur when the phase $\neq \pi$. In the more common commercial shaker design, the oscillators are on separate shafts. By moving the oscillators off the center of gravity (Figure 5.3b):

$$F_1\cos\theta i + F_1\sin\theta j + F_2\cos(\theta+\phi)i + F_2\sin(\theta+\phi)j = 0$$

$$i: \quad F_1\cos\theta + F_2\cos(\theta+\phi) = 0$$
$$j: \quad F_1\sin\theta + F_2\sin(\theta+\phi) = 0$$

Balancing and dividing:

$$\tan\theta = \tan(\theta+\phi)$$

Therefore, $\phi = (2n+1)\pi$ radians n=0,1... will satisfy this condition and can be satisfied at every instant only when both oscillators rotate in the same direction at the same speed (ω_d). For moments:

$$F_1\sin\theta \cdot L_1 - F_2\sin(\theta+\pi) \cdot L_2 = 0 \qquad \text{where } \phi = \pi$$
$$F_1\sin\theta \cdot L_1 + F_2\sin\theta \cdot L_2 = 0$$

Transients can only be zeroed when $\phi = 2n\pi$ n=0,1... Since forces cancel only for ϕ odd and moments cancel only for ϕ even, then it can be concluded that two oscillators mounted at separate centers cannot simultaneously prevent both linear and torsional vibration regardless of the phasing.

If oscillators are rotated counter to one another with $\phi = \pi$ and at the same frequency ω_d, then forces would be zero $\forall t$ but moments would not be zero. In summary, then, for a two-oscillator body:

$$\begin{array}{lll} \phi = 2n\pi & \omega_1 = \omega_2 = \omega_d & \Sigma F \neq 0 \quad \Sigma M = 0 \\ \phi = (2n+1)\pi & \omega_1 = \omega_2 = \omega_d & \Sigma F = 0 \quad \Sigma M \neq 0 \\ 2n\pi < \phi < (2n+1)\pi & & \Sigma F \neq 0 \quad \Sigma M \neq 0 \end{array}$$

The force and moment polygons for the two-oscillator case are shown in Figure 5.3c. It is evident that unless $F_1 = F_2 = F$, the force polygon will not close (zero resultant) which confirms a phase angle of π radians between the functions. Therefore, the masses must rotate in the same direction at the same frequency ω. With this, moments are shown as:

$$-F_1 \sin\omega t \cdot L_1 = F_2 \sin\omega t \cdot L_2$$

Thus:

$$-L_1 = L_2$$

And the only two fixed-mass oscillator system which will impart no motion to the shaker or tree is where both masses connect at the same center (trivial case: $-L_1 = L_2 = 0$). Furthermore, as long as both concentric oscillators rotate in the same direction at ω and $\Sigma m_i r_i = 0$ for some t, then no motion will be imparted to the body $\forall t$ (assuming no acceleration a_t or other external influences).

This produces a very interesting result. Many commercial vibratory fruit and nut harvesters incorporate two fixed-mass oscillators which physically cannot be located at the desired point of no rotation - the tree. In spite of mechanical restrictions to rotation, there is the possibility of moments about the tree, an unwelcome

precursor of bark stress and strain. Mechanical restrictions to rotation seldom exist as most shakers are vertically suspended by three or four hangers to allow free motion, limited only by the damping properties of the hanger bushings and gravity which discourage horizontal and vertical displacement. These configurations cannot prevent small amounts of rotation of the heavy shaker and clamp which easily strain susceptible tree bark during harvesting.

Since a two-oscillator system cannot balance the shaker body within reasonable physical dimensions, a three-oscillator system is examined, Figure 5.4a. The force polygons for a three-oscillator system are shown in Figure 5.4b. The analysis proceeds as follows, Figure 5.4c:

$\Sigma F = 0$ i: $F_1\cos\omega t + F_2\cos(\omega t+\phi_1) + F_3\cos(\omega t+\phi_2) = 0$
j: $F_1\sin\omega t + F_2\sin(\omega t+\phi_1) + F_3\sin(\omega t+\phi_2) = 0$

$\Sigma M_a = 0$ $F_1\sin\omega t\cdot L_1 - F_2\cos(\omega t+\phi_1-90+\psi_1)\cdot L_2 + F_3\cos(\omega t+\phi_2-90-\psi_2)\cdot L_3 = 0$

Where: ϕ_1 and ϕ_2 are relative phase angles
ψ_1 and ψ_2 are relative mounting angles

Several three-oscillator scenarios are now possible. By letting $\omega t \to 0$:

$$\begin{aligned} \text{i:}\quad & F_1 + F_2\cos\phi_1 + F_3\cos\phi_2 = 0 \\ & F_1 = -F_2\cos\phi_1 - F_3\cos\phi_2 \end{aligned}$$

The trivial case is to let $\phi_1 = \phi_2$ and $F_1 = F_2 = F_3 = F$ as shown in Figure 5.5. To satisfy moments, $L_1 = L_2 = L_3 = 0$. However, as $\Sigma F = 0$ for vibration, $\Sigma M = 0$ only about the oscillator's center of rotation. With a tree attached physically at some other point on the body, force vectors would create moments about the tree, that would be damaging

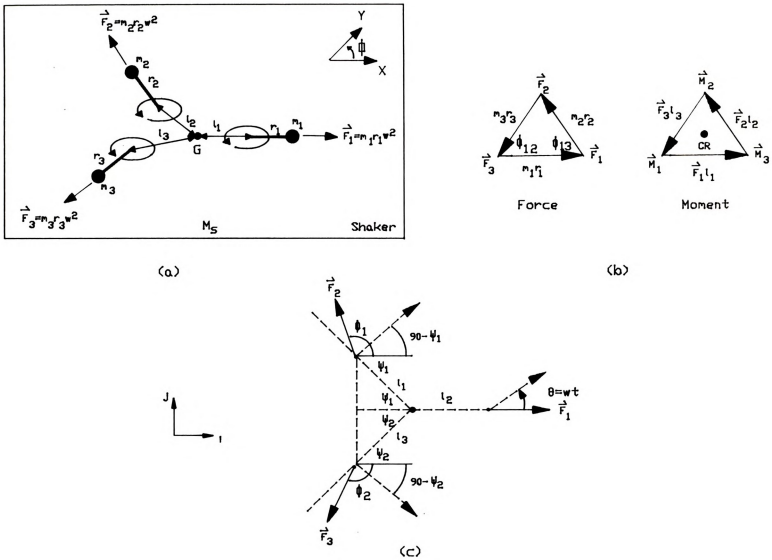

Figure 5.4 Three oscillator shaker excitation (a) general configuration (b) force and moment polygons (c) dynamic balance analysis.

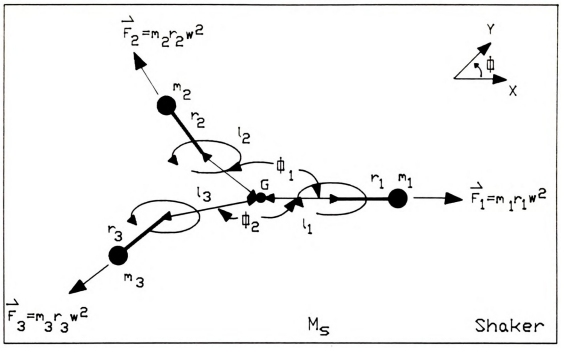

(a)

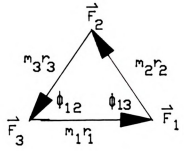

Force

Moment
(Zero)

(b)

Figure 5.5 Three oscillator shaker excitation (a) simplest configuration (b) force and moment polygons.

to the bark.

If $\phi_1 = \phi_2 = \pi$, and $F_3 = F_1 + F_2$ as shown in Figure 5.6, an interesting configuration arises. With $\omega_1 = \omega_2 = \omega_3$ and $L_1 = L_2$ then $\Sigma F = 0$ and $\Sigma M = 0$ $\forall t$. In fact, as long as $\omega_1 = \omega_2 = \omega_3 = \omega$ and $F_1 \cdot L_1 = F_3 \cdot L_2$ with F_2 at the center of gravity and $\Sigma F = 0$, then the system is balanced $\forall t$. The violation here is that F_2 is at the center of gravity which is the desirable location for the tree.

By examining the general equations and force and moment polygons, a third balanced three-oscillator configuration can be determined which is analogous with electrical three-phase phenomena. Field balance methods require that force and moment polygons close for dynamic equilibrium. By examining the moment polygon, we see that if moments are $360^o/n$ out of phase (where n is the number of oscillators) the polygons will close. Applying this theory to the general three-oscillator scenario gives:

$$\Delta\phi = 360^o/n = 120^o$$
$$\phi_0 = 0^o$$
$$\phi_1 = 120^o$$
$$\phi_2 = 240^o$$

Having found a desirable set of relative phase angles, forces can be checked and moments can be used to solve for relative mounting angles (ψ):

$$\text{i:} \quad F_1 + F_2\cos\phi_1 + F_3\cos\phi_2 = 0$$
$$F_1 - 0.5F_2 - 0.5F_3 = 0$$

Any relationship of forces as given above balance the force field. For simplicity, let $F_1 = F_2 = F_3 = F$. Moments are then:

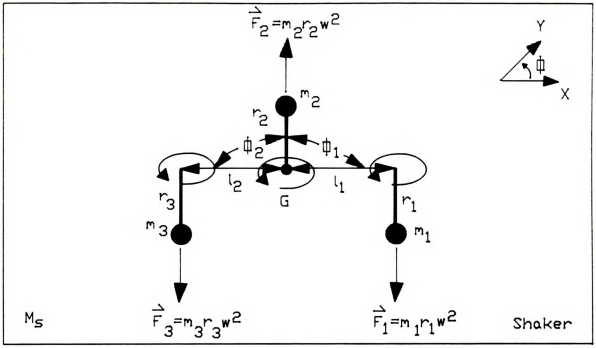

(a)

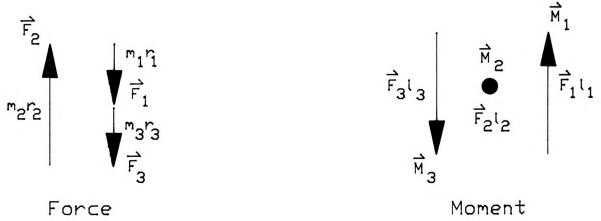

(b)

Figure 5.6 Three oscillator shaker excitation (a) linear configuration (b) force and moment polygons.

$$F_1 \cdot L_1 - F_2\cos(\phi_1 - 90 + \psi_1) \cdot L_2 + F_3\cos(\phi_2 - 90 - \psi_2) \cdot L_3 = 0$$
$$F_1 \cdot L_1 - F_2\sin(\phi_1 + \psi_1) \cdot L_2 + F_3\sin(\phi_2 - \psi_2) \cdot L_3 = 0$$

With the trigonometric identity:

$$\sin(\alpha+\beta) = \sin\alpha \cdot \cos\beta + \cos\alpha \cdot \sin\beta$$

Moments become:

$$F \cdot L_1 - F(0.866\cos\psi_1 - 0.5\sin\psi_1) \cdot L_2 + F(-0.866\cos\psi_2 + 0.5\sin\psi_2) \cdot L_3 = 0$$

Letting $L_1 = L_2 = L_3$:

$$\cos\psi_1 = -\cos\psi_2$$
$$\sin\psi_1 = -\sin\psi_2$$

In order to cancel moments:

$$\tan\psi_1 = 0.866/0.5 \rightarrow \psi_1 = 60^o$$
$$\tan\psi_2 = 0.866/0.5 \rightarrow \psi_2 = 60^o$$

Therefore, with equal forces generated by the oscillators, relative mounting angles of 60^o will also balance moments given the above relative phase angles. This third case is shown in Figure 5.7, indicating balanced forces and moments when masses are $360^o/n$ out of phase and remain at that phase ∀t. This configuration does not require a balancing oscillator at the shaker's center of rotation, thus making this option particularly suitable for a realistic design. A violation occurs in this configuration, however; the masses must rotate in the same direction ∀t for balance which will produce ellipsoidal displacement patterns when the masses are phased, and thus be void of forcing peaks - an undesirable and often ineffective shake pattern for fruit removal. The three in-line design therefore is preferred for its ability to create good patterns of oscillation, Figure 5.6.

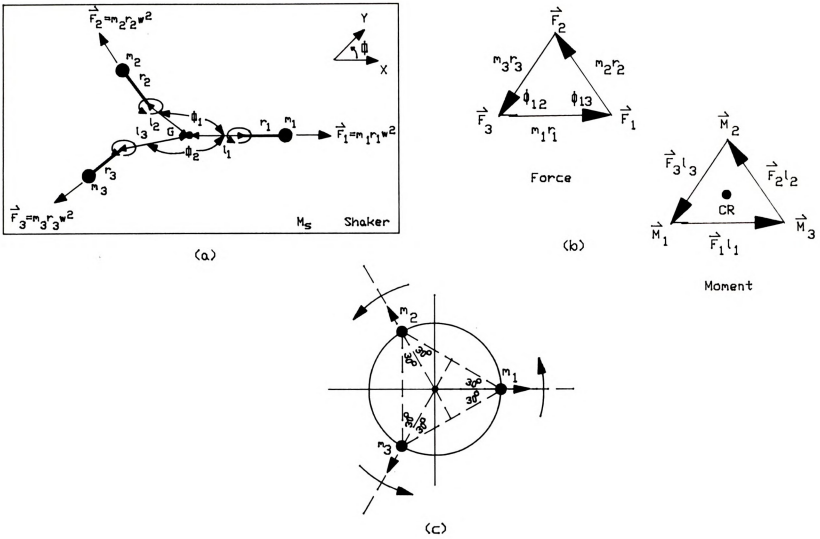

Figure 5.7 Three oscillator shaker excitation (a) physical configuration (b) force and moment polygons (c) trigonometric balance.

Theoretically, the shaken tree is located at the center of rotation. This holds true particularly with large trees. If any one of the three oscillators in the three in-line design is moved off the center line or changed in rotation direction, starting forces or torques are generated, either of which is undesirable. Although two three-oscillator scenarios have been developed which satisfy different aspects of the problem, neither one satisfies both force and moment balance as well as mass counter-rotation for peaked forcing vectors necessary for effective fruit removal.

The next step, therefore, is to examine a four-oscillator system as shown in Figure 5.8. The force polygon closes with the simplest case of $F_1 + F_2 = F_3 + F_4$. Hence, a "double pair" of oscillators can balance forces. The moment field also balances about a point 'G' with this scenario. Geometry and direction of rotation allow us to change the moment vectors without affecting the force balance. In contrast, with the three-oscillator system, changing the direction of rotation changes the force balance, which cannot be corrected by geometry.

The four-oscillator system of Figure 5.8 can be phased to impart no net motion to the body due to the double pair of counter-rotating masses. Let:

$$-\omega_4 = \omega_1 \text{ with } \phi_4 = 180^{\circ}$$
$$\omega_3 = -\omega_2 \text{ with } \phi_3 = 180^{\circ}$$

Where:

$$\omega_1 = \omega_2 = \omega_3 = \omega_4 = \omega$$

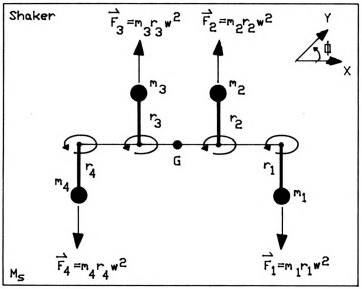

(a)

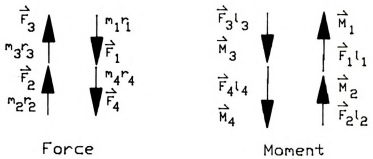

(b)

Figure 5.8 Four oscillator shaker excitation (a) linear configuration (b) force and moment polygons.

$$\Sigma F = 0:$$
$$F_1\cos\omega t\,i + F_1\sin\omega t\,j + F_2\cos(\omega t+\phi_2)i + F_2\sin(\omega t+\phi_2)j +$$
$$F_3\cos(\omega t+\phi_2+\phi_3)i + F_3\sin(\omega t+\phi_2+\phi_3)j + F_4\cos(\omega t+\phi_4)i +$$
$$F_4\sin(\omega t+\phi_4)j = 0$$

Substituting the above values and solving for components:

$$i: \quad F_1\cos\omega t - F_2\cos(\omega t+\phi_2) + F_3\cos(\omega t+\phi_2) - F_4\cos(-\omega t) = 0$$
$$j: \quad F_1\sin\omega t + F_2\sin(\omega t+\phi_2) - F_3\sin(\omega t+\phi_2) - F_4\cos(\omega t) = 0$$

Backsubstituting $F_1 = F_4$ and $F_2 = F_3$:

$$2F_1\cos\omega t - 2F_2\cos(\omega t+\phi_2) = 0$$
$$2F_1\cos\omega t = 2F_2\cos(\omega t+\phi_2)$$

Since $F_2 = F_n > 0$ where F_n is centrifugal force, then $\phi_2 = 0^o$. As expected then, $F_1 = F_2$. Checking moments:

$\Sigma M_{left} = \Sigma M_{right}$:

$$F_1\sin\omega t\cdot L_2 + F_2\sin(\omega t+\phi_2)\cdot L_1 =$$
$$F_3\sin(\omega t+\phi_2+\phi_3)\cdot L_3 + F_4\sin(\omega t+\phi_4)\cdot L_4$$

Substituting the above values:

$$F\sin\omega t\cdot L_2 - F_3\sin\omega t\cdot L_1 = -F\sin\omega t\cdot L_1 + F_3\sin\omega t\cdot L_2$$

Therefore, with $F_1 = F_2 = F_3 = F_4$ and $L_1 = L_4$ and $L_2 = L_3$, with proper phasing, no net torsional or linear motion will be imparted to the platform.

With all masses rotating in the same direction, orbital patterns such as circles, ellipses, hyperboloids, and cardioids can be produced by proper phasing of the four oscillators. Orbital patterns are less desirable than peaked displacement patterns so phasing of counter-rotating masses would be more effective for fruit removal. A hypothetical four-oscillator harvest control system is shown in Figure 5.9a. With two oscillators per shaft, the number of drive motors is half the number of oscillators. A "double mass" shaft is shown in Figure 5.9b. The "double

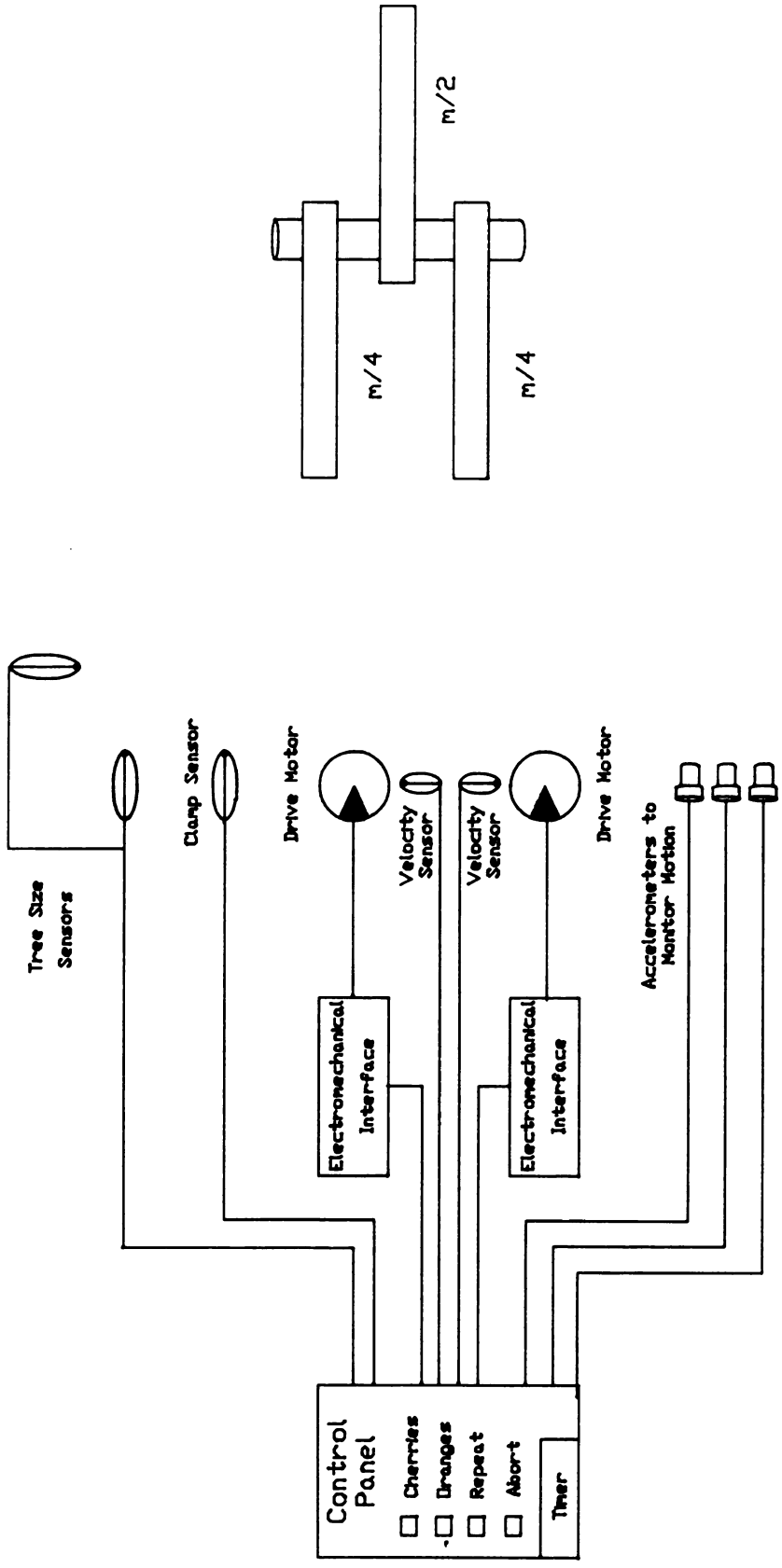

Figure 5.9 (a) Modern potential trunk shaker control panel (b) Couple free 'double mass' shaft.

mass" configuration allows two masses on one shaft to act as a phased pair without a bending couple imposed on the shaft in the balancing configuration.

Since $m_1 r_1 = m_n r_n$ to cancel both forces and moments, a four-oscillator design could be arranged as a "double pair" as long as the pairs of individual masses were spaced equally about the center of rotation of the platform (e.g. the tree) as shown in Figure 5.10. At low frequency, the oscillator masses balance and impart no motion. At the proper shaking frequency, the masses are shifted out of phase to produce a peaked oscillation pattern. Although moments may still exist as in the two-oscillator design, they are minimized by minimizing L. The important feature is to avoid "resonant moments" (at low frequencies) by phase control. A system of 4 separate oscillators would eliminate all undesirable effects, but be more complex in structure to manufacture and control.

In summary, a four-oscillator system provides both a rotating shake pattern with displacement peaks and a force-moment balance for "gallop" avoidance which can be controlled by phasing of fixed-mass oscillators.

b. Variable Eccentricity

The second method of isolating vibration at low unstable frequencies and realizing this energy at higher desirable shake frequencies involves balancing of each individual oscillator in itself. This balancing can be performed by physically changing the inertial properties of

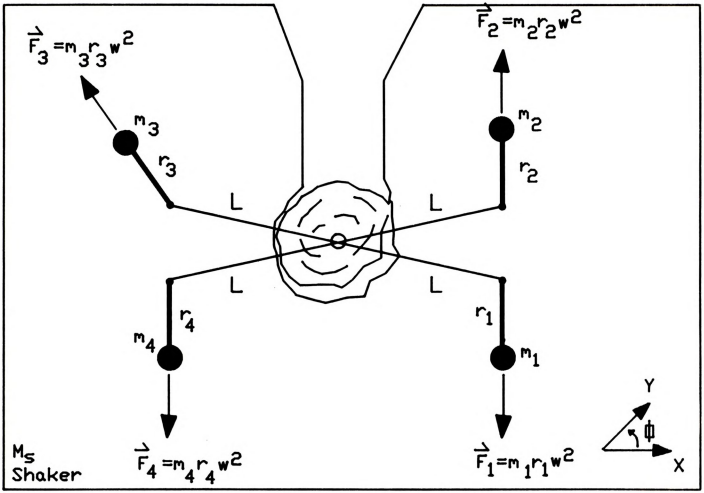

Figure 5.10 Four oscillator shaker excitation with a balanced force distribution about the tree (CR).

the oscillator; a concept which will lead to variation of eccentricity.

The single oscillator generates a force proportional to its mass (m), rotational velocity (ω), and eccentricity (e):

$$F = me\omega^2$$

Therefore, changing the force involves changing the mass, rotational velocity, or eccentricity. Since rotational velocity has the greatest effect on force because of the exponent, it would be obvious to vary ω. However, zero force requires zero velocity which requires passing through low frequencies. This negates the mode evasion strategy, however.

With rotational velocity fixed, two variables remain for control of the force vector. Changing the mass involves a mass transfer to/from the inertial shell. This could be extended to the concept of engaging a fixed mass with a clutch between the oscillator and the shaker body such that even though the oscillator is generating a force, the isolation clutch prevents this force from being transferred to the shaker body. These systems involving a mass or force transfer are difficult to implement, and involve an alternate absorber for the mass or force being isolated. This type of design has historically been unpopular and was not examined in this experiment.

The last variable which can be manipulated is the eccentricity of the fixed mass. If $e \simeq 0$ when ω is small, near the provocative natural resonances, then $F \simeq 0$ and no

motion would occur. Then, when ω is larger, near the desired shake frequency, $e \rightarrow e_{forcing}$ and $F \rightarrow F_{shake}$ resulting in a desirable motion, the intolerable transients having been avoided. Hence, eccentricity was chosen as the variable upon which to base a new design.

Historically, a few shaking devices have been developed with this concept in mind. Most of them involve a heavy flowable medium (oil, BB's) which would be transferred from a balanced position to an unbalanced position by gravity or centrifugal force. Unfortunately, the transfer occurred at very low rotational frequencies, too low for this application. Moreover, there was no positive control of eccentricity in these designs, as they reacted the same each time to centrifugal and gravitational forces.

I wanted positive control over eccentricity, with the possibility of simultaneously controlling the amplitude; therefore I selected an actuator-controlled, fixed-mass variable-eccentricity oscillator design. Several methods were considered for varying the eccentricity (linear, rotary, inclined-screw). For simplicity of construction and ease of connection to an external power unit, I selected a hydraulically controlled fixed-mass pivoted about a primary rotating shaft from a balanced position ($e \approx 0$) to a fully unbalanced position ($e=max$). This system offered the best potential for meeting the goal of resonant mode evasion.

5.2 Modified Shaker: Variable Eccentricity with One Mass

Vibration analysis of a trunk shaker led to the

hypothesis that variable eccentricity may solve the gallop problem. The Friday C-Clamp commercial trunk shaker (Friday Tractor Co., Hartford, MI) was modified in design to accommodate a variable-eccentricity mass.

The Friday Tractor Co. donated a steel mass shell and a 4.92 cm (1.94 in.) diameter steel shaft as used in the fixed-eccentric mass construction for use in construction of an experimental variable-eccentricity mass. Only one variable-eccentricity mass was constructed due to limited time, cost, and space within the shaker body. The other mass was pinned with its center of gravity in the -Y direction using a 2.5 cm (1.0 in.) diameter bolt to prevent interference from movement during design evaluation testing. Because only one variable-eccentricity mass could be developed, conventional shaker tests were conducted at two different shake frequencies (9 Hz and 15 Hz) on three different size cherry trees (6.5, 11.0 and 16.5 cm; 2.5, 4.5, and 6.5 in.) as well as in free shake to determine the effectiveness of individual masses in developing a shake pattern.

Typical displacement results are shown for free shake for analysis and design purposes and for shaking small (6.5 cm, 2.5 in.) trees because of the heavy population of young trees in commercial orchards. Interpretation of X-Y planar motion plots is difficult. Therefore, results are shown for X displacement only at the point of tree attachment.

Displacement traces for individual operation of the

inner mass and outer mass in free shake (Figure 5.11) and in shaking a 6.5 cm (2.5 in.) tree (Figure 5.12) differ very little from one another in frequency content or response time. Occurrence of start-up and shut-down resonance for each treatment were the same within experiments. However, though a start-up transient occurs when shaking 6.5 cm (2.5 in.) trees with individual masses, the decay to steady-state time is much shorter. Resonance on shut-down is still prominent, though decay time from steady-state to zero displacement also occurs much faster. This results from the additive damping factor of the tree. This relation between free shake and tree shake also indicates that part of the resonance component (1.0-2.0 Hz) occurs due to the shaker properties. Though tree damping increases the decay rate of the start-up transient, the low natural frequency of the tree ($\simeq$ 1.0 Hz) still appears to contribute to the shut-down resonance. Amplitude of free shake at steady-state reaches 8-9 mm (0.3-0.4 in.) with transients up to 23 mm (0.9 in.). Steady-state amplitude of a 6.5 cm (2.5 in.) tree shake remains the same (8-9 mm, 0.3-0.4 in.) with transients still reaching 20 mm (0.8 in.).

Results of free shake and shake of a small tree with both masses operating are shown in Figure 5.13. Start-up and shut-down transients are similar to individual mass operation in location of occurrence. A beating phenomena is also present with two mass operation however, evidenced on shut-down where linear displacements go to zero, then

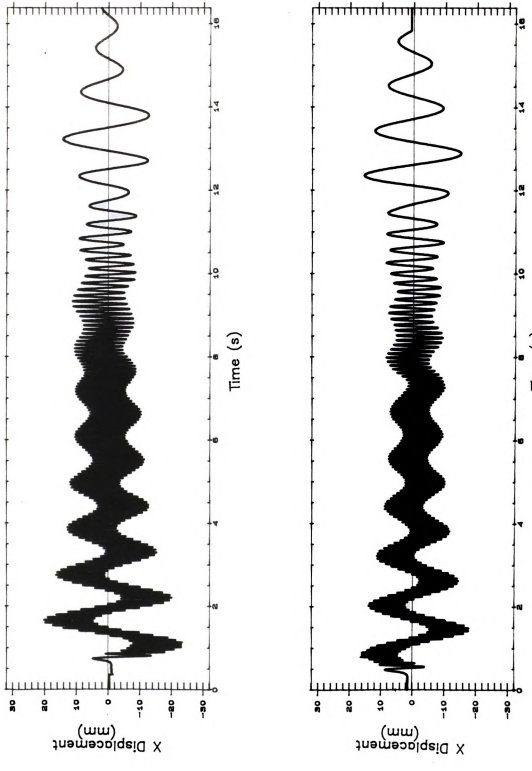

Figure 5.11 Linear (X) motion at shaker clamp with fixed mass, free shake, 15–16 Hz: a–outer mass only, b–inner mass only.

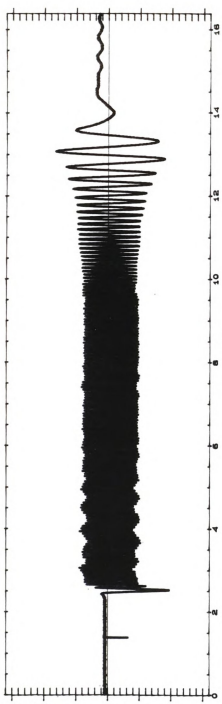

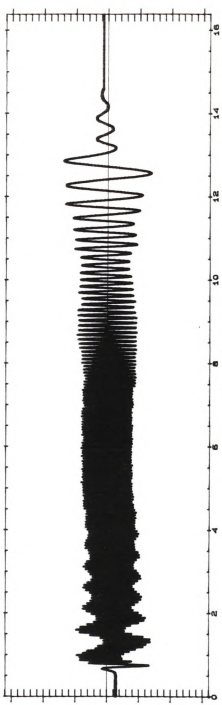

Figure 5.12 Linear (X) motion at the tree with fixed mass, 6.5 cm tree, 15–16 Hz: a–outer mass only, b–inner mass only.

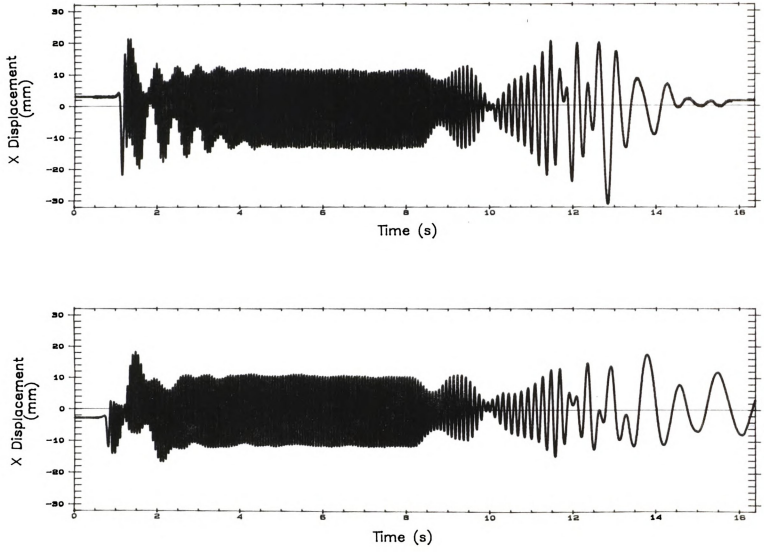

Figure 5.13 Linear (X) motion at shaker clamp with both fixed masses operating 15–16 Hz: a–6.5 cm tree, b–free shake.

rebound to transient maximums. Surprisingly, however, transients with two masses operating are greater when shaking a tree than in free shake; evidence of the contribution of the low natural modes of the tree to the beating phenomena.

Since transients are similar in amplitude and frequency for all treatments, the inner mass was chosen for design modification. This would provide maximum vibratory input to the tree with minimum side effect from shaker torsion.

The variable-eccentricity mass, designed to modify shaker displacement characteristics, is shown in Figure 5.14. A top view and an exploded view are shown in Figure 5.15. Mass 10 in Figure 5.15 is made from a steel shell, appropriately cut in the center for passage of the vertical rotating shaft through the proper arc, and fitted with a hole at each end for the rotary and the hydraulic cylinder pins. Mass 10 was formed with this curved slot 20 so as to engage vertical shaft 14 in the closed position as shown in Figure 5.14. The shell was then filled with molten lead and cooled. Bottom plate 11 and top plate 12 are welded to vertical shaft 14. The free end of mass 10 is rotatably mounted to top plate 12 and bottom plate 11 by shoulder bolt 16 which passes through top plate 12 and fastens into bottom plate 11. The free end of mass 10 is rotatably mounted to piston rod 15 by pin 13.

Vertical shaft 14 contains two internal canals 21,22 which are aligned with a rotating union 24 bolted to union

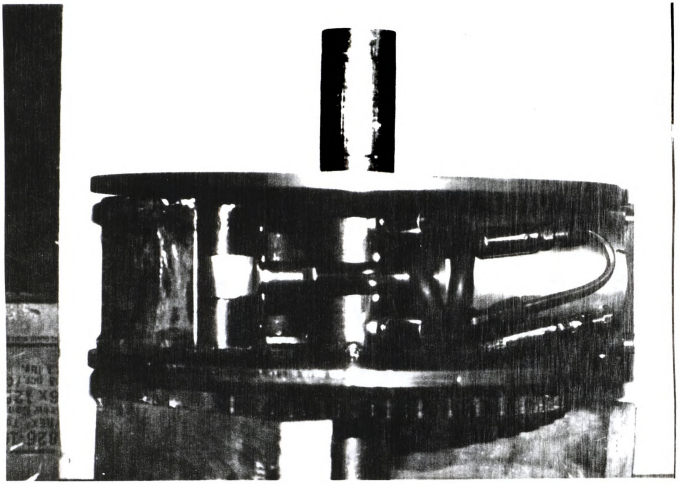

Figure 5.14 Variable-eccentricity shaker mass with positive control.

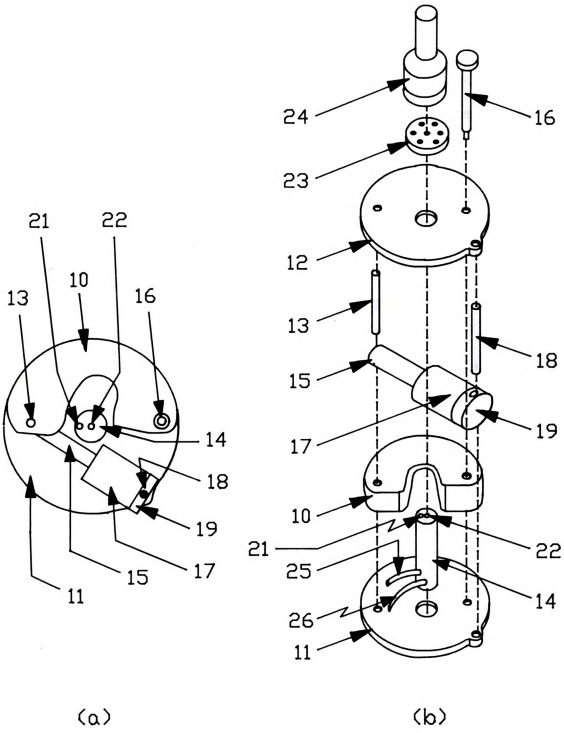

Figure 5.15 Variable eccentric mass design
(a) top view (b) exploded view.

plate 23 for hydraulic fluid passage. Suitable flexible hydraulic hoses 25, 26 transmit hydraulic fluid from vertical shaft 14 to actuator 17.

Operation of a 7.6 cm x 7.6 cm (3.0 in. x 3.0 in.) hydraulic cylinder 17 rotatably mounted to top plate 12 and bottom plate 11 by pin 18 extends and retracts piston rod 15, thus pivoting mass 10 about shoulder bolt 16 causing a change in location of the mass' center of gravity about the center of rotation of vertical shaft 14. In the retracted position, the center of gravity of mass 10 plus cylinder 17 is nearly coincident with the center of vertical shaft 14, thus imparting no unbalance to the rotation. In the extended position, the center of gravity of mass 10 is eccentric, unbalancing the rotating mechanism, thereby generating vibratory shaking forces.

The magnitude of the shaking force can be varied by varying the position of the center of gravity of mass 10 with respect of the center of rotation of shaft 14. The amount of piston rod 15 extension controls the amount of eccentricity, which in turn changes the shaking force and amplitude. In normal operation, vertical shaft 14 would be rotating at the desired shaking frequency whereupon hydraulic cylinder 17 would be controllably engaged and disengaged to pivot mass 10 about shoulder bolt 16 thus varying eccentricity and hence, shaking force and amplitude. Furthermore, the frequency of vibration is controlled by the velocity of rotation of shaft 14. Various shaker patterns

can be developed by adjusting the number, relative size, direction, phase, and frequencies of individual masses.

The experimental variable-eccentricity mass was installed in the shaker body in place of the inside mass (MB). Slight modification of the shaker box frame was necessary since the dimensions of the modified mass were necessarily slightly larger than the fixed mass.

A hydraulic control circuit (Figure 5.16) was assembled to independently vary eccentricity. A 9 cm x 20 cm (3.5 in. x 8.0 in.) hydraulic cylinder was mounted in series with hydraulic actuator 17 as a slave for monitoring the eccentricity of the variable mass enclosed in the shaker body. A flow control valve was used to regulate the velocity of eccentricity engagement providing engagement velocities from 0.0 to 175 mm/s (0.0 to 6.9 in./s) maximum. A pressure regulator limited system pressure to 8275 kPa (1200 psi), as limited by the rotating union design. Hydraulic pressure was tapped from one outlet of the auxiliary PTO pump which would normally power the second rotating mass drive motor.

Initial lab tests indicated that flow and pressure were adequate for proper operation of the new design; the system operated satisfactorily for all tests reported.

Sensors, similar to those employed in the unmodified shaker design, were mounted upon the shaker and subsequently upon cherry trees to evaluate the modified shaker design.

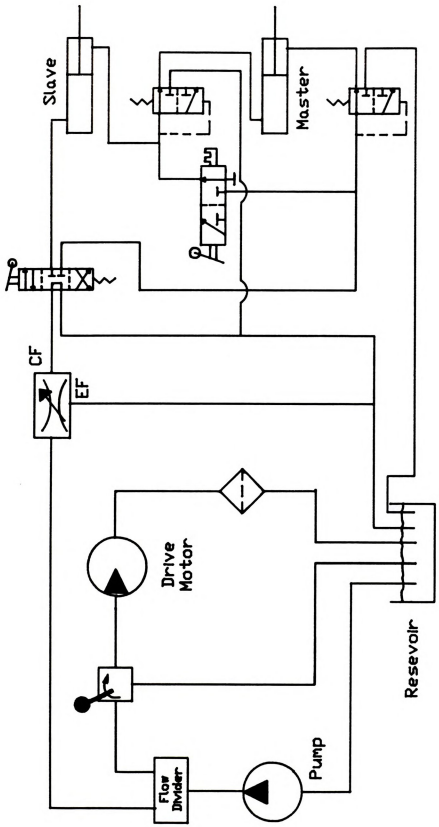

Figure 5.16 Hydraulic circuit used for controlling mass position in variable-eccentricity testing.

5.3 Displacement Results with Variable Eccentricity

Displacement tests of the modified shaker were similar to tests of the unmodified shaker. Two different engine speeds (1500 and 2200 r/min) were utilized on each of three different size Montmorency cherry trees (6.5, 11.0, and 16.5 cm; 2.5, 4.5, and 6.5 in.) as well as in free shake (using a 5 cm x 10 cm board 60 cm long (2.0 in. x 4.0 in. x 24.0 in.) in the clamp in place of a tree). All tests were conducted at the Michigan State University Horticultural Research Orchard.

Instrumentation was the same as that used in the unmodified shaker tests: an X and Y LVDT on the tree, an X and Y accelerometer on the tree, an X and Y accelerometer on the shaker at the shaker-pad interface, and a proximity sensor at the rotating mass shaft. The operation of only one mass eliminated the need for the position sensor on the second mass shaft.

Displacement traces for the modified shaker were calibrated at low frequency against photographic traces obtained by Marshall (1986). Initial observation of photographic displacement traces indicated that torsional motion with the modified shaker design was minimized. Therefore, since recorder channels were limited for transducer input, the X and Y accelerometer at the shaker center of gravity were eliminated.

A position sensor was not available to monitor movement of the cylinder controlling the variable-eccentricity mass,

therefore a Schaevitz Model 7L10VT-Z velocity sensor (Schaevitz Engineering Co., Pennsauken, NJ), was attached to the slave cylinder of the hydraulic eccentricity control circuit. Output was then proportional to the speed of eccentricity engagement and, after integration, proportional to main cylinder displacement, and thus, eccentricity via the approximate calibration equation:

$$e = \left(\int_0^t v\,dt + C\right) * \text{Cal factor}$$

Cal factor = Nonlinear calibration factor accounting for arcuate movement of mass.

Where:
$$\left(\int_0^t v\,dt + C\right)\Big|_{t=0} = 0\Big|_{e=0}$$

Typical eccentricity engagement rate and position plots are shown in Figure 5.17 for shaking of the 6.5 cm (2.5 in.) tree with fast engagement of variable eccentricity and in Figure 5.18 for slow engagement of variable eccentricity. A conventional shake with the single modified mass consisted of engaging full eccentricity prior to start-up of mass rotation. Corresponding rotational frequency versus time plots for the single modified mass are shown in Figures 5.19 (fast engage), 5.20 (slow engage), and 5.21 (conventional pre-engage). Engaging the mass fast had more effect on disturbance of rotational frequency than slow engage, possibly due to the power drawn from the system to maintain the set frequency. The added effect of the sudden change in rotational inertia of the mass may have contributed to the changes in rotational velocity observed. The conventional

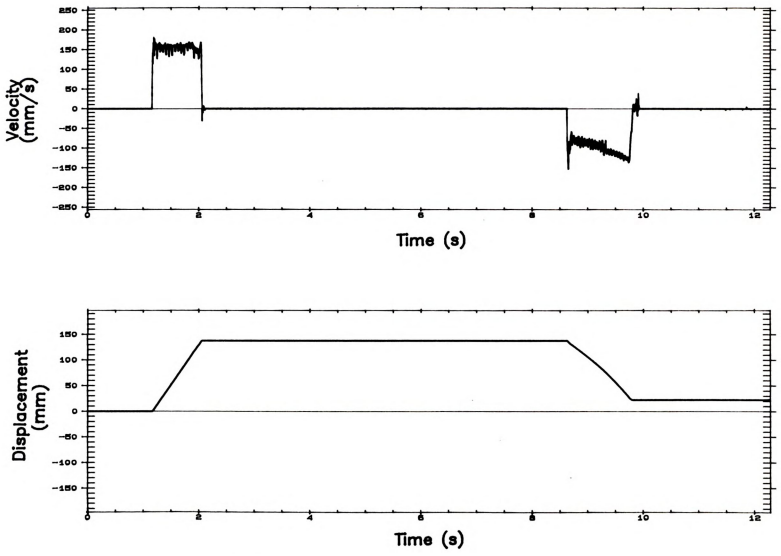

Figure 5.17 Eccentric rod velocity and position when shaking a 6.5 cm tree using fast engagement of eccentricity.

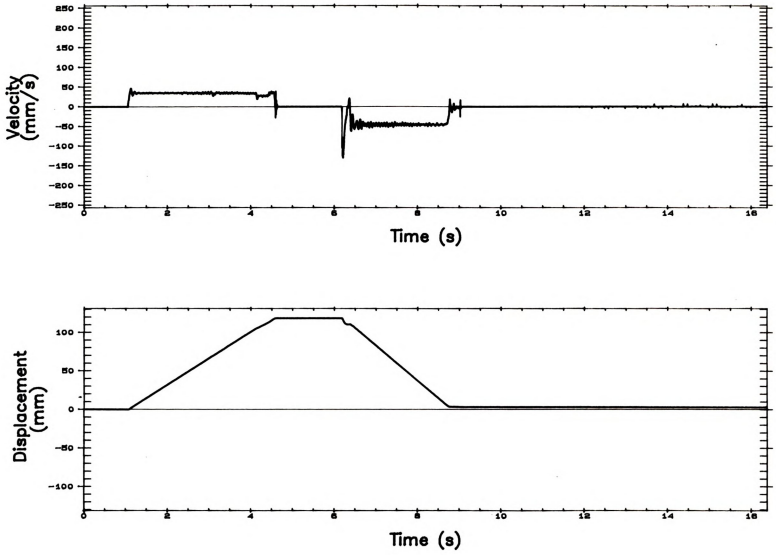

Figure 5.18 Eccentric rod velocity and position when shaking a 6.5 cm tree using slow engagement of eccentricity.

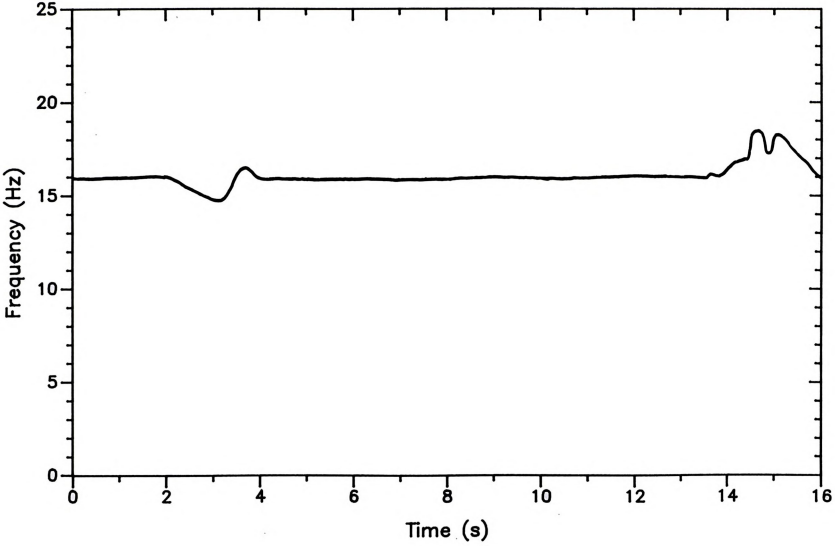

Figure 5.19 Angular velocity of mass rotation for a 15--16 Hz, 6.5 cm tree shake with fast engagement of eccentricity.

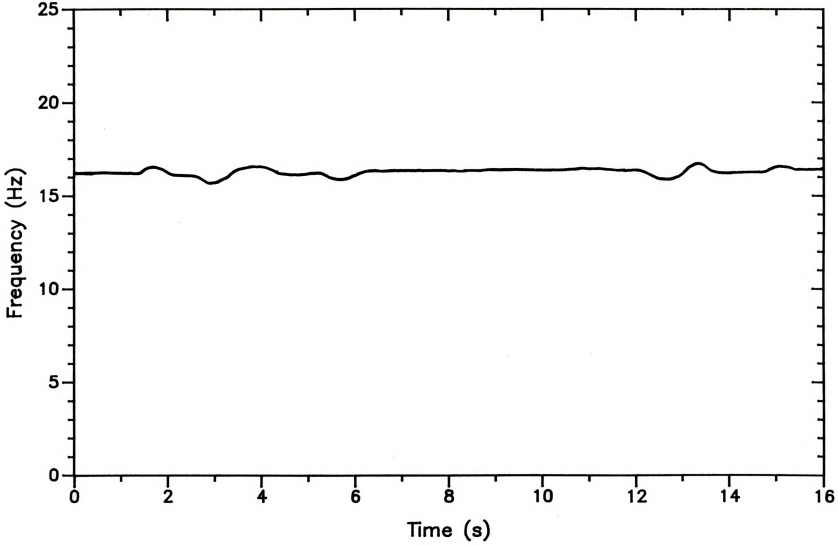

Figure 5.20 Angular velocity of mass rotation for a 15–16 Hz, 6.5 cm tree shake with slow engagement of eccentricity.

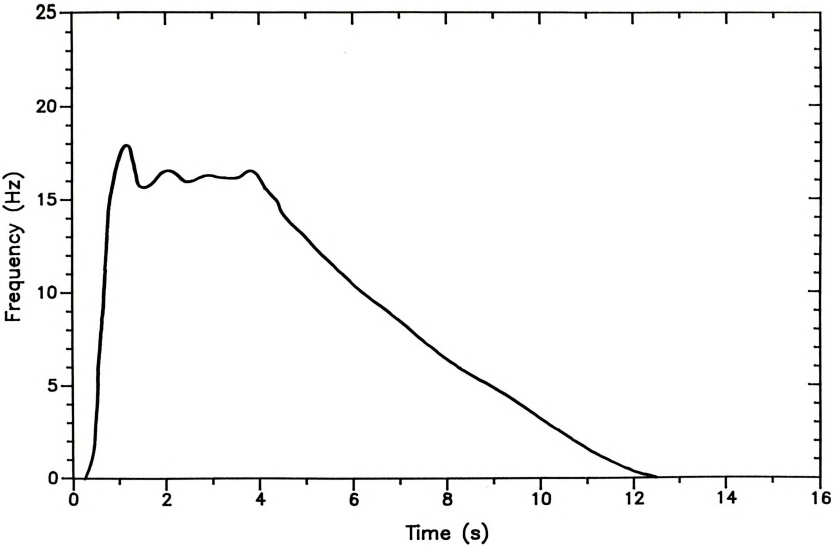

Figure 5.21 Angular velocity of mass rotation for a 15–16 Hz, 6.5 cm tree shake with fixed-eccentricity.

shake still exhibits overshoot and settling to the desired shake frequency; evidence that the system still responds similar to the pre-modified condition. Mass frequency patterns varied insignificantly with tree size or within free shake tests.

Data in the field were recorded using the same Racal four- channel instrumentation tape recorder and a Data 6000 Waveform Analyzer as used in previous tests. Data on the Racal recorder were later transferred to the Data 6000 for floppy disk storage. Data were processed as in Section 4.4 with the velocity sensor traces being integrated and calibrated directly in the Data 6000.

Typical linear X and Y displacement traces at the tree location of the modified shaker are shown for fast mass engagement in free shake (Figure 5.22) and for shaking a 6.5 cm (2.5 in.) tree (Figure 5.24). Planar X-Y motion for free shake is shown in Figure 5.23, with 6.5 cm (2.5 in.) tree motion exhibited in Figure 5.25. In free shake with the modified mass, overall amplitudes are approximately equivalent to the steady-state value of the conventional shake (8-9 mm, 0.3-0.4 in.). Free shake shows a low frequency oscillation envelope similar to that of the fixed-eccentricity data due to the start-up transient, though the magnitude is only 1-2 mm (0.04-0.08 in.) above steady-state; much smaller than the conventional transient of 15 mm (0.6 in.).

This low frequency oscillation envelope is more

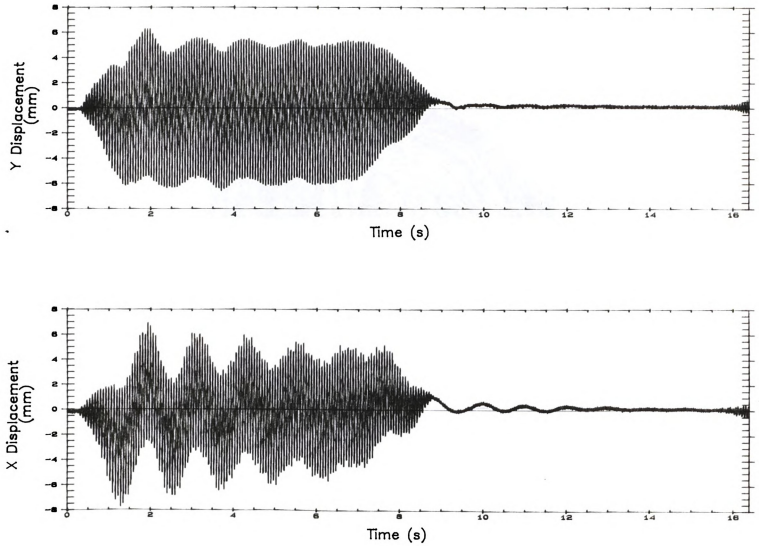

Figure 5.22 X and Y motion at shaker clamp with variable–eccentricity, fast engagement at 15–16 Hz in free shake.

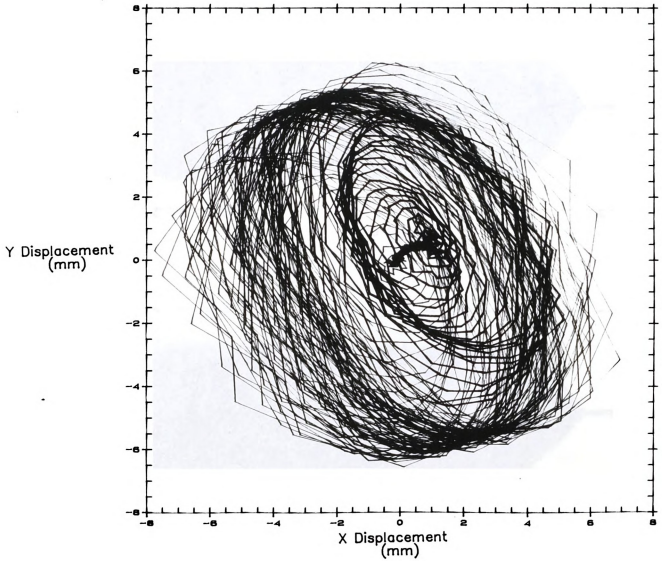

Figure 5.23 X–Y planar motion at shaker clamp with variable–eccentricity, fast engagement at 15–16 Hz in free shake.

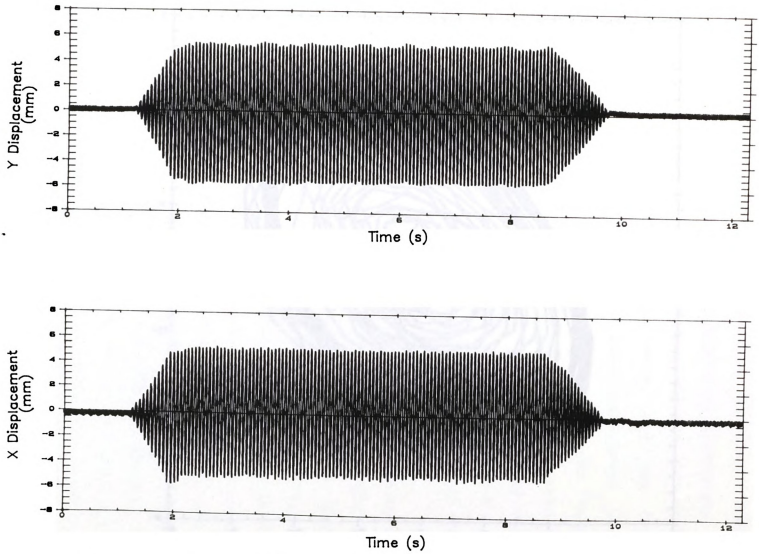

Figure 5.24 X and Y motion at the tree using variable–eccentricity, fast engagement at 15–16 Hz on a 6.5 cm tree.

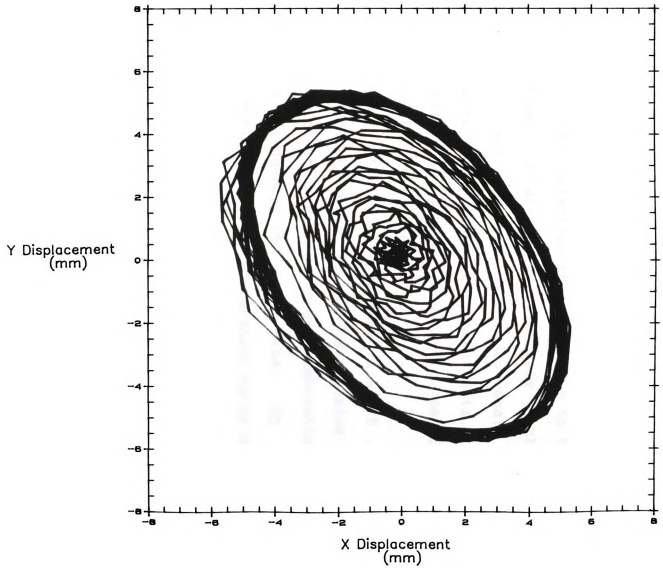

Figure 5.25 X and Y planar motion at the tree using variable–eccentricity, fast engagement at 15–16 Hz on a 6.5 cm tree.

pronounced with fast engagement of eccentricity than with slow engagement due to the greater effect of the inertial pulse on the natural frequency of the shaker body in the pendulum mode when moving the mass to its outer, unbalanced position. Fast engagement was used for subsequent tests, however, because of the speed desirability in commercial harvesting operations. In all tests, the low frequency oscillation in free shake from mass engagement was much greater in the X direction than the Y due to the respective natural modes and varied proportionately to the velocity of mass engagement. However, magnitudes remain very small in comparison to fixed-eccentricity transients. The X-Y planar plot exhibits this as an ellipsoid which oscillates (slides) on a line through its centroid.

When attached to a small tree, X and Y motion starts linearly and reaches a steady-state value approximately equivalent to the steady-state of a conventional shake of equivalent frequency and tree size. No transient or resonant motion is evidenced on start-up or shut-down with only minor overshoot (1 mm, 0.04 in.) at mass engagement evidenced in the X direction; again a result of the fast mass engagement inertial pulse on the natural frequency of the shaker-tree system. This overshoot appears to be proportional to mass engagement and not affected by tree size, in agreement with the mass frequency versus time plots. The ellipse of the planar plot of Figure 5.25 is very uniform, thus requiring a second variable-eccentricity

Table 5.1 Free displacement at shaker clamp and tree displacement resulting from fixed-mass and variable-eccentricity shaker designs (15-16 Hz, 6.5 cm tree, fast mass engagement).

	Maximum Displacement			
	Free Shake		Tree Shake	
	X mm	Y mm	X mm	Y mm
Conventional Fixed-Mass				
a. Both Masses	35	30	52	45
b. Single Mass	38	21	24	23
Modified Variable Eccentricity Mass				
a. Single Mass	16	14	11	11

mass to ensure excitation of different modes of the tree for fruit removal. Table 5.1 summarizes tree displacements incurred by both fixed-mass and variable-eccentricity shaker designs.

From Table 5.1, when a tree is added to the vibrating single mass system, the displacements generally decrease due to the damping property of the tree. However, the beating phenomena of both masses appears in increased displacements during shut-down from steady-state. Values of 15-25 mm (0.6-1.0 in.) to peaks of 40-52 mm (1.6-2.0 in.) occur in the X direction when a tree is shaken. This beating phenomena, as shown in Chapter 4, appears to become harmonic with the tree and shaker bodies and attempts to resonate

around 1.0-2.0 Hz. A pair of variable-eccentricity masses then, when retracted prior to cessation of rotation, would likely avoid these displacements by avoiding beating near this frequency.

The same characteristics are evidenced at lower, nonconventional shaking frequencies (lower frequencies used for testing but not used commercially) indicating that the variable-eccentricity mass concept avoids the majority of transient vibration excited at resonant frequencies which cause excessive displacement and thereby possible excessive stress in tree bark.

Corresponding displacement motion (X and Y) of the shaker next to the pad are shown in Figure 5.26. A planar plot of this motion is shown for shaking a 6.5 cm (2.5 in.) tree in Figure 5.27. Amplitude of motion is nearly the same though X motion is slightly larger than that of the tree (0.5-1.5 mm, 0.02-0.06 in.), possibly because some motion is being absorbed in pad compression. The overall displacement pattern of the shaker is thereby ellipsoidal as is the tree pattern.

Comparison of frequency content of a commercial 15 Hz fixed-mass shaker on a 6.5 cm (2.5 in.) tree (Figure 5.28) and a modified variable-eccentricity shaker with fast mass engagement on the same tree (Figure 5.29) highlights the broad spectrum of frequencies present in the conventional method which are exhibited as peak resonant amplitudes and low frequency oscillations during operation. These low

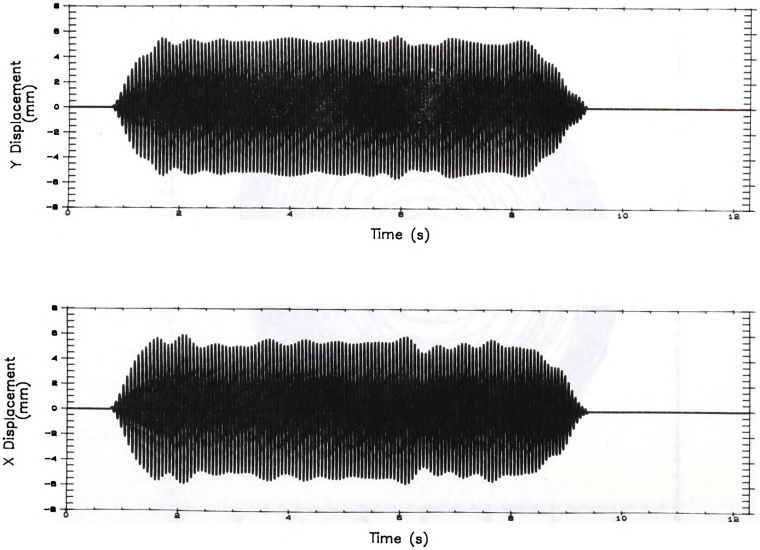

Figure 5.26 X and Y motion at shaker clamp with variable-eccentricity, fast engagement at 15-16 Hz on a 6.5 cm tree.

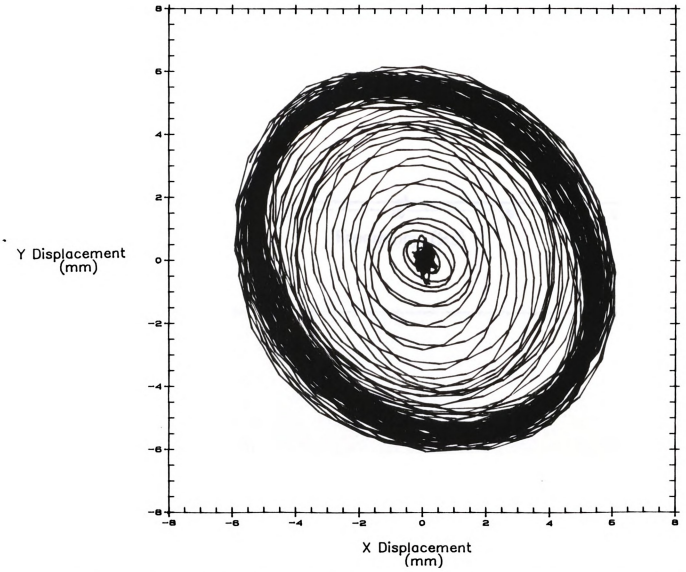

Figure 5.27 X and Y planar motion at shaker clamp with variable–eccentricity, fast engagement at 15–16 Hz on a 6.5 cm tree.

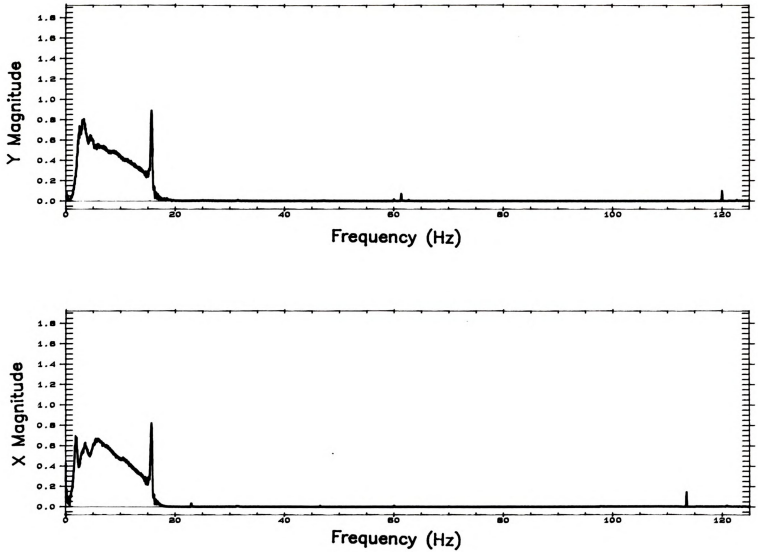

Figure 5.28 Spectral content of vibration when shaking a 6.5 cm tree at 15–16 Hz with conventional fixed-eccentricity.

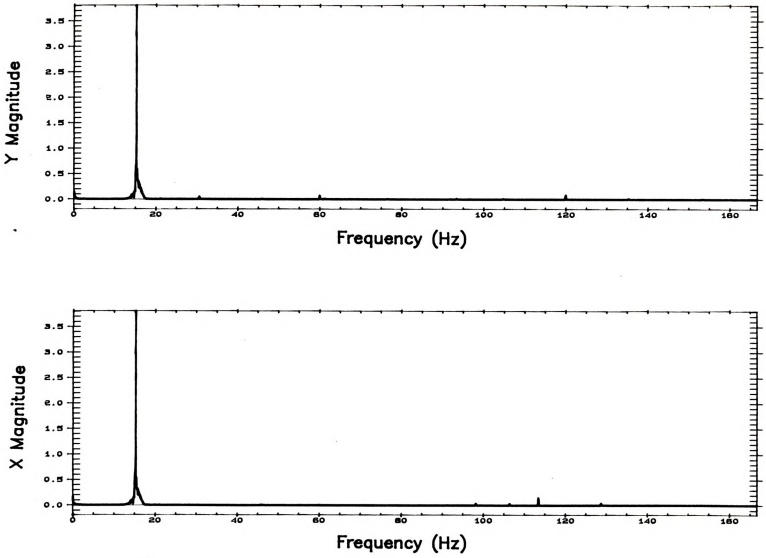

Figure 5.29 Spectral content of vibration when shaking a 6.5 cm tree at 15–16 Hz with fast engagement of eccentricity.

frequency oscillations not only contribute to peak amplitudes for high stress levels in the bark, but may also provide a mechanism for shaker rotation, thereby imparting highly damaging torsion on tree bark. Variable eccentricity eliminates this broad band and allows the shake frequency to be precisely designated.

Justification: "Shift" of the tree-shaker system can be defined as an initial gross displacement (D.C.) from the center of rest or steady-state center of oscillation from which successive oscillatory displacements occur (Figure 5.30). "Drift", on the other hand, can be defined as the path of a changing, noncyclic center of oscillation. Al-Soboh (1986) attempted to model the Friday C-clamp shaker with fixed and variable eccentric inertial driving forces to develop design parameters. Problems with numerical stability in his commercial development program prevented completion of this task. However, in free shake, he found that at high ω and with eccentricity engaged quickly, both shift and drift were kept small.

Modified shaker tests show that shift and drift were nearly zero in all cases and were unaffected by velocity of mass engagement. Shift and drift occurred only near extreme conditions simulating conventional fixed-mass operation. Preceeding variable-eccentricity displacement plots are thus shown only for rapid eccentricity engagement because this would be a preferred characteristic in commercial operation for best harvesting time efficiency.

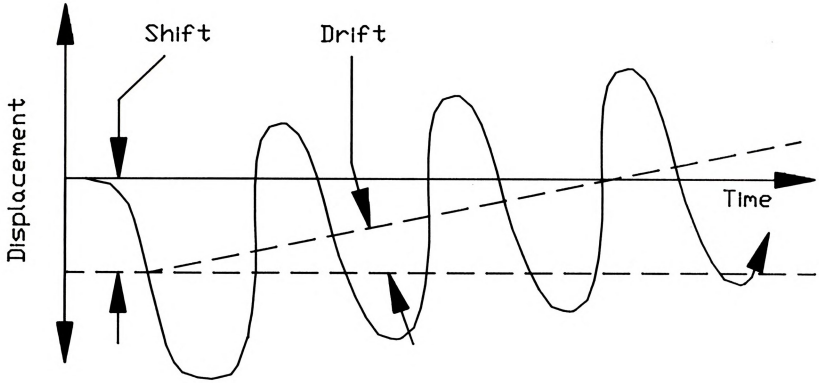

Figure 5.30 Oscillator induced 'shift' and 'drift' on shaker motion.

5.4 Evaluation of Variable Eccentricity Design Performance

The variable-eccentric mass provides a new and improved vibratory actuator for use in shake harvesting fruit and nut bearing trees in which the eccentricity is positively controlled or predetermined by physical mechanics between a balanced condition and a desired maximum unbalanced condition by means of an actuator controlling an inertial mass. The amount of eccentricity and resulting range of shaking amplitudes is controllably varied in a simple, quick operation. Independence of shaking amplitude and shaking frequency gives the operator total shake harvesting control.

Since shaking force and frequency are independently controllable, continuous operation of the primary rotatable shaft which determines the shake frequency is possible for the duration of the entire harvest, thereby eliminating the time and power required for acceleration and deceleration of the masses at each tree. Furthermore, continuous shaft rotation reduces component wear due to acceleration forces and eliminates the need for the operator to reset the shake frequency at each tree.

The most prominent benefit is the provision by this design of an improved tree shaking motion eliminating undesirable and potentially harmful damaging vibrations during transient frequency operation. Since shaking frequency is independent of shaking amplitude, undesired low frequency vibrations are avoided by operating the primary rotating shaft at a higher frequency prior to the

introduction of any vibration-generating unbalance.

5.5 Theoretical Extension to Two Masses

The variable-eccentricity design was experimentally tested with one mass but can be theoretically examined for operation with two masses as shown in Figure 5.31. With one mass located on either side of the tree, any rotation must occur about the tree (a valid assumption particularly with larger trees).

A control system could be constructed to activate the shaking process by starting with a clamp sensor which detects the proper tree position in the clamp jaws and closes the pads around the tree. Both masses would be counter-rotating at shaking speed with zero eccentricity during the clamping operation. Eccentricity would be engaged to start shake, with each mass free wheeling (no phase control). As resonance frequencies are by-passed by the variable-eccentricity design, gallop would be avoided. The desired omni-directional shake with counter-rotating free wheeling masses would be obtained, then the control system would stop the shake by shifting eccentricity back to zero.

The only drawback to this design is the moment about the tree. By moving the masses to either side of the tree, however, and positioning the suspension system close to the masses, the moment arm is small and therefore the moment is minimized. This configuration also guarantees that the center of rotation is at the tree with the forcing vectors

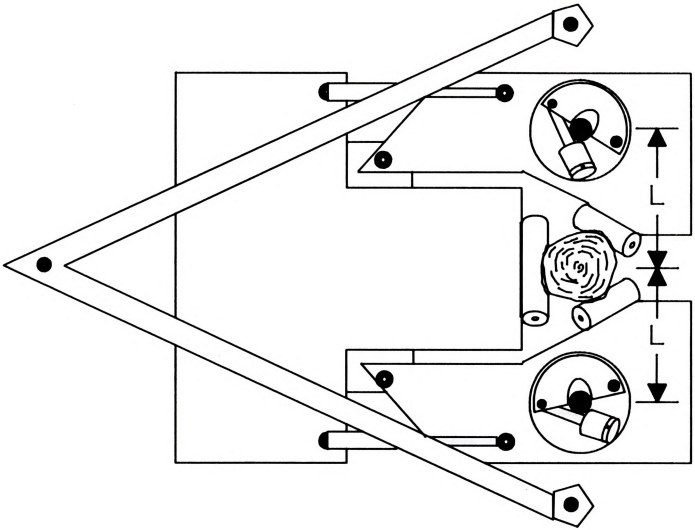

Figure 5.31 Shaker design extension to two variable eccentric oscillators.

lined nearly through the tree. The moment is a maximum when the masses are π radians apart as analyzed in Figure 5.3b:

$$\Sigma F_x = M\ddot{x}: \quad F_2\cos\omega t - F_1\cos(\omega t+\phi)$$
$$\Sigma F_y = M\ddot{y}: \quad F_2\sin\omega t + F_1\sin(\omega t+\phi)$$

Forces are:

$$R = \sqrt{F_x^2 + F_y^2}$$

$$R = \sqrt{F_2^2\cos^2\omega t - 2F_1F_2\cos\omega t\cos(\omega t+\phi) + F_1^2\cos^2(\omega t+\phi)}$$
$$\sqrt{+ F_2^2\sin^2\omega t + 2F_1F_2\sin\omega t\sin(\omega t+\phi) + F_1^2\sin^2(\omega t+\phi)}$$

$F_1=F_2=F$ by $m_1e_1=m_2e_2$

$$R = \sqrt{2F^2 - 2F^2[-\sin\omega t\sin(\omega t+\phi) + \cos\omega t\cos(\omega t+\phi)]}$$

$$R = \sqrt{2F^2 - 2F^2\cos(2\omega t+\phi)}$$

As cosine varies between 0 and $\pm$ 1, the resultant force vector will be $\leq$ 2F and the maximum moment will be 2F$\cdot$L Minimizing L, limiting phase shift to $\pm \pi/2$ radians, and constructing a suspension system to prevent torsional motion are all means to minimize the presence of torsion about the tree.

An elliptical motion with no moment could easily be developed by rotating the masses in phase in the same direction. In fact, shakers have been developed which produce elliptical motions, although fruit removal on some crops is unsatisfactory.

The problems of eliminating gallop and torsion while maintaining frequency and stroke (pattern) control may generally be solved with the variable-eccentricity mass. Unfortunately, with two fixed masses, it is theoretically impossible in any free suspension configuration (except with both fixed masses on the same shaft at the center of

rotation) to cancel both moments and forces.

5.6 Potential in Future Designs

As the current design eliminates many of the problems associated with most of today's fixed-inertia vibratory harvesters, further modification of this mass design to other environments may produce many different shaker patterns for different applications. Alteration of the actuator (hydraulic, electric, etc.), the mass motion (rotational, linear, combined), the primary shaft drive mechanism (gears, belts, direct drive), the number of rotating masses per housing, the direction, speed, eccentricity, and phasing of each of these masses, the plane of activation (horizontal, vertical, inclined), and the division of masses within a housing (one main housing or multiple subhousings) coupled with efficient suspension and clamp systems gives the designer a free hand to achieve practically any desired vibration sequence for a particular need.

CHAPTER 6

SUMMARY

Dynamic forces imposed on fruit tree bark may be beyond acceptable physiological limits, thereby adversely impacting orchard life and harvesting economics. This research consisted of a three-phase systematic plan to reduce bark damage inflicted by the dynamic loading of mechanical fruit tree shaker harvesters. Tests in this research were limited to a single variety and species: Montmorency Cherry, Prunus cerasus. This study involved three steps as follows.

Firstly, an instrumentation system was devised to detect acceleration during shaking on a commercial trunk shaker. Integration and frequency domain spectral analysis were employed to derive peak displacements which could be compared to the tolerable strength of fruit tree bark. Results indicated that transient vibrations during start-up and shut-down of shaker masses may well exceed adopted stress and strain limits even when static clamping forces are at approved levels.

Secondly, based on the peak dynamic bark loading results, a controlled variable-eccentricity trunk shaker was designed, built and tested as one possible method of restricting dynamic bark loading while maintaining

harvesting efficiency and economic feasibility. Transient vibration anomalies present in the original shaker design were eliminated in the variable-eccentricity design, meanwhile preserving selected amplitude and frequency multidirectional shake characteristics.

A preliminary planar kinetic analysis reveals two model configurations for replacing variable-eccentricity with a three-mass fixed-eccentricity system for elimination of start-up and shut-down transients. A four-mass fixed-eccentricity model is also presented which is completely controllable in terms of amplitude, frequency, and phasing.

Thirdly, based on the theory that trees compartmentalize wounded areas, variations with time of tree trunk profiles were studied in seeking indicators of the tree's health status. Because a convenient, nondestructive means of sensing sub-clinical bark damage is currently not available, several signal analysis methods were investigated on measured cross-sectional profiles as a means of nondestructively monitoring the long term effects of trunk shaker harvesting. Preliminary results indicate that the change in radial bandwidth of the trunk profile can diagnose tree damage while a Polar Fourier Analysis may discriminate between internal and external damage and provide an estimate of severity. Cross-correlation of time-spaced frequency signals assisted in detecting profile changes.

The variable-eccentricity design which resulted from this research may significantly reduce bark damage and

orchard decline, particularly in younger, more susceptible orchards. Investment in improved shaker designs of this caliber could provide substantial economic returns, especially since current day orchards have declined 30-50% in productive life from 10 years ago and 30-50% of today's cherry orchards are of nonbearing age.

CHAPTER 7

CONCLUSIONS

1. Tree displacements caused by a fixed-eccentricity, multidirectional C-clamp trunk shaker were determined for cherry tree sizes of 6.5, 11.0, and 16.5 cm (2.5, 4.5, and 6.5 in.) at shaker operating frequencies of 9 Hz and 16 Hz. Steady-state tree displacements in single mass operation ranged from 10-12 mm (0.4-0.5 in.). Two mass operation gave steady-state displacements of 15-25 mm (0.6-1.0 in.). Amplitudes of gallop were found to exceed the steady-state amplitudes by as much as 100%. Torsional motion has been observed to occur, especially during start-up and shut-down transients.

2. Steady-state tree displacements of 10-12 mm (0.4-0.5 in.) were developed by a single mass, controllably variable-eccentricity trunk shaker; the same steady-state displacement as that in the single mass, fixed-eccentricity shaker tests. Start-up and shut-down tree gallop were eliminated with this design. Alternate four-mass, fixed-eccentricity shaker designs can provide similar independent positive control of shake amplitude and frequency.

3. Profile bandwidth provides a first time indicator

of bark damage, having changed 0.5-2.4% on slightly damaged trees to maximums of 13.5% on severely damaged trees in one year. Fourier analysis of the profile, optionally combined with cross-correlation of time-spaced frequency samples, revealed that increases in the second or third harmonic were related to internal or callus damage while increases in higher harmonics (4^{th}-7^{th}) indicated split or protruding bark. The combination of invariant moments 1, 2, and 7 also provided indication of tree trunk profile change resulting from damage.

CHAPTER 8

RECOMMENDATIONS FOR FUTURE RESEARCH

1. TREE PROFILE ANALYSIS: Preliminary methods for defining changes in the profile of a cherry tree trunk over time have been introduced. As image processing equipment becomes more powerful and available, further algorithms for object discrimination and shape analysis need to be investigated. These methods, if integrated into an experimental design for a period of several years, may provide valuable insight into the growth and damage response characteristics of both mechanically harvested and control trees under a multitude of environmental conditions. Physiological basics of tree maturation may be revealed which will aid in future production and harvesting practices.

2. INJURY DETECTION: A convenient, nondestructive means for evaluating sub-clinical bark damage and/or tree stress at minute levels needs to be developed in order to aid research on the effects of orchard production and harvesting practices. If effective, this means could provide a critical link in the communication gap between plant life and humans, thereby providing a daily means by which to monitor plant and orchard condition.

3. SENSOR DEVELOPMENT: Sensor packages are needed to detect both mechanical and biological information from trees (plants) and tree (plant) interaction devices. Sensors are required to relay basic data on stimuli, plant response to stimuli, and plant growth to controllers and research instruments as crucial elements in a strongly needed integrated feedback system which would help control or eliminate nonconducive growing conditions.

4. HARVESTER AND CONTROLLER DESIGN: Agriculture, in general, is heading into an age of total auto-mechanization via microprocessor controlled robots and universal integration via sensor feedback systems. In agriculture, harvesting fruits from woody plants is a most important part of these systems. Harvesters which can efficiently interact with the biological systems without causing damage are necessary. The controllable, variable-eccentricity design of this dissertation needs further development and testing as one feasible solution to the bark damage dilemma on fruit trees. Harvesters of this and other designs need further investigation for their task efficiency and economic potential. Researchers and inventors are just now beginning to apply robotics, intelligent controllers, sensors, and image processing equipment to the harvesting process. Though adequate sensor technology appears to be the current limiting factor, basic biological data integrated into minimum control schemes may provide immediate benefits in damage reduction potential.

5. SYSTEM MANAGEMENT AND SOFTWARE: Efficient mechanization of the harvesting process and the implementation of intelligent controllers may require radical changes in current production and harvesting practice. Environmental control, pruning techniques, and genetic engineering may necessitate a 'total systems' approach to fruit tree management. Efficient, high speed software will be needed to receive information from sensors, then process data, activate controllers, and provide constant information updates on the status of all operations. New integrated systematic techniques for growing, pruning, and harvesting need further investigation as a means of maximizing yield and minimizing adverse physical or biological intervention.

6. SIGNAL PROCESSING: Sensed information in the biological sciences is seldom clean and clear cut. Often, the external stimulus or sensor limitations interfere with the desired signal. As sensors are developed for agricultural applications, it will become increasingly necessary to apply advanced electrical and mechanical signal processing principles in search of new techniques to decipher the sought out message.

BIBLIOGRAPHY

BIBLIOGRAPHY

Abildgaard, W. 1923. Fruit and Nut Harvester. U. S. Patent No. 1,472,262.

Adrian, P. A. and R. B. Fridley. 1958. Mechanical Fruit Tree Shaking. Calif. Agric. 12(10):3,15.

Adrian, P. A. and R. B. Fridley. 1963. Shaker Clamp Design as Related to Allowable Stresses of the Tree Bark. ASAE Paper No. 63-121. Am. Soc. of Agr. Eng., St. Joseph, MI 49085.

Adrian, P. A. and R. B. Fridley. 1965. Dynamics and Design Criteria of Inertia-Type Tree Shakers. Trans. ASAE 8(1):12-14.

Adrian, P. A., R. B. Fridley, D. H. Chaney and K. Uriu. 1965. Shaker-Clamp Injury to Fruit and Nut Trees. Calif. Agric. 19(8):8-10.

Affeldt, H. A. 1984. Digital Analysis of the Dynamic Response within Trunk Shaker Harvester Systems. M.S. Thesis. Mich. State Univ., E. Lansing, MI 48824. 226 p.

Affeldt, H. A., G. K. Brown, J. B. Gerrish and C. J. Radcliffe. 1984. Microcomputer Detection of Dynamic Displacements within Trunk Shaker Pads. ASAE Paper No. 84-1067. Am. Soc. of Agr. Eng., St. Joseph, MI 49085.

Agin, Gerald. J. 1976. SIR Vision Research for Advanced Industrial Automation. Second USA-Japan Computer Conference. pp. 135-148.

ARS. 1964. Mechanizing the Harvesting and Orchard Handling of Fruits. Special Report 22-88. U.S. Dept. of Agriculture. February.

Al-Soboh, G. 1986. A Simulation Study of the Displacement Behavior of a Trunk Shaker System during Cherry Harvest. Ph.D. Dissertation. Mich. State Univ., E. Lansing, MI 48824. 214 p.

Alper, Y. and A. Foux. 1976. Strength Properties of Orange Fruit-Stem Joints. Trans. ASAE 19(3):412-416.

Alper, Y., A. Foux and U. M. Peiper. 1976. Experimental Investigation of Orange Tree Dynamics under Mechanical Shaking. J. Agr. Eng. Res. 21(2):121-131.

Anderson, D. C. 1963. Tree Shaker. U. S. Patent No. 3,105,345.

Aulabaugh, W. E. 1965. Tree Limb Shaker Attachment for Chain Saws. U. S. Patent No. 3,212,250.

Avansino, J. E. 1953. Tree Shaking Mechanism. U. S. Patent No. 2,656,669.

Balsbaugh, P. H. 1950. Nut and Fruit Gatherer. U. S. Patent No. 2,503,990.

Balsbaugh, P. H. 1961. Tree Limb Shaker. U. S. Patent No. 3,013,374.

Balsbaugh, V. L. 1963. Tree Limb Shaker. U. S. Patent No. 3,077,721.

Bartlett, H. 1927. Apparatus for Harvesting Fruit. U. S. Patent No. 1,626,068.

Beljakov, V., P. Manolov and A. Nikolov. 1979. Effect of Mechanical Harvesting using Tree Shakers on the Root System and Physiological Processes of Fruit Trees. Selskostopanska Tehnika 16(6):3-14.

Berger, J. D. 1937. Walnut Tree Shaker. U. S. Patent No. 2,155,311.

Berlage, A. G. and F. M. Willmorth. 1974. Fruit Removal Potential of High Frequency Vibrations. Trans. ASAE 17(2):233-234.

Brandt, R. W. 1964. Tree Clamp with Vibratory Mechanism and Frame. U. S. Patent No. 3,163,458.

Brandt, R. W. 1965. Vibration Generator. U. S. Patent No. 3,220,268.

Brandt, R. W. 1967. Tree Clamping Jaws with Deformable Pads containing Granular Material. U. S. Patent No. 3,318,629.

Brandt, R. W. 1985. Deformable Pad for Tree Clamping Jaws. U. S. Patent No. 4,521,468.

Brinker, R. C. and R. R. Wolf. 1984. Elementary Surveying. Harper and Row Publishers Inc., New York, NY. pp. 249-251.

Brown, G. K. 1980. Harvest Mechanization Status for Horticultural Crops. ASAE Paper No. 80-1532. Am. Soc. of Agr. Eng., St. Joseph, MI 49085.

Brown, G. K. 1982. Res. Leader USDA. Mich. State Univ., E. Lansing, MI 48824. Personal Communication.

Brown, G. K. 1986. Res. Leader USDA. Mich. State Univ., E. Lansing, MI 48824. Personal Communication.

Brown, G. K. and R. M. Perkins. 1967. Harvesting Dates Mechanically. Trans. ASAE 10(4):486-488.

Brown, G. K., J. R. Frahm, R. L. Ledebuhr and B. F. Cargill. 1982. Bark Damage when Trunk Shaking Cherry Trees. ASAE Paper No. 82-1557. Am. Soc. of Agr. Eng., St. Joseph, MI 49085.

Brown, G. K., C. L. Burton and N. L. Schulte. 1984. Progress in Detecting Hidden Bark Damage. ASAE Paper No. 84-1570. Am. Soc. of Agr. Eng., St. Joseph, MI 49085.

Brown, G. K., J. R. Frahm, L. J. Segerlind and B. F. Cargill. 1986. Bark Strengths and Shaker Pads vs Cherry Bark Damage during Harvesting. ASAE Paper in Progress. Am. Soc. of Agr. Eng., St. Joseph, MI 49085.

Bruhn, H. D. 1969. Mechanized Cherry Harvesting and the Relation of Applied Acceleration to Performance. From 'Mechanization of Harvesting Fruits' by J. H. Levin. Proceedings of the 3rd Section Theme 5 VII Int'l. Cong. Agr. Eng., Oct. 6-9, 1969, Baden-Baden, West Germany.

Bukovac, M. J. 1983. Too Much Shaking - A Costly Tool for Cherry Growers. Great Lakes Fruit Growers News, May.

Bukovac, M. J. 1984. Prof. of Horticulture. Mich. State Univ., E. Lansing, MI 48824. Personal Communication.

Burger, C. P., R. B. Hall, D. B. Johnson, E. Baryeh and R. R. Faltonson. 1982. Strain Gages Measure Growth Characteristics of Trees. Trans. ASAE 25(6):1685-1690.

Burke, R. E. 1951. Tree Engaging Device for Tree Shaking Apparatus. U. S. Patent No. 2,567,872.

Burton, C. L. 1987. Asst. Prof., Botany and Plant Pathology, USDA. Mich. State Univ., E. Lansing, MI 48824. Personal Communication.

Burton, C. L., N. L. Schulte-Pason, G. K. Brown and D. E. Marshall. 1986. Influence of Mechanical Harvesting on Cherry Tree Decline. ASAE Paper No. 86-1559. Am. Soc. of Agr. Eng., St. Joseph, MI 49085.

Cargill, B. F., G. K. Brown and M. J. Bukovac. 1982. Factors Affecting Bark Damage to Cherry Trees by Harvesting Machines. Mich. State Univ., CES, AEIS Bull. No. 471. June, 6 pp.

Clarenburg, L. A. 1966. Discussion of "Characteristics of the Powder Particle Shape" by H. H. Hausner. In Particle Size Analysis. The Society for Analytical Chemistry, London, England. p. 27.

Coblentz, R. C. 1973. Harvesting System Using Tree Frame. U. S. Patent No. 3,729,906.

Cooke, J. R. and R. H. Rand. 1969. Vibratory Fruit Harvesting: A Linear Theory of Fruit Stem Dynamics. J. Agric. Eng. Res. 14(3):195-209.

Curray, J. K. 1951. Analysis of Sphericity and Roundness of Quartz Grains. M. S. Thesis in Mineralogy. The Pennsylvania State Univ., University Park.

Devay, J. E., W. H. English, F. L. Lukezic and H. J. O'Reilly. 1960. Mallet Wound Canker of Almond Trees. Calif. Agric. 14(8):8-9.

DeVay, J. E., F. L. Lukezic, W. H. English, W. J. Moller and B. W. Parkinson. 1965. Ceratocystis Canker of Stone Fruit Trees. Calif. Agric. 19(10):2-4.

Diener, R. G., J. H. Levin and B. R. Tennes. 1968. Directional Strength Properties of Cherry, Apple and Peach Bark and the Influence of Limb Mass and Diameter on Bark Damage. Trans. ASAE 11(6):788-791.

Diener, R. G., J. H. Levin and R. T. Whittenberger. 1969. Relation of Frequency and Length of Shaker Stroke to the Mechanical Harvesting of Apples. ARS 42-148. U.S. Dept. Agriculture.

Drake, S. R. 1983. Introduction to the Symposium - The Influence of Mechanical Harvesting on the Quality of Horticultural Crops. Hort. Sci. 18(4):Spec. Insert p.406.

Duda, R. O. and P. E. Hart. 1973. Pattern Classification and Scene Analysis. John Wiley and Sons, Inc. New York, NY.

Edgemond, J. W. 1967. Article Gripping Mechanism. U. S. Patent No. 3,335,556.

Ehrlich, Robert and B. Weinberg. 1970. An Exact Method for Characterization of Grain Shape. Journal of Sedimentary Petrology 40(1):205-212.

Esau, K. 1965. Plant Anatomy. John Wiley and Sons, Inc. New York, NY.

Esch, T. A. 1986. Ph.D. Graduate Student in Agricultural Engineering. Mich. State Univ., E. Lansing, MI 48824. Personal Communication.

Ferguson, J. M. 1963. Limb Shaker. U. S. Patent No. 3,101,583.

Fouch, S. B. 1986. Agricultural Extension Agent, Grand Traverse County, Michigan. Personal Communication.

Frahm, J. R., G. K. Brown and L. J. Segerlind. 1983. Mechanical Properties of Trunk Shaker Pads. ASAE Paper No. 83-1078. Am. Soc. of Agr. Eng., St. Joseph, MI 49085.

Friday, P. L. 1981. Tree Shaking Apparatus. U. S. Patent No. 4,254,608.

Friday Tractor Company. 1982-83. Sales Literature and Personal Communication. Hartford, MI 49057.

Fridley, R. B. 1968. Limb Shaker for Attachment to a Tree. U. S. Patent No. 3,406,508.

Fridley, R. B. 1970. Trunk Shaker for Attachment to a Tree. U. S. Patent No. 3,540,486.

Fridley, R. B. and P. A. Adrian. 1960. Some Aspects of Vibratory Fruit Harvesting. Agricultural Engineering 41(1):28-31.

Fridley, R. B. and P. A. Adrian. 1966. Mechanical Harvesting Equipment for Deciduous Tree Fruits. Calif. Agric. Exp. Sta. Bull. 825.

Fridley, R. B. and P. A. Adrian. 1968. Evaluating the Feasibility of Mechanizing Crop Harvest. Trans. ASAE 11(3):350-352.

Fridley, R. B., G. K. Brown and P. A. Adrian. 1970. Strength Characteristics of Fruit Tree Bark. Hilgardia 40(8):205-223.

Fridley, R. B., H. T. Hartmann, J. J. Mehlschau, P. Chen and J. Whisler. 1971. Olive Harvest Mechanization in California. Calif. Agric. Exp. Sta. Bull. 855.

Fridley, R. B. and C. Yung. 1975. Computer Analysis of Fruit Detachment During Tree Shaking. Trans. ASAE 18(3):409-415.

Gaston, H. P., J. H. Levin and S. Hedden. 1959. Experiments in Harvesting Cherries Mechanically. Quart. Bull. 41(4):805-811. Mich. State Univ. Agr. Exp. Station, E. Lansing, MI 48824. May.

Gebendinger, G. M. 1973. Eccentric Mass Vibrator for the Machines adapted to the Mechanical Harvesting of Olives and Fruits in General. U. S. Patent No. 3,771,768.

Gentry, J. P. 1980. Mechanical Harvesting Desert Grown Grapefruit. ASAE Paper No. 80-1042. Am. Soc. of Agr. Eng., St. Joseph, MI 49085.

Gerrans, W. A. 1966. Fruit and Nut Harvester. U. S. Patent No. 3,248,865.

Gerrans, W. A. 1968. Tree Clamp. U. S. Patent No. 3,367,706.

Gerrans, W. A. 1971. Tree Shaking Mechanism. U. S. Patent No. 3,555,799.

Ghate, S. R. and R. P. Rohrbach. 1980. Natural Frequencies and Associated Mode Shapes for a Two-Branch Structure with an Arbitrary Geometry. Trans. ASAE 23(3):562-567.

Gonzalez, Rafael C. and Paul Wintz. 1977. Digital Image Processing. Addison-Wesley Publishing Co., London.

Goodwin, A. D. 1954. Hydraulic System for Tree Shakers. U. S. Patent No. 2,690,639.

Gould, R. D. 1962. Tree Shaking Device. U. S. Patent No. 3,020,695.

Gould, R. D. 1964. Tree Shaker. U. S. Patent No. 3,120,091.

Gould, R. D. and E. B. Gould. 1954. Tree Shaker. U. S. Patent No. 2,685,775.

Gould, R. D. and J. E. Richter. 1969. Tree Shaking Apparatus. U. S. Patent No. 3,457,712.

Gould, R. D. and J. E. Richter. 1971. Variable Inertia Weight for Tree Shaker. U. S. Patent No. 3,564,825.

Graf, J. 1966. Sizing with Modern Image Analyzers. In Particle Size Analysis by J. D. Stockham and E. G. Fochtman. Ann Arbor Science Publishers, Inc. Ann Arbor, MI. pp. 35-44.

Gustafson, A. E. 1951. Tree Limb Shaker. U. S. Patent No. 2,542,665.

Halderson, J. L. 1966. Fundamental Factors in Mechanical Cherry Harvesting. Trans. ASAE 9(5):681-684.

Harrett, E. F. 1963. Method and Apparatus for Fruit from Trees. U. S. Patent No. 3,084,967.

Hausner, H. H. 1966. Characteristics of the Powder Particle Shape. In Particle Size Analysis. The Society for Analytical Chemistry, London, England. pp. 20-27.

Hedden, S. L., J. D. Whitney and D. B. Churchill. 1984. Trunk Shaker Removal of Oranges. Trans. ASAE 27(2):372-374.

Herbst, B. T. 1964. Tree Shaker. U. S. Patent No. 3,121,304.

Hess, K. H. 1962. Tree Shaking Device with Reel Means. U. S. Patent No. 3,029,585.

Hoag, D. L., J. R. Hutchinson and R. B. Fridley. 1970. Effect of Proportional, Nonproportional and Nonlinear Damping on Dynamic Response of Tree Limbs. Trans. ASAE 13(6):880-884.

Hoag, D. L., R. B. Fridley and J. R. Hutchinson. 1971. Experimental Measurement of Internal and External Damping Properties of Tree Limbs. Trans. ASAE 14(1):20-23.

Hood, C. E., Y. Alper and B. K. Webb. 1979. Tree Shaker. U. S. Patent No. 4,170,100.

Hussain, A. A., G. E. Rehkugler and W. W. Gunkel. 1975. Tree Limb Response to a Periodic Discontinuous Sinusoidal Displacement. Trans. ASAE 18(4):614-617.

Hutchinson, J. R., R. B. Fridley, D. L. Hoag and A. L. Phillips. 1970. Tree Vibrations. Symp. on Structural Dynamics, Loughborough Univ. Tech. Vol. II, pp. D.1.1. to D.1.21.

Johnson, J. 1951. Nut and Fruit Tree Shaking Device. U. S. Patent No. 2,568,193.

Jones, J. P. 1961. Tree Shaker Apparatus. U. S. Patent No. 3,006,130.

Kasa, I. 1975. A Circle Fitting Procedure and its Error Analysis. IEEE Trans. on Instrumentation and Measurement 25(1):8-14.

Kenworthy, A. L. 1974. Sour Cherry-Tree Vigor as Related to Higher Yields and Better Fruit Quality. Agr. Expt. Sta. Res. Report 223, Mich. State Univ., E. Lansing, MI 48824. 4 p.

Khalilian, A., P. Chen and W. J. Chancellor. 1978. Analysis and Testing of a Spring-Loaded Tree Shaker. Trans. ASAE 22(4):756-760.

Kilby, E. D. 1972. Cushioning Device. U. S. Patent No. 3,667,797.

Kronenberg, H. G. 1964. Possibilities for Mechanical Fruit Harvesting. J. Agr. Eng. Res. 9(2):194-196.

Lenker, D. H. and S. L. Hedden. 1968. Optimum Shaking Action for Citrus Fruit Harvesting. Trans. ASAE 11(3):347-349.

Levin, J. H., H. P. Gaston, S. L. Hedden and R. T. Whittenberger. 1960. Mechanizing the Harvest of Red Tart Cherries. Quarterly Bulletin 42(4):42-60. Mich. State Univ. Agr. Exp. Station, E. Lansing, MI 48824. May.

Liang, T., D. K. Lewis, J. K. Wang and G. E. Monroe. 1971. Random Function Modeling of Macadamia Nut Removal by Multiple Frequency Vibration. Trans. ASAE 14(6):1175-1179.

Londo, L. N. 1965. Mechanical Fruit Tree Picker. U. S. Patent No. 3,174,269.

Lowe, E. B. 1955. Tree Vibrating Apparatus. U. S. Patent No. 2,700,268.

Lyons, C. G., Jr. and K. S. Yoder. 1981. Poor Anchorage of Deeply Planted Peach Trees. Hort Sci. 16(1):48-49.

Markwardt, E. D., R. W. Guest, J. C. Cain and R. L. Labelle. 1964. Mechanical Cherry Harvesting. Trans. ASAE 7(1):70-74,82.

Marshall, D. E. 1986. Determining Motion of Mechanical Harvesting Systems with Photographic Techniques. ASAE Paper No. 86-1556. Am. Soc. of Agr. Eng., St. Joseph, MI 49085.

Martin, J. L. 1968. Buffer Member for Tree Shaking Device. U. S. Patent No. 3,414,314.

McEwen, F. L. 1965. Liquid Lubricant Feeding System for Tree Shaking Apparatus. U. S. Patent No. 3,178,875.

McLaughlin, A. L., R. G. Diener, R. E. Adams, K. C. Elliott and S. H. Blizzard. 1976. Comparison of Vertical vs Horizontal Limb Shaker with Regard to Apple Detachment and Bruising. ASAE Paper No. 76-1050. Am. Soc. of Agr. Eng., St. Joseph, MI 49085.

Michigan Department of Agriculture. 1985. Michigan Agricultural Statistics. 88 p. P. O. Box 20008, Lansing, MI 48901.

Michigan Department of Agriculture. 1986. Michigan Agricultural Statistics. 88 p. P. O. Box 20008, Lansing, MI 48901.

Millier, W. F., J. v. d. Werken and J. A. Throop. 1983. A Recoil-Impact Shaker for Semi-Dwarf Apple Trees. ASAE Paper No. 83-1080. Am. Soc. of Agr. Eng., St. Joseph, MI 49085.

Moini, S., J. A. Miles and T. R. Rumsey. 1980. Simulation of Tree Response to Vibration. ASAE Paper No. 80-3526. Am. Soc. of Agr. Eng., St. Joseph, MI 49085.

National Agricultural Statistics Service. 1986. Noncitrus Fruits and Nuts. USDA Agricultural Statistics Board, Washington, D.C. July.

O'Brien, M., B. F. Cargill and R. B. Fridley. 1983. Principles and Practices for Harvesting and Handling Fruits and Nuts. AVI Publishing Co., Inc. Westport, CT.

Orlando, F. P. and R. W. Fitzmaurice. 1981. Vibratory Fruit Harvester. U. S. Patent No. 4,286,426.

Overstreet, L. B. 1969. Tree Shaker. U. S. Patent No. 3,460,329.

Pacheco, A. and G. E. Rehkugler. 1980. Design and Development of a Spring Activated Impact Shaker for Apple Harvesting. Trans. ASAE 23(4):826-830.

Parrish, E. A. Jr. and A. K. Goksel. 1977. Pictorial Pattern Recognition Applied to Fruit Harvesting. Trans. ASAE 20(5):822-827.

Pellerin, R. A., W. F. Millier, A. N. Lakso, G. E. Rehkugler, J. A. Throop and T. E. Allport. 1978. Apple Harvesting with an Inertial vs Impulse Trunk Shaker on Open-Center and Central-Leader Tree--Part I. Trans. ASAE 21(3):407-413.

Pellerin, R. A., W. F. Millier, A. N. Lakso, G. E. Rehkugler and J. A. Throop. 1979. Apple Harvestng with an Inertial vs Impulse Trunk Shaker on Open-Center and Central-Leader Trees--Part II. Trans. ASAE 22(5):983-988.

Pellerin, R. A., W. F. Millier, J. A. Throop, A. N. Lakso and S. G. Carpenter. 1982. Apple Harvesting with a Double Impact Trunk Shaker. Trans. ASAE 25(5):1567-1574.

Peters, R. L. 1980. Method and Apparatus for Shaking Trees Grown in Rows. U. S. Patent No. 4,194,347.

Peterson, D. L., T. Liang and A. L. Myers. 1972. Feasibility Study of Shake Harvesting Macadamia Nuts. Int. Conf. Trop. Subtrop. Agric., ASAE Spec. Publ. Sp-01-72.

Peterson, D. L. and G. E. Monroe. 1973. Automatic-Shaker Sequencing Operation for Tree Crops. ASAE Paper No. 73-1523. Am. Soc. of Agr. Eng., St. Joseph, MI 48905.

Peterson, D. L. and G. E. Monroe. 1974. Continuous Moving Shake-Catch Harvester for Tree Crops. Trans. ASAE 20(2):202-205.

Peterson, D. L., S. S. Miller and T. S. Kornecki. 1985. Over-the-Row Harvester for Apples. Trans. ASAE 28(5):1393-1397.

Phelps, M. E. 1963. Tree Shaker. U. S. Patent No. 3,100,959.

Phillips, A. L., J. R. Hutchinson and R. B. Fridley. 1970. Formulation of Forced Vibrations of Tree Limbs with Secondary Branches. Trans. ASAE 13(1):138-142.

Plummer, C. E. 1969. Tree Shaking Device. U. S. Patent No. 3,457,713.

Pool, S. D. and R. R. Steingas. 1969. Inertia Shaker Construction. U. S. Patent No. 3,479,806.

Pool, S. D. 1971. Tree Clamp Structure. U. S. Patent No. 3,596,972.

Priestley, J. H. 1930. Studies in the Physiology of Cambial Activity III. "The Seasonal Activity of the Cambium". New Phytologist 29:316-354.

Read, B. 1965. Harvesting Device. U. S. Patent No. 3,206,919.

Roberts, W. E. 1959. Tree limb shaking device. U. S. Patent No. 2,867,964.

Rurup, W. F. 1927. Tree Shaking Device. U.S. Patent No. 1,623,497.

Russell, L. C. and E. M. Dowling. 1964. Portable Nut Tree Shaker. U. S. Patent No. 3,132,458.

Santamour, F. S. 1986. Trees Never Heal, They Just Seal. Agricultural Research 34(3):10-11. USDA ARS, Beltsville, MD 20705.

Sarkar, N. 1984. Quality Sorting of Tomatoes using Computer Vision. Ph.D. Dissertation. Rutgers Univ., New Brunswick, NJ.

Savage, B. W. 1971. Tree Shaker. U. S. Patent No. 3,594,999.

Savage, B. W. 1981. Tree Shaker. U. S. Patent No. 4,275,548.

Segerlind, L. J. and B. Weinberg. 1973. Grain Kernel Identification by Profile Analysis. Trans. ASAE 16(2):324-327.

Shipley, R. M. 1967. Tree Shaker Apparatus. U. S. Patent No. 3,358,040.

Shipley, R. M. 1970. Tree Shaking Apparatus. U. S. Patent No. 3,548,578.

Sites, P. W. and M. J. Delwiche. 1985. Computer Vision to Locate Fruit on a Tree. ASAE Paper No. 85-3039. Am. Soc. of Agr. Eng., St. Joseph, MI 49085.

Steingas, R. R. and E. M. Gaul. 1968. Mobile Shaker and Harvesting Machine. U. S. Patent No. 3,362,145.

Stockham, J. D. 1977. What is Particle Size: The Relationship among Statistical Diameters. In Particle Size Analysis by J. D. Stockham and E. G. Fochtman. Ann Arbor Science Publishers, Inc. Ann Arbor, MI.

Sturos, J. A. and J. R. Erickson. 1977. Proposed Systems to Remove Bark and Foliage from Whole-Tree Chips. Trans. ASAE 20(2):206-209.

Sumner, H. R., J. D. Whitney and S. L. Hedden. 1975. Foliage Shaker for Canopy Shaker. Trans. ASAE 16(6):1024-1026.

Tempkins, N. R. 1973. Shaker Head. U. S. Patent No. 3,780,510.

Tennes, B. R. and C. L. Burton. 1977. Continuous Mechanized Harvesting of Horticulural Crops. U. S. Patent No. 4,064,683.

Tennes, B. R. and G. K. Brown. 1980. Mechanical Shaker Assembly for Continuous Harvesting of Fruit. U. S. Patent No. 4,208,861.

Tennes, B. R. and G. K. Brown. 1981. The Design, Development, and Testing of a Sway Bar Shaker for Horticultural Crops---A Progress Report. ASAE Paper No. 81-1059. Am. Soc. of Agr. Eng., St. Joseph, MI 49085.

Timm, E. J. 1986. A Technical and Economic Study of the Slip-Belt and Lubrication System used on Commercial Trunk Shakers. M.S. Thesis, Agr. Eng. Dept., Mich. State Univ., E. Lansing, MI 48824. 105 p.

United Nations. 1986. Population and Vital Statistics Report. Dept. of International, Economic and Social Affairs, New York. Vol. 28(3):1.

U.S.D.A. Joint Council on Food and Agricultural Sciences. 1986. Executive Summary. Joint Council Reports Staff, Washington D. C. 20250.

Upadhyaya, S. K. and J. R. Cooke. 1981. Limb Impact Harvesting, Part III: Model Studies. Trans. ASAE 24(4):868-871,878.

Upadhyaya, S. K., J. R. Cooke and R. H. Rand. 1981a. Limb Impact Harvesting, Part I: Finite Element Analysis. Trans. ASAE 24(4):856-863.

Upadhyaya, S. K., J. R. Cooke, R. A. Pellerin and J. A. Throop. 1981b. Limb Impact Harvesting, Part II: Experimental Approach. Trans. ASAE 24(4):864-867.

Upadhyaya, S. K., R. H. Rand and J. R. Cooke. 1981c. Dynamics of Fruit Tree Trunk Impact. Trans. ASAE 24(4):846-855.

Watson, C. E. 1970. Limb Shaker. U. S. Patent No. 3,491,520.

Westergaard, R., L. Morton and K. Zeiders. 1983. Multiple Pattern Tree Shaking Mechanism. U. S. Patent No. 4,409,782.

Westwood, M. N. 1978. Temperate-Zone Pomology. W. H. Freemont Co., San Francisco, CA. pp. 280-281.

Whitfield, P. M. 1971. Vibrator Means. U. S. Patent No. 3,566,593.

Whitney, J. D., D. B. Churchill, S. L. Hedden and G. H. Smerage. 1986. Measured Trunk shaker and Citrus Tree Trunk Motion. ASAE Paper No. 86-1069. Am. Soc. of Agr. Eng., St. Joseph, MI 49085.

Yung, C. and R. B. Fridley. 1975. Simulation of Vibration of Whole Tree Systems using Finite Elements. Trans. ASAE 18(3):475-481.